Application of one-way laser ranging data to the Lunar Reconnaissance Orbiter (LRO) for time transfer, clock characterization and orbit determination

vorgelegt von
Dipl.-Ing.
Sven Bauer
geb. in Leipzig

von der Fakultät VI - Planen Bauen Umwelt
der Technischen Universität Berlin
zur Erlangung des akademischen Grades

Doktor der Ingenieurwissenschaften
- Dr.-Ing. -

genehmigte Dissertation

Promotionsausschuss:

Vorsitzender:	Prof. Dr. Dr. h.c. Harald Schuh
Gutachter:	Prof. Dr. Jürgen Oberst
Gutachter:	Prof. Dr. Karl Ulrich Schreiber
Gutachter:	Prof. Dr. L.L.A. (Bert) Vermeersen

Tag der wissenschaftlichen Aussprache: 5. Dezember 2016

Berlin 2017

Cumulative PhD Thesis

Application of one-way laser ranging data to the Lunar Reconnaissance Orbiter (LRO) for time transfer, clock characterization and orbit determination

Credit: NASA

Supervised by

Prof. Dr. Jürgen Oberst and Dr. Hauke Hussmann

Released by

Dipl.-Ing. Sven Bauer

Acknowledgement

First I would like to thank Prof. Jürgen Oberst, who gave me the opportunity to write this cumulative thesis within his department for planetary geodesy and supported me extensively throughout my work. Thank you for organizing a stay for me at the NASA's Goddard Space Flight Center which heavily promoted my research and provided me with so many important contacts within my career. A dream from my childhood days became a reality when I walked over NASA grounds, feeling proud to be wearing my badge. Thanks for encouraging me to participate in international conferences and meetings and discussing and reviewing so many parts of my work.

Furthermore I would like to thank Dr. Hauke Hussmann for his consistent support. He was always able to listen to and discuss problems related to my work. He also proof-read large parts of my work, even though he was always very busy himself.

Thanks to Prof. Harald Schuh for being the head of the committee as well as Prof. Karl Ulrich Schreiber and Prof. L.L.A. (Bert) Vermeersen for reviewing my thesis. I am happy to have such a well composed committee for the evaluation of my thesis.

Thanks to the LOLA team who hosted me first in the SOC, than in the SAC and finally the DAC. Every stay was so inspiring and encouraging. I learned so much in such short timeframes. Thanks to everybody in the team for patiently listening and answering to my requests. A very big thank you to Maria Zuber for being such an effective but friendly manager, David Smith who is still so active and keeps on travelling internationally, Greg Neumann who became a close friend and was so supportive and helpful, Erwan Mazarico the only person that I know who can speak faster than I can think and is still right, Mark Torrence for his support and the Porsche ride, David Rowlands for his crazy worldly wisdoms as well as Dandan Mao, Frank Lemoine, Jan McGarry and Xiaoli Sun for their extensive support and expertise. This work would not have been possible without you guys and I am happy to see everyone still alive and kicking.

A very big thank you goes to Dominic Dirkx from TU Delft with whom I collaborated a lot. He patiently reviewed and discussed so many parts of my work which helped so much and most of the time addressed the really complicated aspects of them. Without his support, his collaboration and moreover his expertise this work would not have been completed. Moreover I want to thank my DLR and TUB colleagues for the support, in particular Alexander Stark for the many fruitful discussions and the corrections, Philipp Gläser for his expertise, the table tennis lessons and his sense for business and Gregor Steinbrügge as well as Isabel Haase for their support. Also many thanks to Team One for reviewing the spelling and the grammar of the manuscript.

Finally I would like to thank my family who gave more than anybody else. Thanks to my mom who always supported my ideas and made my childhood dreams come true. Thanks to my grandpa who always supported me as well and saved me from becoming a truck driver. Also thanks to my girl Franziska Peter for supporting me during the tough times and for being such a nice woman. I am so lucky and happy to have you! Finally I also want to thank all the other friends and people who supported me during the tough times during this work.

Abstract

NASA's Lunar Reconnaissance Orbiter (LRO) mission carries a suite of seven instruments with the Lunar Orbiter Laser Altimeter (LOLA) being one of them. Due to a hardware extension the instrument is capable of detecting regular altimetry measurements from the lunar surface and laser pulses from Earth-based ground stations concurrently at a precision of 15 cm. Utilizing the ground-based ranges for orbit determination is a promising technique due to its precision, the simplicity of the hardware extension and the multiple uses of laser altimeters for future missions.

Compared to classical two-way systems, one-way tracking is subject to issues that affect the processing and the application of the data. The fire and the receive times are recorded separately because the respective systems are separate. Furthermore the ranges are a function of state and time which have to be estimated simultaneously from the one-way observable. This requires the simultaneous estimation of the LRO state vector as well as the behavior of its clock and all involved ground station clocks. Within this cumulative thesis the application of one-way laser ranging measurements for LRO's orbit determination is investigated while analyzing the issues in particular.

The method that was developed for the pairing of the fire and the receive times utilizes time conversion from the spacecraft clock kernel and position information from the nominal LRO trajectory. The fire and the receive times were thereby corrected for the influence of atmospheric, instrument specific and relativistic effects. From the processing of observation data covering the whole experimental timeframe of 5 years, statistical values for the experiment and the ground station performance were derived. This data is extremely valuable for mission analysis and simulation.

Furthermore the LRO clock was characterized whereby the average value over all mission phases was estimated to 6.9×10^{-8} for the rate, to 1.6×10^{-12} /day for the aging and to 2.3×10^{-14} /day^2 for the change of aging. Onboard times were referenced to ground times at an accuracy of 166 ns over two and 256 ns over all mission phases via ground to space time transfer. Moreover ground station clock differences were characterized with different methods from common-view ground to ground time transfer. From such simultaneous passes relative offsets ranging from 33 to 560 ns and relative rates ranging from 2×10^{-13} to 6×10^{-12} were estimated between different ground station clocks.

LRO orbit arcs were successfully estimated with inversion software based on batch linear least squares. The simultaneous estimation of LRO's state vector as well as of the correlated LRO and ground station clock parameters required a priori initial and covariance values. These constraints were taken from the nominal LRO trajectory and the characterization of the LRO and the ground station clocks. Within the orbit determination with one-way data only, longer arcs (e.g. 7 and more days) are preferable over shorter arcs since fewer correlated parameters have to be estimated.

The estimated 2 and 7 day long arcs had differences of ≈25 m to the nominal LRO trajectory. This is comparable to results from the literature, which had differences of 5–30 m to the nominal trajectory from orbit determination with one-way laser ranging data only.

With increasing LRO state arc length (e.g. from 2 to 7 days) the accuracy of the estimated trajectories and the post-fit measurement residuals are decreasing due to neglected or simplified effects in the dynamical modeling. Likewise the accuracy of the estimated clock parameters and the post-fit measurement residuals are decreasing with increasing LRO and ground station clock arc length. The polynomial fits only had limited capability to approximate random LRO clock errors and errors due to incomplete corrections of the fire and the receive times within the clock modeling. Furthermore gaps

longer than 12 hours in the observation data coverage significantly decreased the accuracy of the trajectories, the clock parameters and the post-fit measurement residuals.

From the results it was found that the LRO state and the LRO and ground station clock arc lengths can be adjusted so that the maximum arc length and the accumulation of errors are optimized. Thereby the different arc lengths for the state, the LRO and the ground station clocks do not need to be identical.

While utilizing such optimized state and clock arc lengths as well as enhanced dynamical modeling and corrections, further improvement of the LRO positioning derived from orbit determination with one-way laser ranging data should be possible. Then the laser ranging data could provide valuable input within the joint orbit determination of LRO from radio, laser and altimetry data.

Zusammenfassung

Die NASA Raumsonde Lunar Reconnaissance Orbiter (LRO) verfügt über sechs Bordinstrumente, von denen eines das Lunar Orbiter Laser Altimeter (LOLA) ist. Durch eine technische Erweiterung ist das Instrument fähig, die regulären Altimetriemessungen zur Mondoberfläche und gleichzeitig Laserpulse von erdbasierten Bodenstationen mit einer Präzision von 15 cm zu detektieren. Die Bestimmung der Umlaufbahn von LRO mit Hilfe der bodenbasierten Laserentfernungsmessungen ist hinsichtlich der Präzision, der Einfachheit der technischen Realisierung und der Mehrfachnutzung von Laser Altimetern innerhalb zukünftiger Missionen von Interesse.

Da es sich bei den Laserentfernungsmessungen um eine Einweg-Verbindung handelt, weist die Verarbeitung und die Anwendung der Daten im Vergleich zu klassischen Zweiwege-Verbindungen Besonderheiten auf. Die Abschuss und Empfangszeiten werden separat aufgezeichnet, da die jeweiligen Systeme voneinander getrennt sind. Des Weiteren sind die Einweg-Entfernungsmessungen abhängig von Ort und Zeit welche in der Umlaufbahnbestimmung gleichzeitig aus nur einer Beobachtung bestimmt werden müssen. Das erfordert die gleichzeitige Bestimmung des LRO Ortsvektors und dem Verhalten seiner Uhr sowie aller involvierten Bodenstationsuhren. Diese kumulative Dissertation beschreibt die Anwendung der Einweg-Laserentfernungsmessungen für die Umlaufbahnbestimmung von LRO wobei speziell auf die Besonderheiten eingegangen wird.

Die zunächst entwickelte Zuordnungsmethode der Schuss- und Empfangszeiten nutzt Zeitkonvertierungs- und Positionsinformation aus der nominellen LRO Trajektorie. Die Abschuss- und Empfangszeiten wurden dabei für atmosphärische, instrumentenspezifische sowie relativistische Einflüsse korrigiert. Aus der Prozessierung von Beobachtungsdaten über den gesamten Experimentzeitraum von 5 Jahren wurden statistische Mittelwerte für die Experiment- und Bodenstationsperformance abgeleitet. Diese Daten sind äußerst wertvoll für Missionsanalysen und -simulationen.

Des Weiteren wurde die LRO Uhr charakterisiert wobei ein mittlerer Wert von 6.9×10^{-8} für ihre Rate, 1.6×10^{-12} /Tag für ihre Alterung und 2.3×10^{-14} /Tag^2 für die Änderung der Alterung über alle Missionsphasen bestimmt wurde. Mittels ground to space time transfer wurden Bord- zu Bodenzeiten mit einer Genauigkeit von 166 ns über zwei und von 256 ns über alle Missionphasen referenziert. Außerdem wurden mittels Ground to Ground Common-View Time Transfer die Unterschiede zwischen den Bodenstationsuhren mit verschiedenen Methoden charakterisiert. Aus simultanen Pässen wurden relative Offsets von 33 bis 560 ns sowie relative Raten von 2×10^{-13} bis 6×10^{-12} zwischen den Bodenstationsuhren bestimmt.

Mit einer auf einem Batch Linear Least Squares Verfahren basierenden Inversionssoftware wurden erfolgreich Bahnbögen für LRO bestimmt. Die Bestimmung des Ortsvektors von LRO und der zum Teil stark korrelierten LRO- und Bodenstationsuhrenparameter war nur unter Verwendung von a priori Start- und Kovarianzwerten möglich. Diese Werte wurden aus der nominellen LRO Trajektorie und der Charakterisierung der LRO Uhr und der Bodenstationsuhrendifferenzen bezogen. Prinzipiell sind bei der Umlaufbahnbestimmung nur mit Einweg-Daten längere Bahnbögen (zum Beispiel 7 und mehr Tage) kürzeren Bögen vorzuziehen, da weniger korrelierte Parameter gleichzeitig bestimmt werden müssen.

Die bestimmten LRO Bahnbögen mit Längen von 2 und 7 Tagen hatten Unterschiede von ungefähr ≈25 m zur nominellen LRO Trajektorie. Das ist vergleichbar mit Ergebnissen aus der Literatur, die

Abweichungen von 5–30 m zur nominellen Trajektorie bei der Umlaufbahnbestimmung nur mit Einweg-Laserdaten aufwiesen.

Mit zunehmender LRO-Bahnbogenlänge (z.B. von 2 zu 7 Tagen) verschlechterte sich die Genauigkeit der bestimmten Trajektorien und der Messwertresiduen durch vernachlässigte oder vereinfachte Effekte in der dynamischen Modellierung. Ebenso werden die bestimmten Uhrenparameter und die Messwertresiduen mit zunehmender LRO- und Bodenstationsuhrenbogenlänge ungenauer. Die verwendeten Polynome können zufällige LRO-Uhrenfehler und Fehler aufgrund von vernachlässigten oder vereinfachten Korrekturen der Abschuss- und Empfangszeiten bei der Uhrenmodellierung nur begrenzt abbilden. Weiterhin haben Beobachtungsdatenlücken größer als 12 h die Genauigkeit der bestimmten Trajektorien, Uhrenparameter und Messwertresiduen signifikant verringert.

Aus den Ergebnissen hat sich gezeigt, dass die LRO-Bahn- und Uhrenbogenlängen für LRO und die Bodenstationsuhren so eingestellt werden können, dass die maximale Länge und die Akkumulation von Fehlern optimiert ist. Die verschiedenen Bogenlängen für die Bahnbögen sowie die LRO und die Bodenstationsuhren müssen dabei nicht identisch sein.

Unter Verwendung von solchen optimalen Bahn- und Uhrenbogenlängen sowie einer verbesserten dynamischen Modellierung und verbesserter Korrekturen sollte eine weitere Verbesserung der Positionierung von LRO aus der Umlaufbahnbestimmung nur mit Einweg-Daten möglich sein. Dann könnten die Laser Entfernungsmessungen einen wertvollen Beitrag in der gemeinsamen Umlaufbahnbestimmung von LRO aus Radio, Laser und Altimetriedaten leisten.

Structure of the dissertation

On the scientific background of the Lunar Reconnaissance Orbiter (LRO) mission the first chapter will highlight why the investigation of the laser ranging data is relevant and thus provide the research motivation. The introduction follows, providing background about laser ranging, the LRO mission, orbit determination and time transfer. The introduction closes with a description about the various aspects and the content discussed in the research papers. The main part of the cumulative thesis consists of two scientific publications which have been submitted to peer-reviewed journals:

Research paper 1
S. Bauer, H. Hussmann, J. Oberst, D. Dirkx, D. Mao, G.A. Neumann, E. Mazarico, M.H. Torrence, J.F. McGarry, D.E. Smith, M.T. Zuber.
Analysis of one-way laser ranging data to LRO, time transfer and clock characterization.
Accepted manuscript, Published in *Icarus* **283**, Lunar Reconnaissance Orbiter – Part II, February 2017, Pages 38–54. DOI: 10.1016/j.icarus.2016.09.026

Research paper 2
S. Bauer, H. Hussmann, J. Oberst, D. Dirkx, D. Mao, G.A. Neumann, E. Mazarico, M.H. Torrence, J.F. McGarry, D.E. Smith, M.T. Zuber.
Demonstration of orbit determination for the Lunar Reconnaissance Orbiter using one-way laser ranging data.
Accepted manuscript, Published in *Planet. Space Sci.* **129**, September 2016, Pages 32-46. DOI: 10.1016/j.pss.2016.06.005

The subsequent section discusses the implications and the effect of the applied methods or data products on the common and the individual results. The discussion focuses on the effect of

- utilizing existing orbit information,
- the methods for estimating the onboard and the ground station clocks,
- the detail of the dynamical modeling,
- the observation data type and coverage

on the characterization of the clocks, the time transfer and the derived orbit arcs. Finally it is shown how the research question is addressed by the results and how that compares to the current state of research derived from the literature. Moreover aspects of the work that could be improved are discussed, including the outcome and potential methods. On the basis of the results of this work, range-rate observations that could be differenced from the one-way range data, are analyzed regarding potential error influences and attainable accuracy. After discussing the benefits of one-way tracking systems, the results of this thesis are summarized in the synthesis.

The author of this thesis, Sven Bauer, was the main developer of the methods described in the papers from which the presented results were derived. The two papers were improved by the comments of the coauthors and the reviewers. The author received support from colleagues from the German Aerospace Center (DLR) Berlin and from Technische Universität Berlin (TUB). The LOLA team provided the laser ranging data, the nominal LRO trajectory, other data products as well as expertise. The work presented in this thesis was carried out at the Institute for Planetary Research at the German Aerospace Center (DLR) in Berlin Germany. Part of this work was done during a three month long stay at NASA's Goddard Space Flight Center (GSFC) in Greenbelt, Maryland USA.

Content

List of Figures

List of Tables

1 Research motivation

Geodesy is the science of the measurement and mapping of the surface of the Earth (Helmert, 1880). Seeber (2003) builds upon this definition and says that satellite geodesy uses observational and computational techniques in order to provide solutions to geodetic topics by using precise measurements to, from or between mostly Earth-satellites. Following the definition of Seeber (2003) the basic geodetic topics are

- Estimation of global, regional and local three-dimensional positions (e.g. control-point networks),
- Determination of the gravity field of a certain body that a spacecraft is orbiting,
- Measurement and modeling of geodynamical phenomena such as plate tectonics, volcanism, folding, faulting which are caused by mantle convection and can be analyzed from internal activity (magnetic field, gravity field, seismic activity) and mineralogy (Ismail-Zadeh and Tackley, 2010).

NASA's Lunar Reconnaissance Orbiter (LRO) mission, from which the ground-based one-way laser ranging tracking data is used for orbit determination within this work, addresses these topics on the Moon. Besides comprehensive geophysical, geological and geochemical mapping of its surface, geodetic mapping will provide an observational framework for future lunar human and robotic exploration (Zuber et al., 2010). Following Smith et al. (2010a) and Jin et al. (2014) the geodetic grid, the surface slopes and the roughness derived from the Lunar Orbiter Laser Altimeter (LOLA) data (topography and return pulse characteristics) allow for the

- Referencing of measurements on the lunar surface,
- Selecting future landing sites,
- Research of the lunar origin and evolution from its figure,
- Research of gravity anomalies,
- Research of the thermal and loading histories of major lunar impact basins.

The spacecraft that was launched on June 18, 2009 carries further instruments which address the following research topics:

- Characterization of biological effects and property changes of radiation shielding materials due to the deep space radiation environment,
- Mapping the hydrogen on the lunar surface,
- Mapping the temperature in the lunar polar shadowed regions,
- Imaging of the permanently shadowed regions,
- Search near-surface water ice in the lunar polar cold traps,
- Assessment of potential landing sites at meter and smaller-scale for safety analysis,
- Characterization of the illumination conditions at the lunar polar regions (Chin et al., 2007).

Except for the first one, all mission goals rely on the analysis of measurements located on the lunar surface. From the position and the orientation of the spacecraft and its instruments at the time when measurements were taken, they can be referenced to a location on the lunar surface. While the orientation of LRO is measured from the onboard star trackers (Garrick et al., 2010), its trajectory is derived from the utilization of tracking data in orbit determination. The main result from orbit

determination is the trajectory of the spacecraft representing its position as a function of time $\vec{x}(t)$ which is derived by integrating the equations of motion from the initial state. Figure 1 shows schematically how the spacecraft trajectory is derived via orbit determination which allows for the referencing of the measurements to a location and from that the estimation of results provided as data products. Such data products can either be derived from the analysis directly (e.g. mapping), or from the application of the measurements in further parameter estimation (e.g. for a Digital Elevation Model (DEM)).

Within a space mission generally two types of measurements are available for use in orbit determination. They are either ground-based tracking data of the spacecraft or spacecraft-based observations. While most Earth-based ground stations provide the tracking data for use in orbit determination, spacecraft observation data can be derived via different setup. Some missions, such as GRACE and GRAIL, employed a twin spacecraft configuration with dedicated instruments for measuring the distance between them. Such a setup allows for a more accurate estimation of the gravity field than with ground based observations only (Zuber et al., 2013; Seeber, 2003). Furthermore measurements from instruments onboard the spacecraft may provide observations that can be used within orbit determination as well, such as the crossover points – the intersections – of the altimetric profiles that are collected by LOLA (Smith et al., 2010a). Due to their global distribution on the lunar surface, these crossovers are also available at the far side where no ground-based tracking is available.

The quality of the ground- and spacecraft-based measurements thereby influences the quality of the trajectory and the data products. Aspects of the measurements such as observation geometry, coverage in time, in space and on the surface, as well as accuracy and precision define the accuracy, the precision and the resolution of the data products. Improvement of the measurement quality allows for an improvement of the trajectory, the referencing of the measurements to their location on the surface and from that of the data products.

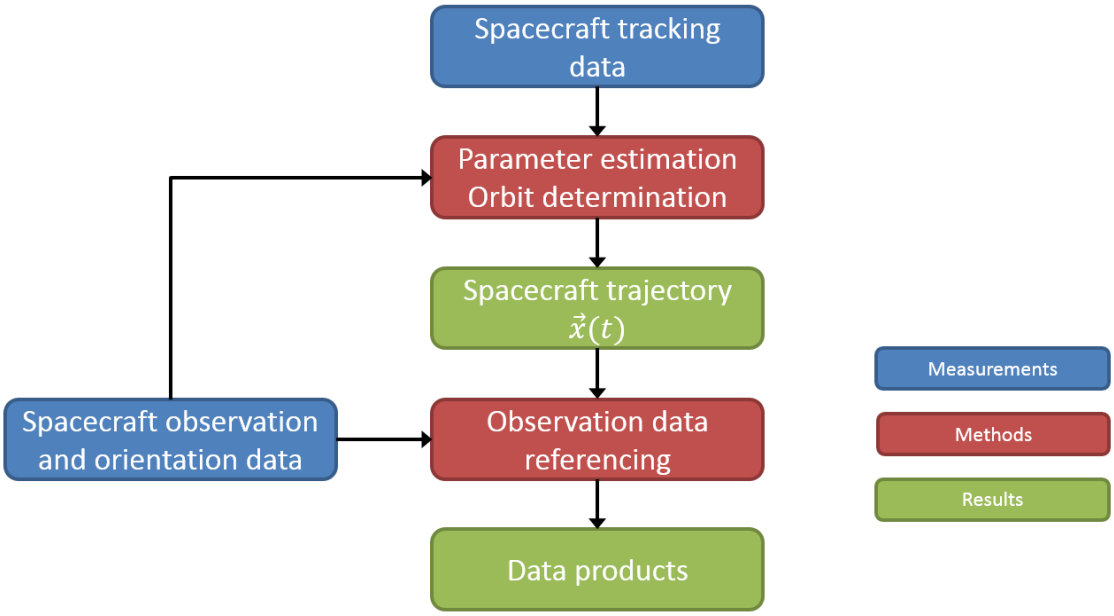

Figure 1: Utilization of measurements (blue boxes) within methods (red boxes) in order to derive results such as data products (green boxes).

Within the LRO mission three types of observations are available as illustrated in Figure 2. While the spacecraft is tracked from Earth ground stations via radio and laser, the crossover points of LOLA's altimetric profiles provide spacecraft-based observations.

The radio tracking of LRO provides ground-based observations consisting of range, range-rate often referred to as Doppler, and angular observations. The range observable is estimated from the round-trip time of the signal, which is measured from the phase shift between the outgoing and incoming signal. The range-rate/Doppler observable is derived from the shift in frequency of the radio signal due to the relative motion between the ground station and the spacecraft. The angular observations provide azimuth and elevation. Due to systematics their accuracy is limited and they are not commonly used for orbit determination. However, they allow for automatic tracking of the spacecraft by keeping the spacecraft in the center of the radio beam over time (Montenbruck and Gill, 2000). LRO is tracked by the ground stations in the S-Band (Mazarico et al., 2012) which is typically operated at frequencies of 2110 to 2120 MHz for the up- and 2290–2300 MHz for the downlink (Montenbruck and Gill, 2000). The radio data has an accuracy of 20–40 cm for the range and 0.3 mm/s to 0.8 mm/s for the Doppler observations (Mazarico et al., 2012). The extreme sensitivity of the Doppler measurements highlights their value for observables such as the orbit and the gravity field for example.

LOLA's main observables are spacecraft-based altimetric measurements between the spacecraft and the lunar surface. The time of flight is detected from the departure and the arrival of photons reflected back from the lunar surface. As the spacecraft moves along in its orbit it collects laser profiles that consist of consecutive altimetry measurements. Over time, these profiles intersect at crossover points (see Figure 3). Since the lunar surface does not change over time due to erosion, the measured height difference between consecutive orbits at those crossover points can be used as an observable in orbit determination. The crossover point measurement precision is limited by the onboard altimeter time-stamp precision, which is 15 cm. While Earth-based tracking techniques can only provide observations on the lunar nearside, crossovers from LOLA altimetry data are also available on the lunar farside.

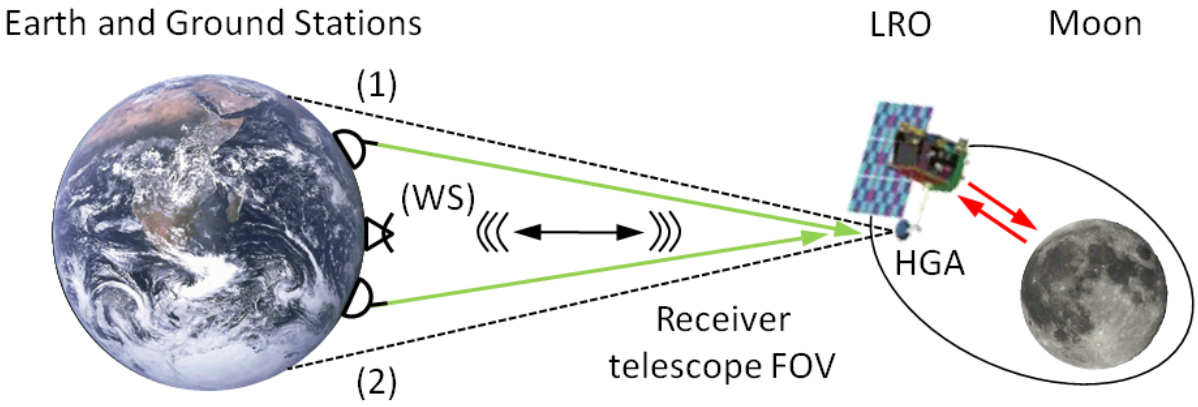

Figure 2: Illustration of the observations that are available within the LRO mission. While the spacecraft is regularly tracked via radio, for example by the White Sands (WS) ground station, laser stations are also ranging to LRO. Here station (1) is ranging during a single pass but station (2) may join for a simultaneous pass if it is in the Field Of View (FOV) of the receiver telescope, which is attached to the High Gain Antenna (HGA). Furthermore LOLA collects altimetric profiles of the lunar surface which provides the crossover points. While the Earth ground stations are ranging to LRO at 532 nm, LOLA is ranging to the lunar surface at 1064 nm.

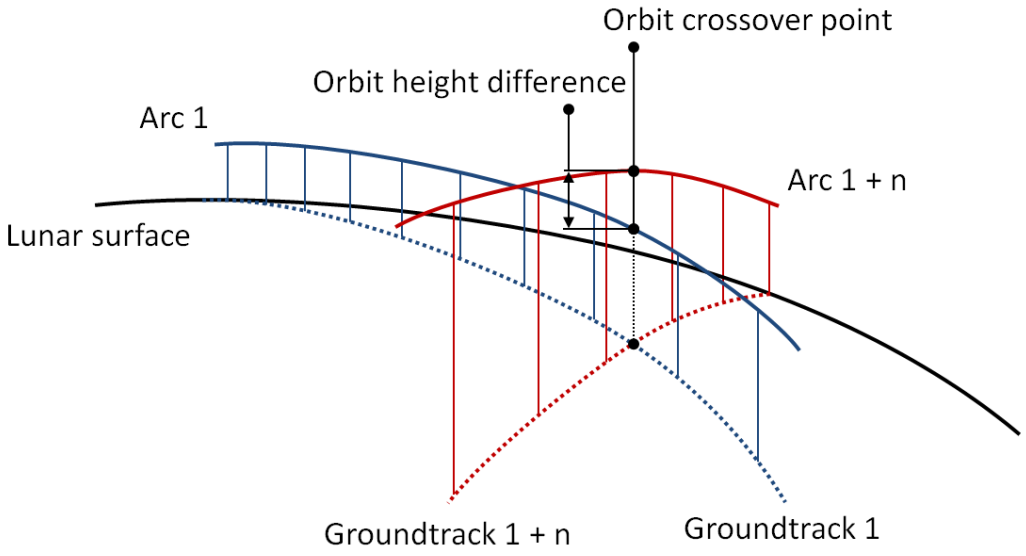

Figure 3: Illustration of the crossover point formation adapted from Smith et al. (2008). Over time LOLA's altimetric profiles of the lunar surface intersect at crossover points. Since the lunar surface does not change over time due to erosion, the height difference between orbits can be used as an observable within orbit determination.

Figure 4 shows the hardware extension that added the laser ranging capability to the LRO mission. The extension consists of a small receiver telescope attached to the High Gain Antenna and a fiber optics cable forwarding an incoming pulse into LOLA detector. The 532 nm pulses from the Earth-based ground stations can then be detected concurrently with 1064 nm pulses reflected from the Lunar surface. Satellite laser ranging is usually carried out in a two-way configuration to specially designed mirrors (retro-reflectors) onboard a spacecraft where a range is derived from the detection of the departure and arrival times of the photons (see section 2). With the laser ranging to the LRO, the range is derived in a 1–way configuration – from the departure time at the station and the arrival time at the LOLA detector. Due to the usage of ultrashort pulses laser ranges are generally very precise. While two-way satellite laser ranging typically achieves a precision of 1.2 cm (Exertier et al., 2006), the 1–way ranging to LRO has a precision of ≈12 cm for the Full Rate (FR) and 6 cm for the averaged Normal Point (NPT) data (see research paper 1). Further features of the experiment and setup are described in research paper 1 in more detail.

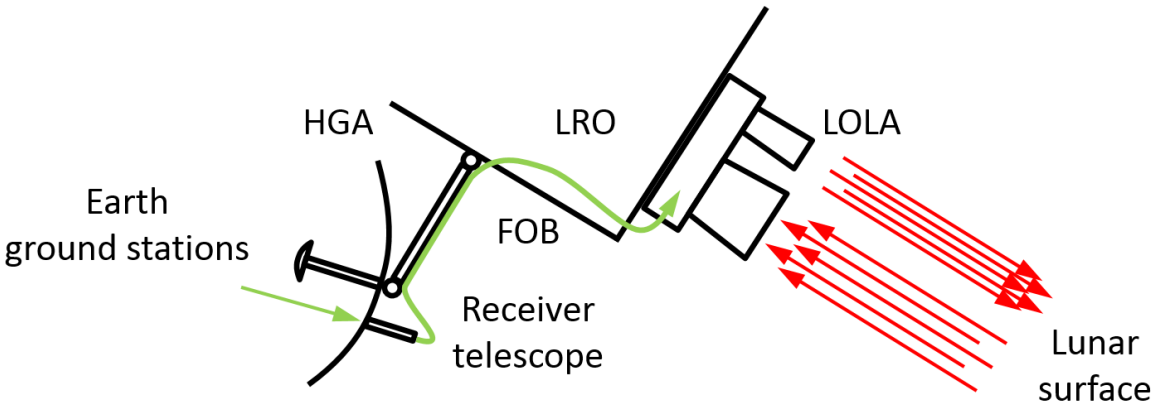

Figure 4: Illustration of the hardware extension that added a laser ranging capability to the LRO mission. Incoming pulses from Earth-based ground stations are received by a telescope which is attached to the High Gain Antenna (HGA) and forwarded into LOLA via a Fiber Optic Bundle (FOB). LOLA then detects the Earth-based signals at 532 nm and the Lunar returns at 1064 nm concurrently.

For comparison Table 1 lists the advantages, disadvantages and the precision of the LRO mission tracking data types which will be discussed subsequently. While the focus will be on the comparison of the ground-based radio and laser ranging observation, the features of the laser altimetry observations are provided for completeness.

Within the LRO mission both the ground-based radio and laser tracking are carried out by a well-developed global network of ground stations. Most of the radio tracking is done by NASA's Deep Space Network (DSN) which has been involved in the tracking of many interplanetary spacecraft such as Voyager, Pioneer and many more (Smith, 1985). Within the DSN the 34 m dishes in Goldstone California USA, Madrid Spain, Canberra Australia as well as the 18 m dishes in White Sands New Mexico USA have been used for the radio tracking of LRO (Mazarico et al., 2012).

The laser ranging stations that were tracking LRO are members of the International Laser Ranging Service (ILRS). While most of the ILRS stations are tracking Earth orbiting satellites, a few have been ranging to lunar and even interplanetary spacecraft. The 10 stations that were tracking LRO are distributed in the USA, the EU, Africa and Australia. Further details about them and their performance within the laser ranging to LRO experiment are provided in research paper 1.

Table 1: Features of the different types of observations which are available within the LRO mission.

	Advantages	**Disadvantages**	**LRO data type and precision**
Radio	+ well developed global network + less sensitive to clouds than laser ranging + automatic tracking of the spacecraft possible + very sensitive Doppler measurements	- more sensitive to troposphere, ionosphere and solar plasma than laser ranging - compared to laser ranging large stations, dishes and amounts of power required	- Range: 20 to 40 cm, - Range-Rate: LRO 0.03 mm/s (Mazarico et al., 2012)
Laser Ranging	+ well developed global network + less sensitive to troposphere, ionosphere and solar plasma than radio + compared to radio techniques small stations, telescopes and amounts of power required + more efficient due to more focused beam than radio + simple and passive hardware extension of LOLA for enabling tracking of LRO + more precise range measurements than radio	- more sensitive to clouds than radio - tracking of spacecraft requires position prediction - data analysis and application (e.g. in orbit determination) is subject to issues compared to two-way data	- Range: 12 cm for the full data and around 6 cm for the averaged NPT data (see LRO data paper)
Altimetric crossover points	+ local measurement + global coverage + effective regarding mass, size and energy consumption + sensitive to spacecraft positioning uncertainties	- specialized single onboard spacecraft unit	- Range: 10 cm (Mazarico et al., 2012)

While radio ranging is less sensitive to clouds, it is more affected by charged particles in the ionosphere, solar plasma and water vapour than laser ranging. The delay of S-Band signals due to the ionosphere can be 0.25–3.75 m in zenith and up to 37.5 m at low elevations. Because ionospheric influence is inversely proportional to the signal wavelength, laser signals (≈$5x10^{14}$ Hz) are much less affected than S-Band signals (≈$2x10^{9}$ Hz). While the tropospheric influence is almost the same for both wavelengths (≈2.5–25 m for S-Band and ≈2.5–29 m for laser ranging) the radio signals are more sensitive to water vapor (≈5–40 cm for S-Band and ≈0.1–0.6 cm for laser ranging). Thereby the ionosphere and the water vapor are parts of the atmosphere which are difficult to model (Rothacher et al., 2000).

The angular observations from the radio tracking allow for the automatic pointing during the tracking of a spacecraft. This is a system advantage over laser ranging, where pointing information need to be predicted from preliminary spacecraft position information. The loss of the contact over a pass due to loss of correct pointing can further reduce the amount of successfully collected tracking data (see research paper 1).

A major difference between ground-based radio and laser stations is the size, the power consumption and the beam width. Table 2 lists these parameters for a representative 34 m DSN radio and an ILRS laser station that were used for the tracking of LRO. The GO1L laser station telescope is 85 times smaller than the radio station dish and needs ≈17800 times less energy than the radio antenna during the tracking of LRO. Since the beam is also 2.87 times more focused, the laser ranging to LRO is more energy efficient than radio tracking of it. Thus laser ranging involves smaller, cheaper and less complicated ground equipment regarding construction and operation.

Compared to the radio and laser ground stations, LOLA is even smaller and requires less energy because it is a dedicated onboard instrument. Moreover its local observations are not affected by Earth's atmosphere. In contrast to radio and laser data, observations are also available on the lunar farside. However, due to a hardware anomaly of LOLA, the data rate is reduced when LRO is in the shadowed by the Moon (Smith et al., 2010b).

Radio Doppler data is very sensitive to small changes in the spacecraft velocity and has been the baseline in orbit determination of LRO (Mazarico et al., 2012). While the LRO radio range precision is at 20–40 cm, the laser data is still 2–3 times more precise after the statistical averaging to NPTs.

Following the approach shown in Figure 1, an improvement in the measurement precision enables an improvement of the spacecraft positioning derived from orbit determination. With that the localization of the measurements becomes more precise, which allows for the generation of more precise data products.

Table 2: Comparison of the performance parameters of a radio and a laser station which were tracking LRO.

	DSS-24	**NGSLR/GO1L**
Datatype	Radio range and Doppler	Laser range
Location	Goldstone Complex, Mohave Desert, California, USA	NASA Goddard Space Flight Center, Greenbelt, Maryland, USA
Size	Dish: 34 m (Layland et al, 1997)	Telescope: 0.4 m (ILRS website, 2016) *
Power	S-Band: 20 KW (Cornish et al, 2014)	1.12 W @ 532 nm (ILRS website, 2016)**
Beam width	S-Band: 0.263 ± 0.02 deg (Slobin et al., 2015)	< 1.6 mrad = 0.0917 deg (ILRS website, 2016)**

* The laser beam is inserted into the telescope for transmission.

** A special laser that was installed for the ranging campaign to LRO was used. The 40 mJ pulses were fired at a 28 Hz rate.

The incorporation of the one-way laser ranging data itself and in combination with other types of tracking data within the LRO orbit determination is a topic of ongoing research. So far Mao et al. (2014), Löcher et al. (2015) and Buccino et al. (2016) reported about the application of laser ranging data alone and in combination with radio data within orbit determination. While Löcher et al. (2015) and Buccino et al. (2016) could not achieve an improvement in positioning, Mao et al. (2014) reported an improvement of 3 m after adding laser to the radio data within orbit determination. Even though the authors reported about the application and the results, the background and the issues of the one-way compared to two-way data were not covered. The fact, that two of three authors could not derive improved positioning from the incorporation of one-way laser ranging to radio data within the LRO orbit determination, highlights the necessity of further research and documentation of the background and the issues.

Since the literature does not cover these aspects comprehensively yet, background about other spacecraft tracking techniques which also utilize one-way observations could be potentially useful. However as described in the following, they are different regarding their technique, their measurements and their observables which makes them not applicable to the LRO orbit determination from one-way laser ranging data.

The Global Positioning System (GPS) utilizes one-way radio ranges sent from Earth-orbiting spacecraft which can be received by any observer. As discussed above, the radio ranges are estimated from the measurement of a phase offset, while laser ranges are derived from pulse detection. Even though GPS features a downlink while the laser ranging to LRO utilizes an uplink, the principle is basically similar. From observations of a synchronized timing reference (either GPS satellites or ILRS ground stations), the position and the time of an observer (e.g. via GPS receiver or for LRO) is estimated. GPS utilizes multiple observations at a time (at least signals from four satellites) from which the observer can estimate his state (X, Y, Z) and time (his clock offset) concurrently. Within the laser ranging to LRO only one observable at a time is available with the regular observations. Even though simultaneous passes provide multiple observations at a time (see Figure 2), the timing of the additional ground station clocks that become involved must also be estimated, introducing further parameters. Within GPS, the spacecraft clocks are kept synchronized so that only the timing of the observer's clock has to be estimated (Easton, 1978). Since the number of simultaneous observations at a time does not cover the number of parameters that have to be estimated with the laser ranging to LRO, the background and the technique of estimating the position and the time via GPS cannot be applied.

The Delta Differential One-way Range (ΔDOR) system utilizes one-way radio ranges from a spacecraft to ground stations to estimate the angular position of a spacecraft in the sky. The radio signal of the spacecraft is received by two distinct ground stations simultaneously and the one-way ranges are inferred from the phase offset. The difference of the arrival times of the signals at the stations form the differential one-way range. This approach cancels errors such as the influence of the clock on the one-way range which improves the accuracy of the observable. With the orientation of the ground stations with respect to each other (baseline) the angular position of the spacecraft in the sky is estimated. From the observation of a close by quasar errors affecting the signals (e.g. atmosphere) are calibrated (Border et al., 1982; Border and Bedrossian, 2015). As within GPS the one-way ranges are measured from a phase offset while the pulse detection is used within the laser ranging to LRO. Furthermore the link is different since the signal from the spacecraft is downlinked and received by multiple ground stations, while LRO receives the signal from a single or multiple ground stations.

Moreover the observable (angular position in the sky) is different so that the background of ΔDOR cannot be applied to the laser ranging for LRO orbit determination.

Also radio range-rate (Doppler) measurements are derived from one-way observations. However, they are measured from a frequency offset and provide a different observable (velocity) compared to the laser ranges (pulse detection and range respectively). Due to the different nature of the observable, the background of the radio range-rate data cannot be used for the LRO laser ranging experiment.

Since no other tracking technique provides background that is applicable to the application of one-way laser ranging data for the LRO orbit determination, the research and the documentation of this topic carried out within this work is of high interest. Due to software limitations (see research paper 2), the work presented in this thesis focuses on the application of one-way laser ranging data within orbit determination only. Furthermore the detailed research on the one-way laser ranging data supports the overall mission goal of a joint orbit determination. Once the issues with the application of the individual datasets (radio, crossovers and laser) is fully understood, the joint application of the different types of the data can be analyzed in detail.

2 Introduction

This section introduces the following aspects: Satellite, Lunar and Interplanetary Laser Ranging – SLR, LLR and ILR respectively. This includes various aspects such as measurement principle, history, applications, setup, hardware, difference of one- and two-way observables, etc. Then the LRO mission with its suite of instruments, their science goals and the spacecraft orbit determination history are described. A basic concept of orbit determination is provided in support in addition to a description of how it is implemented within the estimation software. With these facts the reader will be able to understand the one-way laser ranging experiment to LRO regarding its relation to SLR in general, the implementation in the mission and the spacecraft as well as its application within orbit determination. The final section of the introduction will describe the content and the scope of the papers as well as how they address the overall research question.

2.1 Laser ranging

At first this section will introduce the background, history, setup and applications of Satellite, Lunar and Interplanetary Laser Ranging – SLR, LLR and ILR respectively. Following that, the one- and two-way setup in which the tracking can be carried out is discussed. This includes a discussion of the differences between one- and two-way observables and the effects on the application. Finally the section closes with a description of the general setup of laser ground stations.

Background, history, setup and applications

Mostly SLR is carried out from a ground station to a satellite that is equipped with a retro-reflector – a mirror of special design that reflects light back to its source with a minimum of scattering. The round trip light time is derived from the detection of the outgoing and incoming photons at a ground station. Ultra-short pulses (30–200 ps) allow for range measurements with a precision down to 3 mm (Montenbruck and Gill, 2000). The formation of statistically averaged NPTs allows for even better range measurements with a precision of 1 mm in case of geodetic Earth satellites (Husson et al., 1992). While this two-way setup involves a passive element onboard the spacecraft, both ends on ground and in space can also be active – each including a laser and a detector. If one of the ends only detects incoming

pulses the setup is one-way – as it is the case with the laser ranging to LRO. The detailed features of the different possible setups will be discussed later in this section.

Figure 5 shows the measurement principle of two-way SLR to retro-reflectors onboard a satellite. A laser creates a pulse that is transmitted towards the satellite. While with some setups the laser is attached to the telescope as shown in Figure 5, it can also be inserted to the telescope for the transmission. A part of the transmitted beam gets reflected back to the station and is received by the telescope. From the detected departure and arrival time, the time of flight and in case of retro-reflectors an unambiguous range measurement is derived.

In 1964 a team around Dr. Plotkin carried out the first Satellite Laser Ranging experiment to the Beacon B/Explorer 22 satellite at the Goddard Space Flight Center in the USA (Degnan, 1994). The measurement precision dropped from 2–3 m back then at one order of magnitude with every decade until the 1990's. Nowadays range measurements can be obtained at a few mm precision. Only the development of radio based techniques in the 1990 such as GPS, the Global Navigation Satellite System (GLONASS), the Doppler Orbitography and Radiopositioning Integrated by Satellite (DORIS) and the Precise Range and Range-Rate (PRARE) system allowed for geodetic measurements in a more cost effective manner while providing data products with accuracy comparable to SLR (Degnan, 1994).

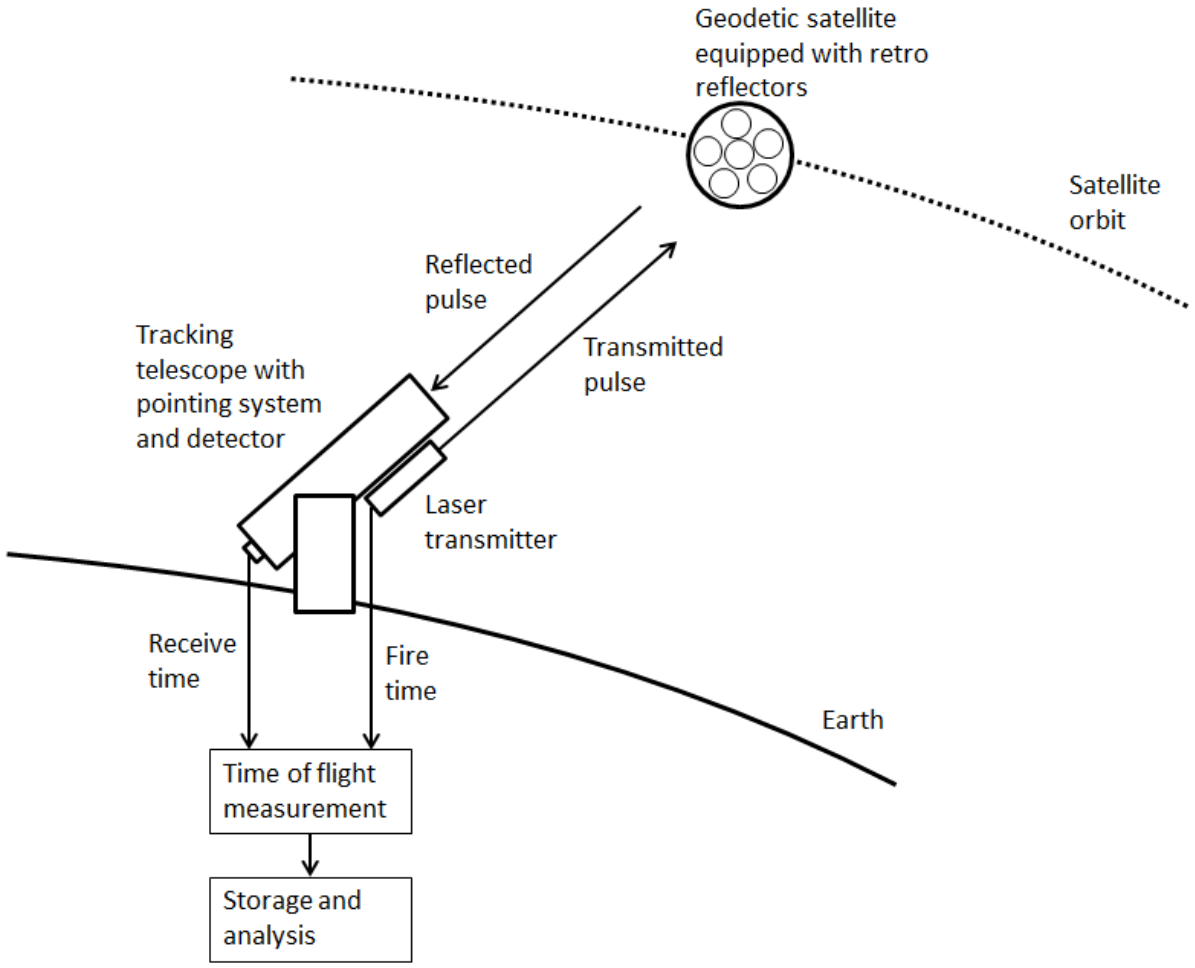

Figure 5: Illustration of the basic principle of two-way Laser Ranging to a Satellite equipped with retro-reflectors adapted from Pearlman et al. (2002). Here a laser pulse is transmitted towards a geodetic satellite which is a sphere with retro-reflectors attached. The reflected pulses are received by the telescope and the time of flight is derived from the detected fire and receive time.

Purely geodetic missions, however, used satellites that had only retro-reflectors attached to a sphere – as shown in Figure 5. These satellites, which were basically cannonballs, had a simple and passive setup and were thus fail safe as well as long lived. The design thereby allowed for a good separation of conservative from non-conservative forces and for cost effective missions (Degnan, 1994).

Stations have been created and operated by nations and organizations world-wide, though many of them are organized within the International Laser Ranging Service (ILRS) which was founded in 1998. Figure 6 shows the global network of stations that are organized within the ILRS. Following Pearlman et al. (2002) the applications and the data products of SLR within the ILRS are:

- Estimation of centimeter accurate satellite orbits,
- Estimation of the Earth orientation parameters, polar motion and length of the day,
- Estimation of the ILRS station coordinates from which tectonic motion can be analyzed for example,
- Estimation of the Earth center of mass and its variation over time,
- Estimation of the terrestrial gravity field – in particular its long wavelength coefficients – and its temporal change,
- Estimation of fundamental physics constants.

Further general applications of SLR are

- Synchronization of remote clocks via time transfer (Degnan, 2002),
- Inflight calibration of e.g. GPS radio tracking receivers (Degnan, 1994),
- Characterization of the atmosphere via two-color Satellite laser ranging (Zagwodzki et al., 1994).

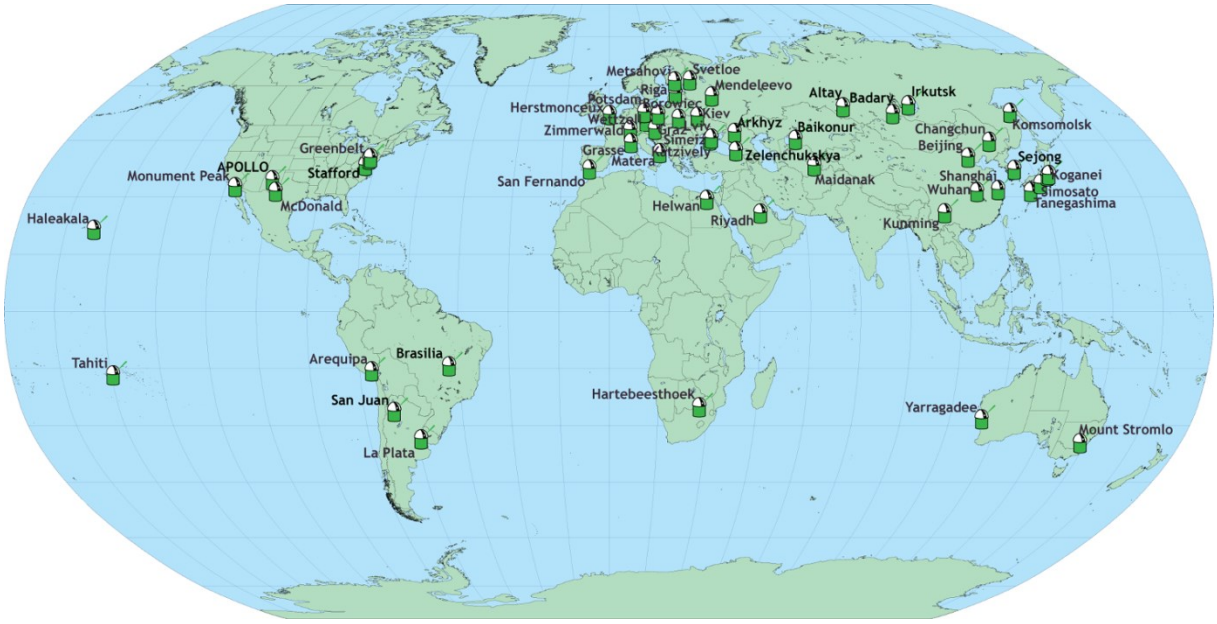

Figure 6: Map of the stations that are organized within the ILRS network (ILRS website, 2016).

Ranging beyond an Earth orbit was initialized with the Lunar Laser Ranging in 1969 when APOLLO 11 delivered the first retro-reflectors to the lunar surfaces. Further retro-reflectors were provided by the following APOLLO missions as well as the Soviet Lunakhod missions. These observations are used for (Gurtner et al., 2005):

- Estimation of the lunar ephemerides and rotation,
- Estimation of the dissipation-caused acceleration,
- Assessment of the lunar interior and the Love numbers,
- Tests of general relativity in particular
    - Of the equivalence principle,
    - If the gravity constant G is changing over time.
- Assessment of the geodetic precession.

Due to large signal loss over the two-way distance to the Moon and back (see equation 1), only a few stations worldwide are able to range to the lunar mirrors. The first and subsequent majority of the measurements came from McDonald station in Texas USA. Later Grasse (OCA) station in France, Haleakala station in Hawaii, Matera station in Italy and finally APOLLO station in New Mexico USA joined the ranging (Murphy, 2013). In the 1970's the creation of one NPT at McDonald station took tens of minutes and had a precision of 3 m. Nowadays APOLLO station generates them within a few minutes and at mm precision (Murphy et al., 2008; Murphy, 2013).

Even though the station performance has been dramatically improved over the past years, ranging towards retro-reflectors beyond a lunar orbit is basically impractical due to high signal loss. For ranging to even further targets such as interplanetary spacecraft, other setups are required which involve detectors and/or active transmitters onboard the spacecraft. Following Neumann et al. (2014) precise laser range measurement over interplanetary distance would provide applications such as:

- Accurate ephemerides of and time transfer to the spacecraft from ground,
- Faster and more efficient communication compared to radio due to higher wavelength and a narrower beam,
- Improved planetary ephemerides and mass distribution within the asteroid belt,
- Estimation of the Astronomical Unit (AU) and its change (AU dot),
- Solar gravitational oblateness from the tracking of asteroids,
- Mars solid tidal dissipation from Phobos tracking,
- Test of general relativity.

Furthermore laser ranging can be used for the inflight calibration of an onboard laser altimeter as it was demonstrated with MLA and LOLA (Sun et al., 2013a). Even though important properties, such as laser beam pointing, are calibrated on the ground before launch, they may change due to the various loads during lift off or the changing environmental conditions in flight.

Since laser altimeters usually have no active pointing mechanism, pointing of the whole spacecraft towards the Earth is required to establish a two-way link. Usually a raster scan on the Earth surface is carried out to account for uncertainties in the spacecraft pointing and laser beam alignment. From a successful two-way link the following properties can be calibrated (Sun et al., 2014; Dirkx, 2015a):

- General ranging and detection capability of the laser and the receiver,
- Laser performance from the measurement of the far field diffraction pattern,

- Laser beam pointing offsets with respect to a selected spacecraft orientation such as, for example, nadir-pointing,
- Receiver boresight and field of view,
- Onboard clock behavior via ground to space time transfer.

ILR was so far mostly carried out occasionally. Successful links have been established to Mars Global Surveyor (Neumann et al., 2006), to MESSENGER (Smith et al. 2006), the lunar orbiter LADEE (D'Ortenzio et al., 2015) and recently to Hayabusa-2 (JAXA website, 2015). Except for LADEE that had its own active laser terminal, all experiments were carried out with onboard laser altimeters and required spacecraft pointing towards the Earth. Besides LLR that started in 1969, only the one-way ranging to LRO has been carried out routinely between 2009 and 2014 beyond an Earth orbit (see LRO data paper). While the one-way laser uplink to LRO does not require active spacecraft pointing towards the Earth (see Figure 2), within the two-way experiment to LOLA, the whole spacecraft had to be turned (Sun et al., 2014).

One- and two-way laser ranging systems, setup, differences and effect on applications

To understand the features of the various possible laser ranging setups – one- and two-way – the link budget equation will be analyzed in the following. Following Degnan (1993) the number of photoelectrons n_p arriving at a detector can be calculated via

$$n_p = \eta_q \left(E_T \frac{\lambda}{hc} \right) \eta_t G_t(\theta) \sigma_{cs}^{m-1} \left(\frac{1}{4\pi R^2} \right)^m A_r \eta_r T_a^m \quad (1)$$

Where η_q is the detector quantum efficiency, E_T the energy of the transmitted laser pulse, λ the laser wavelength, h Planck's constant, c the speed of light, η_t the transmission optics efficiency, G_t the transmitter gain as a function of the off-axis pointing angle θ, σ_{cs}^{m-1} the satellite optical cross-section, R the range between observer and target, A_r the effective telescope receiver area, η_r the receiver optics efficiency and T_a^m the transmissivity of the atmospheric propagation path. Degnan (1993) assumes quasi-gaussian spatial and temporal profiles and provides the transmitter gain G_t for a Gaussian beam with

$$G_t(\theta) = \frac{8}{\theta_f^2} exp\left[-2 \left(\frac{\theta}{\theta_f} \right)^2 \right] \quad (2)$$

where θ_f is the far field divergence half-angle between the beam center and the $1/e^2$ intensity point and θ is the beam pointing error.

The type of the system setup defines m. In case of ranging to retro-reflectors m = 2, while it is m = 1 for all other setups. The increased signal loss – at the 4th power to the distance – highlights the difficulty when ranging to the retro-reflectors on the lunar surface and the necessity of active terminals both on ground and in space for interplanetary laser ranging. Various one- and two-way configurations in which laser ranging can be carried out, are illustrated in Figure 7.

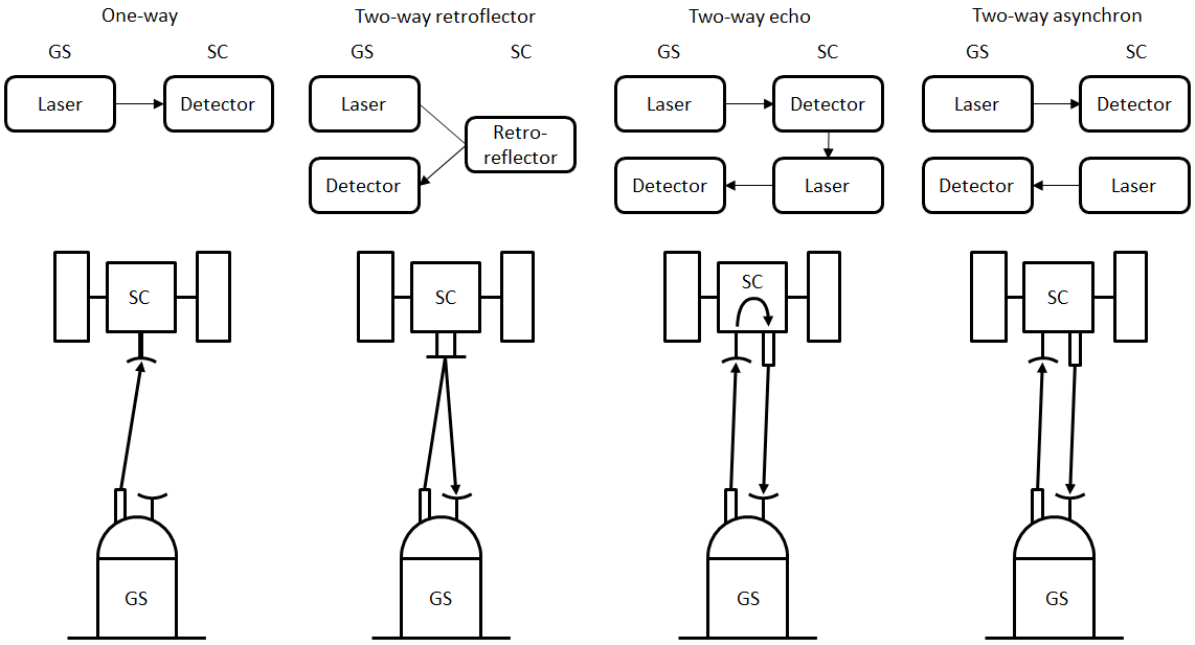

Figure 7: Illustration of various configurations in which laser ranging between a ground station (GS) and a spacecraft (SC) can be carried out.

A one-way link can be either an uplink or a downlink. However, here the discussion will focus on the case of an uplink due to the focus on the laser ranging to LRO experiment. The observable consists of the transmission time t_t of a pulse and its reception time t_r recorded by two separate clocks at different locations. The time tags are recorded separately and have to be paired with each other in a post processing (see research paper 1). Further, the data has to be exchanged via another link – e.g. via radio in case of the LRO mission. Since all clocks have limited stability and are sensitive to environmental influences, the involved clocks won't stay synchronized. This causes a timing error in the one-way range measurement that needs to be estimated concurrently with the state (Dirkx et al, 2015b; Moyer et al., 2000; Asmar et al., 2005). In case of an uplink, the spacecraft is the passive segment since it is only detecting incoming laser pulses. This can be of advantage regarding mass, hardware complexity and energy consumption of the onboard terminal.

Two-way laser ranging to a retro-reflector provides a direct and unambiguous observable since both, the transmission time t_t and the reception time t_r, are measured by one ground station clock at the same location. The setup of the space segment is passive, simple and active hardware is only needed at the ground. Since the requirements regarding mass, size and energy consumption are lower for the ground than for the space segment, this allows for simpler and cheaper hardware. A major drawback is the signal loss that is larger by a power of 2 with the distance compared to other setups (see equation 1).

A significant difference between one- and two-way systems is the effect of timing errors on the range observables. With a one-way system, any offsets in the total times of the involved clocks affect the derived range measurement directly at the speed of light c (see equation 34). Generally the ILRS recommends, that the stations keep their station clock offset to Coordinated Universal Time (UTC) smaller than 100 ns. With that the data products (see above) can be retrieved at millimeter accuracy from two-way ranging to retro-reflectors (Belli et al., 2015 and see the following disucssion). However, an error of 100 ns of the ground station clock with respect to UTC and with that of the fire time would cause an error ≈30 m on a one-way range.

With two-way laser ranging to retro-reflectors, the round trip time is measured by one clock at the same location. If the ground station fire time would have an offset, the satellite would be located at a different position, when the range is actually measured. At an offset of 100 ns, a satellite with a velocity of 7 km/s would be 0.7 mm away from his correct position in the along track direction of his orbit. Since an Earth satellite is typically not moving in the line of sight from the station when it's tracked, the actual error in the range measurement is even smaller. With that, two-way laser ranges to retro-reflectors are much less affected by station clock offsets than one-way ranges – at the satellite velocity and the speed of light c respectively. Consequently with one-way ranges the offsets have to be monitored and reported properly by the stations.

Moreover, two-way ranges to retro-reflectors are only affected by the stability of the involved clocks over their measurement roundtrip time (Dirkx et al., 2015b). A typical stability of $1x10^{-14}$ of a caesium clock causes an offset of only 1.2 fs over a round trip time of 120 ms (≈40000 km) which is neglible. Thereby a round trip time of 120 ms is equivalent to the orbit of a GNSS satellite, which is a distant target for a laser station ranging to a satellite with retro-reflectors. With a one-way system, the clock stability affects the measurements continuously. The offset accumulates over time, depending on the stability of the clock, which affects the total time measurement and with that the one-way range measurement directly at the speed of light c. Over the light trip time from a ground station to LRO in orbit around the Moon (≈1.3 s which is ≈390000 km), this is not relevant. With the LRO onboard clock stability of $1x10^{-13}$ up to 100 s (Cash et al., 2008), this an offset of only 0.13 ps which introduces an error on the range of only 40 µm. However, between 100 and 10000 s the onboard clock stability is at $2x10^{-13}$ (Cash et al., 2008) and so the error becomes larger than 0.5 ns (≈15 cm) and thus detectable by LOLA after ≈42 min. After one LRO orbit with a period of ≈120 min, an offset of 1.4 ns (≈0.4 m) has accumulated which already affects passes from consecutive LRO orbits. Furthermore the LRO onboard clock was sensitive to external influences such as temperature change, which further altered its rate and with that the accumulating offset. This caused a linear trend in the rate accumulating to an offset of 13–39 ns (≈4–12 m) that had sinusoidal variations with amplitudes of 2–6 ns (≈0.6–1.8 m) around it over one day (see section 3.3). The random walk of the LRO clock adds an offset of more than ≈17 ns (≈5 m) over one day with its given stability of $2x10^{-13}$ up to 10000 s. Since these variations affect the one-way observable directly at the speed of light c, such systems are more sensitive to the stability and sensitivity of the involved clocks than two-way systems. However, ground station clocks typically provide better stabilities than onboard clocks and are shielded against external influences properly (see section 3.2).

Over long distances, such as to the Moon, two-way ranging to retro-reflectors is not feasible due to the large signal loss. To overcome this, ranging could be carried out with two active segments on ground and in space either in echo or in asynchronous mode. In echo mode the space segment waits for a received pulse upon which it fires a pulse back to the ground. With long round-trip times (e.g. > 10 minutes) this mode becomes unpractical since pulses are only sent back from the space terminal upon successfully received pulses. However, multiple pulses are required to establish and maintain the correct orientation at both terminals. With breaks between them, it becomes even more difficult to maintain the correct pointing which reduces the number of received pulses even further.

To overcome the difficulties of the echo mode, two-way laser ranging is best carried out in asynchronous mode where both terminals fire independently from each other. From the pairing of transmit and receive times in post processing, one can derive both, the range and clock characterization simultaneously (Degnan, 2002). Even though seperate clocks on ground and in space

are involved as within one-way laser ranging, their offsets can be characterized from the data itself. Furthermore, the stability of the involved clocks affects the measurements only over the light trip time, as it is the case with ranging to retro-reflectors (Dirkx et al., 2015b). However in both, the echo and the asynchronous mode, active onboard terminals with accurate pointing mechanisms are required.

General hardware setup on ground

Figure 8 shows the typical components that are employed within a SLR ground station. The shown setup is valid for two-way retro-reflector and asynchronous ranging. In the case of one-way ranging from the station to a target the downlink is missing. Since the individual setups at the stations can vary heavily, only general components of the ground systems following Dirkx (2015a) are covered.

The Lasers within the transmission assembly (see Figure 8) typically generate a laser pulse at a wavelength of 1064 nm which is often frequency doubled to 532 nm. Short pulse lengths (typically between 30–200 ps) thereby enable range measurements at mm precision (Montenbruck and Gill, 2000). While most of the ILRS stations produce these pulses at frequencies around 10–20 Hz, modern SLR systems achieve firing rates of 1–2 kHz. The energy of the transmitted pulses is typically between 1–100 mJ for the systems ranging at lower frequencies (10–20 Hz) and between 0.1–1 mJ for the kHz systems (see research paper 1; Kirchner and Koidl, 2015).

The generated pulses are forwarded to the transmitter telescope which controls the direction of the laser beam as well as the beam width. Typical values for the beam width are 100 µrad for the full angle (Dirkx, 2015a). While some systems have a separated transmitter and receiver telescope as shown in Figure 8 (e.g. Potsdam station – POT3), other systems use one telescope for both transmission and reception of the pulses (e.g. APOLLO station – APOL). Larger receiver telescope apertures thereby enable the detection of a higher number of photons (see equation 1). The receiver telescope aperture can vary heavily between the stations – while POT3 has an aperture of 0.4 m, APOL has an aperture of 3.5 m and is thus very suitable for LLR (Grunwaldt et al. 2013; Murphy et al., 2007).

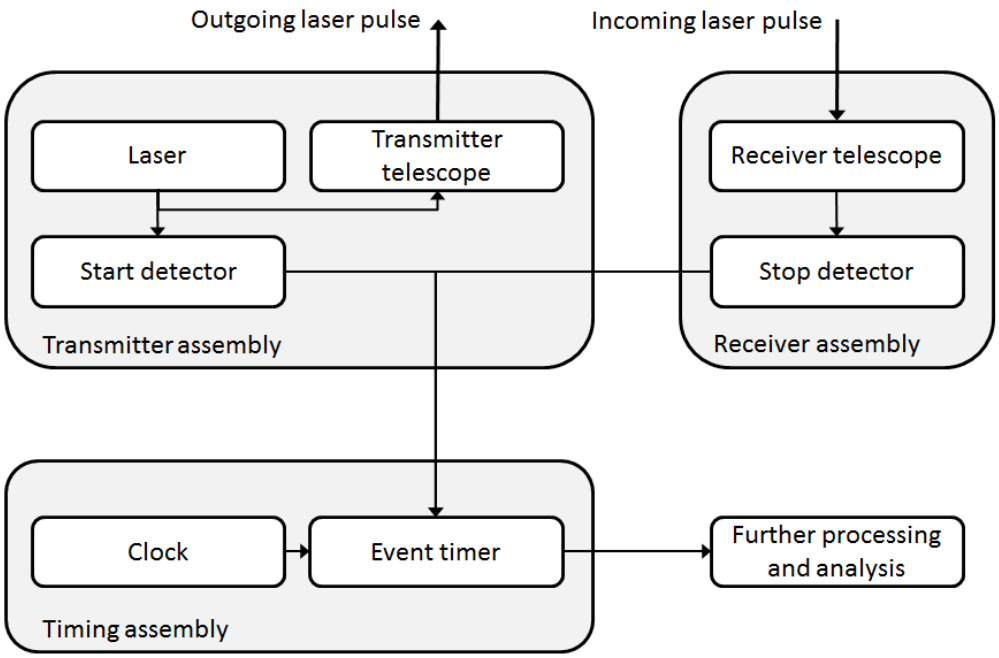

Figure 8: Illustration of the general setup of a transmission and detection system at a laser ranging ground station, adapted from Dirkx (2015a).

On both the transmission and the receiving paths the photons are registered by a detector that records their departure and the arrival. Typically either a Single Photon Avalanche Diodes (SPAD) or a Photon-Multiplier Tube (PMT) is employed (Wood and Appleby, 2004).

The ground station clock needs to be a stable reference. In order to provide accurate timing over longer timeframes, the total referencing in time needs to be maintained accurately or range biases are introduced in the measurements. The types of clocks employed at ground stations that were participating in the ranging to LRO were oscillators, rubidium, cesium and masers (see research paper 1).

The event timer references the departure or the arrival of a photon to the corresponding time provided by the clock. For accurate measurements a resolution below the laser pulse length is required.

The laser creates a pulse that is registered by the start detector. The event timer derives the pulse departure time from the clock. The outgoing pulse is directed and focused by the transmitter telescope based on predicted positioning information of a target. Uncertainties in the predicted positioning can be compensated by an increased beam width. In order to hit the satellite ahead pointing of the telescope needs to be included. In case of a two-way link (either retro-reflector or asynchronous) the receiver telescope collects the photons and forwards them to the stop detector. The event timer reads the pulse arrival time from the stop detector.

Depending on the setup, the fire and receive times have to be further processed. With one-way data the separately recorded fire and receive times have to be paired during post processing (see research paper 1). Two-way ranging to a retro-reflector provides an instantaneous observable if a return pulse was received. Two-way asynchronous laser ranging data also requires a post processing in form of pairing, since the two terminals fire, receive and record the pulses independently from each other.

2.2 LRO mission

In 2004 President Bush formulated the vision for the US space exploration, where one of the goals was the robotic exploration of the lunar surface for research and preparation for future human exploration (Bush, 2004). The LRO mission was the first of the Lunar Precursor Robotic Program (LPRP) which was established in order to fulfill these goals. The comprehensive geodetic, geophysical, geological and geochemical mapping campaign of the mission established an observational framework that supports future lunar exploration (Zuber et al., 2010). As demonstrated by Gläser (2015) for example, future lunar missions can select landing sites on the basis of the LRO mission data products while considering various aspects such as:

- Analyzing the safety of a landing site from the topography, surface slopes and roughness,
- Simulating illumination conditions at a landing site for energy supply considerations and exploration activities by using the Digital Terrain Models and interplanetary ephemerides,
- Selecting places of scientific interest and analyzing surface mobility from the Digital Terrain Models and the images.

For the LRO mission a suite of seven instruments was selected. The instruments addressed the following scientific goals with their measurements (Chin et al., 2007):

- Lunar Orbiter Laser Altimeter (LOLA)

    - From the round trip time of laser pulses directed to and reflected by the lunar surface, altimetric measurements were collected. The instrument featured a five spot laser pattern which provided five atlimetric profiles simultaneously. From that global topography, slopes, surface roughness was derived which enabled a geodetic mapping. Furthermore the data was used for the search for polar water ice in the permanently shadowed regions.
- Lunar Reconnaissance Orbiter Camera (LROC)
    - From the mapping of the lunar surface via wide and narrow angle images, landing site selection was supported, polar illumination conditions were characterized and potential resources identified.
- Lunar Exploration Neutron Detector (LEND)
    - From the mapping of the neutron flux water ice was searched for and the space radiation environment was mapped.
- Diviner Lunar Radiometer Experiment (DLRE)
    - From the measurement of the surface temperature, cold-traps and potential water ice were detected.
- Lyman-Alpha Mapping Project (LAMP)
    - From a global mapping of the surface in the far ultra violet, potential water ice and frost was identified within the polar and permanently shadowed regions only illuminated by star light.
- Cosmic Ray Telescope for the Effects of Radiation (CRaTER)
    - From the investigation of the influence of galactic cosmic rays on a tissue like material, the biological response on background radiation was analyzed.
- Mini Radio-Frequency Technology Demonstrations (Mini-RF)
    - Synthetic Aperture Radar (SAR) imaging supported the search for deposits of water ice on the surface and even below a layer of regolith.

The LOLA data products global topography and a geodetic reference frame are affected by the uncertainty in the radial positioning of the spacecraft. To provide the data products at the defined accuracy, the radial position was required to be known with an accuracy of better than $1\ \mathrm{m}$. Originally the LRO position was expected to be known at 300 m in along- and cross-track and at 10 m in radial direction from S-band radio observations only. Because of this the laser ranging capability was added to the LOLA instrument. So altogether radio, altimetric crossover and laser ranging observations were available for use within the orbit determination process. Their joint application within orbit determination was supposed to provide the positioning of the spacecraft and with that, the data products at the required accuracies as shown in Table 3 (Smith et al., 2010a; Zuber et al., 2010).

The LRO spacecraft itself was regularly tracked by NASA's radio station White Sands in New Mexico as well as by the commercial Universal Space Network (USN). Since the accuracy of this radio tracking data was much better than anticipated, already the radio only solutions from the LOLA team almost achieved the 1 m radial uncertainty requirement. The continuously updated orbit solutions from the LOLA team was used as the nominal trajectory of LRO within this work (see research paper 1 and 2). In their first solution Mazarico et al. (2012) used radio and LOLA's altimetric crossover data along with historical tracking data from the Lunar Orbiters, the APOLLO sub-orbiters, the Lunar Prospector as well as the Clementine mission. With this tracking data they determined LRO's orbit and the gravity field LLGM-1 up to degree and order 150. The radio only orbits estimated with the gravity field had an

uncertainty of 1.6 m in radial and 23.4 m in total direction at the arc overlaps. When adding the crossovers to the solution the uncertainty at the arc overlaps changed to 1.8 m in radial direction and 13.6 m in total (Mazarico et al. 2012). Thereby the individual arcs had a length of 2.5 d on average, with overlaps between 8 and 12 hours between consecutive arcs. This allowed to start and end the individual arcs with observations passes from White Sands station and to monitor the orbit reconstruction quality (Mazarico et al., 2010, 2012 and 2013).

The GRAIL mission was launched in September 2011 and lasted until December 2013. It consisted of two identical co-orbiting spacecraft around the Moon. From the precise measurement of the change of the inter-spacecraft distance, the lunar gravity field could be estimated to unprecedented accuracy on both the near and the far side. During the mission the inter-spacecraft distance and the height above the lunar surface were changed to map the gravity field at different wavelengths (Zuber et al., 2013). While the latest fields have a resolution of up to degree and order 900 (Konopliv et al., 2013; Lemoine et al., 2014), Mazarico et al. (2013) used earlier fields up to degree and order 270 within LRO orbit determination.

The GRAIL gravity field enabled LRO orbit radio only solutions at uncertainties of ≈0.4 m in radial and ≈8.7 m in total direction over all mission phases at the arc overlaps. Due to the significant orbit improvement, all further updates of the LRO orbits were done with radio data only (Mazarico et al., 2013). The most recent solutions of the nominal LRO trajectory incorporated the GRAIL gravity field GRGM900C (Lemoine et al., 2014) up to degree and order 600 (NAIF LRO SPICE archive, 2016). However improving the spacecraft positioning via a joint orbit determination with radio, laser and crossover data still remains an important research topic (see section 1).

Table 3: Accuracy of the LRO positioning and mission data products depending on the types of tracking data used within orbit determination in radial and horizontal direction from Zuber et al. (2010). R stands for radial and H for horizontal.

LOLA data products	S-band tracking	S-band tracking + altimetric crossovers	S-band tracking + altimetric crossovers + laser ranging
Global topography Accuracy/ Resolution	R: 10 m; H: ≈300 m	R: 10 m; H: ≈200 m	R: 1 m; H: 50 m
Polar topography Accuracy/ Resolution	R: 10 m; H: ≈300 m	R: 5 m; H: 200 m	R: 0.1 m; H: 25 m
Surface slopes Accuracy Resolution	2° 300 m	1.5° 200 m	0.3° 25 m
Surface roughness Accuracy Resolution	35 cm ≈5 m	35 cm ≈5 m	35 cm ≈5 m

2.3 Orbit determination and utilized timescales

Orbit determination comprises various methods that are used to estimate the position and the velocity of an orbiting object from given observations. The object can be a satellite in orbit around Earth or a spaceraft orbiting another planet, for example. The estimation of an initial state in the form of coordinates or orbital elements allows one to derive the spacecraft trajectory over time from the integration of the equations of motion (Vetter, 2007; Montenbruck and Gill, 2000).

Within preliminary orbit determination the Keplerian elements are calculated without any a priori knowledge from at least six observations. However, due to the limited accuracy of this method, it is more relevant for the orbit determination of solar system bodies than for orbiting spacecraft. Orbit determination by differential correction improves parameters of interest from their a priori knowledge within an iterative process while using a large set of observations.

Figure 9 illustrates the basic principle of orbit determination by differential correction. From an a priori initial state $\vec{r}_{i=1}$ the trajectory is numerically integrated via the equations of motion within the first iteration ($i = 1$). The features that are incorporated within the equations of motion represent the dynamical model. The accuracy to which they approximate actual physical effects influences the accuracy of the derived trajectory. From this trajectory, artificial observations are computed at the points in time, where actual observations were taken from a ground station to the spacecraft. Since the actual observations were taken by systems with limited accuracy, they scatter around the true orbit at their precision. By saying that the differences between the computed and the actual observations – the residuals – become minimal, a differential improvement of the parameters of interest $\delta\vec{x}$ can be derived via (Vallado, 2001)

$$\delta\vec{x} = (A^T A)^{-1} A^T \vec{b}. \quad (3)$$

The parameters of interest $\delta\vec{x}$ thereby typically consist of the initial state $\vec{r}$ and other spacecraft related parameters. A is the partial derivative matrix and $\vec{b}$ the residual vector containing the differences between the computed observations y_{co} and the actual observations y_{ao} from 1 to n

$$\vec{b} = (y_{ao_1} - y_{co_1}, y_{ao_2} - y_{co_2}, \cdots, y_{ao_n} - y_{co_n})^T. \quad (4)$$

Since $\delta\vec{x}$ is a function of the computed observations which depend on the trajectory integrated from the state, the non-linear least squares problem needs to be solved iteratievely ($i = 1 \ldots m$). The parameters of interest are improved step-wise from their a priori values until their change is smaller than a defined criterion and thus convergence is achieved (Vallado, 2001). From the final iteration $i = m$, the optimized parameters of interest (e.g. nominal initial state $\vec{r}_{i=m}$) are derived from the nominal orbit. This trajectory fits best to the observations that were collected while the spacecraft was flying along the true orbit.

The differential correction is either done with a sequential or a batch estimator. While sequential estimators such as the Kalman filter update the parameters of interest upon new observations, batch estimators utilize all observations at a time within the estimation process. Sequential estimators are typically employed within routine spacecraft operation and batch estimators within scientific applications (Montenbruck and Gill, 2000).

Within this work the LRO orbit determination is done within an estimation software package (Dirkx et al., 2015b) that is based upon the Tudat toolbox (Kumar et al., 2012). More details on the representation of the timescales within the software, the clock error modeling and the observation model for the one-way measurements can be found in section 4.4.1. Section 4.4.2 describes the features of the batch estimation software and the dynamical modeling with details about the gravity field and solar radiation pressure representation for example.

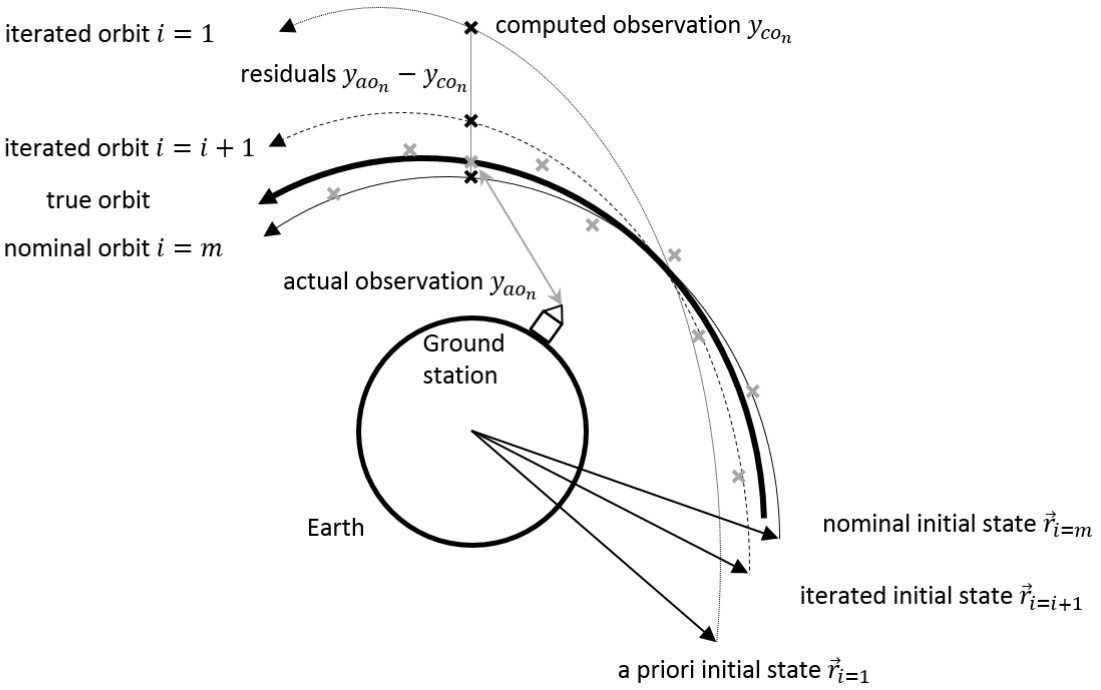

Figure 9: Basic principle of orbit determination from observations via the integration of the equations of motion. The basic concept of the figure was adapted from Vallado (2001).

With the one-way setup, separated clocks record the fire and the receive times at different locations in the solar system. While Earth ground stations record their fire times in Coordinated Universal Time (UTC), the LRO spacecraft in orbit around the Moon records times in Mission Elapsed Time (MET). However, since the Barycentric Dynamical Time (TDB) timescale is commonly used for ephemerides and interplanetary orbit determination, it was selected as the timescale within the orbit determination. The relationship, the differences and conversions between the UTC and the MET timescales and TDB due to relativistic effects are provided in research paper 1. At first Figure 10 in section 3.3 shows the relationship and the conversion accuracies of these timescales. The conversion of the station fire times from UTC to TDB is provided in section 3.5.4 and was taken from the literature. MET is not a common timescale and consequently the formulae required for its conversion to TDB had to be developed. Section 3.5.3 provides this conversion and discusses the differences between MET and TDB. The described differences due to relativistic effects were observed in the results accordingly and are described in section 3.7.2. The SI definition of the second was used within all timescales.

2.4 Time transfer

Time transfer is the transportation of temporal information through space for the comparison and the synchronization of remote clocks (Dirkx 2015a; Vrancken, 2008). An example for time transfer via laser ranging is the T2L2 experiment, which will be described later in this section with more detail. A ground station fires laser pulse towards the JASON-2 spacecraft, which carries the T2L2 experiment. While some part of the laser pulse is reflected back to the station by the retro-reflector, T2L2 also features a detector which measures the arrival of the pulse at the spacecraft in onboard time. From the two-way measurement via the retro-reflector (see section 2.1), the exact light travel time is known after calibration of all delays and error sources. From the comparison of the receive time, derived from the ground station fire and the light time, to the receive time measured by the onboard clock, the offset of the clock to a selected time scale, such as for example UTC, can be measured. This measured offset can also be used for the synchronization of the clock (Exertier et al., 2013).

Comparing the timing of remote clocks at high accuracy is required within Global Navigation Satellite Systems (GNSS), space geodesy, deep space navigation, relativistic physics and astronomy, among others. While radio based time transfer techniques achieve nano and sub-nano second accuracies, optical time transfer provides accuracies at the pico-second level (Vrancken, 2008; Kunimori, 1993).

With GNSS the positioning of an observer is retrieved from the analysis of the timing signal of multiple satellite signals. With signals from at least four satellites, the position and the observer clock offset can be estimated – of which the latter represents time transfer. The GPS timing system and thus the satellite clocks are kept synchronized so that only the observer's clock offset has to be estimated. The time transfer via GPS can be done in multiple configurations. If the offset of the observer's clock is estimated as described earlier, the configuration is one-way. If two observers see the same GPS satellite, they may perform ground to ground time transfer in common-view configuration. In this configuration the spacecraft clock error, as well as errors from the orbit, the atmosphere and the ionosphere cancel, if the distance between the observers is small (small baseline). The time transfer can also be performed via the measurement of the carrier phases of the GPS signal. However, this technique requires significant effort and is subject to ambiguity in the measurement (Lombardi et al., 2001). Another radio-based system is the Two-way system for frequency and time transfer (TWSTFT). With this system two stations are ranging to the same geostationary satellite at the same time – ground to ground time transfer in common-view. The satellite forwards the respective signals to the other station for comparison of the timing difference between the stations (Kirchner et al., 1991).

After a time of 1000 s the stability of the time transfer with the one-way GPS configuration is 5–10 ns, 5 ns with the common-view time transfer between two observers, 20 ps with the carrier phase measurement and < 100 ps with the TWSTFT experiment (Parker and Matsakis, 2004).

The Atomic Clock Ensemble in Space (ACES) experiment is supposed to be installed onboard the International Space Station (ISS) and features a cesium fountain clock and a hydrogen maser. Time transfer can be done via the radio based Microwave Link (MWL) experiment and the European Laser Timing (ELT) experiment, which are both connected to ACES. The MWL experiment is specified to achieve an accuracy of 230 fs after 300 s (Vrancken, 2008). The features and the performance of the ELT experiment will be discussed later with more detail.

Compared to radio techniques, time transfer via laser ranging promises improved accuracy due to the higher wavelength of the optical signals (Leschiutta, 1991). The first ground based laser time transfer experiment was carried out between a laser station located at NASA Goddard Space Flight Center and the 26 km distant U.S. Naval Observatory (USNO), whereby an accuracy of 20–40 ps was achieved. Similar experiments were carried out over a 25 km distance in China at the same time (Leschiutta, 1991).

The first space-borne laser time transfer experiment was the Laser Synchronization from Stationary Orbit (LASSO) experiment. In 1992 the first time transfer link was established between the French Observatoire de la Côte d'Azur (OCA) in Grasse and the US McDonald Observatory in Texas (Lewandowski et al., 1993). The Time Transfer by Laser Link (T2L2) experiment was the follow-on for the LASSO experiment and launched on-board Jason-2 in 2008. As the LASSO experiment T2L2 featured a retro-reflector and a detector and provided time-transfer via a two-way link. This setup allows to measure the unambiguous range to the spacecraft – after applying corrections – and furthermore the offset between the onboard and the ground station clock directly. By comparing the offsets between

different ground stations with respect to the onboard clock, the ground to space time transfer from multiple stations can also be used for the ground to ground time transfer between them (Exertier et al., 2013). The time transfer can be done in common-view (multiple stations are ranging simultaneously) and in non-common view (multiple stations are ranging consecutively). In non-common view the stability of the onboard clock defines the accuracy that can be achieved with the time transfer over a certain time. The onboard clock of the Jason-2 spacecraft was an Ultra Stable Oscillator which had a stability of $\approx 1 \times 10^{-12}$ over up to 100 s (see research paper 1). While the ground to space and the ground to ground time transfer in common view achieved accuracies of up to 10 ps, the ground to ground time transfer in non-common view had an accuracy of 150 ps due to the limited stability of the onboard USO (Exertier et al., 2006).

Besides the MWL experiment, ELT is also connected to ACES for optical time transfer. The principle is equivalent to the two-way link of T2L2. The improved stability of the ACES clocks enables improved ground to space and ground to ground time transfer both in common and non-common view. While the ground to space time transfer achieves an accuracy of 4 ps, the ground to ground time transfer in common-view has an accuracy of 6 ps. Due to the stability of the cesium fountain clock and the H-Maser (1×10^{-14} over up to 10^7 s and 1×10^{-15} over up to 10^5 s respectively; see research paper 1) non-common view time transfer can be carried out globally at an accuracy of 7 ps between all stations that can range to ELT (Schreiber et al., 2009; Schlicht, 2012).

Even though the laser ranging to LRO experiment only features a one-way uplink, ground to space and ground to ground time transfer has been demonstrated (Sun et al., 2013b and research paper 1). Unlike with T2L2 or ELT, the offset between a ground station and the onboard clock cannot be estimated directly (see research paper 1). However, onboard time was referenced to ground time via polynomial fits, at an accuracy of 256 ns over all mission phases representing ground to space time transfer (see research paper 1). Furthermore common view observations from simultaneous passes (see Figure 2) allow for the estimation of the relative ground station clock differences at an accuracy of 500 ps (Sun et al., 2013b). The common-view time transfer can be carried out between all stations that are in the field of view of the receiver telescope. With a field of view of 30 mrad all US stations can range to LRO simultaneously. However, due to required pointing of the HGA, to which the receiver telescope is attached, simultaneous ranging between US and European stations is not possible on a regular basis. As with the T2L2 experiment non-common view time transfer is not feasible due to the limited stability of the LRO USO.

With the one-way data, both the state vector and the timing of the clocks have to be estimated within the orbit determination of LRO. This includes the errors of the LRO and all ground station clocks (see research paper 2). Since the station clocks are not synchronized perfectly, their observations have offsets and trends with respect to each other. These differences can be measured between the clocks of the stations that can range to LRO simultaneously with other stations. The measured differences can be used both for a priori constraints on the ground station clock parameters and as references for comparison of the values estimated within the orbit determination (see research paper 2).

2.5 Content, scope and research questions of the papers

The topic of this thesis and the research papers is the processing, analysis and application of one-way laser ranging data to LRO for

- deriving the Experiment and ground station performance from a statistical dataset analysis,
- characterizing the LRO clock via ground to space and the ground station clock differences via common-view ground to ground time transfer and
- the orbit determination of the spacecraft.

Compared to two-way experiments, the one-way laser ranging experiment to LRO is subject to the following issues which were analyzed within this work in particular:

- The fire and the receive times are recorded separately at the ground station and the spacecraft and have to be paired first. Predictions from the nominal LRO trajectory were used to reference onboard to ground time within research paper 1. Corrections for environmental and hardware influences were applied on the measured and the predicted receive times.
- In contrast to two-way, the one-way observables are affected by timing errors of the involved clocks at the speed of light c. The errors of all clocks on ground and in space have to be modeled and estimated concurrently with the spacecraft state within the orbit determination (see section 2.1). Since one-way observables were not common practice for the involved ILRS stations, the one-way transmit (Tx) delay and the ground station clock offset to UTC were not reported. Therefore a fixed orbit was used to charcterize the involved clocks in research paper 1. While the LRO clock was characterized directly, only the differences between the ground station clocks could be analyzed with the one-way data. These results were used to estimate all involved clocks concurrently with spacecraft state in research paper 2.
- Since the timing parameters were highly correlated, a priori constraints (initial and covariance values) were used to separate them within the estimation. The results of the LRO and ground station clock characterization from research paper 1 were used as the basis for these a priori constraints.
- The ground to ground time transfer can only be done from common-view observations. The limited stability of the LRO clock prevents non-common view time transfer. Furthermore only the differences between the stations and not the total offsets with respect to the spacecraft clock can be estimated from the one-way observables.
- These common-view observations were only made between US stations due to the limited Field of View of the receiver telescope and the required pointing of the HGA towards White Sands (New Mexico, USA). Thus the coverage of the common-view observations in time as well as for certain station combinations is limited and with that the information available for the a priori constraints.
- Due to the limited accuracy of the dynamical, the clock modeling and the corrections of this work, errors were accumulating with increasing state and clock arc length. Those errors were caused by the approximation of the actual dynamical environment as well as the LRO and the ground station clocks (including random walk and the influence of external effects) with this modeling. Consequently those errors affect the accuracy of the results from the orbit determination (trajectories, LRO and ground station clock parameters, post-fit measurement residuals) in combination the observation data coverage.

- While polynomial fits of short length provided a better approximation of clock behavior, more correlated parameter had to be estimated. With polynomial fits of longer length, the approximation of the clocks and with that the accuracy of the results became worse. However, since less correlated parameters have to be estimated, longer arcs are generally of interest for orbit determination with one-way data. But they require accurate modeling and complete corrections in order to provide results of good accuracy over the longer timeframes.

Since the literature so far does not contain extensive reports about the processing, analysis and application of one-way laser ranging data and the issues (see section 1), this cumulative thesis reports about those aspects in particular. The ultimate goal of a joint LRO orbit determination that incorporates all available datatypes (radio, crossover and laser ranging) requires understanding of the application of the individual datasets within orbit determination. Since this thesis provides the background for the application of the one-way laser ranging data to LRO, the ultimate goal of a joint orbit determination is supported as well. Based upon this work and the literature about the application of radio and crossover data (e.g. Mazarico et al., 2012), future work can focus on the joint orbit determination in particular, while utilizing the different datasets with their optimum settings. The research papers 1 and 2 of this cumulative thesis provide the content as described in the following.

Research paper 1 – Analysis of one-way laser ranging data to LRO: performance and calibration of spacecraft and ground station clocks

At first the LRO mission, the laser ranging experiment, the setup of the ground stations, the spacecraft, the LOLA instrument and the observation data is introduced. Furthermore other interplanetary laser ranging and time transfer experiments are described.

The one-way range measurement was obtained from the pairing of the seperate fire and receive times, measured at the station and the satellite respectively. For the pairing, predicted satellite receive times were taken from the nominal LRO trajectory. Corrections for the influence of hardware characteristics, the atmosphere and relativistic effects were applied to the predicted and the measured receive times.

Following that, the methods which were used to analyze single, multiple and simultaneous laser ranging passes are described in order to:

- derive the experiment and ground station performance from a statistical dataset analysis,
- estimate the LRO clock parameters and reference it to other timescales such as TDB via ground to space time transfer,
- estimate the ground station clock differences via ground to ground common-view time transfer.

A fixed orbit (the nominal LRO trajectory) was used for the estimation of the LRO and the ground station clock parameters within research paper 1. The Full Rate (FR) data is derived for every pass of the dataset from an iterative pairing process and statistically averaged to Normal Point (NPT) data while using LRO specific settings. The experiment and ground station performance is valuable information for mission analysis and simulation.

The LRO clock parameters were characterized via polynomial fits either applied over single passes or multiple passes consecutive in time. These fits further provided a referencing of onboard time to the TDB time scale. The ground station clock differences were characterized from the multiple- and

simultaneous-pass analysis via ground to ground time transfer in common-view. The LRO clock parameters and the ground station clock differences derived from different methods were compared with each other in order to evaluate their accuracy. All results were compared with available literature when possible.

The paper closes with a discussion of the effect of the completeness and the accuracy of the corrections, the influence of the length (single, multiple passes) over which the parameters were estimated and the orbit errors on the accuracy of the results.

Research paper 2 – Demonstration of orbit determination for the Lunar Reconnaissance Orbiter using one-way laser ranging data

The introduction is similar to research paper 1 but more oriented towards the orbit determination of LRO. This is followed by a discussion of the random and systematic errors of the one-way measurements in comparison to the errors typically observed within SLR. Furthermore the stability and the environmental sensitivity of the LRO and the ground station clocks is described. Moreover the background about other time transfer experiments, the time scales that were used, the clock error modeling, the observation model as well as the dynamical modeling used within the orbit determination software is provided.

Due to the one-way setup, the state vector and the timing of all involved clocks (LRO and all ground stations) have to be estimated simultaneously, which introduces many highly correlated timing parameters within the estimation. A priori constraints in the form of initial and covariance values were applied in order to separate the LRO state, its clock and all ground station clocks within the estimation. Furthermore it is described how the results from the LRO and ground station clock characterization from research paper 1 were used for the a priori constraints.

Following that, the timeframe selected for the demonstration of LRO orbit determination and the various state and clock arcs are described. Furthermore, the observation data coverage and the LRO orbit features are discussed for the selected timeframe.

The results of the estimated orbit arcs were the trajectories, the LRO and ground station clock parameters as well as post the fit measurement residuals. In order to evaluate the accuracy of the estimated orbit arcs,

- their differences with respect to the nominal LRO trajectory were analyzed,
- the post-fit measurement residuals with respect to the estimated trajectory were analyzed,
- the differences at the overlaps of consecutive arcs were analyzed,
- the estimated empirical accelerations were compared to the literature,
- the LRO clock parameters were compared to the a priori initial and covariance values,
- the ground station clock differences were compared to the a priori initial and covariance values.

Furthermore the results from the orbit arcs with different state and clock arc lengths were compared, in order to research how

- the accuracy of the results is affected by the completeness and the accuracy of the dynamical modeling,

- the accuracy of the results is affected by the approximation of the LRO clock which is defined by its stability and the completeness and accuracy of the correction for various effects,
- well the ground station clock differences were approximated with the different clock arc lengths also by analyzing the incorporation of simultaneous passes within the estimation,
- the accuracy of the results is affected by the observation data coverage in combination with the arc length and the presence of data gaps.

In the following discussion the results as well as the influence of the various aspects on the result accuracy is summarized. The paper closes with a description of various points for future missions which would allow for a better performance of one-way laser tracking systems.

References

Asmar, S.W., Armstrong, J.W., Iess, L. and Tortora, P., Spacecraft Doppler tracking: Noise budget and accuracy achievable in precision radio science observations, *Radio Sci.* **40**, 2005.

Border, J.S., Donivan, F.F., Finley, S.G., Hildebrand, C.E., Moultrie, B. and Skjerve, L.J., 1982. Determining spacecraft angular position with Delta VLBI – The Voyager demonstration. In: Proceeding of the Astrodynamics Conference, Guidance, Navigation and Control and Co-located Conferences. San Diego, USA, August 9th–11th.

Belli, A., Exertier, P., Samain, E., Courde, C., Torre, J.M. and Vernotte, F., 2015. Synchronization of distant Laser stations thanks to Time Transfer by Laser Link : Proposal for a dedicated campaign. In: Proceeding of the ILRS Technical Workshop. Matera, Italy, October 26th -30th.

Border, J.S. and Bedrossian, A., Delta Differential One-way Ranging, 2015, DSN, JPL, CALTEC.

Buccino, D.R., Seubert, J.A., Asmar, S.W. and Park, R.S., Optical Ranging measurement with a lunar orbiter: limitations and potential, *J. Spacecr. Rockets* **53**, 2016.

Bush, G.W., A Renewed Spirit of Discovery: The President's Vision for U.S. Space Exploration, in: The Vision for Space Exploration, 2004, NASA.

Cash, P., Emmons, D. and Welgemoed, J., 2008. Ultrastable oscillators for space applications. In: Proceedings of the 40th Annual Precise Time and Time Interval (PTTI) Meeting. Reston, Virginia, USA, 1st–4th December.

Chin, G., Brylow, S., Foote, M., Garvin, J., Kasper, J., Keller, J., Litvak, M., Mitrofanov, I., Paige, D., Raney, K., Robinson, M., Sanin, A., Smith, D., Spence, H., Spudis, P., Alan Stern, S. and Zuber, M., Lunar Reconnaissance Orbiter overview: The instrument suite and mission, *Spa Sci Rev* **129**, 2007.

Cornish, T., 34-m and 70-m Command, 2014, DSN, JPL, CALTEC.

Degnan, J.J., Millimeter Accuracy Satellite Laser Ranging: a Review, *Contributions of Space Geodesy to Geodynamics: Technology, American Geophysical Union*, 1993.

Degnan, J.J., 1994. Thirty years of laser ranging. In: Proceedings of the 9th International Laser Ranging Service workshop. Canberra, Australia, 7th–11th November.

Degnan, J.J., Asynchronous laser transponders for precise interplanetary ranging and time transfer, *J Geodyn* **34**, 2002.

Dirkx, D., Interplanetary Laser Ranging – Analysis for Implementation in Planetary Science Missions (PhD dissertation), 2015a, Delft University of Technology.

Dirkx, D., Noomen, R., Visser, P.N.A.M., Bauer, S. and Vermeersen, L.L.A., Comparative analysis of one- and two-way planetary laser ranging concepts, *Planet. Space Sci.* **117**, 2015b.

D'Ortenzio, M.V., Bresina, J.L., Crocker, A.R., Elphic, R.C., Galal, K.F., Hunt, D.R., Owens, B.D., Plice, L., Hawkins, A.M. and Policastri, L.A., 2015. Operating LADDEE: mission architecture, challenges, anomalies and success. In: Proceedings of the IEEE Aerospace Conference. Big Sky, Montana, USA, 7th–14th March.

Easton, R.L., The Navigation Technology Program, *Navigation* **25**, 1978.

Exertier, P., Bonnefond, P., Deleflie, F., Barlier, F., Kasser, M., Biancale, R. and Menard, Y., Contribution of laser ranging to Earth's sciences, *C.R. Geosci.* **338**, 2006.

Exertier, P., Samain, E., Courde, C., Martin, N., Torre, J.-M., Oneto, J.-L., Laas-Bourez, M., Guillemot, Ph. and Léon, S., 2013. T2L2: Five years in space. In: Proceedings of the European Frequency and Time Forum & International Frequency Control Symposium (EFTF/IFC). Prague, Czech Republic, 21st–25th June.

Garrick, J., Simpson, J. and Shah, N., 2010. Lunar Reconnaissance Orbiter (LRO) Guidance, Navigation and Control (GN&C) Overview. In: Proceedings of the American Institute of Aeronautics and Astronautics (AIAA) Guidance, Navigation and Control (GN&C) Conference. Toronto, Canada, 2nd–5th August.

Gurtner, W., Noomen, R. and Pearlman, M.R., The International Laser Ranging Service: current status and future developments, *Adv. Space Res.* **36**, 2005.

Gläser, P.A., Evaluation of topography, slopes, illumination and surface roughness of landing sites near the lunar south pole using laser altimetry from the lunar reconnaissance orbiter (PhD dissertation), 2015, Technische Universität Berlin.

Grunwaldt, L., Weisheit, S. and Steinborn, J., 2013. Upgrade of SLR station 7841 Potsdam. In: Proceedings of the 18th International Laser Ranging Service workshop. Fuyjiyoshida, Japan, 11th–15th November.

Helmert, F.R.: Die mathematischen und physikalischen Theorieen der höheren Geodäsie, 1880, Teubner Verlag.

Husson, V.S., 1992. Historical MOBLAS system characterization. In: Proceedings of the 8th International Laser Ranging Service workshop. Annapolis, Maryland, USA, 18th–22nd May.

International Laser Ranging Service (ILRS) Website. <http://ilrs.gsfc.nasa.gov> retrieved in July 2016.

Ismail-Zadeh, A. and Tackley, P., Computational methods for geodynamics, 2010, Cambridge University Press.

The Optical Link Experiment with the Laser Altimeter (LIDAR), Japanese Aerospace Exploration Agency (JAXA) website announcement <http://www.hayabusa2.jaxa.jp/topics/20151225_02_e/> retrieved in August 2016.

Jin, S., Arivazhagan, S., Zhang, T., Lunar Geodesy and Sensing: Methods and Results from Recent Lunar Exploration Missions, in: Planetary Geodesy and Remote Sensing, 2014, CRC Press.

Kirchner, D., Two-way time transfer via communication satellites, *Proceedings of the IEEE* **79**(7), 1991.

Kirchner, G. and Koidl, F., Laser ranging to space debris from Graz laser station, *Vermessung & Geoinformation* **2+3**, 2015.

Konopliv, A.S., Park, R.S., Yuan, D.N., Asmar, S.W., Watkins, M.M., Williams, J.G., Fahnestock, E., Kruizinga, G., Paik, M., Strekalov, D., Harvey, N., Smith, D. and Zuber, M., The JPL lunar gravity field to spherical harmonic degree 660 from the GRAIL Primary Mission, *J. Geophys. Res.: Planets* **118**, 2013.

Kumar, K., Abdulkadir, Y., van Barneveld, P., Belien, F., Billemont, S., Brandon, E., Dijkstra, M., Dirkx, D., Engelen, F., Gondelach, D., van der Ham, L., Heeren, E., Iorfida, E., Leloux, J., Melman, J., Mooij, E., Musegaas, P., Noomen, R., Römgens, B., Ronse, A., Leite Pinto Secretin, T., Tong Minh, B., Vandamme, J. and, Persson, S., 2012. TUDAT: a modular and robust astrodynamics toolbox. In: Proceedings of the 5th International Conference on Astrodynamic Tools and Techniques (ICATT). ESTEC/ESA, Noordwijk, The Netherlands, 29th May–1st June.

Kunimori, H., Takahashi, F., Itabe, T. and Yamamoto, A., 1993. Laser ranging application to time transfer using geodetic satellite and to other Japanese space programs. In: Proceedings of the 8th International Laser Ranging Service workshop. Annapolis, Maryland USA, 18th–22th May.

Layland, J.W. and Rauch, L.L., The evolution of technology in the deep space network: A history of the Advanced Systems Program, *TDA Progress Report* **42-130**, 1997.

Lemoine, F. G., Goossens, S., Sabaka, T. J., Nicholas, J. B., Mazarico, E., Rowlands, D. D., Loomis, B. D., Chinn, D. S., Neumann, G. A., Smith, D. E. and Zuber, M. T., GRGM900C: a degree 900 lunar gravity model from GRAIL primary and extended mission data, *Geophys. Res. Lett.* **41**, 2014.

Leschiutta, S., Time synchronization using laser techniques, *Proceedings of the IEEE* **79**, 1991.

Lewandowski, W., Petit, G., Baumont, F., Fridelance, P., Gaignebet, J., Grudler, P., Veillet, Ch., Wiant, J. and Klepczynski, W.J., 1993. Comparison of LASSO and GPS time transfers. In: Proceedings of the 25th Annual Precise Time and Time Interval (PTTI) Applications and Planning Meeting. Marina Del Rey, California, USA, November 29th –December 2nd.

Lombardi, M.A., Fundamentals of Time and Frequency, in: The Mechatronics Handbook, 2001, CRC Press.

Löcher, A., Hofmann, F., Gläser, P., Haase, I., Müller, J., Kusche, J. and Oberst, J., Towards improved lunar reference frames: LRO orbit determination, in: International Association of Geodesy Symposia, Springer, 2015.

Mao, D., Sun, X., McGarry, J., Mazarico, E., Torrence, M., Rowlands, D., Neumann, G., Barker, M., Golder, J., Smith, D. and Zuber, M., 2014. LRO orbit determination with laser ranging data. In:

Proceedings of the 19th International Laser Ranging Service workshop Annapolis. Maryland, USA, 27th–31st October.

Mazarico, E., Lemoine, F.G., Han, S.-C. and Smith, D.E., GLGM-3: a degree-150 lunar gravity model from the historical tracking data of NASA Moon orbiters, *JGR* **115,** 2010.

Mazarico, E., Rowlands, D.D., Neumann, G.A., Smith, D.E., Torrence, M.H., Lemoine, F.G. and Zuber, M.T., Orbit determination of the Lunar Reconnaissance Orbiter, *J. Geod.* **86**, 2012.

Mazarico, E., Goossens, S., Lemoine, F., Neumann, G., Torrence, M., Rowlands, D., Smith, D. and Zuber, M., 2013. Improved orbit determination of lunar orbiters with lunar gravity fields obtained by the GRAIL mission. In: Proceedings of the 44th Lunar and Planetary Science Conference (LPSC). Woodlands, Texas, USA, 18th–23rd March.

Montenbruck, O. and Gill, E., Satellite Orbits, 2000, Springer.

Moyer, T.D, Formulation for Observed and Computed Values of Deep Space Network Data Types for Navigation, 2000, NASA, JPL, CALTEC.

Murphy, T., Adelberger, E., Battat, J., Carey, L., Hoyle, C., Leblanc, P., Michelsen, E., Nordtvedt, K., Orin, A., Strasburg, J., Stubbs, C., Swanson, H. and Williams, E., The Apache Point Observatory Lunar Laser-ranging Operation: Instrument Description and First Detections, *Publ. Astron. Soc. Pac.* **120,** 2008**.**

Murphy, T.W., Lunar laser ranging: the millimeter challenge, *Rep. Prog. Phys.* **76**, 2013.

NAIF LRO SPICE archive. <ftp://naif.jpl.nasa.gov/pub/naif/pds/data/lro-l-spice-6-v1.0/lrosp_1000/> retrieved in July 2016.

Neumann, G. A., Cavanaugh, J. F., Coyle, D. B., McGarry, J., Smith, D. E., Sun, X., Torrence, M., Zagwodski, T. W. and Zuber, M. T., 2006. Laser ranging at interplanetary distances. In: Proceedings of the 15th International Laser Ranging workshop. Canberra, Australia, 15th–20th October.

Neumann, G.A., Barker, M.H., Mao, D., Mazarico, E., McGarry, J.F., Smith, D.E., Sun, X., Torrence, M.H. and Zuber, M.T., 2014. Interplanetary laser ranging: the quest for 1 AU. In: Proceedings of the 19th International Laser Ranging Service workshop. Annapolis, Maryland, USA, 27th–31st October.

Parker, T. and Matsakis, D., Time and frequency dissemination: Advances in GPS transfer techniques, *GPS World* **15**, 2004.

Pearlman, M.R., Degnan, J.J. and Bosworth, J.M., The international laser ranging service, *Adv. Space Res.* **30**, 2002.

Rothacher, M., Vorlesungsskriptum Erdmessung und Satellitengeodäsie 2, 2000, TU München.

Schlicht, A., 2012. The European Laser Timing Experiment (ELT) and Data Centre (ELT-DC), In: Mitteilung des Bundesamtes für Kartographie und Geodäsie, Proceeding of the 17th International Workshop on Laser Ranging. Wettzell, Deutschland, 16th–20th May, 2011.

Schreiber, U., Prochazka, I., Lauber, P., Hugentobler, U., Schafer, W., Cacciapuoti, L. and Nasca, R., 2009. The European Laser Timing (ELT) experiment on-board ACES. In: Proceedings of the 23rd European Frequency and Time Forum (EFTF 2009). Neuchâtel, Switzerland.

Seeber, G., Satellite Geodesy, 2003, de Gruyter.

Slobin, S.D., 34-m BWG Stations Telecommunications Interfaces, 2015, NASA, JPL, CALTEC.

Smith, J.G., Communicating through deep space, *J. Br. Interplanet. Soc.* **38**, 1985.

Smith, D., Zuber, M., Sun, X., Neumann, G., Cavanaugh, J., McGarry, J. and Zagwodzki, T., Two-way laser link over interplanetary distance, Science **311**, 2006.

Smith, D., Zuber, M., Lemoine, F., Torrence, M. and Mazarico, E., 2008. Orbit determination of LRO at the Moon. 16th International Workshop on Laser Ranging. Poznan, Poland, October 13th–17th.

Smith, D.E., Zuber, M.T., Jackson, G.B., Cavanaugh, J.F., Neumann, G.A., Riris, H., Sun, X., Zellar, R.S., Coltharp, C., Connelly, J., Matuszeski, A., Ott, M., Rowlands, D.D., Zagwodzki, T., Torrence, M.H., Katz, R., Kleyner, I., Peters, C., Liiva, P., Coltharp, C., Schmidt, S., Ramsey, L., Scott, V.S., Unger, G., Danny C. Krebs, Novo-Gradac, A.D., Shaw, G.B. and Yu, A.W., The Lunar Orbiter Laser Altimeter Investigation on the Lunar Reconnaissance Orbiter Mission, *Space Sci Rev* **150**, 2010a.

Smith, D.E., Zuber, M.T., Neumann, G.A., Lemoine, F.G., Mazarico, E., Torrence, M.H., McGarry, J.F., Rowlands, D.D., Head, J.W., Duxbury, T.H., Aharonson, O., Lucey, P.G., Robinson, M.S., Barnouin, O.S., Cavanaugh, J.F., Sun, X., Liiva, P., Mao, D.-d., Smith, J.C. and Bartels, A.E., Initial observations from the Lunar Orbiter Laser Altimeter (LOLA), *Geophys. Res. Lett.* **37**, 2010b.

Sun, X., Abshire, J.B., McGarry, J.F., Neumann, G.A., Smith, J.C., Cavanaugh, J.F., Harding, D.J., Zwally, H.J., Smith, D.E. and Zuber, M.T., Space Lidar Developed at the NASA Goddard Space Flight Center—The First 20 Years, *IEEE J. Sel. Topics Appl. Earth Observ. in Remote Sens* **6**, 2013a.

Sun, X., Skillman, D.R., McGarry, J.F., Neumann, G.A., Mao, D., Torrence, M.H. and Hoffman, E., 2013b. Time transfer between satellite laser ranging stations via simultaneous laser ranging to the Lunar Reconnaissance Orbiter. In: Proceedings of the 18th International Laser Ranging workshop. Fujiyoshida Japan, 11th–15th November.

Sun, X., Barker, M.K., Mao, D., Marzarico, E., Neumann, G.A., Skillman, D.R., Zagwodzki, T.W., Torrence, M.H., Mcgarry, J. and Smith, D.E. and Zuber, M.T., 2014. In-orbit calibration of the Lunar Orbiter Laser Altimeter via two-way laser ranging with an Earth station. In: Proceedings of the American Geophysical Union, Fall Meeting. San Francisco, California, USA, December 15th–19th.

Vallado, D.A., Fundamentals of Astrodynamics and Applications, 2001, Microcosm.

Vetter, J.R., Fifty Years of Orbit Determination: Development of Modern Astrodynamics Methods, *Johns Hopkins APL Tech Dig* **27**, 2007.

Vrancken, P., Characterization of T2L2 (Time Transfer by Laser Link) on the Jason 2 ocean altimetry satellite and Micrometric laser ranging (PhD dissertation), 2008, Université Nice Sophia Antipolis.

Wood, R. and Appleby, G., Satellite laser ranging, in: Handbook of Laser Technology and Applications, Institute of Physics, 2004.

Zagwodzki, T., McGarry, J.,Degnan, J., Abbot, A., Varghese, T., Oldham, T., Selden, M., Chabot, R., Fitzgerald, J. and Grolemund, D., 1994. Two-Colour Wavelength Ranging at NASA 's 1.2 Meter

Telescope Tracking Facility. In: Proceedings of the 9th International Laser Ranging Service workshop. Canberra, Australia, 7th–11th November.

Zuber, M.T., Smith, D.E., Zellar, R.S., Neumann, G.A., Sun, X., Katz, R.B., Kleyner, I., Matuszeski, A., McGarry, J.F., Ott, M.N., Ramos-Izquierdo, L.A., Rowlands, D.D., Torrence, M.H. and Zagwodzki, T.W., The Lunar Reconnaissance Orbiter laser ranging investigation, *Space Sci. Rev.* **150**, 2010.

Zuber, M.T., Smith, D.E., Lehman, D.H., Hoffman, T.L., Asmar, S.W. and Watkins, M.M., Gravity Field of the Moon from the Gravity Recovery and Interior Laboratory (GRAIL) Mission, *Science **339***, 2013.

3 Research paper 1

Analysis of one-way laser ranging data to LRO, time transfer and clock characterization.

S. Bauer[1], H. Hussmann[1], J. Oberst[1,2,3], D. Dirkx[4,5], D. Mao[6], G.A. Neumann[7], E. Mazarico[7], M.H. Torrence[8], J.F. McGarry[7], D.E. Smith[9], M.T. Zuber[9].

[1]German Aerospace Center (DLR), Berlin, Germany, contact: sven.bauer@dlr.de,
[2]TU Berlin, Germany,
[3]Moscow State University for Geodesy and Cartography (MIIGAiK), Russia,
[4]TU Delft, Netherlands,
[5]Joint institute for VLBI ERIC, Dwingeloo, Netherlands,
[6]Sigma Space Corporation, Lanham, MD, USA,
[7]NASA Goddard Space Flight Center, Greenbelt, MD, USA,
[8]Stinger Ghaffarian Technologies Inc., Greenbelt, MD, USA,
[9]Massachusetts Institute of Technology, Cambridge, MA, USA.

Abstract

We processed and analyzed one-way laser ranging data from International Laser Ranging Service ground stations to NASA's Lunar Reconnaissance Orbiter (LRO), obtained from June 13, 2009 until September 30, 2014.

We pair and analyze the one-way range observables from station laser fire and spacecraft laser arrival times by using nominal LRO orbit models based on the GRAIL gravity field. We apply corrections for instrument range walk, as well as for atmospheric and relativistic effects.

In total we derived a tracking data volume of ≈3000 hours featuring 64 million Full Rate and 1.5 million Normal Point observations. From a statistical analysis of the dataset we evaluate the experiment and the ground station performance. We observe a laser ranging measurement precision of 12.3 cm in case of the Full Rate data which surpasses the LOLA timestamp precision of 15 cm. The averaging to Normal Point data further reduces the measurement precision to 5.6 cm.

We characterize the LRO clock by estimating its rate, aging and the change of it throughout the mission time with fits. These fits also provide referencing of onboard time to the TDB time scale at a precision of 166 ns over two and 256 ns over all mission phases, representing ground to space time transfer. Furthermore we measure ground station clock differences from the fits as well as from simultaneous passes which we use for ground to ground time transfer from common view observations. We observed relative offsets ranging from 33 to 560 ns and relative rates ranging from 2×10^{-13} to 6×10^{-12} between the ground station clocks during selected mission phases. We study the results from the different methods and discuss their applicability for time transfer.

Keywords

Laser ranging, one-way, Lunar Reconnaissance Orbiter, time transfer

3.1 Introduction

NASA's Lunar Reconnaissance Orbiter (LRO) was launched on June 18, 2009 and entered its lunar orbit five days later. The goal of the mission is to carry out a comprehensive geophysical, geological and geochemical mapping campaign to establish an observational framework for future lunar exploration (Zuber et al., 2010).

One of the seven instruments onboard LRO is the Lunar Orbiting Laser Altimeter (LOLA), which was developed at NASA's Goddard Space Flight Center (GSFC), measuring the surface elevation, slope and roughness. From these data a global topographic model and a high-accuracy geodetic grid are derived. LOLA is also capable of detecting laser pulses from Earth ground stations. These one-way range measurements add a new type of tracking data to the mission (Zuber et al., 2010; McGarry et al., 2011 and 2013).

For precise referencing of the orbital remote sensing data, the accuracy and precision of LRO positioning throughout the mission is critical (Zuber et al., 2010). The baseline of the LRO tracking and orbit determination was realized by radio observations from Earth via NASA's White Sands station and the Universal Space Network (USN) in combination with LOLA's altimetric crossovers. The accuracy of this nominal LRO trajectory which we use in our analysis is reported to be ≈9 m overall at the arc overlaps of trajectories consecutive in time (Mazarico et al. 2012 and 2013). Recent solutions of that trajectory used the GRAIL gravity field GRGM900C (Lemoine et al., 2014) up to degree and order 600 (LRO SPICE archive, 2015). The ultimate goal is to combine the various tracking data sets for refined orbit determination to support Lunar precision mapping (Zuber et al., 2010).

Most of the laser ranging experiments beyond an Earth orbit have only been carried out sporadically as for example to Mars Global Surveyor and MESSENGER (Neumann et al., 2006, Smith et al. 2006a). Beside the two-way laser ranging to the mirrors on the lunar surface since the 1970s (Degnan, 1994), only the one-way ranging to LRO has been carried out routinely between June 30, 2009 and September 30, 2014 (McGarry et al. 2013).

Mao et al. (2014a) demonstrated the application of laser ranging data for analysis of the LRO clock and orbit determination. Trajectories derived from various combinations of different types of tracking data were compared in order to assess their consistency. They found that the application of improved gravity fields from the GRAIL mission supports orbit determination with one-way laser ranging data to a quality comparable to radio data based results. Sun et al. (2013a) also used the same laser uplink for demonstration of data transmission which highlights the versatility of the laser ranging to LRO experiment.

Furthermore Sun et al. (2013b) and Mao et al. (2014b) reported about simultaneous passes from multiple stations. They demonstrated the measurement of differences between and the synchronization of remote ground station clocks with the one-way data thus performing ground to ground time transfer. Other optical time transfer experiments like the time transfer by laser link (T2L2) and the European Laser Timing (ELT) have a two-way setup. They derive ground to space and ground to ground time transfer by using an onboard retro-reflector and a detector which provides an active uplink (Exertier et al., 2013; Schreiber et al., 2009).

While previous data analyses have been carried out in the early stages of the experiment (Bauer et al., 2013), we now use all data obtained between July 16, 2009 and September 10, 2014. This report describes the application of the nominal LRO trajectory for the pairing, processing and the analysis of

the one-way range measurements as well as the characterization of the onboard clock and the ground station clock differences by time transfer.

We analyze the derived dataset regarding criteria such as pass length, ratio of successfully paired to actually fired shots and measurement precision. From the averaging of these values either over all or all passes of a certain station, we derive the overall and the ground station performance.

Furthermore we use approaches based on the analysis of single and multiple passes in order to characterize the LRO clock by estimating its parameters offset, rate, aging and its change and derive a referencing of onboard to ground time (ground to space time transfer). While we use these terms for the clock parameters they are equivalent to the terms phase, frequency, frequency drift and change of frequency drift respectively, which are used within the time and frequency community. By comparing the parameters derived from the single- and the multiple-pass analysis, we get estimates of their accuracy and precision. We further use the multiple-pass analysis and simultaneous passes to characterize the timing differences between ground station clocks (ground to ground time transfer). Measuring their relative offsets and rates enables the monitoring of their timing.

Section 3.2 describes the setup and the features of the ground stations that are ranging to LRO along with their timing system stabilities. Section 3.3 provides the setup of the spacecraft and the laser ranging data and discusses the LRO clock stability. Section 3.4 compares optical two-way time transfer experiments regarding their performance and difference to the time transfer experiment done with the one-way laser ranging data to LRO. Section 3.5 explains our data processing methods for the pairing, processing and the formation of the Normal Point data as well as the corrections that we apply. In section 3.6 we introduce our data analysis methods that utilize either single, multiple or simultaneous passes. The results on the dataset statistics, the characterization of the LRO clock and the ground station clock differences are presented in section 3.7. In section 3.8 we discuss these results and draw conclusion from our work.

3.2 Ground stations

LRO is tracked by selected ground stations of the International Laser Ranging Service (ILRS – Pearlman et al., 2002), which differ in their equipment and characteristics as listed in Table 4. Table 5 shows the corresponding stability values of their timing systems. For completion the stability of the LRO onboard clock is added as well, while it is discussed in section 3.3 with more detail. With stations in the US, Europe, South Africa (HARL) and Australia (YARL) a global coverage of LRO is basically provided.

Contrary to other established stations, the stations YARL, GODL, MONL and HARL are trailer-based Mobile Laser Ranging Station (MOBLAS). These stations were deployed by NASA in the 1970's for a global tracking of the SEASAT mission (Husson et al., 1992) and have similar hardware and performance characteristics.

Table 4: Equipment and characteristics of the ILRS ground stations that range to LRO taken from Mao et al. (2011), McGarry et al. (2011) and the ILRS website (2015)

Code	ID	Location	Coordinates in Lat., Long. and Height	Firing rate in Hz	SF*	Potential received shots per sec	Pulse width in ns	Energy expected at LRO in fJ/cm²	Type of timing system
MDOL	**7080**	McDonald, Texas, USA	30.6802° N 104.0152° W 2006 m	10	No	2 to 4	0.20	1 to 10	Cesium
YARL**	**7090**	Yarragadee, Australia	29.0464° S 115.3467° E 244 m	10	No	2 to 4	0.15	1 to 3	Rubidium
GODL**	**7105**	Greenbelt, Maryland, USA	39.0206° N 76.8277° W 19 m	10	No	2 to 4	0.15	1 to 3	H-Maser
MONL**	**7110**	Monument Peak, California, USA	32.8917° N 116.4227° W 1842 m	10	No	2 to 4	0.15	1 to 3	Rubidium
GO1L	**7125**	Greenbelt, Maryland, USA	39.0206° N 76.8277° W 19 m	28	Yes	28	< 8	1 to 5	H-Maser
HARL**	**7501**	Hartebeesthoek, South Africa	25.8897° S 27.6861° E 1407 m	10	No	2 to 4	0.20	1 to 3	Rubidium
ZIML	**7810**	Zimmerwald, Switzerland	46.8772° N 7.4652° E 951 m	14	Yes	14	0.06	1 to 3	OCCO***
HERL	**7840**	Herstmonceaux, United Kingdom	50.8674° N 0.3361° E 75 m	14	Yes	14	0.10	1 to 3	H-Maser
GRSM	**7845**	Grasse, France	43.7546° N 6.9216° E 1323 m	10	No	2 to 4	0.20	1 to 10	Cesium
WETL	**8834**	Wettzell, Germany	49.1444° N 12.8780° E 665 m	14	Yes	14	0.01	1 to 10	H-Maser

*) Synchronized firing.
**) MOBLAS Stations.
***) Oven controlled crystal oscillator.

Table 5: Stabilities of various ground station timing systems (Lombardi, 2001) and the LRO onboard clock (Cash et al., 2008).

Type	Stability @ noise floor	Averaging period τ in s
Quartz OCXO/OCCO*	$1x10^{-12}$	1 to 10^2
Rubidium	$1x10^{-12}$	10^3 to 10^5
Cesium/Atomic	$1x10^{-14}$	10^5 to 10^7
H-Maser	$1x10^{-15}$	10^3 to 10^5
LRO onboard clock OCXO*	$7x10^{-14}$	40

*) Oven Controlled Crystal Oscillator

3.3 Spacecraft and data setup

The ranging to LRO as illustrated in Sun et al. (2013a) is done from either one or multiple stations at a time. In order to receive laser shots from Earth ground stations, an optical receiver, the Laser Ranging Telescope was added to the high gain communication antenna which is always pointing towards Earth – in particular, to the White Sands radio station, New Mexico, US, when it is in view. A fiber optic cable is forwarding incoming laser pulses into the LOLA instrument for detection.

From a distance of 381000 km the Laser Ranging Telescope Field Of View of 30 mrad covers a circular surface segment with a diameter of ≈11433 km. With this Field of View all US stations to range to LRO simultaneously while the LRO antenna is pointed at White Sands (Ramos et al., 2009).

LOLA has five channels which are designed to receive and detect the 1064 nm lunar return pulses from the laser beams, resulting in five altimetry measurements at a time ideally. The Silicon Avalanche Photodiode (SiAPD) is also able to detect signals at a wavelength of 532 nm (Ramos-Izquierdo et al., 2009), which is commonly used by ILRS ground stations for the ranging to Earth orbiting satellites (Smith et al., 2006b). It is shown in Ramos-Izquierdo et al. (2009) how the signals at both wavelengths are merged. With this setup the regular signals from ILRS Earth ground stations and the returns from the lunar surface can be detected concurrently with the same instrument. Since the LOLA time stamp precision is 0.5 ns, the precision of derived range measurements is ≈15 cm.

While the stations record their fire times in UTC, LOLA measures the arrival of laser shots in Mission Elapsed Time (MET), which is the internal timing system of the LRO onboard clock. Within our work we use the Barycentric Dynamical Time (TDB) time scale because it is commonly used for ephemerides and interplanetary orbit determination. Figure 10 illustrates the relation of these timing systems and their conversion along with the corresponding accuracies. The officially provided data product for the conversion of MET to UTC is the spacecraft clock kernel (SCLK) which has an accuracy of ±3 ms. Within this work we derive a conversion from fits (ground to space time transfer) with an accuracy of ± 256 ns over all mission phases (see section 3.6.2 and 3.7.2).

The LOLA instrument is operating in 28 Hz cycles, which are illustrated in Figure 11. One major frame with a length of 1 second consists of 28 minor frames with a length of ≈35.7 ms each, which include two windows for receiving laser pulses. First, the Earth Range Gate is open for 8 ms, awaiting incoming laser pulses from ground stations. After that the LOLA fires its laser towards the lunar surface ≈9.6 ms after t_0 – the beginning of a minor frame. Then, the Lunar Range Gate is open for 5 ms and awaits laser returns from the Lunar surface (Riris and Cavanaugh, 2009).

The maximum number of range measurements can be made, when a ground station is firing with frequency and phase matching the LOLA 28 Hz cycle, as it is the case for the GO1L station. For some stations ranging at half of this frequency (e.g. WETL firing at 14 Hz), the number of successful measurements is correspondingly smaller. For other stations ranging at 10 Hz (e.g. MOBLAS), shots fall on average at least twice per second in the Earth range gate (compare Table 4). A near-real-time feedback via radio with a delay down to 45 s helps the stations during operation to check whether shots are received and if they fire in phase with the LOLA cycle.

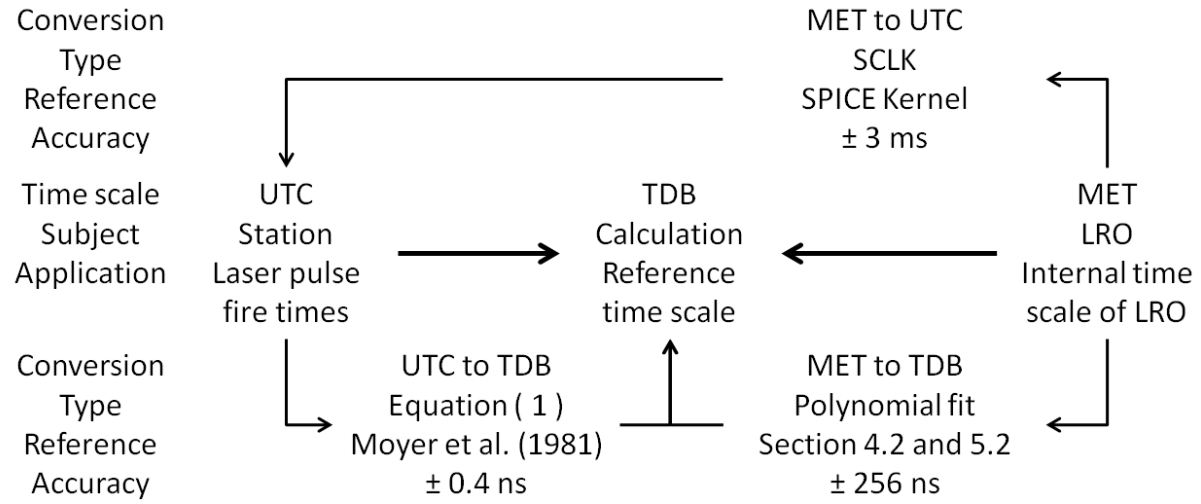

Figure 10: Utilized time scales with their relation and their conversion accuracies.

The timestamps for the detection of the incoming laser pulses are derived from the LRO onboard clock which is an Ultra Stable Oscillator (USO). While the ground station clocks have stabilities of $1x10^{-12}$ to $1x10^{-15}$ over periods of 10^3 to 10^7 s, the LRO onboard clock achieves its best stability of $7x10^{-14}$ after an averaging period of 40 s (see Table 5). Generally it is at $1x10^{-13}$ between 1 and 100 s and at $2x10^{-13}$ up to 10000 s at constant temperatures (Cash et al., 2008). This stability adds up to an error in the range of 0.3 to 3 mm and up to 60 cm respectively. The accumulating range error becomes larger than the LOLA timestamp precision after 2500 s. Since the LRO USO stability does not become larger than $2x10^{-13}$ after an orbital period of LRO of ≈120 min (7200 s) no additional once per orbit error is introduced by the onboard clock.

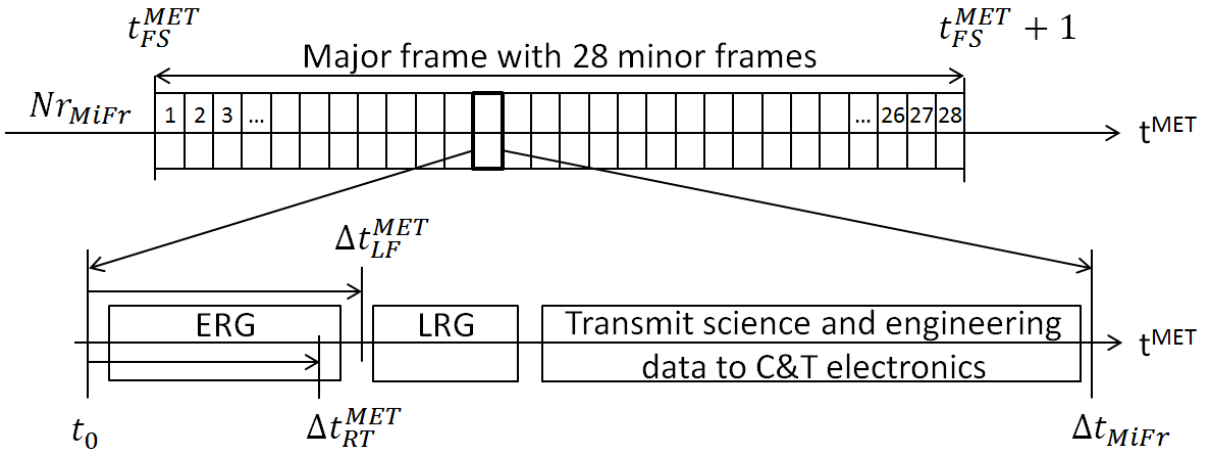

Figure 11: Timing of a LOLA major frame with its 28 minor frames (Nr_{MiFr}) which is spanning over one full second (t_{FS}^{MET}). All events are measured in Mission Elapsed Time (MET). One frame contains the Earth Range Gate (ERG) and the Lunar Range Gate (LRG). Both the laser receive time (Δt_{RT}^{MET}) and the LOLA laser fire time (Δt_{LF}^{MET}) are referenced to t_0, which marks the beginning of a minor frame. The LOLA laser fires ≈9.6 ms after t_0. The rest of the minor frame that has a total length of Δt_{MiFr}≈35.7 ms, is used to transmit science and engineering data to the Command & Telemetry (C&T) electronics.

Following Cash et al. (2008) the response of the LRO USO to temperature variation is $1–3x10^{-12}$ /°C. We saw variations with an amplitude of 0.3°C over one day which causes a maximum change in the rate of $0.3–0.9x10^{-12}$ accordingly. Variations due to changes in the power consumption of close by instruments or the orbit height can cause further changes of the rate. These variations accumulate to an offset of 13–39 ns over one day, when we use a sinusoidal function for the integration of it. The resulting range error of ≈4–12 m has an average linear trend of $1.5–4.5x10^{-13}$. We observed remaining sinusoidal variations around the linear trend with amplitudes of ≈2–6 ns. If we assume that a sinusoidal curve with a period of one day has a turnover point every 21600 s, the remaining variations have an average rate of $\approx\pm1–3x10^{-13}$ between these points. Since the LRO clock stability is $2x10^{-13}$ over up to 10000 s, this average rate is at or below this value. Since no correction was available for the change of the rate due to temperature change within our work yet, the resulting periodic and the further changes mix with the stochastic noise of the LRO clock. The incomplete corrections affect the approximation of it via the polynomial fits (see section 3.6.1, 3.6.2 and 3.7.2). Because the ground station clocks are not subject to temperature change due to proper housing, their approximation is only affected by their stability.

Compared to the LOLA timestamp precision of 15 cm, Exertier et al. (2006) reported random errors below that within Satellite Laser Ranging (SLR) in general. They found a 7 – 12 mm random error for Full Rate and 1 – 3 mm for Normal Point data. The errors are thereby coming from the ground station laser, detector, timer, clock and other dependencies as well as from the atmosphere and the target signature. Further the calibration of the station hardware, the atmosphere itself as well as the target signature introduce a systematic error of 8–19 mm. The systematic errors are larger than the random ones with the one-way setup as well. The errors are thereby coming from the LRO onboard and the ground station clocks, the orbit that we use for the predictions as well as the modeling accuracy of the environment (atmosphere) as it will be shown with the results (section 3.5). The target signature error is not present with the one-way setup.

3.4 Time transfer via LRO laser ranging and other optical experiments

The two-way laser time transfer experiments T2L2 and ELT allow for the direct estimation of the offset between station and onboard clock (ground to space time transfer). This offset can be further used to measure the differences or synchronize remote ground station clocks (ground to ground time transfer). In case of T2L2 the offsets of all participating stations to the onboard clock are used to estimate the difference between them either in non-common and common view (Exertier et al., 2013).

Both the T2L2 and the ELT experiment feature a similar setup consisting of a retro-reflector, a detector (providing an active uplink) and a timing system and are tracked by ILRS ground stations. The T2L2 experiment was launched onboard the Jason-2 satellite in 2008 and utilizes its USO (Exertier et al., 2013). The ELT experiment will make use of the Atomic Clock Ensemble in Space (ACES) onboard the International Space Station (ISS) which will include both an atomic clock and an H-Maser (Schreiber et al., 2009).

With the laser ranging to LRO we pair a predicted receive to a measured receive time to complete the one-way observable (section 3.5.4). Unlike with the two-way T2L2 and ELT experiment an unbiased range measurement (via the retro-reflector) is not available in order to estimate the offset between the ground station and the onboard clock directly. Due to the prediction the ground to space time transfer is affected by orbit errors, modeling and random errors of the LRO clock and errors of the corrections (see section 3.6.2 and 3.7.2). However as it will be shown in section 3.6.2 (multiple-pass

analysis) and section 3.6.3 (simultaneous pass analysis) we can estimate the differences between the ground station clocks. Thereby the multiple pass analysis allows for common and non-common and the simultaneous pass analysis for common view time transfer whereby the latter one is insensitive to orbit and LRO clock errors (see section 3.6.3). The accuracy of the time transfer from the simultaneous passes is below LOLA's timestamp accuracy and thus only limited by the precision of the instrument which is 500 ps (see section 3.6.3 and Sun et al., 2013b). Contrary the accuracy of the ground to space time transfer – which we measure from the 1–σ variation of the post-fit measurement residuals – is affected by the errors from the orbit, the LRO clock modeling, random errors and incomplete corrections.

Table 6 shows a comparison of the performance of the two-way T2L2 and the ELT as well as the one-way LRO laser ranging time transfer experiment. Both two-way experiments achieve accuracies around and below 10 ps for ground to space and ground to ground time transfer. With non-common view time transfer, the ELT achieves much better accuracies than the T2L2 experiment due to the more stable clocks (Atomic and H-Maser compared to USO – see Table 5) even over one ISS orbit. With that the ELT experiment will enable global time transfer between all stations that can range to its detector.

With the LRO laser ranging experiment we used polynomial fits for the characterization of the LRO clock from which we also derived the ground to space time transfer. Compared to the T2L2 and the ELT experiment the timeframes over which the ground to space time transfer is carried out are much longer (see Table 6). Comparing the accuracy (166 and 256 ns over 56 days and 5 years respectively) to the accuracy of the nominal LRO trajectory (30 ns), we see that the influence of the orbit errors is smaller than the other errors together. As it will be shown (see section 3.6.2, 3.6.3 and 3.7.3) ground to ground time transfer is only possible in common view. Non-common view measurements would become subject of too much interpretation with the accumulated errors from the orbit, the modeling and the random errors of the LRO clock and the incomplete corrections. As reported by Sun et al. (2013b) and confirmed with our results in section 3.7.3, the time transfer with common-view laser ranging observations to LRO achieves an accuracy of 500 ps over the average pass length.

Table 6: Performance comparison of the T2L2, the ELT and the LRO laser ranging time transfer experiment taken from Exertier et al. (2006), Schlicht (2012) and the results of this work respectively. The performance is compared for ground to space and ground to ground time transfer in common view (CV) and non-common view (NCV).

Experiment	Setup	Ground to	Accuracy	Averaging period τ
T2L2	Two-way	Space	<10 ps	1000 s
		Ground CV	≈10 ps	1000 s
		Ground NCV	150 ps	300 s
ELT	Two-way	Space	4 ps	300 s
		Ground CV	6 ps	300 s
		Ground NCV	7 ps	≈5400 s*
LRO LR	One-way	Space	166 ns**	56 d
		Ground CV	500 ps	≈2000 s***
		Ground NCV	-	-

*) Dead time of one orbit cycle (Schlicht, 2012) which we assumed to ≈90 min for the ISS

**) Accuracy estimated from the 1–σ variation of the post-fit measurement residuals (see the discussion in this section).

***) Average length of a LRO laser ranging pass (see section section 3.7.1)

Compared to the T2L2 experiment onboard the Earth-bound Jason-2 spacecraft, the distance between the ground stations and LRO is much larger. Due to the different observation geometry, the LRO laser ranging time transfer can tolerate larger uncertainties in the spacecraft positioning than the T2L2 project (Sun et al., 2013b). However since the T2L2 experiment was a dedicated time transfer experiment it still achieves a better performance than the time transfer carried out via the laser ranging to LRO (see Table 6).

3.5 Data processing methods

The laser measurements are affected by various influences that we correct for. While the corrections for atmospheric and relativistic effects cover systematic influences, the range walk correction addresses random errors that affect the data measurement precision. Following that the pairing of the separated one-way data and the formation of the Normal Point (NP) from the Full Rata (FR) data is described.

3.5.1 Correction for atmospheric effects

While the laser pulses travel through the atmosphere they are decelerated for which we apply an atmospheric correction Δt_{AC} to the measurements. Following Rothacher (2000) we can neglect the influence of the ionosphere on an optical signal. For the troposphere we use the standard model from Marini and Murray (1973) where we input the environmental conditions recorded by the stations. The conditions, their change and the resulting correction are listed in Table 7 for an example pass where GO1L station ranged to LRO on September 14, 2009 at 15:52 UTC for ≈45 min.

In contrast to ranging campaigns involving Earth satellites, the elevation change during a LRO pass and thus the change of the correction is small over a long timeframe (8° over 45 min – see Table 7). Also, the Lunar target is usually at high elevations, so that we set the correction to an averaged value, as shown in Table 7 with the example pass. While some stations provide continuous meteo measurements throughout their pass, many only provide one meteo measurement. Hence we use just one correction value for each passes. In case of the example pass this constant correction value causes an error in time of ≈±0.2 m (≈±0.7 ns) and in rate of ≈5×10^{-13} over the length of the pass (45 min). The error introduced by the simplified atmospheric correction is small than the other errors as it will be shown in section 3.7.3.

The introduced rate difference of ≈5×10^{-13} with the example pass (see section 3.5.1) is only half the magnitude of the LRO clock random errors (2×10^{-13}) and the missing LRO clock rate correction due to temperature variation ($4.5+3\times10^{-13}$ at max) together (≈1×10^{-12}). Furthermore the difference in rate is accumulating an offset only throughout an individual pass if conditions are changing. Contrary the random LRO clock errors and errors due to the incomplete corrections are accumulating varying offsets over the whole clock arc length (e.g. 28, 56 days or 5 years).

Table 7: Environmental conditions and resulting laser signal delay for an example laser ranging pass from GO1L station to LRO on September 14, 2009.

Time of the pass	Pressure in mbar	Temperature in K	Humidity in %	Elevation in °	Correction	
					in ns	in m
Begin	1010.0	299.65	68	53	10.3	3.09
End	1009.4	299.85	66	45	11.6	3.48
Difference	0.6	0.2	2	8	1.3	0.39
				Averaged to	**10.9**	**3.27**

Further atmospheric effects on laser ranging measurements such as attenuation, scintillation and beam wander are below the LOLA measurement precision (Dirkx et al., 2014) and thus neglected within this analysis.

3.5.2 Correction for range walk

The LOLA time tags of the received pulses are affected by a range walk bias. Due to the impulse response of the LOLA detector electronics, the shape of a recorded receive pulse is distorted which causes the trailing edge to be delayed (see Figure 12). Because the peak centroid is averaged from the leading and trailing edge at a threshold, the delay causes an offset on the receive times. Over a whole pass this correction reduces the measurement precision.

The single pulses are corrected for range walk with an empirical formula from Mao et al. (2011) via

$$\Delta t_{RWC} = 6.0 \cdot \sqrt{36.0 + P_{Station} \cdot (PW - 1)^2} \quad (5)$$

where PW is the pulse width, measured in ns and $P_{Station}$ a station correction factor. We used a series of passes to estimate an optimal empirical correction factor for each station. First a correction factor was estimated for every pass following the requirement, that the measurement precision σ_{MP} becomes minimal. From that series of optimized values, a single $P_{Station}$ was averaged for every station as listed in Table 8. Due to a different pairing and processing our values are different to the values from Mao et al. (2011).

Without the range walk correction, the measurement precision is usually around 30 to 50 cm. After applying the correction the observation data reaches the LOLA timestamp precision of 15 cm. Even though the minimal measurement precision requirement is a simplified approach for the estimation of the station parameters, it is sufficient within the empirical formula.

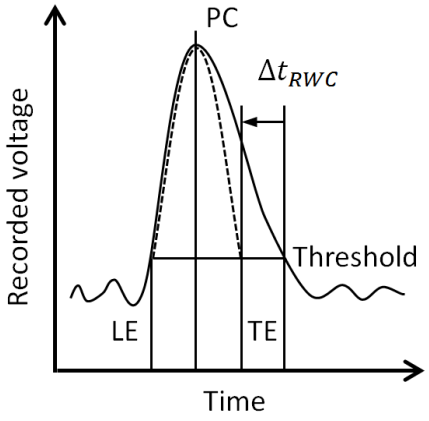

Figure 12: The receive time of a recorded pulse is taken from the Peak Centroid (PC) which is averaged from the Leading Edge (LE) and Trailing Edge (TE) at a threshold. The range walk causes the trailing edge to be delayed which results in a biased receive time. The solid line represents the distorted and the dashed line the corrected pulse.

Table 8: Estimated $P_{Station}$ values for the various ground stations.

Code	ID	$P_{Station}$
MDOL	**7080**	0.18
YARL	**7090**	0.20
GODL	**7105**	0.19
MONL	**7110**	0.21
GO1L	**7125**	0.10
HARL	**7501**	0.20
ZIML	**7810**	0.19
HERL	**7840**	0.21
GRSM	**7845**	0.19
WETL	**8834**	0.21

3.5.3 Correction for relativistic effects

The rate of a clock is influenced by the gravitational potential φ at its location and its velocity v with respect to the solar system barycenter. Since a ground station and the LRO clock are at different locations and move with different velocities, we correct the measurements for the resulting

differences due to relativistic effects. While the station fire times are converted from UTC to TDB with equation 12 from section 3.5.4, we derive a relationship between TDB and MET for the LRO clock in the following. Further information on the transformation between various time scales can be found in Kaplan (2005).

The Barycentric Coordinate Time (TCB) represents the time measured by an atomic clock located at the Solar System Barycenter. Moyer et al. (1971) describe the influence on the rate of a clock by the gravitational potential φ at the clocks location and its velocity v with respect to the solar system barycenter with the ratio

$$\frac{dt^{Clock}}{dt^{TCB}} = \left[1 - \frac{2\varphi}{c^2} - \left(\frac{v}{c}\right)^2\right]^{\frac{1}{2}} \quad \text{by using} \quad \varphi = \sum \frac{\mu_i}{r_i} = \sum \frac{G \cdot m_i}{r_i}. \tag{6}$$

Thereby c is the speed of light and φ is calculated from the gravitational parameter μ_i of the planets and their distance r_i with respect to the spacecraft. By using equation 6 the difference in rate between the LRO clock which measures MET and TCB is

$$\frac{dt^{MET}}{dt^{TCB}} = \left[1 - \frac{2\varphi_{LRO}}{c^2} - \left(\frac{v_{LRO}}{c}\right)^2\right]^{\frac{1}{2}}. \tag{7}$$

Thereby we calculate the potential at the location of the spacecraft with respect to the Solar System Barycenter with

$$\varphi_{LRO}(t) = \sum \frac{\mu_i}{|r_{i-LRO}(t)|} = \frac{\mu_{SUN}}{|r_{SUN-LRO}(t)|} + \frac{\mu_{EARTH}}{|r_{EARTH-LRO}(t)|} + \frac{\mu_{MOON}}{|r_{MOON-LRO}(t)|}. \tag{8}$$

Following (Kaplan, 2005) TDB only differs constant in rate to TCB and is defined as

$$\frac{dt^{TDB}}{dt^{TCB}} = 1 - L_b = 1 - 1.550519768 \times 10^{-8}. \tag{9}$$

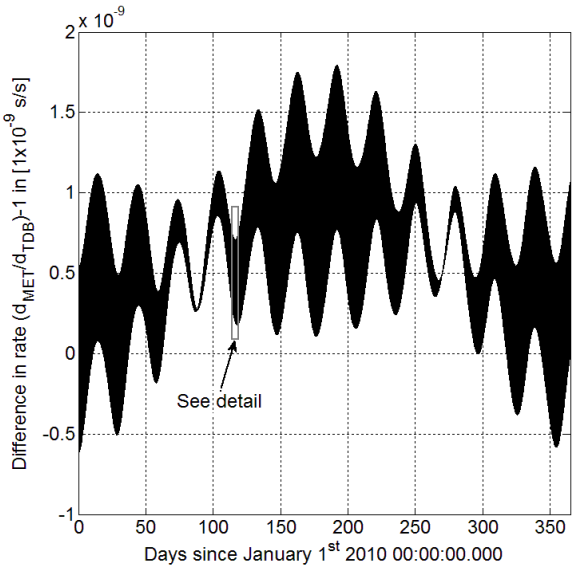

Figure 13: Normalized difference in rate between MET and TDB throughout 2010. Variations due to the orbit of LRO around the Sun and the Earth are visible.

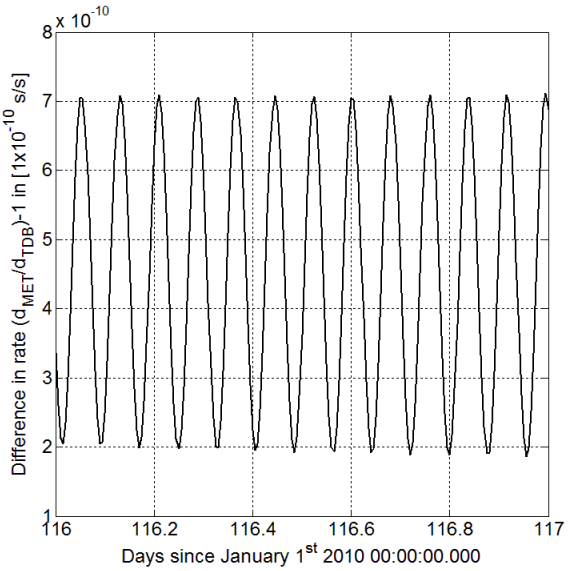

Figure 14: Detail of the normalized difference in rate between MET and TDB for one day. Note the different scales. Variations due to the orbit of LRO around the moon are visible.

By combining equation 7 and 9 we can describe the difference in rate between MET and TDB with the ratio

$$\frac{\frac{dt^{MET}}{dt^{TCB}}}{\frac{d\,t^{TDB}}{d\,t^{TCB}}} = \frac{dt^{MET}}{dt^{TDB}} = \frac{\left[1-\frac{2\varphi_{LRO}}{c^2}-\left(\frac{v_{LRO}}{c}\right)^2\right]^{\frac{1}{2}}}{1-L_b}. \quad (10)$$

Figure 13 shows the difference in rate plotted as $dt^{MET}/dt^{TDB} - 1$ between MET and TDB throughout the year 2010. The annual variation due to the elliptical orbit of the Earth-Moon system around the Solar System Barycenter and the 28 day variation due to the orbit of the Moon around the Earth can be identified. In addition, there is the variation due to the orbit of LRO around the Moon with a period of ≈120 min (see Figure 14). By integrating the difference in rate over time from an epoch t_e we can derive the offset between MET and TDB for a certain date t_d with

$$\Delta t_{RC} = \int_{t_e}^{t_d} \frac{dt^{MET}}{dt^{TDB}}\, dt. \quad (11)$$

3.5.4 Pairing of the fire and receive times

As the fire and receive events are recorded separately at the ground stations and on board of LRO, the two independent clock readings have to be paired in order to establish the complete range measurement. Such pairs are also called biplets within the SLR community. In case of two-way experiments such as T2L2 that carry a detector and a retroreflector such pairs are called triplets (Exertier et al., 2011).

The fire times from the stations are converted by using

$$t^{TDB} = t^{UTC} + 32.184 + \Delta t_{LS} + \Delta t_{PT} \quad (12)$$

from Kaplan (2005), where t^{TDB} is the resulting TDB time from a given UTC time t^{UTC}. Δt_{LS} is the number of leap seconds for a given year and Δt_{PT} are the periodic terms which incorporate the eccentricity of the Earth orbit and perturbations of it by other planets. The derivation of the formula and the precise calculation of the Δt_{PT} can be found in Moyer et al. (1981).

We use the nominal LRO trajectory in form of the Spacecraft and Planet Kernel (SPK) within the software SPICE to get a predicted TDB receive time t_{PRT}^{TDB} from

$$t_{FT}^{TDB} + \Delta t_{LT}^{TDB} + \Delta t_{AC} = t_{PRT}^{TDB}. \quad (13)$$

t_{FT}^{TDB} is the TDB fire time at the ground station, Δt_{LT}^{TDB} the predicted light time from the nominal LRO trajectory and Δt_{AC} the correction for atmospheric effects (see section 3.5.1). While the fire times from the station are influenced by the accuracy of the station calibration, the light time is affected by the nominal trajectory accuracy.

We calculate the MET receive time t_{RT}^{MET} from the single parts contained in the RDR files (see Figure 11) to which we apply the corrections with

$$t_{RT}^{MET} = t_{FS}^{MET} + Nr_{MiFr} * \Delta t_{MiFr} + \Delta t_{RT}^{MET} + \Delta t_{RWC} + \Delta t_{RC}. \quad (14)$$

Thereby t_{FS}^{MET} are the full MET seconds, Nr_{MiFr} the number of the minor frame, Δt_{MiFr} the length of a minor frame and Δt_{RT}^{MET} the MET receive time of a pulse after t_0. We correct for range walk Δt_{RWC} and relativistic effects Δt_{RC} as described in section 3.5.2 and 3.5.3 respectively.

The RDR files also contain the LOLA laser fire event in MET and converted with the SCLK in UTC which we further convert to TDB with equation 12. We derive a TDB converted receive time t_{CRT}^{TDB} from a MET receive time t_{RT}^{MET} by using a linear fit applied to these LOLA laser fire events. The accuracy of the SCLK conversion is ±3 ms coming from the accuracy of the SCLK (see Figure 10). Even though this accuracy is too coarse for laser ranging data analysis itself, it is sufficient for the pairing. Since a single Earth Range Gate does not record more than one laser pulse and the cycle frequency is 28 Hz, the time between consecutive receiving events is always at least ≈0.0277 s. This setup enables the unique identification of a pair even at an accuracy of ±3 ms.

We identify all converted receive times t_{CRT}^{TDB} as potential receives that range 0.1 s around a predicted receive time t_{PRT}^{TDB} for every fire time t_{FT}^{TDB} of a pass. By saying that the difference Δt_{RT}^{TDB} between the predicted and the converted receive times shall become minimal, we can find a corresponding pair with

$$\Delta t_{RT}^{TDB} = t_{PRT}^{TDB} - t_{CRT}^{TDB}. \quad (15)$$

By comparing Δt_{RT}^{TDB} for all paired shots of a pass, offsets can be detected and outliers removed in an iterative process. The derived TDB and MET link becomes more accurate after replacing the TDB converted receive times t_{CRT}^{TDB} with the predicted TDB receive times t_{PRT}^{TDB} from the nominal LRO trajectory.

Figure 15 to Figure 17 show the pairing of an observation pass from November 15, 2011 when the WETL station in Southern Germany was ranging to LRO between 00:51 and 01:24 UTC. Figure 15 shows the light time of the predicted (Δt_{LT}^{TDB}) and the paired converted receiving events ($t_{PRT}^{TDB} - t_{CRT}^{TDB}$) which have a difference of 535.3 µs on average throughout this pass. The difference shown in Figure 16 is caused by the limited SCLK accuracy. By fitting a 4th order polynomial to this difference Δt_{RT}^{TDB}, we can remove the observed offsets and trends and yield the measurement precision σ_{MP} of the laser ranging pass from the 1–σ variation as shown in Figure 17. For this particular pass we find a precision of 7.70 cm, which attests the high quality of the ranging experiment. Figure 17 also shows the measurement precision of the NP data that is averaged from the FR data as described in the next section.

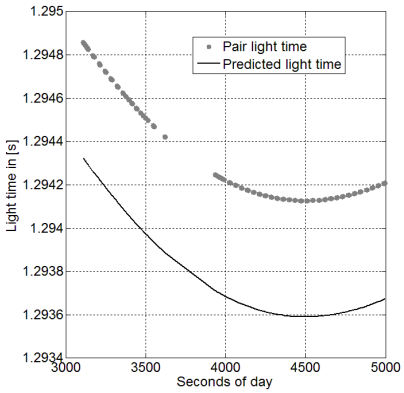

Figure 15: Light time for the prediction from the nominal LRO trajectory (line) and the paired shots that were converted with the SCLK (dots).

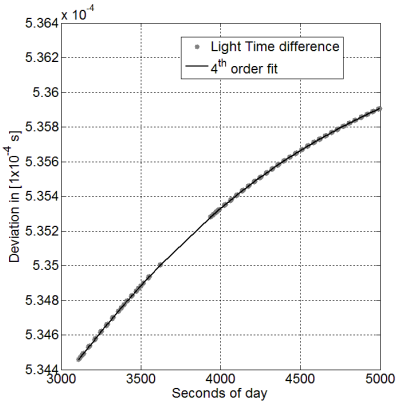

Figure 16: Difference between the light time of the prediction and the paired shots (dots). 4th order fit (solid line) added.

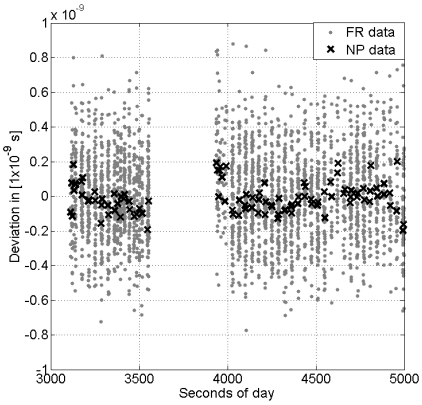

Figure 17: Deviation of the paired shots with respect to the 4th order fit from which the measurement precision is derived. Deviation is shown in dots for the FR and in asterisks for the NP data.

3.5.5 Normal Point formation

NP's are the official station data product for SLR observations within the ILRS community (Torrence et al., 1984). The formation from the FR data reduces the data amount, while improving precision and balancing station system dependent variations via an averaging. Because of these advantages we use NP's that have all corrections applied within the further applications.

Our NP's incorporate the TDB fire, the TDB predicted receive and the MET receive time. Following the NP formation guidelines of Torrence et al (1984), the observations are grouped into bins which start at midnight. As defined by the ILRS guideline for LRO, the bin length is 5 s and a NP is formed if there is more than 1 observation per bin (ILRS website, 2016). We use the TDB predicted receive times for the binning and group the MET receive times accordingly in order keep up the previously derived pairing.

In case of the example pass the measurement precision σ_{MP} reduces from 7.70 to 2.60 cm and the number of paired shots from 2791 to 104 after the averaging of the FR to the NP data (see Figure 17). The reduction of the data volume simplifies the processing of a larger number of passes in further applications.

3.6 Data analysis methods

This section describes how we utilize single, multiple and simultaneous passes to derive the experiment and ground station performance, characterize the LRO clock and the ground station clock differences by time transfer. We model the LRO and the ground station clock differences with polynomial fits after applying the corrections to the measurements.

3.6.1 Single-pass analysis

We analyze the single passes of the dataset regarding the criteria described in the following and shown in Figure 18. From the overall or per station averaged values we derive the statistical experiment and the station performance respectively. The measurement precision σ_{MP} is derived from the 1–σ variation of the receive times as described in section 3.5.4.

From the number of fired shots Nr_{FS} and the pass length Δt_{PL} we get the station fire frequency

$$f_{SF} = {Nr_{FS}}/{\Delta t_{PL}}. \quad (16)$$

With the number of paired shots Nr_{PS} and the pass length Δt_{PL} we get the paired shots per second as a frequency via

$$f_{PS} = {Nr_{PS}}/{\Delta t_{PL}}. \quad (17)$$

We calculate the ratio between the number of fired and paired shots with

$$Rat_{PtFS} = {Nr_{PS}}/{Nr_{FS}}. \quad (18)$$

Further we characterize the LRO clock from the single-passes by applying a first order linear fit $f_{Single-pass}$ on the TDB and MET receiving times from which we measure the parameters offset $\Delta\tau^{(0)}_{Single-pass}$and rate $\Delta\tau^{(1)}_{Single-pass}$ with

$$t^{MET} - t_0^{MET} = f_{Single-pass}(t^{TDB}) = \sum_{i=0}^{1} \Delta\tau^{(i)}_{Single-pass} \times (t^{TDB} - t_0^{TDB})^i. \quad (19)$$

We use the paired measured MET and predicted TDB receive times for t^{MET} and t^{TDB} respectively with t_0^{MET} and t_0^{TDB} being their reference epoch respectively.

We do not estimate the higher order parameters clock parameters aging $\Delta\tau^{(2)}_{Single-pass}$ and its change $\Delta\tau^{(3)}_{Single-pass}$ from single passes since they are too short. While a single pass is ≈33 minutes long on average (see section 3.7.1), the LRO clock aging value is around 1.6x10^{-12} /day^2 over all mission phases (see section 3.7.2). This aging value causes an offset of 71 ps over the length of an average pass which is equivalent to 2.1 cm. Since this offset is below the LOLA time stamp precision the higher order parameters cannot be measured from the single passes directly but from the long term change of the rate.

The LRO clock parameters estimated from the single passes are affected by random errors of the LRO clock, the incomplete corrections as well as by errors from the nominal LRO trajectory. Systematics and trends on the predicted receive times from the nominal trajectory as well as on the predicted and the measured receive times from the random LRO clock errors and the incomplete corrections over a single pass introduce errors on the estimated LRO clock parameters.

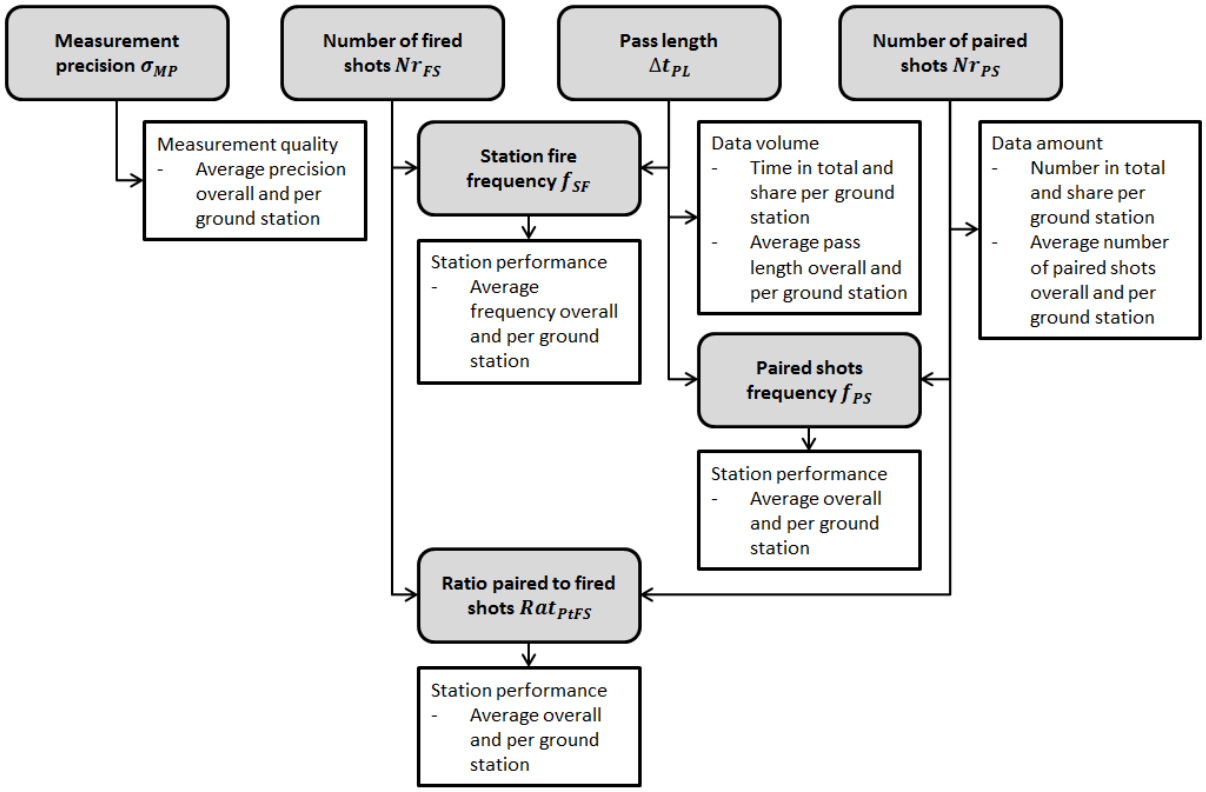

Figure 18: Single pass analysis criteria and derived properties.

3.6.2 Multiple-pass analysis

Beside the single-pass analysis, we use a 3rd order polynomial fit applied to multiple passes consecutive in time to approximates the actual LRO clock trend as shown in Figure 19. We characterize the LRO clock by estimating its parameters offset, rate, aging and its change from the fit and the ground station clock differences from the pass residuals with respect to it (ground to ground time transfer). Further the fit provides referencing of the MET to the TDB time scale (ground to space time transfer) similar to the SCLK (see section 3.2 and Figure 19).

The timeframe over which we apply the fit typically is one mission phases (≈28 d) since the nominal LRO trajectory is grouped accordingly. Changes of the LRO clock rate due to external effects can further shorten the timeframe. If the fit is applied over longer timeframes (e.g. multiple mission phases) the pass residuals will feature jumps due to the grouping of the nominal trajectory.

The 3rd order fit provides the offset $\Delta\tau^{(0)}_{Multi-pass}$, the rate $\Delta\tau^{(1)}_{Multi-pass}$, the aging $\Delta\tau^{(2)}_{Multi-pass}$ and its change $\Delta\tau^{(3)}_{Multi-pass}$via

$$t^{MET} - t_0^{MET} = f_{Multi-pass}(t^{TDB}) = \sum_{i=0}^{3} \Delta\tau^{(i)}_{Multi-pass} \times (t^{TDB} - t_0^{TDB})^i \quad (20)$$

As within equation 23 we use the paired measured MET and predicted TDB receive times for t^{MET} and t^{TDB} respectively. A manual editing is used to remove outlying passes while applying the fit.

Furthermore we characterize the differences between the ground station clocks in time and rate from the pass residuals of common view observations with respect to the fit as shown in Figure 20 (ground to ground time transfer). The relative offsets and rates between simultaneous passes (e.g. from $GS1$ and $GS2$ in Figure 20) are derived from the difference between the estimated offsets with

$$\Delta\tau^{(0)}_{Multi-pass\ GS1\ GS2} = \Delta\tau^{(0)}_{GS1} - \Delta\tau^{(0)}_{GS2} \quad (21)$$

and the rates with

$$\Delta\tau^{(1)}_{Multi-pass\ GS1\ GS2} = \Delta\tau^{(1)}_{GS1} - \Delta\tau^{(1)}_{GS2}. \quad (22)$$

Even though the fit features jumps if applied over more than one mission phase, it allows to monitor the long term station timing behavior with respect to each other.

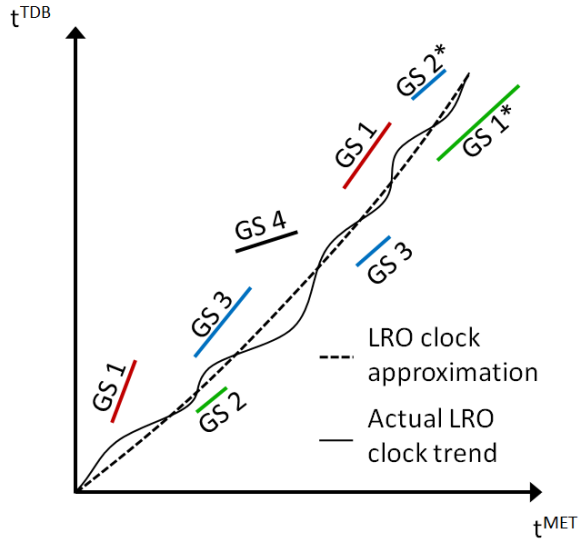

Figure 19: Approximation of the actual LRO clock trend from multiple passes and their individual TDB and MET links, different ground stations (GS) are indicated by their labels, solid line represents the actual LRO clock trend and the dashed line the approximation from the 3rd order fit. The passes marked with an * are simultaneous passes (common-view observations).

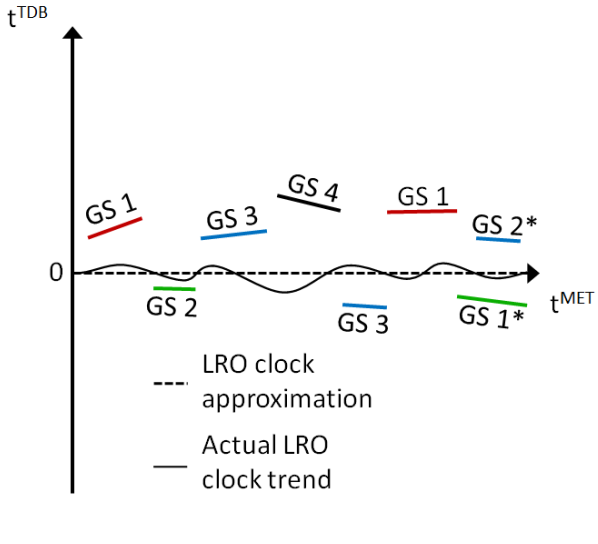

Figure 20: Residuals of multiple passes with respect to the LRO clock approximation (dashed line), from which relative offsets and rates between the ground station passes can be derived. The actual LRO clock trend is added for comparison. The passes marked with an * are simultaneous passes (common-view observations).

The approximation from the 3rd order fit does not exactly represent the actual LRO clock trend (see Figure 19 and Figure 20). Deviations between the approximation and the actual LRO clock trend can be seen in the post-fit measurement residuals. Remaining trends and systematics in the residuals are caused by random LRO clock errors, incomplete corrections and the nominal LRO trajectory.

Pass residuals which we also use for the analysis of ground station clock differences during SM02 and SM03 in section 3.7.3, are shown in Figure 24. Table 9 provides an overview about the characteristics (accuracy from the 1–σ variation of the residuals, length as well as data coverage) of fits we applied during the mission phases SM02 and SM03 (see section 3.7.2 and 3.7.3). Since the reported accuracy of the nominal trajectory (9 m≈30 ns) is more than 5 times smaller than the accuracy of the fits, the random errors of the LRO clock and the errors from the incomplete corrections are larger.

To a certain extent random errors and missing corrections can be compensated by the polynomial fit. But the long-term approximation cannot cover all short-term variations due to the limited order of the fit. However due to the averaging of the fit the referencing of MET to TDB is possible even with data gaps of up to 3 and 5 days (see Table 9). Even though the approximation of the actual LRO clock trend is probably even less good during the data gaps compared to when observation data is available, the continuous coverage is provided.

Even though the long-term approximation does not represent the short term variations of the LRO clock very well, ground station clock differences can be measured from common view observations. The differences are thereby less affected from LRO clock approximation, orbit, random LRO clock and correction errors than the referencing itself. In an ideal case the errors would cancel out during a common-view observation (see section 3.6.3 as well as Figure 19 and Figure 20). However some errors are present within the multiple-pass analysis and affect the measurements from common-view observations (see section 3.7.3). The measurement of differences from consecutive passes (non-common view time transfer) becomes unfeasible since too many errors are accumulating between passes. Furthermore the nominal LRO trajectory error (30 ns) was at the order of magnitude of the ground station clock differences in some cases (see section 3.7.3), limiting the validity of the measured values.

Table 9: Laser data coverage and pass residuals with respect to the 3rd order polynomial fits that were applied during the mission phases SM02 and SM03.

Mission phase	**SM02**	**SM03**
Length in days	28	26
Number of selected passes	66	88
Average gap between consecutive passes in h	9.16	5.94
Largest gap between consecutive passes in d	≈5	≈3
Pass residuals with respect to the fit from their 1–σ variation in ns	170.97	160.08

3.6.3 Simultaneous passes

While usually one station is scheduled to range to LRO at a time, also simultaneous ranging by multiple stations is possible, as long as all stations are in the field of view of the receiver. These common-view observations allow the measurement of timing differences (time transfer) of the participating ground station clocks. The measured differences are thereby insensitive to orbit and LRO clock errors and are resolved at the LOLA time stamp precision of 500 ps (Sun et al., 2013b).

In total we saw approximately 1215 simultaneous sessions within our dataset consisting of two or more stations ranging to LRO. For ≈52 % of them the time in between consecutive simultaneous passes was less than 0.5 days (≈5 LRO orbits). For 26 % the time in between them was 0.5 to 1.5 days and for the other 21 % 1.5 to 25 days. Almost all of the simultaneous passes were carried out between US stations. Because of the limited Field Of View of the Laser Ranging Telescope and the required pointing of the high gain communication antenna towards White Sands ground station simultaneous passes between US, EU and even Australian stations are mostly unfeasible.

Figure 21 shows a simultaneous pass from the ground stations 7125 (GO1L) and 7110 (MONL) on November 29th, 2010 at 14:28 UTC. LOLA itself cannot distinguish the laser pulses coming from different stations and the first pulse in the Earth range gate closes it. We pair the fire and the receive times as described in section 3.5.4 and apply all corrections. We use 4th order polynomial fits (f_{GS1} and f_{GS2}) on the paired predicted TDB and measured MET receive times of the passes from both stations. These fits provide links between MET and TDB for both ground stations with

$$t^{TDB}_{PRT\,GS1} = f_{GS1}(t^{MET}_{RT}) \text{ and } t^{TDB}_{PRT\,GS2} = f_{GS2}(t^{MET}_{RT}). \quad (23)$$

Here and in the following all TDB and MET times from the passes are normalized with t_0^{TDB} and t_0^{MET} derived from the pass starting first as in equation 19 and 20.

Both fits (f_{GS1} and f_{GS2}) contain the signatures of the LRO clock as well as the respective ground station clock errors. Since the stations ranged to LRO simultaneously the difference between the LRO clock signatures contained within both fits is negligible. This fact implies that the variation of the LRO clock rate due to temperature change has no effect when measuring ground station clock differences from simultaneous passes. We thus measure the difference between the ground station clocks from the remaining differences after we corrected for the local atmospheric influence at the stations. Since incoming pulses cannot be detected concurrently by LOLA we derive the difference between the TDB times referenced to the same MET times from the fits via

$$\begin{aligned} f_{GS1}(t^{MET}) - f_{GS2}(t^{MET}) &= t^{TDB}_{RRT\,GS1} + \Delta t^{TDB}_{RRT\,GS1} - t^{TDB}_{RRT\,GS2} - \Delta t^{TDB}_{RRT\,GS2} \\ &= \; t^{TDB}_{RFT\,GS1} + \Delta t^{TDB}_{RFT\,GS1} + \Delta t^{TDB}_{LT\,GS1}(t^{TDB}_{RFT\,GS1} + \Delta t^{TDB}_{RFT\,GS1}) \\ &\quad -t^{TDB}_{RFT\,GS2} - \Delta t^{TDB}_{RFT\,GS2} - \Delta t^{TDB}_{LT\,GS2}(t^{TDB}_{RFT\,GS2} + \Delta t^{TDB}_{RFT\,GS2}). \end{aligned} \quad (24)$$

The TDB fire times t^{TDB}_{FT} from the stations are affected by clock offsets and we separate them into a real TDB fire time and an offset due to the station clock offset ($t^{TDB}_{RFT} + \Delta t^{TDB}_{RFT}$). Analogously we separate the predicted receive time t^{TDB}_{PRT} into a real TDB receive time and an offset propagated from the ground station clock offset ($t^{TDB}_{RRT} + \Delta t^{TDB}_{RRT}$).

The predicted TDB light time ($\Delta t^{TDB}_{LT}(t^{TDB}_{RFT} + \Delta t^{TDB}_{RFT})$) that we get from the nominal LRO trajectory is affected by the station offsets as well. Assuming a typical ground station offset of 100 ns and an orbital LRO velocity of ≈1 km/s we see that the spacecraft is moving 0.1 mm during such a time interval. Since this distance is equivalent to a difference of ≈0.3 ps in the light time, the influence of the ground station clock offsets on the predicted light time is negligible.

We regroup equation 24 for the difference of the ground station clocks, derive the predicted TDB light time $\Delta t^{TDB}_{LT\,GS1}(t^{TDB}_{RFT\,GS1})$ only from the real TDB fire time and get

$$\begin{aligned} \Delta t^{TDB}_{RFT\,GS1} - \Delta t^{TDB}_{RFT\,GS2} = &-t^{TDB}_{RFT\,GS1} - \Delta t^{TDB}_{LT\,GS1}(t^{TDB}_{RFT\,GS1}) + t^{TDB}_{RRT\,GS1} + \Delta t^{TDB}_{RRT\,GS1} \\ &+t^{TDB}_{RFT\,GS2} + \Delta t^{TDB}_{LT\,GS2}(t^{TDB}_{RFT\,GS2}) - t^{TDB}_{RRT\,GS2} - \Delta t^{TDB}_{RRT\,GS2}. \end{aligned} \quad (25)$$

The difference of the real TDB fire time (t_{RFT}^{TDB}) plus the real predicted TDB light time ($\Delta t_{LT}^{TDB}(t_{RFT}^{TDB})$) to the real TDB receive time (t_{RRT}^{TDB}) is zero for both stations. Further the difference between the real predicted TDB receive times ($t_{RRT\ GS1}^{TDB} - t_{RRT\ GS2}^{TDB}$) in equation 24 is zero since perfectly synchronized clocks would provide identical MET to TDB links. With that we can simplify equation 25 to

$$f_{GS1}(t^{MET}) - f_{GS2}(t^{MET}) = \Delta t_{RRT\ GS1}^{TDB} - \Delta t_{RRT\ GS2}^{TDB} = \Delta t_{RFT\ GS1}^{TDB} - \Delta t_{RFT\ GS2}^{TDB}. \quad (26)$$

Thus the real ground station clock differences are equivalent to the modelled differences between predicted TDB receive times that are referenced to the same MET receive times via the fits (when assuming perfect ground station clocks in the model). We thus derive the ground station clock difference from the difference between the fits $f_{GS1}$and f_{GS2} for the same MET times. By applying a linear fit to the difference $f_{GS1}(t^{MET}) - f_{GS2}(t^{MET})$ throughout a simultaneous pass, we measure the relative offset $\Delta\tau_{Simu-pass\ GS1\ GS2}^{(0)}$ and the relative rate $\Delta\tau_{Simu-pass\ GS1\ GS2}^{(1)}$ between the ground station clocks $GS1$ and $GS2$ with

$$\Delta t_{GS}^{TDB} = \Delta t_{RRT\ GS1}^{TDB} - \Delta t_{RRT\ GS2}^{TDB} = \sum_{i=0}^{1} \Delta\tau_{Simu-pass\ GS1\ GS2}^{(i)} \times (t^{MET})^i . \quad (27)$$

Since we work in the TDB time scale, we measure the ground station clock differences in TDB.

Figure 22 shows the difference Δt_{GS}^{TDB} for the example, whereby the 7125 (GO1L) pass provides the reference t_0^{TDB} and $t_0^{MET}$for the normalization since it is the pass starting first within the example common view observation. We measured a relative offset of ≈39 ns at the beginning of the pass and a relative rate of ≈-1.9x10^{-12} between the 7125 and the 7110 station clock.

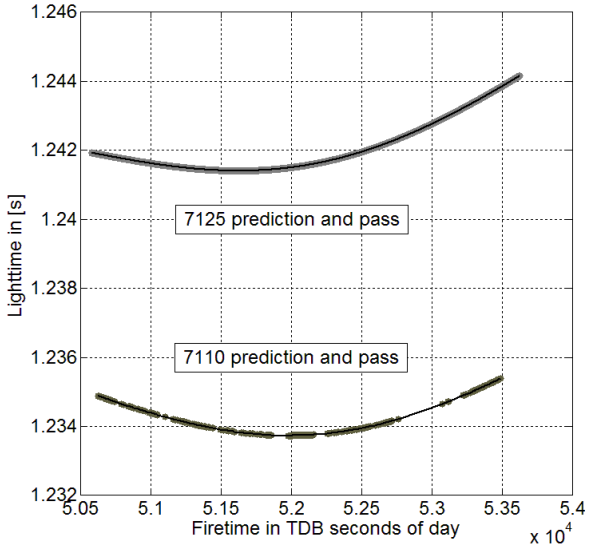

Figure 21: Predicted and paired light times for the passes from 7125 and 7110 ground station. The paired receive times for the two ground stations are both represented with the same dots to highlight the fact that the LOLA detector cannot distinguish between the station pulses.

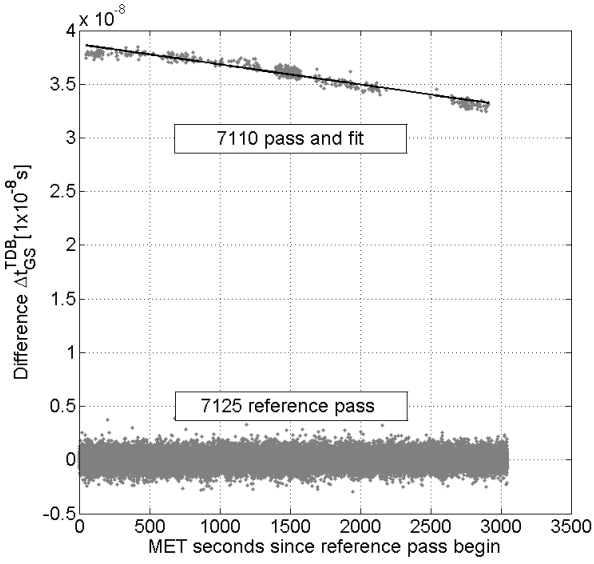

Figure 22: Difference Δt_{GS}^{TDB} of the predicted TDB receive times paired to the same MET receive times from the two ground stations. The 7125 (GO1L) pass is chosen as reference for the normalization since it is the pass starting first. A linear fit was applied to the 7110 pass to measure the timing differences.

3.7 Results

Section 3.7.1 provides the results of the statistical single-pass analysis from which we derive the experiment and the ground station performance. In section 3.7.2 we present and compare the results of the LRO clock characterization coming from the single- and the multiple-pass analysis. Section 3.7.3 presents and compares the results of the ground station clock differences, estimated from the multiple-pass and the simultaneous pass analysis. We discuss the results and draw conclusions in section 3.8.

3.7.1 Experiment and ground station performance

The laser ranging data covers a period from June 2009 until end of September 2014, including the mission phases Commissioning (CO), Nominal Mission (NO01–NO13), Science Mission (SM01–SM26) and Extended Mission (ES01–ES25). The nominal LRO trajectory coverage begins July 13, 2009, while we started to process laser ranging passes from July, 16 2009 on. Due to missing orientation data the nominal LRO trajectory has gaps in coverage during mission phase ES25 (Mazarico, personal communication). Thus our dataset covers the timeframe from June 16, 2009 until the September 10, 2014 – the end of the mission phase ES24.

Table 10 shows the statistical results for all successfully paired and analyzed passes. While the stations fired at an overall average frequency of 11.68 Hz, 2.68 shots per second could actually be paired. In comparison to the predicted number of received shots per second (see Table 4), the number of actually paired shots per second is lower for all stations. While for most stations $\approx 10\%$ of the fired shots can be paired, GO1L achieves a ratio Rat_{PtFS} of ≈49% due to the synchronized firing to LOLA in frequency and phase. While the number of paired shots (6427 per pass on average) is heavily varying from station to station, the NP formation reduces (241 per pass on average) and balances the number of paired shots between the stations. The average pass length Δt_{PL} is ≈33 min.

Altogether we successfully paired a total number of 64.9 million FR observations which got averaged to 1.6 million NP observations – a reduction by a factor of ≈41.7. With the averaging of the paired FR shots to one NP every five seconds for every station, their paired shot shares become more balanced regardless their fire frequency.

We retrieved a total volume of 3120.44 h of FR and 2918.13 h of NP data. The NP data volume is smaller than the FR data volume, because NP's were only formed when there was more than 1 observation per bin (see section 3.5.5). Further we only processed and analyzed passes that had more than 50 shots in case of the FR and more than 20 shots in case of the NP data. The largest share of tracking data in time comes from stations located in the US with ≈74%, while YARL station in Australia provides ≈20% and the EU stations ≈5%.

The overall average measurement precision σ_{MP} of 12.3 cm confirms and even supersedes the LOLA time stamp accuracy of 15 cm and demonstrates the good precision of the one-way laser ranging data. With the NP formation the precision gets improved by a factor of 2.2 to 5.6 cm. The MOBLAS stations show similar performance with f_{SF}, Rat_{PtFS} and σ_{MP} due to their similar equipment.

The shares of data volume we derived per station agree with values reported by McGarry et al. (2011) and Mao et al. (2014a) – see Table 11. We derived a different total volume than McGarry et al. (2011) since they analyzed the data early on during the experiment. Further our volume is different to Mao et al. (2014a) because of a different processing.

Table 10: Dataset statistics for the ground stations that range to LRO for the FR and the NP data. The overall and per station averaged values provide the experiment and the ground station performance.

ID / Station / Criteria	Type of data	7080 MDOL	7090* YARL	7105* GODL	7110* MONL	7125 GO1L	7501* HARL	7810 ZIML	7840 HERL	7845 GRSM	8834 WETL	Total or Average	Ratio
Station fire frequency in Hz	**FR**	8.74	9.95	9.12	9.49	26.81	9.52	11.34	13.06	7.93	10.77	**11.68**	**4.36**
Paired shots frequency in Hz	**FR**	0.76	1.10	0.93	1.25	13.14	0.74	2.98	3.98	0.86	1.09	**2.68**	
Ratio of paired to fired shots in %	**FR**	8.6	11.4	10.1	13.1	48.8	7.8	26.4	30.3	11.0	11.0	**17.8**	-
Total pass length w.r.t. to total amount of observation data in %	**FR**	10.33	20.30	6.49	24.70	32.96	0.90	1.52	0.47	2.06	0.27	**3120.44 h**	**1.07**
	NP	10.10	19.89	6.12	24.64	34.23	0.83	1.50	0.48	1.92	0.27	**2918.13 h**	
Average pass length in s	**FR**	1846	1776	2651	2557	2431	1831	1294	1637	1566	2041	**1963**	-
Measurement precision in cm	**FR**	9.5 ± 3.1	9.1 ± 1.9	11.6 ± 4.5	11.3 ± 4.8	18.3 ± 4.1	8.6 ± 2.3	7.8 ± 0.8	27.4 ± 10.6	9.7 ± 4.8	9.9 ± 7.7	**12.3±4.5**	**2.20**
	NP	5.5 ± 3.1	3.8 ± 1.7	7.4 ± 5.3	7.5 ± 5.6	8.3 ± 5.3	4.0 ± 1.4	2.2 ± 0.8	7.8 ± 3.8	3.9 ± 1.6	5.7 ± 10.4	**5.6±3.9**	
Nr. of paired shots w.r.t. total Nr. of shots in %	**FR**	1.49	4.40	1.21	5.89	85.11	0.13	1.03	0.35	0.33	0.06	**64865805**	**41.61**
	NP	6.70	18.97	5.05	25.4	39.88	0.53	1.34	0.57	1.46	0.11	**1558657**	
Average Nr. of paired shots per pass	**FR**	1538	2223	2850	3522	36248	1506	5064	7117	1438	2764	**6427**	**26.67**
	NP	179	241	301	378	418	164	167	275	168	117	**241**	

*) MOBLAS station

Table 11: Laser ranging data volumes reported from different Authors.

Values from	MDOL	YARL	GODL	MONL	GO1L	HARL	ZIML	HERL	GRSM	WETL	Total in hours
This work	10.10	19.89	6.12	24.64	34.23	0.83	1.50	0.48	1.92	0.27	**2918.13**
McGarry et al. (2013)	11	15	9	28	33	1	1	1	1	<1	**3448.08**
Mao et al. (2014a)	10.91	14.31	7.78	28.58	32.71	0.76	1.48	1.46	1.90	0.12	**4173.60**

3.7.2 LRO clock analysis

We characterized the LRO clock by estimating its offset $\Delta\tau^{(0)}$, rate $\Delta\tau^{(1)}$, aging $\Delta\tau^{(2)}$ and its change $\Delta\tau^{(3)}$ on a single- and a multiple-pass basis as described in section 3.6.1 and 3.6.2 with data from the mission phases CO until ES24.

To compare the estimated parameters from both approaches the results from the single pass analysis were grouped and averaged mission phase wise as the fits were applied within the multiple-pass analysis. In order to derive the higher order parameters aging and its change from the single pass analysis, a 2nd order polynomial fit was applied to the estimated rates. Within some mission phases external events like solar flares influenced the clock and we further split the timeframe during one mission phase over which we apply the multiple-pass analysis fits. The single-pass analysis results were then grouped accordingly. Due to the grouping of the single-pass LRO clock parameters analog to the multiple-pass analysis for the comparison, the same averaging is applied. Due to that averaging, errors that affect the single-pass clock parameters (see section 3.6.1) are compensated as within the multiple-pass analysis (see section 3.6.2). Since both approaches are subject to the same random LRO clock errors, imperfect corrections and errors from the nominal trajectory, differences in the results are coming from the order of the applied fits and the averaging.

Since the ground station clocks have time biases with respect to each other, their single passes have varying time biases with respect to the mean trend of the multiple-pass analysis fit. We thus only evaluated the offset values $\Delta\tau^{(0)}$ from the multiple-pass analysis. Since they are represented in seconds at orders of 10 billion s and at LOLA timestamp precision (e.g. 35049494.9986398742 s at the beginning of ES09 and normalized to January 1, 2009 00:00:00.000) we focus on the presentation of the estimated rate, the aging and its change.

The estimated rate is shown and listed normalized via $\Delta\tau^{(1)} - 1$ in all figures and tables. Figure 23 shows the LRO clock rate $\Delta\tau^{(1)} - 1$ estimated from both approaches, as well as the effect of the relativistic corrections. Variations with an annual monthly and orbital period (120 min) were detected in the LRO clock rate due to relativistic effects. The corrected clock rates from the single- and multiple-pass analysis follow the same trend and show identical behavior regarding changes and jumps.

Table 15 and Table 16 (supplementary material) provide the clock parameters rate, aging and its change estimated from both approaches and their differences for all mission phases (CO until ES24). Averaged clock parameters and their differences are given in Table 12.

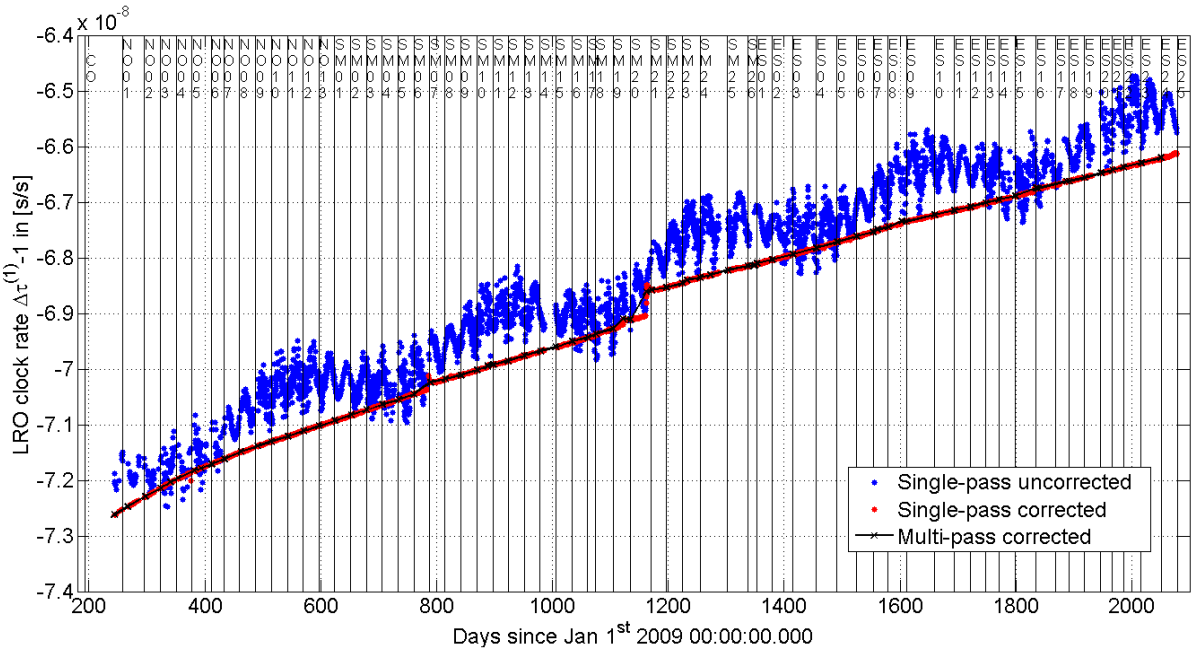

Figure 23: Estimated LRO clock rate $\Delta\tau^{(1)} - 1$ on a single-pass basis uncorrected (blue dots) and corrected for relativistic effects (red dots). The LRO clock rate estimated from the multiple-pass analysis is represented by the black line with crosses for the data points. The various mission phases are marked by the vertical lines along with their names.

The overall mean LRO clock rate is ≈8500 times larger than the 1–σ variation of the differences between the two approaches. Because of large changes in the LRO clock rate due to external influences during SM19 and SM20 (see Figure 23), the differences of the parameters are larger than during other mission phases.

The overall mean aging value is ≈1.4 times larger than the 1–σ variation of the differences. For the change of the aging the overall mean value is ≈3.9 times smaller than the 1–σ variation of the differences (see Table 12).

Table 12: LRO clock parameters estimated from single- and multiple-pass analysis and their differences. The results from Table 15 and Table 16 (supplementary material) were averaged over the mission phases as listed.

	Day	Single-pass analysis			Multiple-pass analysis			1–σ variation of the differences		
Averaged Mission phase	**since Jan 1st 2009**	$\Delta\tau^{(1)} - 1$ **10^{-8}**	$\Delta\tau^{(2)}$ **10^{-12} /day**	$\Delta\tau^{(3)}$ **10^{-14} /day²**	$\Delta\tau^{(1)} - 1$ **10^{-8}**	$\Delta\tau^{(2)}$ **10^{-12} /day**	$\Delta\tau^{(3)}$ **10^{-14} /day²**	$\Delta\tau^{(1)}$ **10^{-12}**	$\Delta\tau^{(2)}$ **10^{-12} /day**	$\Delta\tau^{(3)}$ **10^{-14} /day²**
CO	250.87	-7.2627	4.41	-2.99	-7.2624	3.77	-0.13	-2.93	0.65	-2.87
NO01–NO13	435.85	-7.1692	2.08	0.63	-7.1692	2.26	-1.12	6.85	0.49	2.13
SM01–SM26	1014.92	-6.9468	1.58	-5.06	-6.9469	2.07	-8.61	10.55	1.59	10.99
ES01–ES24	1725.63	-6.7103	1.11	-1.05	-6.7103	0.99	-1.96	5.22	0.76	9.07
CO–ES24	**1144.77**	**-6.9103**	**1.54**	**-1.69**	**-6.9104**	**1.75**	**-2.99**	**8.11**	**1.18**	**9.20**
Averaged from both approaches during CO-ES24: rate, aging, change of aging								**-69103.5**	**1.64**	**-2.34**

The higher order terms aging $\Delta\tau^{(2)}$ and its change $\Delta\tau^{(3)}$ describe smaller changes than the rate (see section 3.6.1) and are thus more sensitive to uncertainties. Since the nominal LRO trajectory is an averaged result from an orbit determination, the estimated parameters are affected by the inherent state errors. The precision of the estimated parameters is limited by the accuracy of the trajectory, the corrections and random LRO clock errors. The accuracy of the aging and the change of the aging depend on the length of timeframe over which they are averaged – e.g. one pass or one mission phase.

Our LRO clock rate agrees with the rate of Mao et al. (2014a) except for a small offset due to the selected reference. While we estimate our parameters with respect to TDB, Mao et al. (2014a) estimated them with respect to the GO1L clock.

The fit from the multiple-pass analysis provides a referencing of the TDB and the MET time scale similar to the SCLK-based conversion (ground to space time transfer). We estimate the accuracy of this referencing from the 1–σ variation of the pass residuals with respect to the averaged trend (see Figure 20, Table 9 and Figure 24). The 1–σ variation of the pass residuals over both mission phases SM02 and SM03 is 166.25 ns. This value supersedes the accuracy of the SCLK based conversion by a factor of ≈18000. When analyzing the residuals throughout all processed mission phases (CO–ES24), we achieved a 1–σ variation of 256.07 ns, which is ≈11700 times better than the accuracy of the SCLK based conversion. For this result many GO1L passes were manually edited along with other outliers due to offsets at the 10 µs magnitude with respect to the other ground station clocks. Since the accuracy of the nominal LRO trajectory is reported to be 30 ns (9 m at the arc overlaps) its influence on the accuracy of the referencing is smaller than the random LRO clock errors and the errors from the incomplete corrections. These errors are compensated by the averaging of the 3rd order fit to some extent. The accuracy of the estimated LRO clock parameters and the TDB and MET link (ground to space time transfer) demonstrate the potential of the laser ranging data for these applications.

3.7.3 Ground station clock analysis from time transfer

We used both the multiple-pass analysis and the simultaneous pass analysis to derive the timing differences between ground station clocks. We measured the relative offsets $\Delta\tau^{(0)}_{GS1\ GS2}$ and rates $\Delta\tau^{(1)}_{GS1\ GS2}$ with both approaches and compare their results.

We chose the mission phases SM02 and SM03 for a comparison, because we found good coverage with simultaneous passes between the three stations 7080 MDOL, 7110 MONL and 7125 GO1L. We focused on these three US stations due to limited coverage of simultaneous passes with other stations. During that timeframe we successfully paired eleven passes between two and five passes between three of the ground stations. The simultaneous passes from three stations were handled like three simultaneous passes from two stations. Within the multiple-pass analysis fit we used the single passes from one station as well as all simultaneous passes from two or three stations. In order to enable a direct comparison of the two methods we only compared timing differences at simultaneous passes (common-view time transfer).

Figure 24 and Figure 25 show the relative offsets derived with multiple-pass and the simultaneous pass analysis respectively. Table 13 lists the values we measured for each ground station combination on two dates. Accordingly Figure 26 and Figure 27 show the relative rates while the measured values are listed in Table 14 similarly. The passes selected for the comparison are highlighted and numbered from 1 to 6 in the figures and the tables.

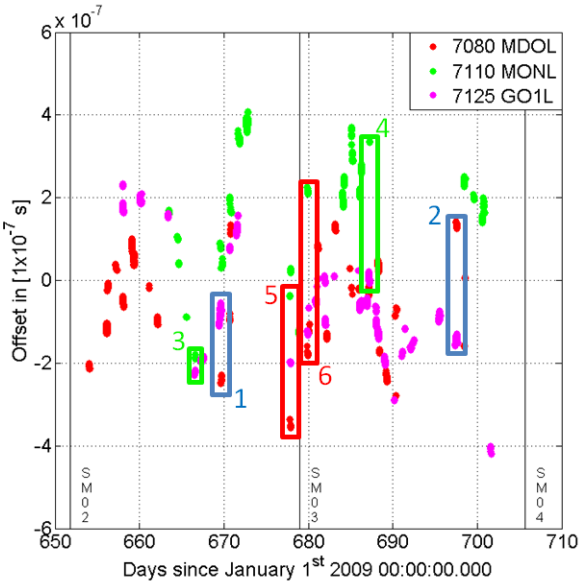

Figure 24: Relative ground station offsets $\Delta\tau^{(0)}_{Multi-pass\ GS1\ GS2}$ measured from the time residuals with respect to the averaged trend from the multiple-pass analysis. The boxes highlight the data from two ground stations which were used to estimate the relative offset. The measured values can be found via their numbers in Table 13.

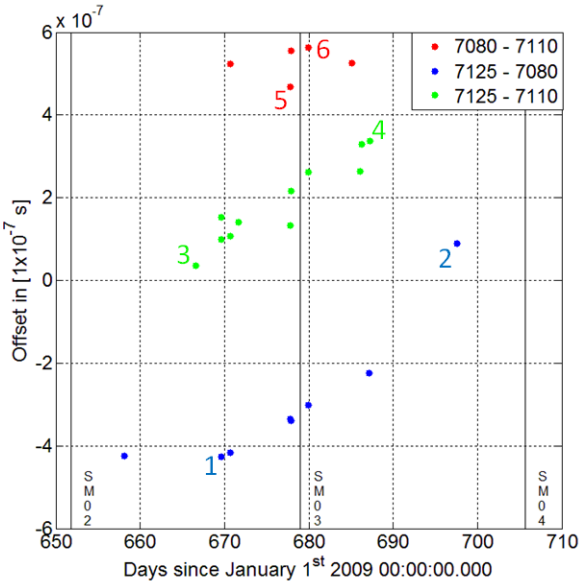

Figure 25: Relative ground station offsets $\Delta\tau^{(0)}_{Simu-pass\ GS1\ GS2}$ measured from the simultaneous passes. The measured values can be found via their numbers in Table 13. All relative offsets measured from the simultaneous passes increase over time.

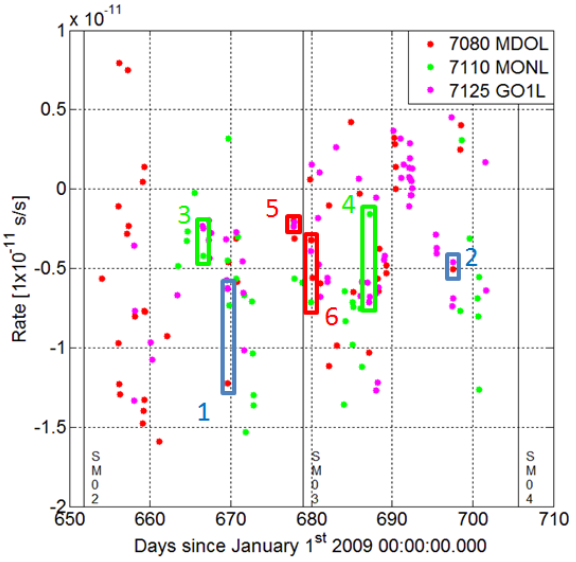

Figure 26: Relative ground station rates $\Delta\tau^{(1)}_{Multi-pass\ GS1\ GS2}$ measured from the rate residuals with respect to the averaged trend from the multiple-pass analysis. The boxes highlight the data from two ground stations which were used to estimate the relative offset. The measured values can be found via their numbers in Table 14.

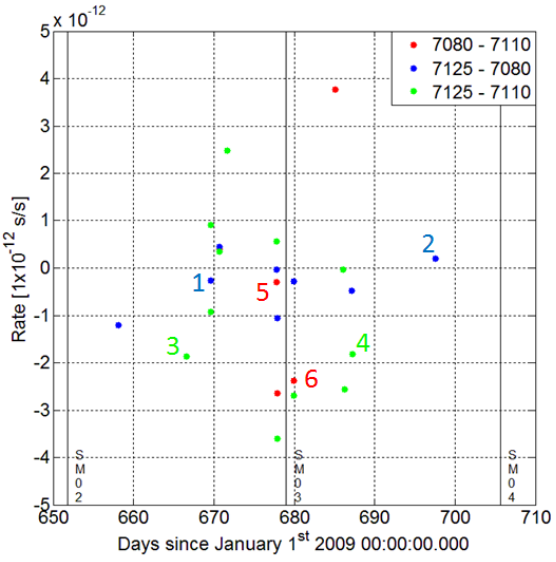

Figure 27: Relative ground station rates $\Delta\tau^{(1)}_{Simu-pass\ GS1\ GS2}$ measured from the simultaneous passes. The measured values can be found via their numbers in Table 14

Table 13: Comparison of relative ground station (GS) clock offsets $\Delta\tau^{(0)}_{GS1\ GS2}$ measured from the multiple-pass and the simultaneous pass analysis.

Station combination		Days since Jan 1st 2009	Nr.	Relative GS offset in ns measured from		Ratio
GS 1	GS 2			Multiple-pass analysis	Simultaneous pass	
GO1L 7125	MDOL 7080	669.7	1	-190	-430	+2.26
		697.5	2	+280	+90	+3.11
GO1L 7125	MONL 7110	666.6	3	+33	+35	+1.06
		687.2	4	+340	+340	+1.00
MDOL 7080	MONL 7110	677.8	5	+300	+470	+1.57
		679.9	6	+400	+560	+1.40

During the selected timeframe we measured relative ground station clock offsets $\Delta\tau^{(0)}_{GS1\ GS2}$ between 33 ns and 560 ns (Table 13). The offsets estimated with the two approaches agree quite well for the two ground stations 7125 GO1L and 7110 MONL (Nr. 3 and 4) and less good for the station combination 7080 MDOL and 7110 MONL (Nr. 5 and 6). The station combination 7125 GO1L and 7080 MDOL showed the largest difference (Nr. 1 and 2).

We measured the relative rates $\Delta\tau^{(1)}_{GS1\ GS2}$ between the ground station clocks to values between $2\text{x}10^{-13}$ and $6\text{x}10^{-12}$ during the selected timeframe (see Table 14). The relative rates agree less good than the relative offsets because they are more sensitive to uncertainties the nominal LRO trajectory and from the corrections. The measured values basically agree with the stability values Cash et al. (2008) reported for the timing systems that are utilized at the ground stations (see Table 4 and Table 5).

Overall simultaneous passes are more suitable for measuring the differences than the multiple-pass analysis since they are less affected by uncertainties. LRO clock and orbit errors do not affect the accuracy of the ground to ground time transfer (Sun et al., 2013b) which only leaves local differences between the ground stations, coming from their clocks and local atmospheric conditions. Thus they allow for direct ground to ground time transfer at an accuracy of at least 500 ps (LOLA timestamp accuracy). However there needs to be frequent coverage with simultaneous passes between all ground stations for continuous monitoring of their differences.

While the values from the multiple-pass analysis are affected by random LRO clock, correction and orbit errors, the fit provides better coverage for monitoring the station timing behavior. Even stations from different continents, which are too much separated for simultaneous ranging, could be analyzed. However due to the limited stability of the LRO clock ($2\text{x}10^{-13}$ over 10000 s, results in 480 ns which is ≈145 m over 28 days, one mission phase) the measurement of timing differences in non-common view is not very accurate since it becomes subject of too much interpretation (see Figure 23).

In order to quantify the effect due to variations of the local atmospheric condition between the stations, we estimated the 1–σ variation of the tropospheric corrections around its mean value for all single and simultaneous passes during SM02 and SM3. Since the 1–σ variation of 8.26 ns around a mean value of 18.1 ns is smaller than the relative offsets themselves, the differences between the stations due to local atmospheric conditions are small.

Table 14: Comparison of relative ground station (GS) rates $\Delta\tau^{(1)}_{GS1\ GS2}$ measured from the multiple-pass and the simultaneous pass analysis.

Station combination		Days since Jan 1st 2009	Nr.	Relative GS rate diff. in 1x10^{-12} measured from		Ratio
GS 1	GS 2			Multiple-pass analysis	Simultaneous pass	
GO1L	MDOL	669.7	1	-5.97	-0.26	+23.23
7125	7080	697.5	2	-0.42	+0.20	-2.16
GO1L	MONL	666.6	3	-1.72	-1.88	+1.09
7125	7110	687.2	4	+5.24	-1.82	-2.88
MDOL	MONL	677.8	5	-0.31	-0.31	+1.03
7080	7110	679.9	6	-3.91	-2.37	+1.65

3.8 Discussion and conclusion

International Laser Ranging Service ground stations performed one-way laser ranging to NASA's Lunar Reconnaissance Orbiter in orbit around the Moon. These measurements complement the radio and the altimetric crossover observations with an additional type of tracking data.

By using the nominal LRO trajectory, we pair and analyze the one-way laser ranging data. The paired predicted and measured receive times provide a link between the TDB and the MET time scale. We apply various corrections on both the predicted and the measured receive times. The results of our processing and analysis are affected by the random errors of the LRO clock, the completeness of the corrections and the errors of the nominal LRO trajectory. The random LRO clock errors and the errors due to the incomplete corrections affect the approximation of the LRO clock with the polynomial fits and with that the estimated LRO clock parameters. However applying fits over longer timeframes (e.g. one mission phase) allows to compensate these as well as errors from the nominal trajectory due to the averaging over time to some extent. Furthermore the accuracy of 9 m (30 ns at the arc overlaps) the nominal trajectory allows us to accurately investigate various aspects of the experiment and its components. The properly assessment of the coupling between the signature of the orbital dynamics and the clock errors would require a concurrent orbit determination and clock parameter estimation, which is outside the scope of this article. Bauer et al. (2016) analyzed such coupling in detail while using the one-way measurements for demonstration of LRO orbit determination.

We derived ≈3000 hours of tracking data that feature 64 million Full Rate observations at a precision of 12.6 cm which confirms and even supersedes the LOLA timestamp accuracy of ≈15 cm. The averaging to Normal Points reduces this amount to 1.5 million observations with a measurement precision of only 5.6 cm and further removes the effect of ground station characteristics. Beside the experiment and the ground station performance, the statistical analysis provides information for laser ranging data simulations from a worldwide ground station network to a target beyond an Earth orbit. These information are of interest within mission analysis as carried out by Turyshev et al. (2010) and Dirkx et al. (2014 and 2015) for example.

From the analysis of single and multiple passes we derived the LRO clock parameters offset, rate, aging and its change through the mission time. By comparing the parameters from both approaches we derived estimates on their precision. Over all mission phases we estimated the rate to an overall average value of 6.9x10^{-8} and at a precision of 8.1x10^{-12}, the aging to an overall average value of 1.6x10^{-12} /day and at a precision of 1.2x10^{-12} /day and the change of the aging to an overall average value of 2.3x10^{-14} /day^2 and at a precision of 9.2x10^{-14} /day^2. We further referenced the MET to the TDB time scale, thus performing ground to space time transfer, at an accuracy of 166 ns over two and 256 ns

over all mission phases. A manual data editing is thereby used to remove outliers and derive a link of good quality. Since the nominal LRO trajectory error is 30 ns, the influence of random LRO clock errors and the incomplete corrections on the referencing were larger.Furthermore we carried out ground to ground time transfer by analyzing the residuals of different ground station passes with respect to the multiple-pass analysis fit and measuring them directly with the simultaneous pass analysis. We compare the results by measuring the differences during simultaneous passes (common-view time transfer). We measured the relative offsets to values between 33 ns and 560 ns and the relative rates between $2x10^{-13}$ and $6x10^{-12}$. The simultaneous pass analysis provides accurate station clock differences at the LOLA timestamp precision of 500 ps since it is insensitive to orbit and LRO clock errors. Compared to the simultaneous pass analysis, the multiple-pass analysis is affected by nominal LRO trajectory errors (30 ns), random LRO clock errors and the incomplete corrections. Because of these errors the station differences from the multiple-pass analysis are less accurate if measured from simultaneous passes and unfeasible if measured from consecutive passes due to the accumulation of errors. However the multiple-pass analysis allows to monitor the station clock behavior over longer timeframes and even between stations from different continents.

While laser ranging ground stations typically measure times of flight very precise, the application of one-way data requires an accurate total referencing of the fire times. Simultaneous passes can be used to track the timing differences of the ground station clocks or for time transfer from a well referenced master station as long as there is frequent coverage with passes between all stations. Therefore the Field Of View of a receiver onboard a spacecraft should be wide enough, so that ranging even from widely spaced stations can occur as with the upcoming ELT experiment for example. A good strategy could be scheduling simultaneous passes between consecutive stations once around the globe in regular time intervals.

To improve the accuracy of the corrections and thus the results, the variation of the LRO clock rate due to temperature change could be incorporated within future work. Further the modeling of the atmospheric corrections could be improved by applying a continuously updated instead of just one averaged correction value if continuous meteo data is available throughout a pass.

Overall the results from the characterization of the LRO and the ground station clock differences provide information that are required for the LRO orbit determination based on one-way laser ranging data. Due to the one-way setup the LRO initial state and all involved timing systems in space and on ground have to be estimated simultaneously which introduces many correlated parameters. Applying the values from the clock characterization in form of a priori initial and covariance values allows for the estimation of all parameters as demonstrated by Bauer et al. (2016). The joint orbit determination utilizing the radio, altimetry and laser data shall enable improvement of the spacecraft positioning and the data product accuracy finally.

Acknowledgements

S. Bauer, H. Hussmann and D. Dirkx were supported by the ESPaCE project, EC FP7 Grant Agreement 263466. Major parts of this work were carried out while the first author very much enjoyed a research visit at NASA Goddard Space Flight Center (GSFC). J.O. was hosted by MIIGAiK and supported by the Russian Science Foundation, project #14-22-00197. We thank two anonymous reviewers for their very constructive comments.

References

Bauer, S., Oberst, J., Hussmann, H., Gläser, P., Schreiber, U., Mao, D., Neumann, G.A., Mazarico, E., Torrence, M.H., McGarry, J.F., Smith, D.E. and Zuber, M.T., 2013. Reduction and analysis of one-way laser ranging data from ILRS ground stations to LRO. In: Proceedings of the 6th ESA International Workshop on Tracking, Telemetry and Command Systems for Space Applications. ESA-ESOC, Darmstadt, Germany, 10th–13th September.

Bauer, S., Hussmann, H., Oberst, J., Dirkx, D., Mao, D., Neumann, G.A., Mazarico, E., Torrence, M.H., McGarry, J.F., Smith, D.E. and Zuber, M.T., Demonstration of orbit determination for the Lunar Reconnaissance Orbiter using one-way laser ranging data, *Planet. Space Sci.* **129**, 2016.

Cash, P., Emmons, D. and Welgemoed, J., 2008. Ultrastable oscillators for space applications. In: Proceedings of the 40th Annual Precise Time and Time Interval (PTTI) Meeting. Reston, Virginia, USA, 1st–4th December.

Degnan, J.J., 1994. Thirty years of laser ranging. In: Proceedings of the 9th International Laser Ranging Service workshop. Canberra, Australia, 7th–11th November.

Dirkx, D., Noomen, R., Prochazka, I., Bauer, S. and Vermeersen, L., Influence of atmospheric turbulence on planetary transceiver laser ranging, *Adv. Space Res.* **54**, 2014.

Dirkx, D., Noomen, R., Visser, P.N.A.M., Bauer, S. and Vermeersen, L.L.A., Comparative analysis of one- and two-way planetary laser ranging concepts, *Planet. Space Sci.* **117**, 2015.

Exertier, P., Bonnefond, P., Deleflie, F., Barlier, F., Kasser, M., Biancale, R. and Menard, Y., Contribution of laser ranging to Earth's sciences, *C.R. Geosci.* **338**, 2006.

Exertier, P., Samain, E. and Guillemot, P., 2011. T2L2 /J2: how to distribute the data. In: Proceedings of the Ocean Surface Science Team (OSTS) Meeting. San Diego, CA, USA, 19th–21st October.

Exertier, P., Samain, E., Courde, C., Martin, N., Torre, J.-M., Oneto, J.-L., Laas-Bourez, M., Guillemot, Ph. and Léon, S., 2013. T2L2: Five years in space. In: Proceedings of the European Frequency and Time Forum & International Frequency Control Symposium (EFTF/IFC). Prague, Czech Republic, 21st–25th June.

Husson, V.S., 1992. Historical MOBLAS system characterization. In: Proceedings of the 8th International Laser Ranging Service workshop. Annapolis, Maryland, USA, 18th–22nd May.

International Laser Ranging Service (ILRS) Website. <http://ilrs.gsfc.nasa.gov> retrieved in July 2016.

Kaplan, G. H., The IAU Resolutions on Astronomical Constants, Time Scales, and the Fundamental Reference Frame, *U.S. Naval Observatory Circular* **179**, 2005.

Lemoine, F. G., Goossens, S., Sabaka, T. J., Nicholas, J. B., Mazarico, E., Rowlands, D. D., Loomis, B. D., Chinn, D. S., Neumann, G. A., Smith, D. E. and Zuber, M. T., GRGM900C: a degree 900 lunar gravity model from GRAIL primary and extended mission data, *Geophys. Res. Lett.* **41**, 2014.

Lombardi, M.A., Fundamentals of Time and Frequency, in: The Mechatronics Handbook, 2001, CRC Press.

Mao, D., Torrence, M., McGarry, J., Golder, J., Barker, M., Mazarico, E., Sun, X., Neumann, G., Smith, D. and Zuber M., 2011. Laser Ranging Status Report. LOLA team meeting. Purdue University, Indiana USA, 25th October.

Mao, D., Sun, X., McGarry, J., Mazarico, E., Torrence, M., Rowlands, D., Neumann, G., Barker, M., Golder, J., Smith, D., and Zuber, M., 2014a. LRO orbit determination with laser ranging data. In: Proceedings of the 19th International Laser Ranging Service workshop Annapolis. Maryland, USA, 27th–31st October.

Mao, D., Sun, X., Skillman, D., McGarry, J., Hoffman, E., Neumann, G., Torrence, M., Smith, D. and Zuber, M., 2014b. Time-transfer experiments between satellite laser ranging ground stations via one-way laser ranging to the Lunar Reconnaissance Orbiter. In: Proceedings of the 19th International Laser Ranging Service workshop. Annapolis, Maryland, USA, 27th–31st October.

Marini, J.W. and Murray, C.W., Correction of Laser Range Tracking Data for Atmospheric Refraction at Elevations Above 10 Degrees, NASA Report X-591-73-351, 1973, Goddard Space Flight Center.

Mazarico, E., Rowlands, D.D., Neumann, G.A., Smith, D.E., Torrence, M.H., Lemoine, F.G. and Zuber, M.T., Orbit determination of the Lunar Reconnaissance Orbiter, *J. Geod.* **86**, 2012.

Mazarico, E., Goossens, S., Lemoine, F., Neumann, G., Torrence, M., Rowlands, D., Smith, D. and Zuber, M., 2013. Improved orbit determination of lunar orbiters with lunar gravity fields obtained by the GRAIL mission. In: Proceedings of the 44th Lunar and Planetary Science Conference (LPSC). Woodlands, Texas, USA, 18th–23rd March.

McGarry, J., Clarke, C., Mao, D. and Torrence. M., 2011. The First ILRS laser transponder mission: laser ranging to NASA's Lunar Reconnaissance Orbiter. In: Proceedings of the 17th International Laser Ranging workshop. Bad Koetzting Germany, 16th–20th May.

McGarry, J.F., Sun, X., Mao, D., Horvath, J., Donovan, H., Clarke, C., Hoffman, E., Cheek, J., Zagwodzki, T.W., Torrence, M.H., Barker, M.K., Mazarico, E., Neumann, G.A., Smith, D.E. and Zuber, M.T., 2013. LRO-LR: Four years of history-making laser ranging. In: Proceedings of the 18th International Laser Ranging workshop. Fujiyoshida Japan, 11th–15th November.

Moyer, T.D., Mathematical Formulation of the Double-Precision Orbit Determination Program (DPODP), Technical Report 32-1527, 1971, NASA, JPL, CALTEC.

Moyer, T.D., Transformation from Proper Time on Earth to Coordinate Time in Solar System Barycentric Space-Time Frame of reference Part 1, *Celest. Mech.* **23**, 1981.

NAIF LRO SPICE archive. <ftp://naif.jpl.nasa.gov/pub/naif/pds/data/lro-l-spice-6-v1.0/lrosp_1000/> retrieved in July 2016.

Neumann, G. A., Cavanaugh, J. F., Coyle, D. B., McGarry, J., Smith, D. E., Sun, X., Torrence, M., Zagwodski, T. W. and Zuber, M. T., 2006. Laser ranging at interplanetary distances. In: Proceedings of the 15th International Laser Ranging workshop. Canberra, Australia, 15th–20th October.

Pearlman, M.R., Degnan, J.J. and Bosworth, J.M., The international laser ranging service, *Adv. Space Res.* **30**, 2002.

Ramos-Izquierdo, L., Scott III, V.S., Connelly, J., Schmidt, S., Mamakos, W., Guzek, J., Peters, C., Liiva, P., Rodriguez, M., Cavanaugh, J. and Riris, H., Optical system design and integration of the Lunar Orbiter Laser Altimeter*, Appl. Opt.* **48**, 2009.

Riris, H. and Cavanaugh, J., Calibration document for the Lunar Orbiter Laser Altimeter (LOLA), 2009, NASA, Goddard Space Flight Center.

Rothacher, M., Vorlesungsskriptum Erdmessung und Satellitengeodäsie 2, 2000, TU München.

Schlicht, A., 2012. The European Laser Timing Experiment (ELT) and Data Centre (ELT-DC), In: Mitteilung des Bundesamtes für Kartographie und Geodäsie, Proceeding of the 17th International Workshop on Laser Ranging. Wettzell, Deutschland, 16th–20th May, 2011.

Schreiber, U., Prochazka, I., Lauber, P., Hugentobler, U., Schafer, W., Cacciapuoti, L. and Nasca, R., 2009. The European Laser Timing (ELT) experiment on-board ACES. In: Proceedings of the 23rd European Frequency and Time Forum (EFTF 2009). Neuchâtel, Switzerland.

Smith, D., Zuber, M., Sun, X., Neumann, G., Cavanaugh, J., McGarry, J. and Zagwodzki, T., Two-way laser link over interplanetary distance, Science **311**, 2006a.

Smith, D., Zuber, M., Torrencec, M., McGarry, J. and Pearlman, M., 2006b. Laser Ranging to the Lunar Reconnaissance Orbiter (LRO). In: Proceedings of the 15th International Laser Ranging workshop. Canberra Australia, 15th–20th October.

Sun, X., Skillman, D.R., Hoffman, E.D., Mao, D., McGarry, J.F., McIntire, L., Zellar, R.S., Davidson, F.M., Fong, W.H., Krainak, M.A., Neumann, G.A., Zuber, M.T. and Smith, D.E., Free space laser communication experiments from Earth to the Lunar Reconnaissance Orbiter in lunar orbit, *Opt. Express* **21**, 2013a.

Sun, X., Skillman, D.R., McGarry, J.F., Neumann, G.A., Mao, D., Torrence, M.H. and Hoffman, E., 2013b. Time transfer between satellite laser ranging stations via simultaneous laser ranging to the Lunar Reconnaissance Orbiter. In: Proceedings of the 18th International Laser Ranging workshop. Fujiyoshida Japan, 11th–15th November.

Torrence, M.H., Klosko, S.M. and Christodoulidis, D.C., 1984. The Construction and Testing of Normal Points at Goddard Space Flight Center. In: Proceedings of the 5th International Laser Ranging workshop. Herstmonceux, UK, 10th–14th September.

Turyshev, S.G., Farr, W., Folkner, W.M., Girerd, A.R., Hemmati, H., Murphy, T.W., Williams, J.G. and Degnan, J.J., Advancing tests of relativistic gravity via laser ranging to Phobos, *Exp. Astron.* **28**, 2010.

Zuber, M.T., Smith, D.E., Zellar, R.S., Neumann, G.A., Sun, X., Katz, R.B., Kleyner, I., Matuszeski, A., McGarry, J.F., Ott, M.N., Ramos-Izquierdo, L.A., Rowlands, D.D., Torrence, M.H. and Zagwodzki, T.W., The Lunar Reconnaissance Orbiter laser ranging investigation, *Space Sci. Rev.* **150**, 2010.

Supplementary material. LRO clock parameters

Table 15 and Table 16 list the LRO clock parameters estimated with the single- (section 3.6.1) and the multiple-pass analysis (section 3.6.2) as well as their difference. The single-pass parameters were grouped and averaged mission phase wise for a direct comparison.

Table 15: Supplementary material – LRO clock parameters estimated with single- and multiple-pass analysis for the mission phases CO until SM26 along with the difference.

	Method	Single-pass analysis			Multiple-pass analysis			1–σ variation of the differences		
Mission phase name	Days since Jan 1st 2009	$\Delta\tau^{(1)} - 1$ 10^{-8}	$\Delta\tau^{(2)}$ 10^{-12} /day	$\Delta\tau^{(3)}$ 10^{-14} /day²	$\Delta\tau^{(1)} - 1$ 10^{-8}	$\Delta\tau^{(2)}$ 10^{-12} /day	$\Delta\tau^{(3)}$ 10^{-14} /day²	$\Delta\tau^{(1)}$ 10^{-12}	$\Delta\tau^{(2)}$ 10^{-12} /day	$\Delta\tau^{(3)}$ 10^{-14} /day²
CO	244.07934	-7.2627	4.41	-2.99	-7.2624	3.77	-0.13	-2.94	0.64	-2.87
NO_01	266.85491	-7.2479	3.28	-0.82	-7.2476	3.12	-0.48	-2.51	0.20	-0.31
NO_02	297.08011	-7.2306	3.20	-0.16	-7.2291	2.96	0.04	-14.82	0.28	-0.19
NO_03	323.88015	-7.2137	2.42	4.33	-7.2144	3.85	-3.17	7.23	-1.47	7.53
NO_03	340.35298	-7.2041	2.68	0.82	-7.2039	2.66	1.97	-1.98	0.02	-1.14
NO_04	354.04899	-7.1975	2.59	-0.18	-7.1965	2.35	-0.11	-10.37	0.26	-0.07
NO_05	381.94425	-7.1834	2.07	0.63	-7.1830	2.00	1.64	-3.34	0.09	-1.02
NO_05	392.98888	-7.1783	2.76	-3.14	-7.1789	2.75	-4.02	5.79	-0.02	0.87
NO_06	411.80282	-7.1704	2.16	-0.03	-7.1710	2.21	-0.30	6.11	-0.03	0.27
NO_07	434.47752	-7.1607	1.73	1.12	-7.1614	1.98	0.49	6.86	-0.23	0.60
NO_08	462.43974	-7.1487	0.83	3.43	-7.1486	1.75	0.44	-1.65	-0.92	2.96
NO_09	491.42192	-7.1381	1.30	1.64	-7.1383	1.88	0.22	2.03	-0.58	1.42
NO_10	514.91883	-7.1295	1.04	1.19	-7.1305	1.32	0.78	10.00	-0.24	0.40
NO_11	543.17526	-7.1204	1.12	1.72	-7.1210	1.42	1.19	5.30	-0.27	0.50
NO_12	570.67653	-7.1113	2.07	-0.97	-7.1113	1.89	-0.50	0.01	0.17	-0.46
NO_13	596.73580	-7.1028	1.90	-0.08	-7.1025	1.71	0.13	-2.55	0.16	-0.22
SM_01	624.05911	-7.0932	1.81	-0.16	-7.0928	1.71	0.18	-3.54	0.08	-0.34
SM_02	652.50906	-7.0836	1.73	0.52	-7.0829	1.48	0.85	-7.30	0.24	-0.33
SM_03	679.19662	-7.0742	1.99	-0.41	-7.0734	1.58	0.44	-8.01	0.40	-0.85
SM_04	705.81334	-7.0637	0.55	3.21	-7.0638	1.03	1.90	0.59	-0.48	1.35
SM_05	734.37676	-7.0555	2.42	-1.27	-7.0549	2.02	-0.38	-6.39	0.43	-0.93
SM_06	761.31328	-7.0449	1.73	0.75	-7.0448	1.78	-0.02	-0.95	-0.07	0.78
SM_07	789.66901	-7.0237	-0.17	3.51	-7.0238	-0.11	3.14	1.35	-0.06	0.35
SM_08	814.96756	-7.0178	0.86	1.27	-7.0183	0.86	1.16	5.72	0.02	0.14
SM_09	842.05148	-7.0108	1.47	0.37	-7.0110	1.32	0.50	1.93	0.11	-0.13
SM_10	870.24819	-7.0019	1.90	-2.39	-7.0021	1.41	0.25	2.03	0.50	-2.60
SM_10	887.95890	-6.9933	-0.73	8.96	-6.9946	2.51	-15.82	13.60	-3.23	25.04
SM_11	897.81335	-6.9920	0.84	1.34	-6.9924	1.05	0.83	3.51	-0.21	0.48
SM_12	923.77265	-6.9856	1.30	0.90	-6.9852	0.85	2.02	-3.57	0.44	-1.15
SM_13	951.76751	-6.9766	1.56	-0.31	-6.9760	1.21	0.57	-5.40	0.33	-0.87
SM_14	979.03614	-6.9674	-0.09	10.45	-6.9676	1.69	-3.97	2.13	-1.78	14.63
SM_15	1005.91635	-6.9615	1.64	-0.08	-6.9605	1.37	0.47	-9.55	0.30	-0.55
SM_16	1034.02144	-6.9526	1.99	-1.05	-6.9506	1.55	0.15	-19.58	0.42	-1.16
SM_17	1061.35148	-6.9432	0.66	5.00	-6.9432	1.82	-1.38	-0.02	-1.16	6.38
SM_18	1075.07070	-6.9378	1.38	0.90	-6.9370	1.89	-0.48	-8.27	-0.54	1.36
SM_19	1104.75628	-6.9274	0.86	6.94	-6.9273	0.67	6.93	-1.17	0.24	-0.03
SM_19	1122.16091	-6.9110	-0.49	-17.17	-6.9101	-2.09	-6.90	-9.51	1.60	-10.18
SM_20	1134.87393	-6.9108	0.57	1.94	-6.9112	0.71	1.64	3.92	-0.14	0.33
SM_20	1161.75727	-6.8583	18.14	-171.69	-6.8621	23.21	-179.74	37.73	-5.10	7.80
SM_21	1171.31798	-6.8567	-0.46	3.28	-6.8582	0.26	1.79	14.96	-0.72	1.51
SM_22	1196.96409	-6.8524	1.04	0.51	-6.8534	1.25	0.24	9.55	-0.20	0.27
SM_23	1223.80217	-6.8458	2.16	-7.32	-6.8461	1.51	-1.36	3.28	0.69	-5.96
SM_23	1232.44447	-6.8398	0.26	2.46	-6.8401	0.26	2.31	2.26	0.00	0.13
SM_24	1255.27557	-6.8349	0.95	0.00	-6.8356	1.35	-0.70	6.51	-0.36	0.69
SM_24	1272.79251	-6.8308	1.04	1.64	-6.8310	0.97	1.69	2.67	0.03	-0.07
SM_25	1302.95045	-6.8222	0.86	0.24	-6.8222	0.85	0.35	-0.14	0.04	-0.12
SM_26	1337.0648	-6.8158	0.85	6.35	-6.8149	2.16	-35.48	-8.53	-1.31	41.85
SM_26	1348.3012	-6.8117	2.07	-20.90	-6.8140	8.18	-56.83	22.87	-6.12	35.96

Table 16: Supplementary material – LRO clock parameters estimated with single- and multiple-pass analysis for the mission phases ES01 until ES24 along with the difference.

	Method	**Single-pass analysis**			**Multiple-pass analysis**			**1–σ variation of the differences**		
Mission phase name	**Days since Jan 1st 2009**	$\Delta\tau^{(1)} - 1$ **10^{-8}**	$\Delta\tau^{(2)}$ **10^{-12} /day**	$\Delta\tau^{(3)}$ **10^{-14} /day²**	$\Delta\tau^{(1)} - 1$ **10^{-8}**	$\Delta\tau^{(2)}$ **10^{-12} /day**	$\Delta\tau^{(3)}$ **10^{-14} /day²**	$\Delta\tau^{(1)}$ **10^{-12}**	$\Delta\tau^{(2)}$ **10^{-12} /day**	$\Delta\tau^{(3)}$ **10^{-14} /day²**
ES_01	1353.14437	-6.8107	1.12	0.90	-6.8103	1.47	-0.39	-3.56	-0.36	1.27
ES_02	1379.69253	-6.8040	1.56	-0.34	-6.8039	1.57	-0.30	-1.43	-0.03	-0.04
ES_03	1414.85936	-6.7943	1.56	-0.20	-6.7937	1.23	0.23	-5.62	0.30	-0.43
ES_04	1455.8192	-6.7824	1.21	0.62	-6.7827	1.41	0.22	2.69	-0.16	0.39
ES_05	1490.9681	-6.7710	0.95	1.05	-6.7719	1.19	0.54	8.91	-0.27	0.48
ES_06	1524.9696	-6.7614	1.21	0.55	-6.7618	1.34	0.07	4.43	-0.11	0.48
ES_07	1553.8928	-6.7527	0.77	8.21	-6.7537	1.80	-2.94	9.97	-1.03	11.29
ES_07	1561.61776	-6.7491	0.86	1.79	-6.7495	0.96	1.02	3.97	-0.10	0.80
ES_08	1579.80045	-6.7446	1.99	-2.46	-6.7449	1.46	-0.48	2.91	0.51	-2.02
ES_08	1603.0288	-6.7349	0.54	-2.02	-6.7344	-0.97	9.51	-4.32	1.50	-11.55
ES_09	1611.30959	-6.7347	1.12	-0.04	-6.7353	1.37	-0.24	5.64	-0.23	0.20
ES_10	1659.66243	-6.7239	1.38	-0.28	-6.7231	0.86	0.96	-8.13	0.52	-1.24
ES_11	1694.18582	-6.7147	0.85	0.52	-6.7151	1.18	0.01	3.31	-0.34	0.50
ES_12	1721.76028	-6.7088	1.21	0.18	-6.7085	1.11	0.41	-3.65	0.10	-0.23
ES_13	1747.75185	-6.7024	1.73	-1.34	-6.7014	0.94	1.01	-10.57	0.77	-2.32
ES_14	1770.86794	-6.6965	1.64	-1.19	-6.6957	1.05	0.53	-7.34	0.64	-1.73
ES_15	1798.93687	-6.6887	1.04	0.60	-6.6881	0.55	1.43	-5.64	0.49	-0.83
ES_16	1835.06086	-6.6756	0.71	0.63	-6.6756	0.75	0.44	0.04	-0.04	0.19
ES_16	1869.04061	-6.6684	-0.56	19.41	-6.6689	1.08	0.76	4.87	-1.64	18.45
ES_17	1887.33396	-6.6629	0.58	0.10	-6.6626	-1.99	39.28	-2.78	2.57	-39.18
ES_18	1891.85374	-6.6624	1.38	-0.13	-6.6627	1.32	-0.16	3.54	0.05	0.02
ES_19	1918.89661	-6.6557	1.90	-2.24	-6.6560	2.00	-3.48	3.36	-0.12	1.28
ES_20	1947.10838	-6.6475	0.68	2.46	-6.6477	1.08	0.86	1.14	-0.40	1.58
ES_21	1967.57812	-6.6431	1.99	-1.87	-6.6427	1.63	-0.99	-3.38	0.34	-0.85
ES_22	1986.09873	-6.6379	1.73	-1.05	-6.6375	1.24	0.03	-4.46	0.47	-1.07
ES_23	2016.52961	-6.6299	1.04	0.33	-6.6298	1.11	0.31	-1.05	-0.04	0.02
ES_24	2050.80498	-6.6202	0.01	4.40	-6.6205	0.14	4.10	2.83	-0.13	0.28
Average & Variation		**-6.9103**	**1.78**	**-2.27**	**-6.9104**	**2.02**	**-4.01**	**8.11**	**1.36**	**12.32**

4 Research paper 2

Demonstration of orbit determination for the Lunar Reconnaissance Orbiter using one-way laser ranging data

S. Bauer[1], H. Hussmann[1], J. Oberst[1,2,3], D. Dirkx[4,5], D. Mao[6], G.A. Neumann[7], E. Mazarico[7], M.H. Torrence[8], J.F. McGarry[7], D.E. Smith[9], M.T. Zuber[9].

[1]German Aerospace Center (DLR), Berlin, Germany, contact: sven.bauer@dlr.de,
[2]TU Berlin, Germany,
[3]Moscow State University for Geodesy and Cartography, Russia,
[4]TU Delft, Netherlands,
[5]Joint Institute for VLBI ERIC, Dwingeloo, Netherlands,
[6]Sigma Space Corporation, Lanham, MD, USA,
[7]NASA Goddard Space Flight Center, Greenbelt, MD, USA,
[8]Stinger Ghaffarian Technologies Inc., Greenbelt, MD, USA,
[9]Massachusetts Institute of Technology, Cambridge, MA, USA.

Keywords

One-way laser ranging, orbit determination, LRO

Abstract

We used one-way laser ranging data from International Laser Ranging Service (ILRS) ground stations to NASA's Lunar Reconnaissance Orbiter (LRO) for a demonstration of orbit determination.

In the one-way setup, the state of LRO and the parameters of the spacecraft and all involved ground station clocks must be estimated simultaneously. This setup introduces many correlated parameters that are resolved by using a priori constraints. Moreover the observation data coverage and errors accumulating from the dynamical and the clock modeling limit the maximum arc length.

The objective of this paper is to investigate the effect of the arc length, the dynamical and modeling accuracy and the observation data coverage on the accuracy of the results.

We analyzed multiple arcs using lengths of 2 and 7 days during a one-week period in Science Mission phase 02 (SM02, November 2010) and compared the trajectories, the post-fit measurement residuals and the estimated clock parameters. We further incorporated simultaneous passes from multiple stations within the observation data to investigate the expected improvement in positioning. The estimated trajectories were compared to the nominal LRO trajectory and the clock parameters (offset, rate and aging) to the results found in the literature.

Arcs estimated with one-way ranging data had differences of 5–30 m compared to the nominal LRO trajectory. While the estimated LRO clock rates agreed closely with the a priori constraints, the aging parameters absorbed clock modeling errors with increasing clock arc length. Because of high correlations between the different ground station clocks and due to limited clock modeling accuracy, their differences only agreed at the order of magnitude with the literature. We found that the incorporation of simultaneous passes requires improved modeling in particular to enable the expected improvement in positioning. We found that gaps in the observation data coverage over 12 hours (≈6 successive LRO orbits) prevented the successful estimation of arcs with lengths shorter or longer than 2 or 7 days with our given modeling.

4.1 Introduction

NASA's Lunar Reconnaissance Orbiter (LRO) was launched on June 18th, 2009 and reached its lunar orbit five days later. A comprehensive geophysical, geological and geochemical mapping of the Moon is carried out by the spacecraft in order to establish an observational framework for future lunar exploration (Zuber et al., 2010).

The Lunar Orbiting Laser Altimeter (LOLA) is one of the seven instruments onboard LRO. Its main science objectives are the derivation of a global topographic model and a high-accuracy geodetic grid. LOLA is also able to receive laser pulses from Earth-based International Laser Ranging Service (ILRS) ground stations (Pearlman et al, 2002) at a single-shot precision of 15 cm. This precision is further reduced to <6 cm with an averaging of the Full Rate to Normal Point data (Bauer et al., 2016). The ranging to LRO as illustrated in Sun et al. (2013) is done from either one or multiple stations at a time. In order to receive laser shots from Earth ground stations, an optical receiver, the Laser Ranging Telescope was added to the high gain communication antenna. A fiber optic cable is forwarding incoming laser pulses into the LOLA instrument for detection. LOLA is designed so that the Earth and the Lunar return pulses can be detected concurrently with the same instrument. Further details about the ground station characteristics, the spacecraft setup including LOLA's hardware extension and the data setup can be found in Bauer et al. (2016). Both LOLA's altimetry data and the one-way range measurements provide additional observational data that complement the regular radio tracking data for orbit determination (Zuber et al., 2010; McGarry et al., 2011, 2013).

The accuracy and precision of the LRO positioning throughout the mission is critical to enable a precise referencing of the remote sensing data. From the combination of the various tracking data sets the orbit determination of LRO shall be improved in order to support Lunar precision mapping (Zuber et al., 2010).

Most of the interplanetary laser ranging experiments have been carried out only occasionally as for example to Mars Global Surveyor, MESSENGER (Neumann et al., 2006; Smith et al. 2006) and LADEE (D'Ortenzio et al., 2015). Only the ranging to LRO and the retroreflectors on the lunar surface has been done on a routine basis. While the one-way laser ranging experiment has been carried out between June 30, 2009 and September 30, 2014 (McGarry et al. 2013), two-way Lunar Laser Ranging is done since the 1970s already (Degnan, 1994). While usually one ground station is ranging to LRO at a time, other stations can join for simultaneous observations.

The LRO spacecraft is regularly tracked by NASA's radio station White Sands in New Mexico as well as by the commercial Universal Space Network (USN). From the radio tracking data the LOLA team estimates the nominal LRO trajectory via orbit determination (Mazarico et al., 2012). Within early updates of the orbit they further used LOLA's altimetric crossover data for improved solutions. Derived from the differences at the arc overlaps of trajectories consecutive in time, this nominal LRO trajectory had an overall accuracy of 23 m for the radio only and 14 m for the radio and crossover solutions (Mazarico et al., 2012). The individual arcs had a length of 2.5 days, which is typical for the orbit determination of lunar orbiters (Konopliv et al., 2001; Mazarico et al., 2010, 2012, 2013).

While using the GRAIL gravity field within the estimation, Mazarico et al. (2013) derived updated solutions that had a total average difference of ≈9 m at the arc overlaps over all mission phases. The GRAIL mission enabled a global estimation of the lunar gravity field to unprecedented precision from the inter-distance measurement of two co-orbiting spacecraft (Zuber et al., 2013). The most recent

solutions of the nominal LRO trajectory that we use within this work incorporates the GRAIL gravity field GRGM900C (Lemoine et al., 2014) up to degree and order 600 (LRO SPICE archive, December 2015).

The application of laser ranging data for both LRO clock analysis and orbit determination was first reported by Mao et al. (2014a). Their 2-week laser-ranging-data-only arcs had differences in total of 5–30 m with respect to the nominal LRO trajectory being thus comparable in accuracy with the radio-based result. Löcher et al. (2015) and Buccino et al. (2016) also estimated orbits comparable to the radio-based results while using laser data. Except for Mao et al. (2014), the authors could not derive an improvement in positioning when using both radio and laser data within the LRO orbit determination. Since the reasons have not been reported yet, one aspect of this work is the analysis of the inherent issues of the one-way laser data application in particular.

Sun et al. (2013) and Mao et al. (2014b) reported results from simultaneous passes by multiple stations and utilized them for ground to ground time transfer with one-way data. Furthermore the positioning was expected to improve with simultaneous passes due to the geometry and the additional observations (Neumann et al., 2014). Other optical time transfer experiments like the time transfer by laser link (T2L2) and the European Laser Timing (ELT) have a two-way setup from which they derive ground to space and ground to ground time transfer (Exertier et al., 2013; Schreiber et al., 2009).

Bauer et al. (2016) characterized the LRO and the ground station clocks from single, multiple as well as simultaneous passes. They estimated the parameters offset, rate, aging and change of aging for the LRO and relative offsets and rates for the ground station clocks (ground to ground time transfer) while keeping the orbit fixed by using the nominal LRO trajectory. Within this work we also use the terms offset, rate, aging and change of aging which are equivalent to phase, frequency, frequency drift and change of frequency drift respectively as used within the time and frequency community.

This work extends the former demonstration of orbit determination based on one-way laser ranging data only by Bauer et al. (2014) from a timeframe of 5 to 7 days. Furthermore variations in the length of the trajectory and the LRO clock arc were used to research the requirements of the one-way data application within orbit determination.

In section 4.2 we discuss the errors arising from the ranging measurement and the involved clocks on ground and in space. Section 4.3 provides a comparison of optical one- and two-way time transfer experiments and their measurement accuracy. In section 4.4 we provide the theoretical background of the observation model, the estimation software with its dynamical modeling as well as the a priori constraints we apply to the state and all clocks. Further we describe the timeframe we selected for demonstration of orbit determination including the observation data coverage, characteristics of the LRO orbit, the detailed setup of the various arcs we estimated and how we analyze the estimated results. Section 4.5 presents our estimated trajectories with their post-fit measurement residuals, the LRO clock parameters and the ground station clock differences that we estimated and compares them to the literature. Section 4.6 will discuss the results and draw conclusions.

4.2 Measurement and clock errors

Compared to the nominal timestamp precision of 15 cm (0.5 ns) of the Full Rate LOLA data, Exertier et al. (2006) reported random errors below that within SLR. They found a 7–12 mm random error for Full Rate and 1–3 mm for Normal Point data. The errors are thereby coming from the ground station laser, detector, timer, clock and other dependencies as well as from the atmosphere and the target

signature. The calibration of the station hardware, the atmosphere itself as well as the target signature introduce a systematic error of 8–19 mm.

With the ranging to LRO the LOLA time stamp accuracy is above the random error reported within SLR. With the one-way setup the systematic errors are larger than the random errors. The errors are thereby coming from the LRO onboard and the ground station clocks, the orbit that is used to complete the one-way observable as well as the modeling accuracy (see section 4.4.2). Since only an uplink is used, target signature errors are not present.

The one-way observable is affected by the ground station and LRO clock stability, since their errors affect their time tags (Dirkx, 2015a and see equation 34). Table 17 shows stability values of typical ground station timing systems as well as of the LRO onboard clock.

While the ground station clocks have good stabilities over long periods ($1x10^{-12}$ to $1x10^{-15}$ over 10^3 to 10^7 s), the LRO onboard clock achieves its best stability of $7x10^{-14}$ after an averaging period of 40 s. Overall the Ultrastable Oscillator (USO) has a stability of $1x10^{-13}$ between 1 and 100 s and $2x10^{-13}$ between 10^3 to 10^5 s at constant temperatures (Cash et al., 2008). The accumulated range error of 0.3 mm, 3 mm and 60 cm respectively becomes larger than the LOLA timestamp precision after 2500 s. Since the LRO USO stability is still at $2x10^{-13}$ after an orbital period of LRO of ≈120 min (7200 s) no additional once per orbit error is introduced by the onboard clock.

The response of the LRO USO rate to temperature variation is reported to be $1–3x10^{-12}$ /°C (Cash et al., 2008). We saw variations with an amplitude of 0.3°C over one day that caused a maximum change in the rate of $0.3–0.9x10^{-12}$ accordingly. These variations result in an accumulating offset of 13–39 ns over one day while using a sinusoidal function for the integration. This range error of ≈4–12 m over one day has an average linear trend of $1.5–4.5x10^{-13}$. We observed remaining sinusoidal variations around that linear trend with an amplitude of ≈2–6 ns which. Assuming that the sinusoidal curve with a period of 1 day has a zero or a turnover point every 21600 s, the remaining variations have an average difference in rate of $≈±1–3x10^{-13}$ between these points. Since the LRO clock stability becomes larger than $2x10^{-13}$ after 10,000 s, the average rate difference is at or below this value. Since no correction was available for the change of rate due to temperature change within our work yet this effect influences the LRO clock approximation with polynomial fits (see section 4.5.1 and 4.5.2). While the periodic temperature variation mostly stays the same over the days, changes in the power consumption of nearby instruments or the orbit height can cause further changes of the temperature and thus the rate. Since the actual temperature variation is not as steady as assumed within our simplification, the periodic and further changes due to external effects mix with the stochastic noise of the clock. Because the ground station clocks are not subject to temperature change due to proper housing, their approximation is only affected by their stability.

Table 17: Stabilities of various ground station clock systems (Lombardi, 2001) and the LRO onboard clock (Cash et al., 2008).

Type	Stability @ noise floor	Averaging period τ in s
Quartz OCXO/OCCO*	$1x10^{-12}$	1 to 10^2
Rubidium	$1x10^{-12}$	10^3 to 10^5
Cesium/atomic	$1x10^{-14}$	10^5 to 10^7
H-Maser	$1x10^{-15}$	10^3 to 10^5
LRO USO OCXO*	$7x10^{-14}$	40

*) Oven Controlled Crystal Oscillator.

4.3 Time transfer with the LRO laser ranging and other experiments

The differences between the ground station clocks which we use within the estimation and for the comparison of our parameters are derived from time transfer experiments. The two-way laser time transfer experiments T2L2 and ELT feature a similar setup consisting of a retro-reflector, a detector (providing an active uplink) and a timing system and are tracked by ILRS ground stations. The T2L2 experiment was launched onboard the Jason-2 satellite in 2008 and utilizes its USO (Exertier et al., 2013). The ELT experiment will make use of the Atomic Clock Ensemble in Space (ACES) onboard the International Space Station (ISS) which will include both an atomic clock and an H-Maser (Schreiber et al., 2009). Due to the two-way setup the offset between a ground station and the onboard clock can be estimated directly (ground to space time transfer). From the offsets with respect to the onboard clock the differences between the stations are measured or remote ground station clocks are synchronized (ground to ground time transfer).

Both experiments achieve accuracies around and below 10 ps for ground to space and ground to ground time transfer. With non-common view time transfer, the ELT achieves much better accuracies than the T2L2 experiment due to the more stable clocks (Atomic and H-Maser compared to USO – see Table 17) even over one ISS orbit. With that the ELT experiment will enable global time transfer between all stations that can range to its detector.

With the one-way laser ranging we cannot derive the ground to ground time transfer from the offsets of the ground station to the onboard clock. However it is possible to measure the differences between ground station clocks directly when using the LRO clock as common reference (Bauer et al., 2016). The measured relative offsets between ground station clocks from common view LRO passes achive an accuracy of 500 ps (Sun et al., 2013).

4.4 Method

Figure 28 schematically shows how the various components and steps, which will be explained in the following, are related with each other.

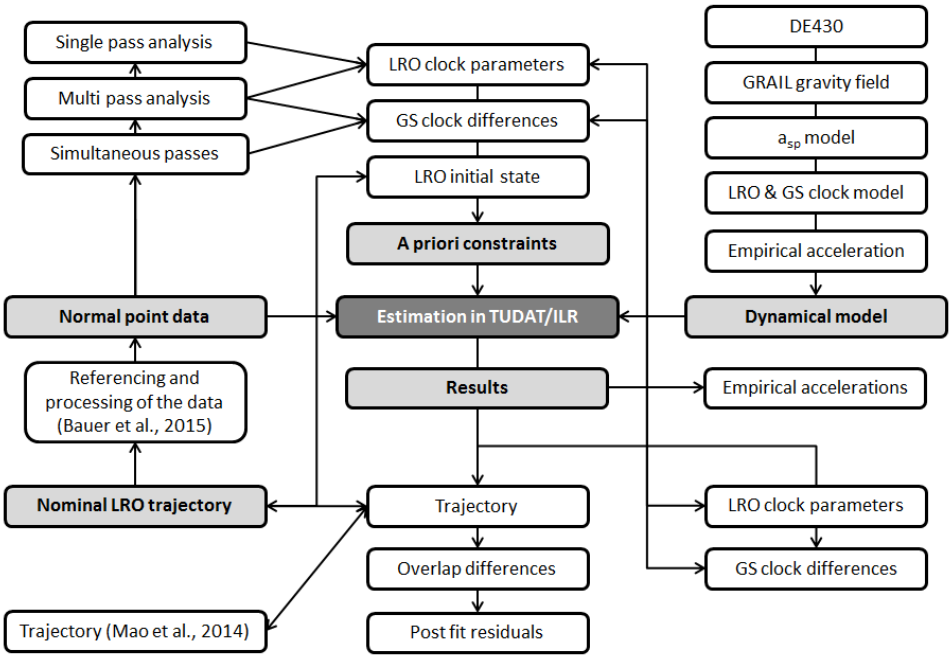

Figure 28: Schematic overview of the relation of the various aspects of the LRO orbit determination. The gray shading highlights important major parts.

4.4.1 Time scales, clock error modeling and observation model

The theoretical description in this section closely follows the approach from Dirkx et al. (2015b) since it is employed in their estimation software which we use for the LRO orbit determination.

Depending on the velocity and the gravitational potential at the location of a clock, the rate at which local time passes varies due to relativistic effects (Einstein, 1907). We assume that a clock reads local proper time at an observer's location. We convert its times to a global timescale such as Barycentric Dynamical Time (TDB), in order to retrieve ranges that we can use within orbit determination. We use the TDB time scale since it is commonly used for ephemerides and interplanetary orbit determination.

All clocks are affected by instabilities, desynchronization, external effects and aging. We assume they register a measured proper time $\tilde{\tau}$ that differs from local proper time τ by

$$\tilde{\tau} = \tau + \Delta\tau = \tau + \Delta\tau_S + \Delta\tau_D \quad (28)$$

where $\Delta\tau_S$ are stochastic and $\Delta\tau_D$ deterministic errors. Our clock modeling consists of a 2nd order polynomial fit with which we estimate accumulating stochastic and deterministic errors after correcting the observation data for the influence of the atmosphere, the detector range-walk and relativistic effect on the LRO clock as reported in Bauer et al. (2016). We fit its errors via

$$\Delta\tau_{LRO} = \sum_{i=0}^{c} \Delta\tau_{LRO}^{(i)} (\tau - \tau_0)^i \quad (29)$$

where τ_0 is a reference epoch, $\Delta\tau_{LRO}^{(0)}$ the offset, $\Delta\tau_{LRO}^{(1)}$ the rate and $\Delta\tau_{LRO}^{(2)}$ the aging parameter. The errors are fitted analog for the ground station (GS) clocks 1 to n via

$$\Delta\tau_{GS\,n} = \sum_{i=0}^{2} \Delta\tau_{GS\,n}^{(i)} (\tau - \tau_0)^i. \quad (30)$$

τ_0 is the same reference epoch as for the LRO clock, $\Delta\tau_{GS\,n}^{(0)}$ the offset, $\Delta\tau_{GS\,n}^{(1)}$ the rate and $\Delta\tau_{GS\,n}^{(2)}$ the aging parameter of the ground station clock n.

On a global timescale the one-way range $s_{LRO-GS}^{(1)}$ consists of a transmission time t_t at the ground station and a receive time t_r at LRO

$$s_{LRO-GS}^{(1)} = c(t_r - t_t) + \Delta s_{LRO-GS}^{(1)}. \quad (31)$$

c is the speed of light and $\Delta s_{LRO-GS}^{(1)}$represents the range correction due to relativistic effects and the atmosphere.

The ground station and the LRO clock measure the transmission ($\widetilde{\tau_t}$) and the receive event ($\widetilde{\tau_r}$) in their proper time. Due to the one-way setup these records are separated and we first pair corresponding events with each other as described in Bauer et al. (2016). After that we retrieve the proper range from a pair via

$$\tilde{s}_{LRO-GS}^{(1)} = c(\widetilde{\tau_r} - \widetilde{\tau_t}) + \Delta s_{LRO-GS}^{(1)}. \quad (32)$$

By using

$$t_i = t_i(\tau_i(\tilde{\tau}_i)) \quad (33)$$

we convert measured proper time $\tilde{\tau}_i$ of a clock to true proper time τ_i and then to global time t_i. By using equation 31 in equation 32 we retrieve

$$\tilde{s}^{(1)}_{LRO-GS} = c(t_r - t_t + \Delta t_{LRO}(t_r) - \Delta t_{GS}(t_t)) + \Delta s^{(1)}_{LRO-GS} + \epsilon_{s^{(1)}_{LRO-GS}}, \quad (34)$$

where $\Delta t_{LRO}(t_r)$ and $\Delta t_{GS}(t_t)$ represent the time measurement error at the two clocks respectively and $\epsilon_{s^{(1)}_{LRO-GS}}$ the errors of the observed range which are independent from the clock. The latter are e.g. instrument detection accuracy, pulse length, signal strength variations and others. By using the global range from equation 31 we rewrite equation 34 as

$$\tilde{s}^{(1)}_{LRO-GS} = s^{(1)}_{LRO-GS} + c(\Delta t_{LRO}(t_r) - \Delta t_{GS}(t_t)) + \Delta s^{(1)}_{LRO-GS} + \epsilon_{s^{(1)}_{LRO-GS}}. \quad (35)$$

Equation 35 shows that the measured proper range differs from the global range by the errors of the involved clocks and the errors which are independent from the clock.

Within the software the observation model for the one-way range from a ground station to LRO is implemented via

$$s^{(1)}_{LRO-GS}(t = t_t) = \left| x_{LRO}\left(t_t + \frac{s^{(1)}_{LRO-GS}}{c}\right) - x_{GS}(t_t)\right| + \Delta s^{(1)}_{LRO-GS}(t_t, t_r) + c(\Delta t_{LRO}(t_r) - \Delta t_{GS}(t_t)). \quad (36)$$

Thereby t_t is the global transmission time at the ground station, x_{LRO} the position of LRO, x_{GS} the position of the ground station and t_r the global reception time at LRO. Since the one-way range depends on both the state and the timing of LRO, both have to be estimated from the same observable which is an inherent drawback of the one-way setup. Further the errors of the LRO and all involved ground station clocks have to be adjusted as well.

4.4.2 Estimation software and dynamical model

We derive the LRO orbit arcs by using a software package (Dirkx et al., 2014) that is based upon the Tudat toolbox (Kumar et al., 2012).

Because of the one-way setup we estimate the spacecraft state and the parameters of all involved clocks simultaneously (see equation 35 and 36). We estimate an initial state (position $\vec{r}_{0,LRO}$ and velocity $\vec{v}_{0,LRO}$) at a certain epoch. The orbit arcs are determined from the integration of the equations of motion from the estimated state. Further we estimate the clock parameters offset, rate and aging for the LRO ($\Delta\tau^{(0)}_{LRO}$, $\Delta\tau^{(1)}_{LRO}$, $\Delta\tau^{(2)}_{LRO}$) and all involved ground station clocks 1 to n ($\Delta\tau^{(0)}_{GS\,n}$, $\Delta\tau^{(1)}_{GS\,n}$, $\Delta\tau^{(2)}_{GS\,n}$). For longer arcs we estimate empirical accelerations in along- and cross-track direction ($a_{emp,AT}$, $a_{emp,CT}$) to compensate for accumulating un-modeled dynamic effects.

We apply a priori initial values and covariances on the many correlated parameters that we have to estimate simultaneously (see section 4.4.3). During the estimation all parameters are adjusted iteratively from their initial values within a non-linear batch least squares optimization as described by Montenbruck and Gill (2000). We use a time step of 5 s within the integration of the equations of motion.

Within the dynamical model (see Figure 28) we used the ephemeris file DE430 (Folkner et al., 2014), in form of Spacecraft and Planetary Kernel (SPK) files for the position of the planets and the Moon.

We applied the GRAIL gravity field GGRM900C (Lemoine et al., 2014) for the representation of the lunar gravity field. We truncated the field at degree and order 180 within the estimation to reduce computation time.

We applied a "cannon-ball" model (Montenbruck and Gill, 2000) to account for the solar radiation pressure. The spacecraft is represented by a reference surface of 10m² while we assume its radiation pressure coefficient to 1.2. The spacecraft mass is changing due to the usage of fuel during maneuvers. We set it to its corresponding value during the timeframe over which we estimated the orbit. Further effects such as varying radiation pressure due to changing orientation and self-shadowing are not included. Also thermal radiation and reflected sunlight from the lunar surface are not included. Thermal radiation may cause an offset of 1–2 meters over an arc length of 2.5 days in the case of LRO (Mazarico, personal communication, 2015), i.e., 6 m over our maximal orbit arc length of 7 days. Regarding sunlight reflected from the surface we expect a total error around 9 m over 7 days for a lunar spacecraft in a 50 km circular orbit (Floberghagen et al., 1999). With both effects added to 15 m over 7 days we obtain a constant acceleration below $5x10^{-11}$ m/s² which is covered by the empirical accelerations that were estimated to values at the order of $1x10^{-9}$ to $1x10^{-8}$ m/s² (see section 4.5.1).

Since both the state and the clocks have to be estimated with the one-way setup, errors accumulate from the imperfect modeling of the dynamics and the clock with increasing arc length. Errors of the dynamical modeling are coming from un-modeled or simplified effects within the force model such as the solar radiation pressure for example. Within the clock modeling the 2nd order polynomial fit can approximate the inherent stochastic noise of a clock only with limited accuracy (see Figure 1 of Dirkx et al. 2015b). Furthermore the completeness and the accuracy of the corrections applied to the observation data defines how much systematics remain that have to be fitted as well. While we correct the observation data for the influence of the atmosphere, the detector range-walk and relativistic effects, the change of the LRO clock rate due to temperature change is missing. Besides the stochastic noise that is caused by the limited stability of a clock, remaining systematics have to be covered by the fits as well and affect the LRO clock approximation (see section 4.2). The accumulating errors affect the estimated trajectories, their post-fit residuals and the clock parameters.

The usage of shorter clock arcs (per pass at minimum) results in more parameters that have to be estimated and leads to high correlations between the state and the clocks. Since they provide a better approximation of the stochastic clock trend, the per pass measurement post fit residuals become small. However the estimated clock parameters tend to scatter because they represent the stochastic trend during a short timescale. Furthermore they absorb signal from the state because of the correlations which also causes the trajectories to become less good.

With longer clock arcs the state and the clock become less correlated. However the errors from the dynamical modeling and the less good clock approximation are accumulating. Even though the fit represents the clock trend on average, the errors due to the stochastic noise around it increase the post-fit residuals. Furthermore the errors are absorbed by the clock parameters and let their values deviate. The trajectories also become less good since the dynamical modeling errors are accumulating, which can be absorbed by the estimation of empirical accelerations to some extent.

Overall an optimum arc length needs to be found for the state and the clocks with one-way data which provides a balance between the accuracy of the trajectory, the post-fit residuals, the clock parameters and the number of correlated parameters. The arc length thereby depends on the accuracy of the corrections, the dynamical and the clock modeling as well as the stability of the involved clocks. The optimum arc length could thereby be different for the LRO and the ground station clocks.

4.4.3 A priori constraints

The a priori constraints (initial values and covariances) which we use to separate and estimate the correlated state and the involved clocks are shown in Table 18.

We use the nominal LRO trajectory to derive the initial LRO state vector at a certain epoch. We do not constraint the initial state tightly by defining large covariances. With that we check if we retrieved trajectories in agreement with the nominal trajectory after adjustment of all parameters.

Bauer et al. (2016) characterized the LRO clock from the analysis of single and multiple passes while keeping the orbit fixed. We used these parameters to define a priori initial values and covariance as described in the following.

We define the initial value of the LRO clock offset to zero, since we already applied various corrections to the one-way ranges represented by the $\Delta s^{(1)}_{LRO-GS}$ term in equation 31. The large covariance of 10 ms allows for the adjustment of all involved clocks simultaneously (see equation 35).

The LRO clock rate has been determined accurately by Bauer et al. (2016) to a total value around $7\text{x}10^{-8}$ with variations slightly below $1\text{x}10^{-11}$ from single and multiple passes. Therefore, we define the initial value to the specific rate during the timeframe and constrain it with a covariance of $1\text{x}10^{-11}$. This covariance value also is in agreement with the 3-σ variation of the single pass rates around their linear trend that we observed during the selected timeframe (see Figure 35 in section 4.5.2). Within certain arcs the rate was constrained to $1\text{x}10^{-13}$ in order to limit their variation due to error accumulation.

The LRO clock aging with its small value of $1.4\text{x}10^{-17}$ /s ($1.2\text{x}10^{-12}$ /day) is especially sensitive to errors (Bauer et al., 2016). Our approximation of the LRO clock with the 2nd order polynomial fit covers stochastic clock noise less good with increasing arc length. Errors accumulate and are absorbed by the aging which is why we retrieved values at the order of $1\text{x}10^{-13}$ /s ($8.6\text{x}10^{-9}$ /day) with long clock arcs (see section 4.5.2). Tight a priori covariance constraints could mitigate the error absorption by the aging but as a result the estimated trajectories would become less good. In favor of agreement of the estimated trajectories with the nominal LRO trajectory we allow for absorption of errors and define the a priori aging covariance to $1\text{x}10^{-15}$ /s ($8.6\text{x}10^{-11}$ /day).

Table 18: A priori initial and covariance values applied in the estimation.

Type	Parameter	Symbol	A priori constraints		
			Initial value	Covariance	Unit
Initial state	Position	$\vec{r}_{0,LRO}$	Taken from the nominal trajectory	$1\text{x}10^{+06}$	m
	Velocity	$\vec{v}_{0,LRO}$		$1\text{x}10^{+03}$	m/s
LRO clock	Offset	$\Delta\tau^{(0)}_{LRO}$	0	10	ms
	Rate	$\Delta\tau^{(1)}_{LRO}$	-7.078e-08	$1\text{x}10^{-11}$, $1\text{x}10^{-13}$	-
	Aging	$\Delta\tau^{(2)}_{LRO}$	$1\text{x}10^{-15}$ ($8.6\text{x}10^{-11}$)	$1\text{x}10^{-15}$ ($8.6\text{x}10^{-11}$)	/s (/day)
Ground station Clocks 1…n	Offset	$\Delta\tau^{(0)}_{GS\,n}$	0	10	ms
	Rate	$\Delta\tau^{(1)}_{GS\,n}$	0	$1\text{x}10^{-11}$	-
	Aging	$\Delta\tau^{(2)}_{GS\,n}$	0	$1\text{x}10^{-12}$ ($8.6\text{x}10^{-8}$)	/s (/day)
Constant empirical Accelerations	Along-track	$a_{emp,AT}$	0	$1\text{x}10^{-09}$	m/s^2
	Cross-track	$a_{emp,CT}$	0	$1\text{x}10^{-09}$	m/s^2

As it will be seen in section 4.5.3, the estimation cannot separate the ground station timing differences exactly to the measured numbers. Due to that we only define a priori covariance and no initial constraints for the offsets and the rates of the ground station clocks. The a priori offset covariance is set to 10 ms to match the LRO clock a priori offset covariance. The a priori rate covariance is set to the upper limit of $1x10^{-11}$ that Bauer et al. (2016) measured between the stations. The ground station clock aging covariance is constrained with $1x10^{-12}$ /s ($8.6x10^{-8}$ /day) in order to allow for absorption of clock modeling errors as we did with the LRO clock aging.

4.4.4 Selected timeframe, data coverage and LRO orbit characteristics

LRO carries out various types of maneuvers at regular intervals. While yaw flips are scheduled every 6 months in order to keep the single solar panel aligned towards the sun, station keeping maneuvers were done every month and separate the overall mission into the various mission phases (commissioning – CO, nominal mission – NO01 to NO13, science mission – SM01 to SM26 and extended science mission – ES01 to ES26). In addition, desaturation maneuvers are usually carried out every two weeks to unload the reaction wheels of the spacecraft (Mazarico, 2012). The desaturation maneuvers limit the maximum free flight phase to 14 days at a time, which is the maximum possible length of orbit arcs without maneuvers. Longer arcs thereby reduce the number of correlated parameters that have to be estimated. With our modeling we found a compromise between the minimum and maximum possible arc length, the observation data coverage and the degradation of the result due to modeling errors when using a length of 2 and 7 days.

We selected a timeframe of 7 days during SM02 to demonstrate orbit determination for LRO. Figure 29 shows the tracking data coverage during that timeframe (upper plot) and the orbit arcs we estimated (lower plot). In order to research the effect of the arc length on the results (see section 4.4.2), we estimated multiple 7-day and 2-day long arcs. While the 7-day arcs Nr. 1–4 all covered the same timeframe with variations in the clock modeling, the 2-day arcs Nr. 5–10 were consecutive with overlaps of up to one day. We discuss the detailed setups of the arcs with their variations in the modeling and their tracking data coverage in section 4.4.5.

We selected observational data from the three ground stations YARL, GO1L and MONL since they had the largest number of passes per station during the selected timeframe. We only used data from 3 ground stations in order to limit the number of correlated clocks that have to be estimated simultaneously (see section 4.4.1 and 4.4.2). The passes from the three stations are shown in Figure 29 and individually listed with their characteristics in Table 24 (appendix). Table 19 lists the station coordinates, the total number of single and simultaneous passes, as well as averaged performance criteria of the stations.

The stations YARL and MONL are trailer-based Mobile Laser (MOBLAS) stations which were deployed by NASA in the 1970s in order to support the global SEASAT mission tracking (Husson, 1992). They have similar measurement characteristics due to their similar hardware (see Table 19). While their measurement precision is smaller, GO1L provides longer passes with more shots in case of the full rate data, due to the local characteristics of the laser system (higher pulse width and 28 Hz synchronized fire frequency respectively – Bauer et al., 2016).

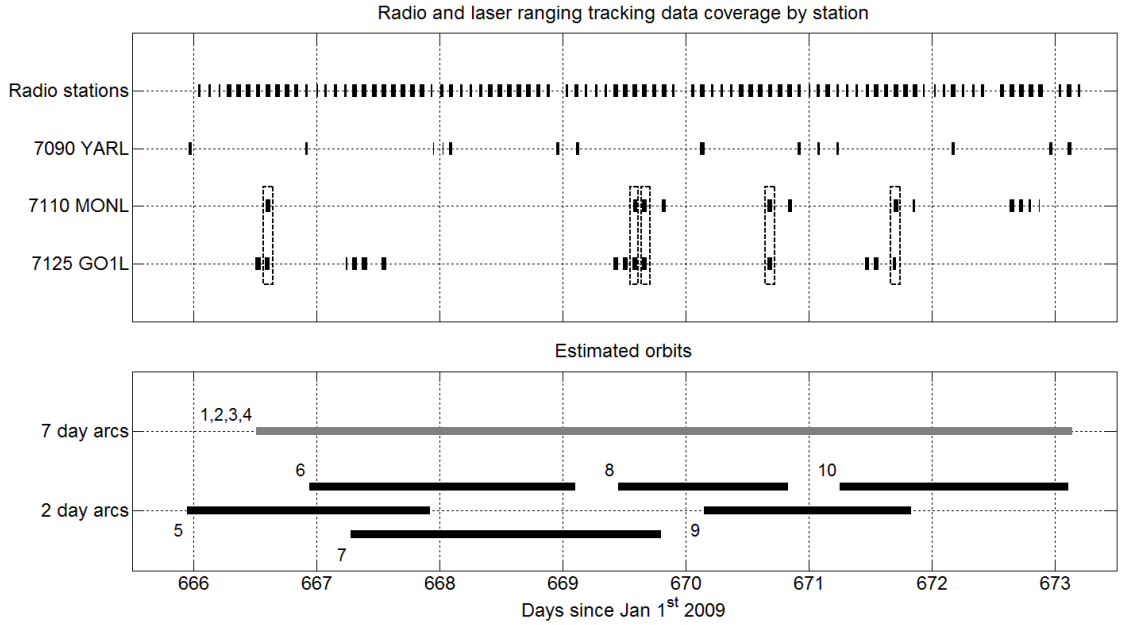

Figure 29: The upper plot provides the coverage of LRO laser ranging data from the stations YARL, MONL and GO1L and radio (range+Doppler) data. The dashed rectangles indicate simultaneous passes. The radio passes from various stations consisting of range and Doppler measurements are added for comparison. For simplification the radio data is not grouped by type or different stations. The lower plot shows the numbered 7-day and 2-day orbit arcs that we estimated in gray and black respectively. The 7-day arcs Nr. 1 to 4 cover the same timeframe while having variations in the LRO clock arc length as well as the observation data and are thus represented by one line. The consecutive overlapping 2-day arcs are shown separately. The detailed setup will be described in section 4.4.5 in detail for all orbit arcs. From the coverage of the orbits it can be seen which laser ranging passes were utilized to estimate them.

Table 19: List of the ground stations from which we used tracking data during the selected timeframe with their characteristics. Various performance criteria are listed which were averaged per station from the overall pass list in Table 24 (appendix). We used the observation data in the Normal Point format.

					Total		**Average*** **		
Station	**Name**	**Location**	**Coordinates**	**Timing system**	**Nr. of passes**		**Pass length**	**Nr. of shots**	**Measure-ment precision**
ID			**Lat.,Long.,Elev.**		**Single**	**SP****	**In min**		**In cm**
7090	**YARL***	Dongara, Western Australia, Australia	29.0464° S 115.3467° E 244 m	H-Maser	15	0	31.0	201	3.25
7110	**MONL***	Mt. Laguna, California, USA	32.8917° N 116.4227° W 1842 m	Rubidium	7	5	36.4	210	3.69
7125	**GO1L**	Greenbelt, Maryland, USA	39.0206° N 76.8277° W 19 m	H-Maser	8	5	46.0	483	6.28
				Total/average value	**30**	**10**	**37.6**	**298**	**4.40**

*) MOBLAS stations.

**) Simultaneous passes.

***) Normal Point data used.

From October 29th to November 5th 2010 there was high data coverage between the 2 US stations, with single and simultaneous passes. Even though there are no simultaneous passes between the US (GO1L and MONL) and the Australian station (YARL), the latter provides an important share of tracking data from the southern hemisphere. Thus the YARL observation data improves the observation geometry and the distribution of tracking data throughout an Earth day.

During the selected timeframe there is a laser ranging pass every 4 hours with an average length of ≈38 min. While the minimum time between two following passes is 134 min (consecutive orbit revolutions), there are 3 gaps longer than 12 h (see Figure 29). While two gaps are around 12 h (12.4 hours on day 666 and 12.2 h on day 670) one gap has a length of 20 h (20.4 hours on day 668). While the laser ranging dataset features passes from 10 stations, these data gaps are present within this work since we only used data from 3 stations within the estimation.

For comparison Figure 29 also shows the coverage of radio range and Doppler data from different stations. There are 88 radio passes, with an average length of 41.9 min and a maximum gap of 3.3 h during the timeframe. There are more than twice as many radio than laser ranging passes and their coverage is denser. These Doppler passes were used for the estimation of the nominal LRO trajectory (Mazarico et al., 2012).

We estimate the orbits from the laser ranging data in the Normal Point format as described in Bauer et al. (2016) with the LRO specific settings on the length and minimum number of measurements per bin (International Laser Ranging Service (ILRS), 2016). The full rate observations are grouped into bins with a length of 5 seconds starting at midnight. If there is more than one measurement per bin, they are averaged to one Normal Point. An empirical station specific range walk correction is applied to the observation data (Bauer et al., 2016).

During the selected timeframe LRO moves in an almost circular orbit with an eccentricity of $\approx 6 \times 10^{-3}$ (see Figure 30). While LRO's orbital plane remains fixed in inertial space, its orientation relative to the observing stations changes significantly, as expressed by the angle α (see Figure 31). Within our chosen timeframe LRO's orbital plane is initially seen "face-on" (α of 0°/180°) and finally in "edge-on" view (α of 90°/270°). While the cross-track direction is constrained well with range measurements at a "face-on" view, the along track directions have larger uncertainties in our orbit reconstruction, similar to effects observed in radio science data analysis (Mazarico et al., 2012).

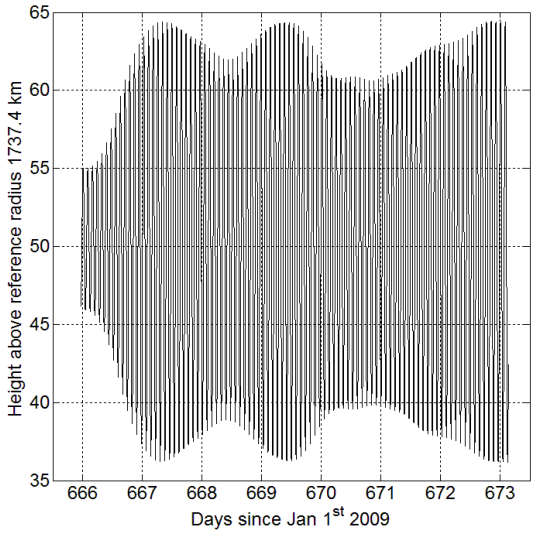

Figure 30: Height of LRO above the surface, with reference radius of 1734.1 km (Archinal et al., 2011).

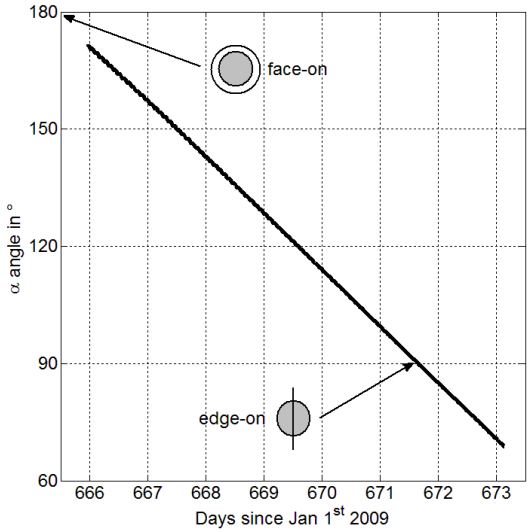

Figure 31: α expresses the angle between the Earth – LRO vector and the orbital plane of LRO around the moon and thus an LRO orbit view-on angle from the Earth. The "face-on" and "edge-on" views from the Earth onto the orbital plane are illustrated for angles of 180° and 90°, respectively.

4.4.5 Setup of the estimated orbit arcs

Figure 32 shows the detailed setup of the 7-day (Nr. 1 to 4) and the 2-day (Nr. 5 to 10) orbit arcs that we introduced in Figure 29.

The arcs Nr. 1 to 4 all cover the same timeframe (day 666.51 until 673.14 since January 1st 2009). We estimated the trajectory and the ground station clocks once over the 7 days. Because we modified the LRO clock arc length and the observation data we retrieved 4 different arcs. Within arc Nr. 1 and 2 we estimated the LRO clock per day, yielding 7 clock arcs with a length of ≈1 day each. Within arc 3 and 4 we estimated the LRO clock once per full period, yielding 1 clock arc with a length of ≈7 days. In addition we introduced simultaneous passes to the observation data for both types of clock modeling (per day and per full period) to analyze how well they can be incorporated with the current modeling. Beside all single passes, we utilized one of the simultaneous passes within the arcs Nr. 1 and 3 and both within the arcs Nr. 2 and 4.

The arcs Nr. 5 to 10 have a length of ≈2 days which is close to the typical length used for lunar spacecraft within orbit determination (Konopliv et al., 2001; Mazarico et al., 2010, 2012 and 2013). Further they are set up so that they have overlaps around one day (see Figure 32), from which we evaluate their consistency. We estimate a trajectory and a set of LRO and ground station clock parameters over the full period of 2 days separately for every arc.

Arc Nr. 7 is longer than the others due to a 20 hours data gap on day 668 (see Figure 29). More observation passes had to be added to enable the estimation of that arc. The other arcs have only minor variations of their length due to individual observation pass selection.

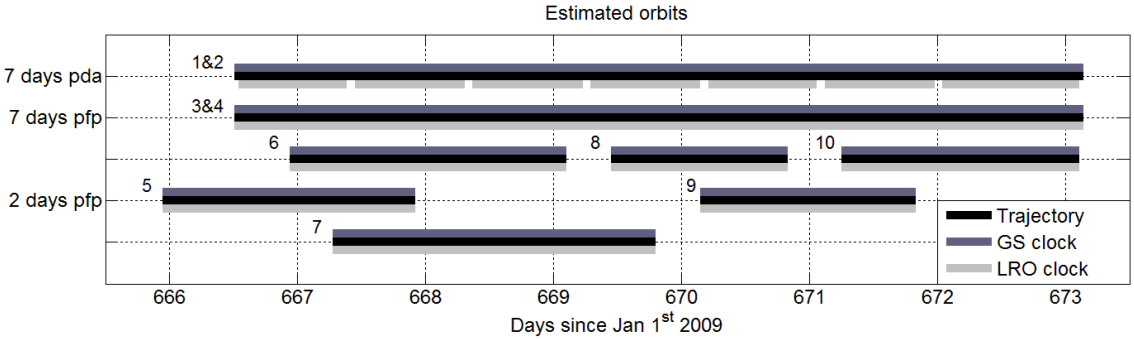

Figure 32: Detailed setup of the estimated orbits, which consist of a trajectory, a LRO and a ground station clock arc. While the lines illustrate the length of the certain arcs – black for trajectory, dark gray for the ground station clocks and light gray for the LRO clock – the numbers label the orbits. We distinguished between orbits with a length of 7 days and 2 days, where we estimated the LRO clock either per day (pda) or per full period (pfp) over the arc. In case of the 7-day arcs Nr. 1 and 3 we further modified the observation data by adding simultaneous passes, resulting in a different trajectory but with the same coverage.

For the 7 day long arcs Nr. 1–4 we estimated empirical accelerations in order to absorb errors from un-modeled or simplified dynamic effects (see section 4.4.2) that accumulate with increasing arc length. We did not incorporate simultaneous passes within the 2-day arcs because since they caused too much degradation.

4.4.6 Analysis of the estimated trajectories and clock parameters

As a result of a single orbit arc we obtained its trajectories, the post-fit measurement residuals, the LRO and ground station clock parameters as well as the empirical accelerations that we iterated from their a priori initial values and covariances.

We compared our estimated trajectories to the nominal LRO trajectory in the directions – along- , cross-track, radial and total for evaluation of their accuracy. Further we compared our differences to the differences of 5–30 m that Mao et al. (2014a) observed between their laser ranging data only orbits and the nominal LRO trajectory. With the 2-day arcs we further compare the differences to the nominal trajectory to the differences at the arc overlaps to evaluate their agreement.

From remaining trends of the measurement post-fit residuals we check the result precision and the modeling accuracy. Since post-fit residuals only allow for an analysis of the precision, we evaluate the trajectory accuracy from the comparison to the nominal LRO trajectory.

We compared our estimated LRO and ground station clock parameters to their a priori constraints as well as the literature. With that we check if they were estimated within their a priori constraints and how they were affected by variations of the clock arc length and clock modeling errors.

In case of the LRO clock parameters we focus on the comparison of the rate and aging. Since the offset represents a reference value and absorbs the mean clock error, as well as a mean range bias per arc it does not provide a valuable comparison.

With the ground station clocks we further compared differences in offset and rate to the corresponding differences from Bauer et al. (2016). Within this work we derived the differences for the comparison from the total offset and rate values of certain ground station combinations.

The arcs Nr. 1–10 provided us with a variety in the length of the trajectory and the clock arcs. In order to analyze the effect of the arc length on the results with the given modeling accuracy (see section 4.4.2), we compare their trajectories, their post-fit residuals and their clock parameters. Furthermore we evaluate how well the simultaneous passes were incorporated with the current modeling by comparing the results of the 7-day arcs with and without them.

4.5 Results

In this section we present the results of the 7-day and the 2-day arcs (see section 4.4.5). After evaluating the trajectories and their measurement post-fit residuals in section 4.5.1, we analyze the LRO clock parameters in section 4.5.2 and the ground station clock differences in section 4.5.3.

4.5.1 Difference to the nominal LRO trajectory and post-fit measurement residuals

Table 20 lists the differences to the nominal LRO trajectory and the post-fit measurement residuals of the estimated 7-day and 2-day arcs with their specific features. In case of the 7-day arcs these are the clock modeling and the simultaneous passes. With the 2-day arcs these are the overlap lengths and differences.

Overall the differences with respect to the nominal LRO trajectory are within the reported range of 5–30 m from Mao et al. (2014a) for the best 7-day arc Nr. 3 and for the mean difference of the 2-day arcs. Increasing the arc length from 2 to 7 days increased the differences to the nominal trajectory as shown with the difference of the 7-day arc Nr. 2 compared to the mean difference of the 2-day arcs. The estimation of constant empirical accelerations once over the 7-day arcs absorbed errors from the dynamical modeling. Due to that the 7-day arc Nr. 3 achieved differences to the nominal trajectory comparable to the mean difference of the 2-day arcs (≈25 m).

Table 20: Averaged values of the 7 and the 2-day arcs with the differences with respect to the nominal LRO trajectory as well as the measurement post-fit residuals.

Arc						Other	
Nr.	**Begin**	**End**	**Length**	**Difference to nominal LRO trajectory**	**Measurement residuals**	**Estimation Lengthx Number**	**SP included**
	Days since 2009 Jan 1st			**m**	**m**	**–**	**–**
1	666.51	673.14	6.63	35.11	3.69	Per day 7x1	No
2				42.78	4.01		Yes
3				23.79	6.76	Per full period 1x7	No
4				31.39	7.23		Yes
Nr.	**Begin**	**End**	**Length**	**Difference to nominal LRO trajectory**	**Measurement residuals**	**Overlap length**	**Overlap diff**
	Days since 2009 Jan 1st			**m**	**m**	**Day**	**m**
5	665.97	667.95	1.98	14.63	0.37		
6	666.91	669.13	2.22	31.58	2.03	1.04	34.55
7	667.25	669.83	2.58	18.50	1.46	1.88	39.51
8	669.42	670.86	1.44	37.16	0.19	0.41	57.06
9	670.12	671.86	1.74	35.69	0.29	0.74	71.92
10	671.22	673.14	1.92	12.15	1.19	0.64	22.95
Mean			**–**	**24.95**	**0.92**	**–**	**40.61**

While we estimated empirical accelerations on the order of $1x10^{-9}$ to $1x10^{-8}$ m/s², Mazarico et al. (2012) reported values one to two order of magnitude smaller within their LRO orbit determination. The estimation of larger empirical accelerations is caused by our less accurate dynamical modeling compared to Mazarico et al. (2012). Since the incorporation of empirical accelerations once per revolution provided no improvement while increasing the number of correlated parameters we only estimated constant empirical accelerations.

The estimation of the LRO clock per day within the 7-day arcs (Nr. 1 and 2) enabled a better approximation of its trend by the 2nd order polynomial fit. Over the shorter clock arc length less stochastic noise and variations due to temperature change have to be approximated with the fit. The accumulation of less errors allows for smaller post-fit residuals compared to the arcs where the LRO clock was estimated over the full period of 7 days (Nr. 3 and 4 – see Figure 33). With the 2-day arcs both the state and the LRO and the ground station clocks were adjusted separately for every arc. Because of that they had even smaller post-fit residuals e.g. of only 0.19 m for arc Nr. 8 (see Table 20).

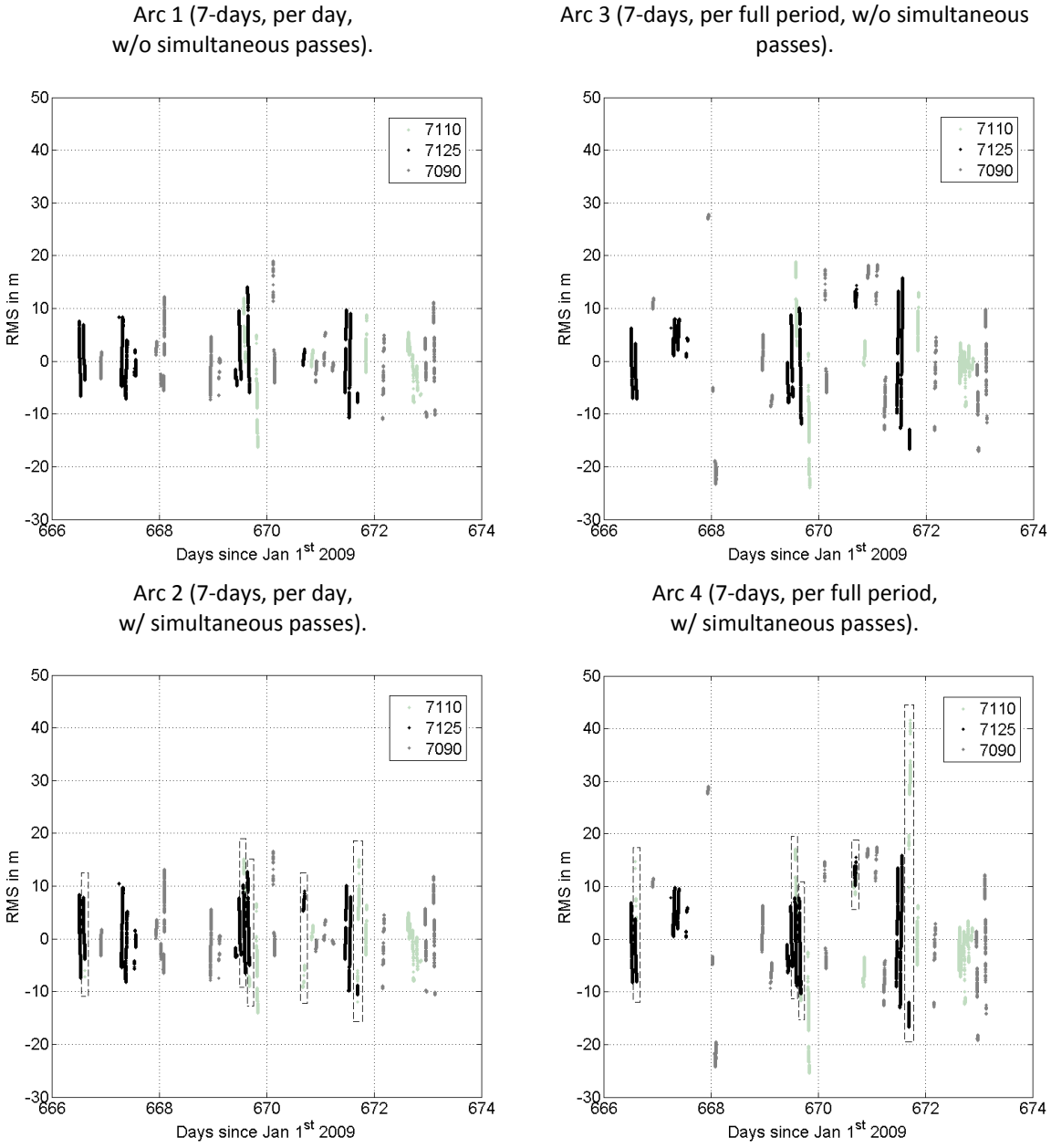

Figure 33: Measurement post-fit residuals with respect to the estimated trajectory of the 7-day arcs 1 to 4.

The arc overlap differences of the consecutive 2-day arcs were larger than their differences to the nominal trajectory (see Table 20). Thus the estimated trajectories were generally in agreement with the nominal trajectory even though they were scattered around it. The data gaps on day 668 (20.4 h) and on day 670 (12.2 h) that affected the arcs Nr. 7, 8 as well as 9, caused their overlaps to have large deviations in particular.

If only single passes are used from the observation data the 7-day arcs yield smaller differences to the nominal LRO trajectory and post-fit residuals for both types of clock modeling (per day and per full period). Even though it is expected that simultaneous passes should improve the solution (Neumann et al., 2014) the opposite seems to be the case – see Table 20 and Figure 33.

The simultaneous passes were carried out by stations with different timing systems which is why they had differences in offset and rate with respect to each other. However in case of perfect dynamical and clock modeling their measurement residual differences should be close to the observation data precision (≈15 cm). Since the 2nd order fit that we apply over the full timeframe of 7 days cannot represent the stochastic noise of the correlated ground station clocks well enough, the measurement residual differences exceed the observation data precision at the simultaneous passes (see section 4.4.2 and 4.5.3). Since the passes were carried out simultaneously their approximation is not affected by the completeness and accuracy of the LRO clock corrections.

Since the simultaneous passes could not be resolved at the LOLA timestamp precision yet, more accurate dynamical and clock modeling is required in order to enable their successful application. Within the estimation we did not utilize the simultaneous passes as constraint (e.g. post-fit residuals at observation data precision) but used them as two separate single passes to benchmark our dynamical and clock modeling.

The Figure 36 to Figure 38 (supplementary material) provide the differences to the nominal LRO trajectory of all arcs as well as the overlap differences of the 2-day arcs. Exemplarily the differences to the nominal trajectory of the best 7-day arc Nr. 3 and the best 2-day arc Nr. 10 are shown in Figure 34.

The 2-day arc along- and cross-track differences to the nominal trajectory show a dependency on the alpha angle as reported by Mazarico et al. (2012) – see Figure 37 (supplementary material). At the beginning of the timeframe α is almost 180° (“face-on” – see Figure 31) which enables a better estimation of the cross-track than the along-track elements. Accordingly the cross-track differences of the arcs Nr. 5, 6 and 7 are smaller than their along-track differences. Towards day 671.5 α becomes 90° (“edge-on”- see Figure 31) resulting in better resolved along-track than cross-track elements as it is the case with the arcs Nr. 8, 9 and 10. This change of the along- and the cross-track accuracy with the alpha angle is also present with differences of the arc overlaps – see Figure 38 (supplementary material) for the overlaps of the arcs 5 and 6, 6 and 7 compared to the overlaps of the arcs 7 and 8, 8 and 9, 9 and 10.

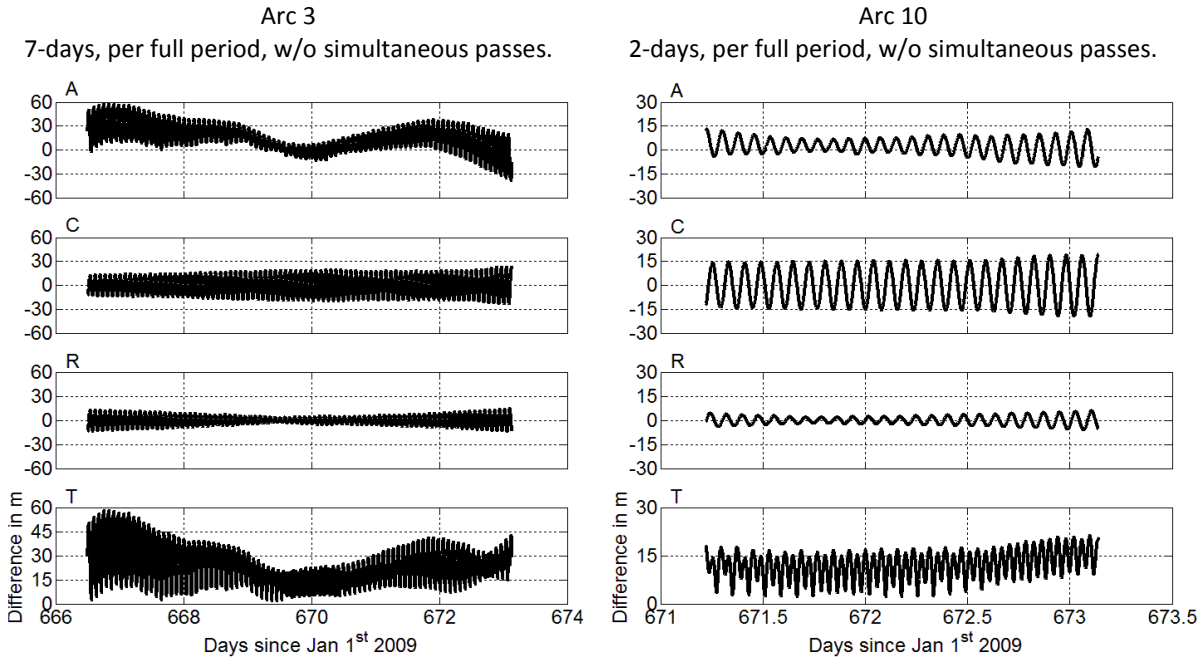

Figure 34: Difference of the best 7-day and 2-day arc with respect to the nominal LRO trajectory in the satellite coordinate system directions along- (A), cross-track (C), radial (R) and total (T). Note the change in the scale of the time and the differences between the two arcs.

4.5.2 LRO clock parameters rate and aging

Figure 35 shows the LRO clock rate parameters $\Delta\tau^{(1)}_{LRO}$ we estimated from the applied 2nd order fit for all arcs. All estimated rate values are shown at the beginning of their state arcs respectively over which they are constant.

The rate estimated following Bauer et al. (2016) for every single or over multiple (here all plotted) passes is added. A linear fit was added to the rates of the single passes with their 3-σ error of ≈±1x10^{-11} for comparison. Neglecting the change of aging (≈-2.2x10^{-14} /day² from Bauer et al., 2016) causes an error of ≈1x10^{-12} in the rate over the 7 days. Since this error is below the rate uncertainty of 1x10^{-11} this linear fit is acceptable within the comparison. The rates derived from the linear fit of single passes also were the basis for the LRO clock rate a priori constraints in section 4.4.3.

While Bauer et al. (2016) used a fixed orbit (nominal trajectory) to derive the clock parameters, we adjust both the state and the clocks within this work. Due to the good accuracy of the nominal trajectory (9 m at the arc overlaps), the values derived with it provide a good comparison. Due to the fixed orbit they are affected by its state errors. However they become more accurate when estimated over multiple passes covering a longer timeframe.

While the LRO clock rates also can be estimated well from single passes, the aging of the selected timeframe (≈1.6x10^{-12} /day from Bauer et al.; 2016) only causes a difference of ≈3 cm over the average laser ranging pass length of ≈38 min. Since this difference is below the LOLA timestamp precision the aging value needs to be averaged over a longer timeframe with the multiple-pass analysis.

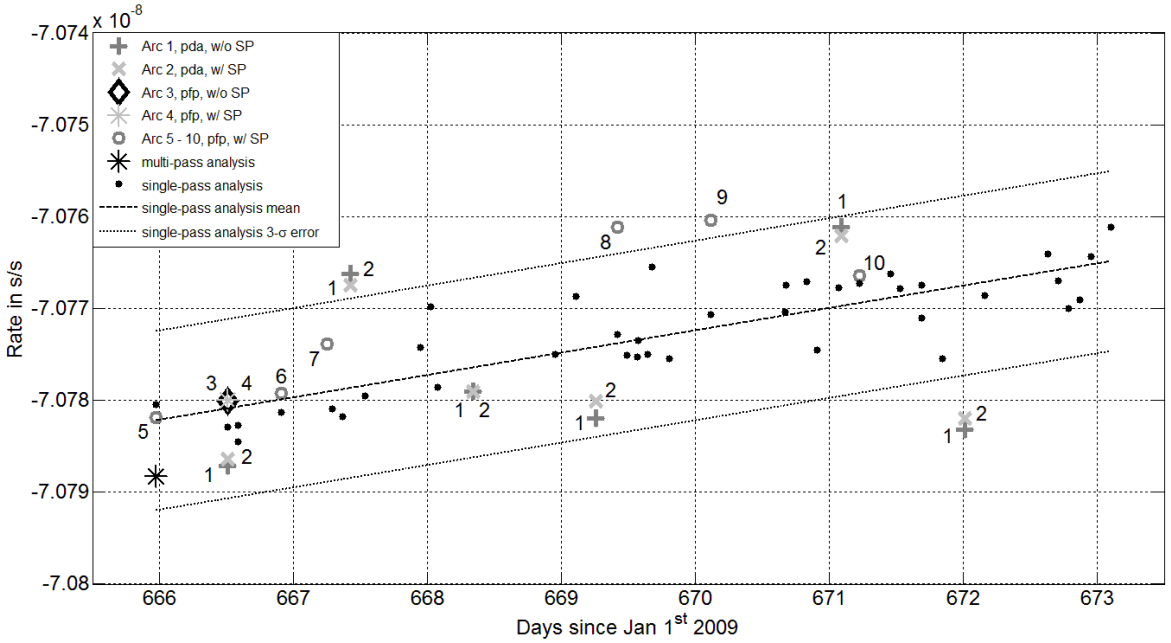

Figure 35: Estimated LRO clock rate $\Delta\tau_{LRO}^{(1)}$ of the 7-day and 2-day arcs numbered from 1 to 10 with their variation of the LRO clock modeling (pda – per day and pfp – per full period) and the observation data (with or without simultaneous passes). For comparison the rate values from the analysis (single- and multiple-pass) based on the nominal LRO trajectory are added. For the values from the single pass analysis, the 3-σ error bounds are added.

With that the rates were estimated to values within the 3-σ error of the single pass rates except for the arcs Nr. 1 and 2 on day 667 and 672 within the arcs Nr. 1 and 2 as well as for arc Nr. 8 and 9. In case of the arcs Nr. 1 and 2 the outliers represent the varying LRO clock trend enabled by the shorter clock arc length of one day (see section 4.4.2). With the 2-day arcs the data gaps on day 668 and 670 that affect the arcs Nr. 7, 8 and 9 caused the estimated rates to be more off than for the arcs Nr. 5, 6 and 10. The incorporation of simultaneous passes within the 7-day arcs did not change the estimated rate significantly (see Figure 33). Mao et al. (2011) reported a similar rate of ≈7x10^{-8} during our selected timeframe. The rates differ by ≈8x10^{-9} since they use UTC as time scale while we use TDB.

While the arcs Nr. 5–10 had an a priori covariance constraint of 1x10^{-11} on the rate, the arcs Nr. 1–4 were constrained with a covariance of 1x10^{-13} to prevent further error absorption by the parameters.

The LRO clock aging parameters $\Delta\tau_{LRO}^{(2)}$ we estimated from the 2nd order polynomial fit are listed in Table 21 for the 7-day arcs Nr. 1–4 and in Table 22 for the 2-day arcs Nr. 5–10. Both tables also list the values estimated with a single and multiple pass (here all plotted) analysis following Bauer et al., 2016. We applied a linear fit to the aging values of the single passes for interpolating them to the beginning of the clock arcs for a direct comparison.

Table 21: Estimated LRO clock aging $\Delta\tau_{LRO}^{(2)}$ from the single-pass analysis, the multiple-pass analysis and the arcs where the LRO clock was estimated per full period over the 7-days (orbit arc length).

Begin date of the clock arc in days since 2009 Jan 1st	Aging $\Delta\tau_{LRO}^{(2)}$ in /day					
	Single-pass analysis	Multiple-pass analysis	Per day simultaneous passes		Per full period simultaneous passes	
			Not Included	Included	Not Included	Included
			Arc 1	Arc 2	Arc 3	Arc 4
666.5	+2.1x10^{-10}	+2.4x10^{-12}	+2.5x10^{-12}	+2.7x10^{-12}	-1.2x10^{-8}	-2.9x10^{-9}
667.4	+2.4x10^{-10}		-2.8x10^{-11}	-2.7x10^{-11}		
668.3	+2.7x10^{-10}		-4.6x10^{-12}	-4.0x10^{-12}		
669.3	+3.0x10^{-10}		-2.3x10^{-12}	-4.2x10^{-12}		
670.2	+3.4x10^{-10}		+1.0x10^{-11}	+1.3x10^{-11}		
671.1	+3.7x10^{-10}		-2.1x10^{-12}	-1.8x10^{-11}		
672.0	+4.0x10^{-10}		+2.0x10^{-12}	+1.8x10^{-12}		
Average	**+3.0x10^{-10}**	**–**	**-3.1x10^{-12}**	**-5.1x10^{-12}**	**–**	**–**

The aging values estimated over 1 day (per day within the 7-day arcs) agreed best with the multiple-pass analysis value of ≈2.4x10^{-12} /day. When estimated over 2 days we saw intermediate agreement and over 7 days (per full period within the 7-day arcs) worse agreement (see Table 21 and Table 22). The incorporation of simultaneous passes within the 7-day arcs did not change the aging parameters significantly (see Table 21). While the oscillators of the New Horizons and the GRAIL mission had aging values of 1x10^{-11} /day and 7x10^{-11} /day (Weaver et al. 2004, 2010), our multiple-pass analysis and the 7-day arc per day values are in agreement with the LRO clock aging reported by Mao et al. (2011) of 3.2x10^{-12} /day.

The 2nd order polynomial is only a rough approximation of the inherently stochastic nature of the clock noise (see Figure 1 of Dirkx et al. 2015b). Accordingly the stochastic noise and periodic variations due to temperature change were not captured by the fit and affected the clock parameters as well as the post fit residuals. While the LRO clock rate was mostly in agreement with it's a priori constraints even when estimated over 7 days, the aging was significantly increasing with increasing clock arc length due to error absorption – also as enabled by the a priori constraints. The increase of the post-fit measurement residuals due to accumulating clock modeling errors also can be seen in in Figure 33.

Table 22: Estimated LRO clock aging $\Delta\tau_{LRO}^{(2)}$ from the single-pass analysis, the multiple-pass analysis and the arcs where the LRO clock was estimated per full period over the 2-days (arc length).

Arc	Begin	End	Aging $\Delta\tau_{LRO}^{(2)}$ in /day		
Nr.	Days since 2009 Jan 1st		Single-pass analysis	Multiple-pass analysis	Per full period
5	665.97	667.95	+1.9x10^{-10}	+2.4x10^{-12}	+3.7x10^{-11}
6	666.91	669.13	+2.2x10^{-10}		-9.5x10^{-10}
7	667.25	669.83	+2.3x10^{-10}		-5.8x10^{-11}
8	669.42	670.86	+3.1x10^{-10}		+7.0x10^{-11}
9	670.12	671.86	+3.4x10^{-10}		+7.1x10^{-11}
10	671.23	673.14	+3.7x10^{-10}		-3.5x10^{-10}
Average			**+2.8x10^{-10}**	**–**	**-5.5x10^{-11}**

4.5.3 Ground station clock differences

Table 23 shows the ground station clock differences we estimated compared to the differences that Bauer et al. (2016) measured from common view time transfer during the selected timeframe. Because of the limited accuracy of the clock modeling we could not estimate the differences to the exact values

from Bauer et al. (2016). However we estimated reasonable differences since at first the relative rates agree with the floor stability values of the timing systems used at the ground stations – Rubidium and H-Maser with noise floor stabilities at $1x10^{-15}$ to $1x10^{-12}$ (see Table 17 and Table 19). Furthermore the differences are not larger than the upper limits measured by Bauer et al. (2016), except for the 2-day arc upper relative offset of 1000 ns. While this relative offset is too large to be realistic it highlights the absorption of clock modeling errors by the clock parameters in particular.

As shown with equation 34, the errors of the LRO and all involved ground station clocks have to be estimated simultaneously. The a priori constraints separate the LRO from the ground station clocks. While the errors from the ground station clocks are smaller than the LRO clock errors (similar stabilities but over longer timeframes – see section 4.2), multiple stations have to be estimated with errors at the same order of magnitude. Furthermore the 2nd order polynomial fit cannot approximate the complete stochastic noise of the ground station clocks over the timeframe of 2 and 7 days. Due to the limited clock model accuracy and high correlations of all clock parameters we cannot estimate them to their actual values Furthermore the post-fit measurement residuals of the simultaneous passes were not at LOLA's observation data precision (see Figure 34). Applying individual a priori constraints for each of the ground stations also showed no improvement, since we could not separate the highly correlated clocks with the current modeling well enough.

Table 23: Comparison of the ground station clock differences (relative offsets and rates) estimated by Bauer et al. (2016) and from the 7-day and the 2-day arcs.

	Relative offset order of magnitude	**Relative rates order of magnitude**
7-day arcs	10–100 ns	$1x10^{-15}$ to $1x10^{-12}$
2-day arcs	10–1000 ns	$1x10^{-13}$ to $1x10^{-11}$
Bauer et al. (2016)	1–100 ns	$1x10^{-13}$ to $1x10^{-11}$

4.6 Discussion and conclusions

We used observation passes collected from ILRS ground stations to LRO for a demonstration of orbit determination with one-way laser ranging data only. We selected a timeframe of 7 days from October 28th to November 5th 2010 during the mission phase SM02.

Due to the one-way setup, the state of LRO and all involved clocks (LRO and all ground station clocks) have to be estimated simultaneously. Furthermore the errors of both the dynamical and the clock modeling accumulate with increasing arc length. The accumulation of errors thereby depends on the completeness and the accuracy of the corrections, the modeling accuracy and the stability of the involved clocks. Thus an optimum arc length is required in order to achieve a balance between the accuracy of the estimated trajectories, the measurement post-fit residuals and all clock parameters. These aspects represent inherent drawbacks of one-way data in general – compared to two-way data for example.

We used a priori constraints to separate and estimate the state as well as all involved and correlated clocks. Our a priori constraints on the LRO initial state as well as the LRO and ground station clock parameters from Bauer et al. (2016) were derived from or while using the nominal LRO trajectory respectively. The estimated trajectories were also compared to the nominal trajectory and the clock parameters to their a priori constraints. With that we utilized a radio-based product for the analysis of laser data, the a priori constraints and as a reference for comparison of the results. However due to

the good accuracy of the trajectory (9 m ≈30 ns at the arc overlaps) it provides an accurate basis and reference.

We estimated multiple 7- and 2-day long arcs within the selected timeframe. The best 7-day arc had a difference of 23.95 m to the nominal LRO trajectory and post-fit measurement residuals of 6.76 m. On average the consecutive 2-day arcs had a difference to the nominal trajectory of 24.95 m, post-fit residuals of 0.92 m and arc overlap differences of 40.91 m. The differences to the nominal trajectory were in the range that Mao et al. (2014a) observed with their 2-week long laser ranging arcs (5–30 m). The larger overlap differences of the 2-day arcs indicate that they were scattered around the nominal trajectory. Extending the state and the clock arc length from 2 to 7 days increased the difference to the nominal LRO trajectory (≈25 m to ≈42 m) and the post-fit measurement residuals (≈1 m to ≈7 m). The estimation of empirical accelerations within the 7-day arcs absorbed errors from the dynamical modeling and enabled the estimation of 7-day arcs with differences to the nominal trajectory comparable to the 2-day arcs (≈25 m).

We observed a relationship between the ratio of along- and cross-track differences and the alpha angle (angle between vector Earth-LRO and normal vector of LRO's orbital plane) as observed by others during LRO orbit determination (Mazarico et al., 2012).

We estimated the LRO clock rate to values in agreement with the a priori constraints. Except for outliers due to shorter clock arc lengths and data gaps, they were within the 3-σ range ($\pm 1 \times 10^{-11}$) of the linear trend from the single pass rates. We estimated an average LRO clock aging value of -3.1×10^{-12} /day with a clock arc length of 1 day, of -5.5×10^{-11} /day with a length of 2 days and of 1.2×10^{-8} /day with a length of 7 days. Using methods from Bauer et al. (2016) we estimated an aging value of 2.4×10^{-12} /day during the selected timeframe. Contrary to the LRO clock rate, the aging becomes significantly larger with increasing clock arc length because the stochastic LRO clock noise and the variations due to temperature change become approximated less good by the clock model (2nd order polynomial fit).

We estimated ground station clock differences at the order of 10 to 1000 ns for the relative offset and 1×10^{-15} to 1×10^{-11} for the relative rates. Except for the outlying offset of 1000 ns the values are in agreement with the relative offsets and rates of Bauer et al. (2016). Further the relative rates agree with the noise floor stability values of the timing systems which were used at the stations. Because of the limited clock modeling accuracy, errors at similar magnitudes and high correlations between the ground station clock parameters, the differences could not be estimated to the exact values of Bauer et al. (2016). Furthermore the measurement post-fit residuals of the simultaneous passes were not at LOLA'S observation data precision.

Overall our estimation was capable of producing orbit arcs with one-way laser data only to an accuracy comparable to radio-based orbit arcs, while using less than half the number of tracking passes (40 laser compared to 88 radio passes). The incorporation of simultaneous passes did not change the estimated trajectories, the post-fit measurement residuals and the clock parameters significantly.

While the random errors observed within SLR typically limit the measurement accuracy, they are smaller than the LOLA timestamp precision with the LRO laser ranging experiment. Compared to two-way for example systematic errors are dominating with the one-way setup. They are coming from the station and the spacecraft hardware, their calibration, their timing systems and have to be modeled and estimated as well. Because all errors have to be estimated within the orbit determination simultaneously, a priori constraints are required to separate the state and all involved clocks as well as

sufficient observation data coverage. Within our work we saw that gaps over 12 h degraded the result accuracy significantly in particular with arcs with a shorter length (2 days). We saw that the accuracy of the trajectories, their post-fit measurement residuals and the clock parameters became worse with increasing arc length due to errors in the modeling. Because of that an improvement of the corrections, the dynamical and the clock modeling should improve the result accuracy which should be the case with the simultaneous passes in particular.

To improve the dynamical modeling, we propose to implement a geometrical 3D spacecraft model. Such a model would allow for an improved solar radiation pressure model including effects of changing orientation of the spacecraft and self-shadowing. Additionally, indirect solar radiation pressure and thermal radiation could be incorporated. In order to improve the clock approximation, the response of the LRO clock due to thermal variation could be incorporated. If the change of the LRO clock rate can be modeled better, its approximation becomes better allowing for better residuals also over longer arc lengths. The LRO clock approximation could further be improved by using an optimum clock arc length for the LRO and the ground station clocks. With an improved approximation, the application of a priori timing information should provide an even better separation of the involved clocks. With that less errors accumulate, which should improve the accuracy of the estimated trajectories, their post-fit residuals and the clock parameters. Moreover an improved approximation might enable the application of observation data from more than 3 stations which could close gaps in the selected observation data and further improve the result accuracy.

Finding an optimum on the state and clock arc length, that balances the trajectory, the post-fit measurement and the clock parameter accuracy would require a more extensive variation of the arc lengths. Since the observation data coverage was not coherent enough with our given modeling, arcs with further variations in the length did not provide comparable results. That has already become apparent with the adjustment of the length of arc Nr. 7 due to a ≈20 h data gap. In order to achieve results comparable to the other 2 day arcs it had to be extended to incorporate more observation data.

While a two-way laser ranging system is affected less from systematic errors than a one-way system, it requires additional and active hardware onboard the spacecraft. With a one-way ranging system the stabilities of the onboard and ground station clocks are key for the performance. While ground station clocks already provide good stabilities, onboard clocks are subject to requirements on mass and power consumption which results in a limited performance. However recent developments as the Deep Space Atomic Clock already demonstrated a stability of $1x10^{-15}$ /day (Ely et al., 2012) which promises better orbit determination. If multiple stations are participating in a ranging campaign, there clocks should be well referenced to a common reference such as UTC. Otherwise simultaneous passes could be used to measure their differences from common view observations. With the given stability of the DSAC, the accurate measurement of the differences also might be possible in non-common view as with the ELT experiment for example.

Overall the one-way laser ranging to LRO experiment provides a comprehensive dataset to study the capabilities and challenges of this type of tracking data. Since only minor hardware extensions on an existing instrument were required, this tracking technique is promising for future missions that carry a laser altimeter such as the Jupiter Icy Moons Explorer (JUICE) mission from ESA.

Acknowledgements

S. Bauer, H. Hussmann and D. Dirkx were supported by the ESPaCE project, EC FP7 Grant Agreement 263466. Major parts of this work were carried out while the first author very much enjoyed a research visit at NASA Goddard Space Flight Center (GSFC). J.O. was hosted by MIIGAiK and supported by the Russian Science Foundation, project #14-22-00197. We thank two anonymous reviewers for their very constructive comments.

References

Archinal, B.A., A'Hearn, M.F., Bowell, E., Conrad, A., Consolmagno, G.J., Courtin, R., Fukushima, T., Hestroffer, D., Hilton, J.L., Krasinsky, G.A., Neumann, G.A., Oberst, J., Seidelmann, P.K., Stooke, P., Tholen, D.J., Thomas, P.C. and Williams, I.P., Report of the IAU working group on cartographic coordinates and rotational elements, *Celest. Mech. Dyna. Astron* **109**, 2011.

Bauer, S., Dirkx, D., Hussmann, H., Oberst, J., Mao, D., Neumann, G., Mazarico, E., Torrence, M., McGarry, J., Smith, D. and Zuber, M., 2014. Implementation of one-way laser ranging data into LRO orbit determination. In: Proceedings of the 19th International Laser Ranging Service workshop. Annapolis, Maryland, USA, 27th–31st October.

Bauer, S., Hussmann, H., Oberst, J., Dirkx, D., Mao, D., Neumann, G.A., Mazarico, E., Torrence, M.H., McGarry, J.F., Smith, D.E. and Zuber, M.T., Analysis of one-way laser ranging data to LRO, time transfer and clock characterization, *Icarus* **283**, 2017.

Buccino, D.R., Seubert, J.A., Asmar, S.W. and Park, R.S., Optical Ranging measurement with a lunar orbiter: limitations and potential, *J. Spacecr. Rockets* **53**, 2016.

Cash, P., Emmons, D. and Welgemoed, J., 2008. Ultrastable oscillators for space applications. In: Proceedings of the 40th Annual Precise Time and Time Interval (PTTI) Meeting. Reston, Virginia, USA, 1st–4th December.

D'Ortenzio, M.V., Bresina, J.L., Crocker, A.R., Elphic, R.C., Galal, K.F., Hunt, D.R., Owens, B.D., Plice, L., Hawkins, A.M., Policastri, L.A., 2015. Operating LADDEE: mission architecture, challenges, anomalies and success. In: Proceedings of the IEEE Aerospace Conference. Big Sky, Montana, USA, 7th–14th March.

Degnan, J.J., 1994. Thirty years of laser ranging. In: Proceedings of the 9th International Laser Ranging Service workshop. Canberra, Australia, 7th–11th November.

Dirkx, D., Vermeersen, L., Noomen, R. and Visser, P., Phobos laser ranging: numerical geodesy experiments for Martian system science, *Planet. Space Sci.* **99**, 2014.

Dirkx, D., Interplanetary Laser Ranging – Analysis for Implementation in Planetary Science Missions (PhD dissertation), 2015a, Delft University of Technology.

Dirkx, D., Noomen, R., Visser, P.N.A.M., Bauer, S. and Vermeersen, L.L.A., Comparative analysis of one- and two-way planetary laser ranging concepts, *Planet. Space Sci.* **117**, 2015b.

Einstein, A., Über das Relativitätsprinzip und die aus demselben gezogenen Folgerungen, *Jahrb. Radioakt. Elektron.* **4**, 1907.

Ely, T.A., Koch, T., Kuang, D., Lee, K., Murphy, D., Prestage, J., Tjoelker, R. and Seubert, J., 2012. The deep space atomic clock mission. In: Proceedings of the 23rd International Symposium on Space Flight Dynamics (ISSFD). Pasadena, California, USA, October 29th–November 2nd.

Exertier, P., Bonnefond, P., Deleflie, F., Barlier, F., Kasser, M., Biancale, R. and Menard, Y., Contribution of laser ranging to Earth's sciences, *C.R. Geosci.* **338**, 2006.

Exertier, P., Samain, E., Courde, C., Martin, N., Torre, J.-M., Oneto, J.-L., Laas-Bourez, M., Guillemot, Ph. and Léon, S., 2013. T2L2: Five years in space. In: Proceedings of the European Frequency and Time Forum & International Frequency Control Symposium (EFTF/IFC). Prague, Czech Republic, 21st–25th June.

Floberghagen, R., Visser, P. and Weischede, F., Lunar albedo force modeling and its effect on low lunar orbit and gravity field determination, *Adv. Space Res.* **23**, 1999.

Folkner, W.M., Williams, J.G., Boggs, D.H., Park, R.S. and Kuchynka, P., The planetary and lunar ephemerides DE430 and DE431, *IPN Prog. Rep.* **42-196**, 2014.

Husson, V.S., 1992. Historical MOBLAS system characterization. In: Proceedings of the 8th International Laser Ranging Service workshop. Annapolis, Maryland, USA, 18th–22nd May.

International Laser Ranging Service (ILRS) Website. <http://ilrs.gsfc.nasa.gov> retrieved in July 2016.

Lemoine, F. G., Goossens, S., Sabaka, T. J., Nicholas, J. B., Mazarico, E., Rowlands, D. D., Loomis, B. D., Chinn, D. S., Neumann, G. A., Smith, D. E. and Zuber, M. T., GRGM900C: a degree 900 lunar gravity model from GRAIL primary and extended mission data, *Geophys. Res. Lett.* **41**, 2014.

Lombardi, M.A., Fundamentals of Time and Frequency, in: The Mechatronics Handbook, 2001, CRC Press.

Konopliv, A.S., Asmar, S.W., Carranza, E., Sjogren, W.L. and Yuan, D.N., Recent gravity models as a result of the lunar prospector mission, *Icarus* **150**, 2001.

Kumar, K., Abdulkadir, Y., van Barneveld, P., Belien, F., Billemont, S., Brandon, E., Dijkstra, M., Dirkx, D., Engelen, F., Gondelach, D., van der Ham, L., Heeren, E., Iorfida, E., Leloux, J., Melman, J., Mooij, E., Musegaas, P., Noomen, R., Römgens, B., Ronse, A., Leite Pinto Secretin, T., Tong Minh, B., Vandamme, J. and and, Persson, S., 2012. TUDAT: a modular and robust astrodynamics toolbox. In: Proceedings of the 5th International Conference on Astrodynamic Tools and Techniques (ICATT). ESTEC/ESA, Noordwijk, The Netherlands, 29th May–1st June.

Löcher, A., Hofmann, F., Gläser, P., Haase, I., Müller, J., Kusche, J. and Oberst, J., Towards improved lunar reference frames: LRO orbit determination, in: International Association of Geodesy Symposia, Springer, 2015.

Mao, D., McGarry, J., Torrence, M., Neumann, G., Mazarico, E., Barker, M., Sun, X., Rowlands, D., Golder, J., Zagwodzki, T., Cavanaugh, J., Zuber, M. and Smith, D., 2011. Laser ranging experiment on Lunar Reconnaissance Orbiter: timing determination and orbit constraints. In: Proceedings of the 17th International Workshop on Laser Ranging. Bad Kötzting, Germany, 16-20 May.

Mao, D., Sun, X., McGarry, J., Mazarico, E., Torrence, M., Rowlands, D., Neumann, G., Barker, M., Golder, J., Smith, D. and Zuber, M., 2014a. LRO orbit determination with laser ranging data. In: Proceedings of the 19th International Laser Ranging Service workshop Annapolis. Maryland, USA, 27th–31st October.

Mao, D., Sun, X., Skillman, D., McGarry, J., Hoffman, E., Neumann, G., Torrence, M., Smith, D. and Zuber, M., 2014b. Time-transfer experiments between satellite laser ranging ground stations via one-way laser ranging to the Lunar Reconnaissance Orbiter. In: Proceedings of the 19th International Laser Ranging Service workshop. Annapolis, Maryland, USA, 27th–31st October.

Mazarico, E., Lemoine, F. G., Han, S.-C. and Smith, D. E., GLGM-3: a degree-150 lunar gravity model from the historical tracking data of NASA Moon orbiters, *JGR* **115,** 2010.

Mazarico, E., Rowlands, D.D., Neumann, G.A., Smith, D.E., Torrence, M.H., Lemoine, F.G. and Zuber, M.T., Orbit determination of the Lunar Reconnaissance Orbiter, *J. Geod.* **86**, 2012.

Mazarico, E., Goossens, S., Lemoine, F., Neumann, G., Torrence, M., Rowlands, D., Smith, D. and Zuber, M., 2013. Improved orbit determination of lunar orbiters with lunar gravity fields obtained by the GRAIL mission. In: Proceedings of the 44th Lunar and Planetary Science Conference (LPSC). Woodlands, Texas, USA, 18th–23rd March.

McGarry, J., Clarke, C., Mao, D. and Torrence. M., 2011. The First ILRS laser transponder mission: laser ranging to NASA's Lunar Reconnaissance Orbiter. In: Proceedings of the 17th International Laser Ranging workshop. Bad Koetzting Germany, 16th–20th May.

McGarry, J.F., Sun, X., Mao, D., Horvath, J., Donovan, H., Clarke, C., Hoffman, E., Cheek, J., Zagwodzki, T.W., Torrence, M.H., Barker, M.K., Mazarico, E., Neumann, G.A., Smith, D.E. and Zuber, M.T., 2013. LRO-LR: Four years of history-making laser ranging. In: Proceedings of the 18th International Laser Ranging workshop. Fujiyoshida Japan, 11th–15th November.

Montenbruck, O. and Gill, E., Satellite Orbits, 2000, Springer.

Neumann, G. A., Cavanaugh, J. F., Coyle, D. B., McGarry, J., Smith, D. E., Sun, X., Torrence, M., Zagwodski, T. W. and Zuber, M. T., 2006. Laser ranging at interplanetary distances. In: Proceedings of the 15th International Laser Ranging workshop. Canberra, Australia, 15th–20th October.

Neumann, G.A., Barker, M.H., Mao, D., Mazarico, E., McGarry, J.F., Smith, D.E., Sun, X., Torrence, M.H. and Zuber, M.T., 2014. Interplanetary laser ranging: the quest for 1 AU. In: Proceedings of the 19th International Laser Ranging Service workshop. Annapolis, Maryland, USA, 27th–31st October.

Pearlman, M.R., Degnan, J.J. and Bosworth, J.M., The international laser ranging service, *Adv. Space Res.* **30**, 2002.

Schreiber, U., Prochazka, I., Lauber, P., Hugentobler, U., Schafer, W., Cacciapuoti, L. and Nasca, R., 2009. The European Laser Timing (ELT) experiment on-board ACES. In: Proceedings of the 23rd European Frequency and Time Forum (EFTF 2009). Neuchâtel, Switzerland.

Smith, D., Zuber, M., Sun, X., Neumann, G., Cavanaugh, J., McGarry, J. and Zagwodzki, T., Two-way laser link over interplanetary distance, Science **311**, 2006.

Sun, X., Skillman, D.R., Hoffman, E.D., Mao, D., McGarry, J.F., McIntire, L., Zellar, R.S., Davidson, F.M., Fong, W.H., Krainak, M.A., Neumann, G.A., Zuber, M.T. and Smith, D.E., Free space laser communication experiments from Earth to the Lunar Reconnaissance Orbiter in lunar orbit, *Opt. Express* **21**, 2013.

Weaver, G., Reinhart, M. and Miranian, M., 2004. Developments in ultra-stable quartz oscillators for deep space reliability. In: Proceedings of the 36th Annual Precise Time and Time Interval (PTTI) Systems and Applications Meeting. Washington, DC, USA, 7th–9th December.

Weaver, G., Garstecki, J. and Reynolds, S., 2010. The performance of ultra-stable oscillators for the Gravity Recovery and Interior Laboratory (Grail). In: Proceedings of the 42nd Annual Precise Time and Time Interval (PTTI) Systems and Applications Meeting. Reston, Virginia, USA, 15th–18th November.

Zuber, M.T., Smith, D.E., Zellar, R.S., Neumann, G.A., Sun, X., Katz, R.B., Kleyner, I., Matuszeski, A., McGarry, J.F., Ott, M.N., Ramos-Izquierdo, L.A., Rowlands, D.D., Torrence, M.H. and Zagwodzki, T.W., The Lunar Reconnaissance Orbiter laser ranging investigation, *Space Sci. Rev.* **150**, 2010.

Appendix – Observation data table

Table 24: Appendix – List of the single and simultaneous laser ranging to LRO one-way observation passes during the 7 days timeframe with their times, length and characteristics. We used the observation data in the form of Normal Points.

Station		Pass			Average**		
ID	Name	SP*	Begin	End	Length	Nr. of Shots	Precision
			Days since 2009 Jan 1st		min		cm
7090	YARL		665.97	665.99	21.6	132	3.1
7125	GO1L		666.51	666.54	53.9	640	8.1
7125	GO1L	*	666.59	666.62	50.7	609	3.9
7110	MONL	*	666.59	666.62	46.6	31	2.4
7090	YARL		666.91	666.93	28.0	259	3.4
7125	GO1L		667.29	667.33	53.7	626	6.5
7125	GO1L		667.37	667.41	52.1	541	9.5
7125	GO1L		667.53	667.57	45.2	180	7.1
7090	YARL		667.95	667.95	08.5	94	2.6
7090	YARL		668.03	668.03	09.7	92	2.8
7090	YARL		668.08	668.10	33.8	317	3.0
7090	YARL		668.95	668.97	26.9	278	3.1
7090	YARL		669.11	669.13	35.2	202	3.2
7125	GO1L		669.42	669.45	42.1	465	4.7
7125	GO1L		669.49	669.53	53.3	600	5.4
7125	GO1L	*	669.57	669.61	53.2	632	6.4
7110	MONL	*	669.57	669.61	45.8	332	5.6
7125	GO1L	*	669.65	669.68	53.2	575	7.4
7110	MONL	*	669.67	669.68	14.8	74	2.6
7110	MONL		669.81	669.83	38.2	249	3.3
7090	YARL		670.12	670.16	53.2	255	4.1
7110	MONL	*	670.67	670.70	48.4	174	4.0
7125	GO1L	*	670.68	670.71	36.4	245	6.6
7110	MONL		670.83	670.86	44.0	329	4.1
7090	YARL		670.91	670.93	31.3	306	2.6
7090	YARL		671.07	671.09	32.2	82	4.5
7090	YARL		671.23	671.25	30.8	236	3.1
7125	GO1L		671.46	671.49	42.8	464	4.6
7125	GO1L		671.53	671.57	53.2	615	7.8
7125	GO1L	*	671.69	671.69	7.54	92	3.6
7110	MONL	*	671.69	671.73	50.4	147	3.8
7110	MONL		671.85	671.86	19.9	176	2.7
7090	YARL		672.16	672.19	38.7	114	3.4
7110	MONL		672.63	672.67	53.1	433	5.7
7110	MONL		672.71	672.74	43.7	320	3.9
7110	MONL		672.79	672.81	25.7	200	3.5
7110	MONL		672.87	672.87	05.9	55	2.7
7090	YARL		672.95	672.98	37.9	236	2.9
7090	YARL		673.11	673.14	45.8	213	3.6
7090	YARL		665.97	665.99	21.6	132	3.1
Total	**40**	**10**	**Mean**	**Value**	**37.6**	**298**	**4.4**

*) Simultaneous passes.

**) Normal Point data used.

Supplementary material

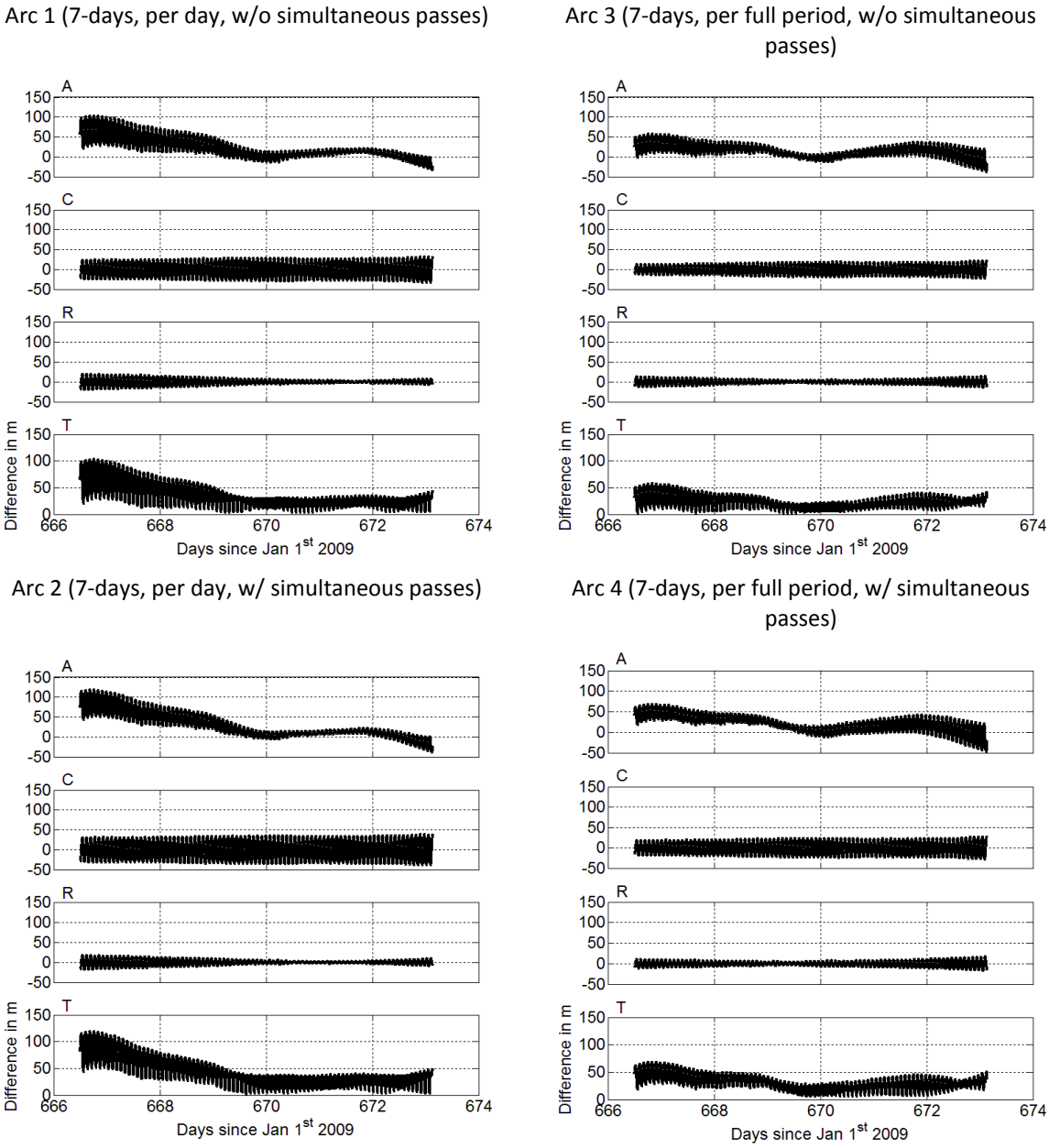

Figure 36: Supplementary material – Difference of the 7-day arcs with respect to the nominal LRO trajectory in the satellite coordinate system directions along- (A), cross-track (C), radial (R) and total (T).

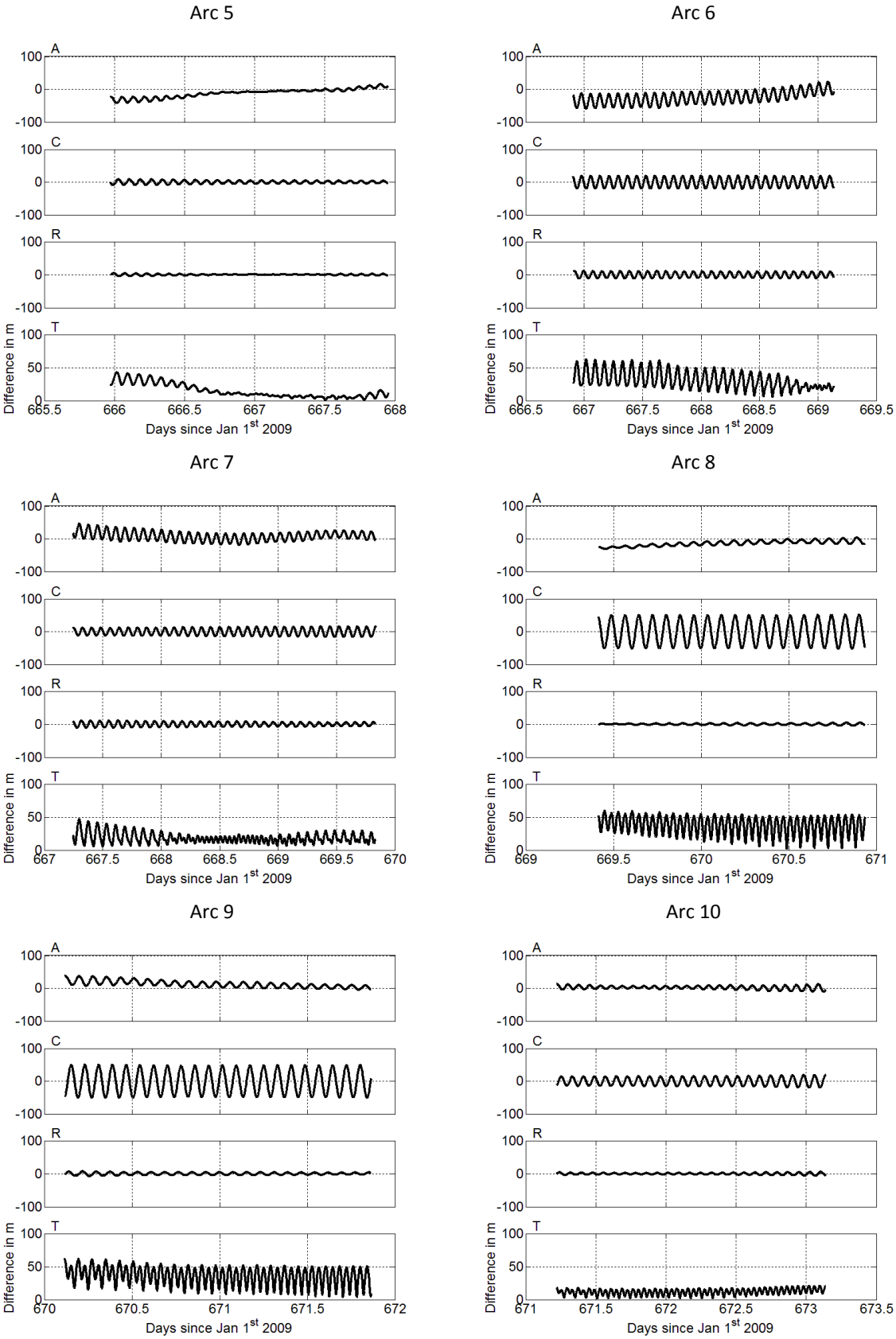

Figure 37: Supplementary material – Difference of the 2-day arcs with respect to the nominal LRO trajectory in the satellite coordinate system directions along- (A), cross-track (C), radial (R) and total (T).

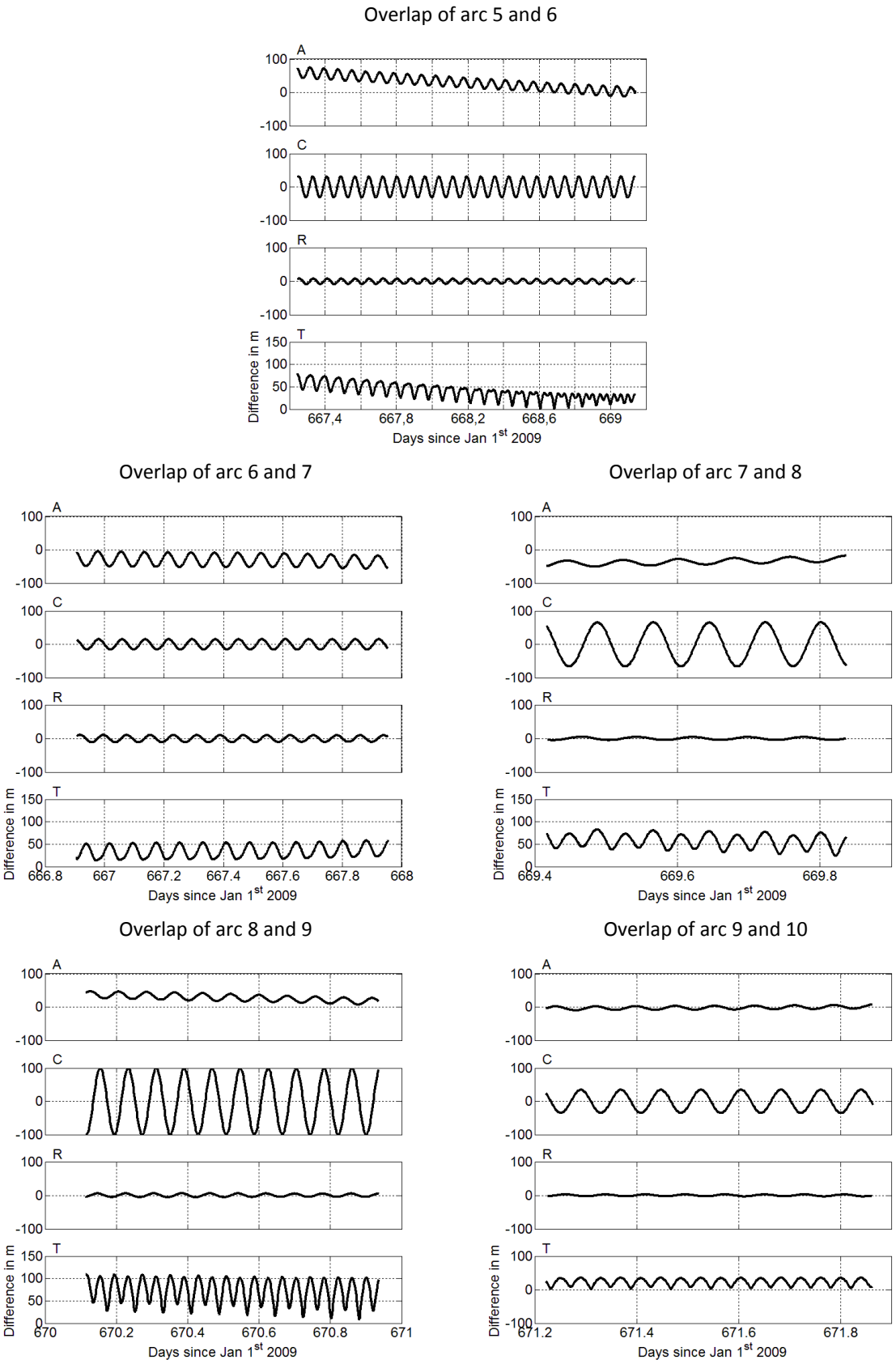

Figure 38: Supplementary material – Difference of the 2-day arcs at the overlaps in the satellite coordinate system directions along- (A), cross-track (C), radial (R) and total (T).

5 Discussion

This section merges and discusses the methods and the individual results from the two research papers and outlines how they address the overall research topic. To support this, Figure 39 shows the various elements of the research papers and how they relate with each other. The individual elements will be picked up in the text while their effects on the results are discussed.

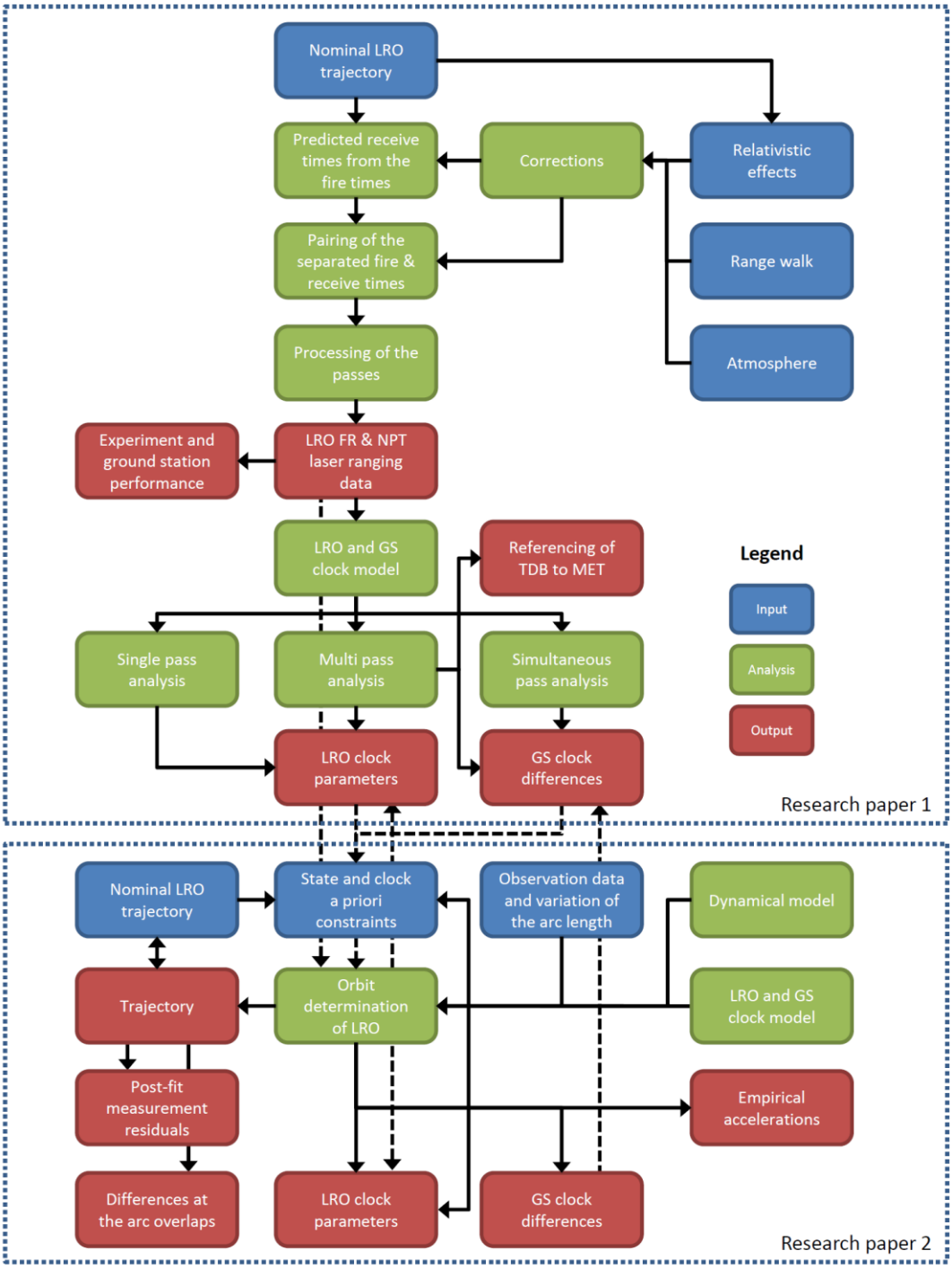

Figure 39: Elements of the two research papers and their relation. The blue boxes represent input, the green boxes analysis and the red boxes output elements. GS stands for ground station, FR for Full Rate, NPT for Normal Point, TDB for Barycentric Dynamical Time and MET for Mission Elapsed Time. The dashed arrows mark results from research paper 1 that have been used for input or for comparison within research paper 2.

Thereby the subsections are grouped by the implications of the nominal LRO trajectory, the clock estimation, the dynamical modeling, the observation data type and coverage as well as Normal Point (NPT) data formation. Following that, the current status of the incorporation of the one-way laser ranging data within orbit determination is discussed and future research directions are provided. Furthermore, the potentially attainable accuracy of differenced range-rate measurements is then analyzed on the basis of the results of this work. Finally, the section closes with a general discussion about the benefits of one-way laser tracking for orbit determination.

5.1 Implications of the nominal LRO trajectory

The nominal LRO trajectory was used extensively within both research papers (see Figure 39). In research paper 1, the orbit was kept fixed by using the nominal LRO trajectory to characterize the involved clocks. In research paper 2, the a priori constraints were taken from the nominal trajectory for the state directly and from the clock characterization from research paper 1 – which was based on the nominal LRO trajectory as well. The clock parameters derived within the orbit determination are compared to the results from research paper 1 as well. In the following it is discussed how the results were affected by the application of the nominal trajectory with its errors.

Influence on the pairing of the fire and the receive times

In research paper 1 the nominal trajectory was used for the pairing of the separated fire and receive times and completes the one-way observable with a predicted receive time (see equation 13). Furthermore it provides the state vector of the spacecraft with respect to selected bodies of the solar system. The spacecraft state was used to calculate the relativistic corrections that were applied on the MET receive times, which were measured by the LRO onboard clock (see Figure 39).

Deriving the state vector of the spacecraft from the trajectory simplifies both the pairing and the calculation of the correction. If no a priori spacecraft state vector is available, the pairing would need to be done in a combined inversion for the spacecraft state vector, the timing of all clocks and the pairing of the separated data, while the corrections would need to be adjusted as well. The LRO state vector and the timing would need to be integrated from an a priori state, providing a preliminary trajectory that would be used for the pairing. After the pairing, differential improvement of the parameters of interest could be derived via the residuals within the inversion. This process would need to be repeated until convergence is reached. Thereby the pairing would need to be repeated on every iteration until it is established correctly.

Utilizing the nominal LRO trajectory allows for a separate pairing resulting in a simpler processing and application of the data within orbit determination. Furthermore the analysis of various aspects (LRO and ground station clock characterization, MET to TDB referencing as well as experiment and ground station performance – see research paper 1) can be carried out by using the nominal trajectory.

The pairing is very robust against uncertainties in the positioning. Due to the 28 Hz cycle the minimum time between consecutive receive events is ≈27.7 ms as illustrated in Figure 40. The Earth Range Gate detects only one event during the time window of 8 ms (see section 3.3 in research paper 1).

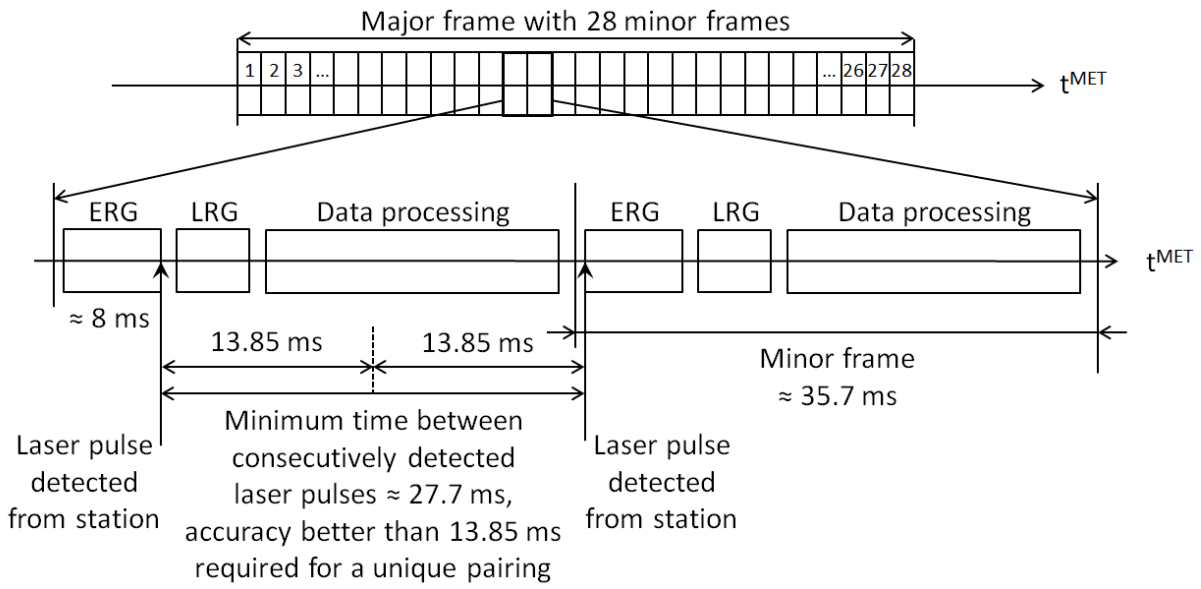

Figure 40: Setup of two consecutive LOLA minor frames which illustrates the minimum time between consecutively detected laser pulses. The minor frame contains three main parts; the Earth Range Gate (ERG), the Lunar Range Gate (LRG) and the processing of the data (see section 3.3 in research paper 1).

In order to pair a single MET receive time to its corresponding TDB receive time, at first a conversion between MET and TDB is required, such as provided by the Spacecraft Clock Kernel (SCLK). This conversion has to be more accurate than half of the minimum time between consecutively received events, which is 13.85 ms (see Figure 40). However, an accuracy of at least ±9 ms might be more suitable for an unambiguous and successful pairing. With its uncertainty of ±3 ms the SCLK is ≈4 times more accurate and ≈3 times in case of an accuracy of ±9 ms.

In the next step the nominal LRO trajectory is used to derive a light time and from that a predicted receive time, which is used for the pairing (see section 3.5.4). Besides the MET to TDB time conversion also the nominal LRO trajectory has to fulfill the accuracy requirement. The minimum a priori conversion accuracy of 13.85 ms translates into a distance of 4155 km (2700 km in case of 9 ms). Consequently the pairing can be carried out with quite coarse spacecraft positioning information. Since the nominal LRO trajectory has an accuracy of ≈9 m (30 ns) at the arc overlaps, it is accurate enough for the pairing. Once the pairing is established, it provides a more accurate link between MET and TDB then the SCLK. Also the operational orbit, provided by the Flight Dynamics Facility (FDF), would be accurate enough for the pairing with its accuracy of 250 m at max (Slojkowski, 2014).

It could be assumed that patterns in the MET receive times could allow for a pairing with even less accurate time conversion and positioning information. However, since only ≈10 % of the shots from most of the stations are actually detected by LOLA (see section 3.7.1 in research paper 1), fire time patterns cannot be expected to be present in the receive times.

Influence on the relativistic correction

The nominal LRO trajectory is further used to derive the position and the velocity of LRO with respect to selected bodies of the solar system for the calculation of the relativistic corrections (see section 3.5.3 of research paper 1 and Figure 39). The position of the Sun, the Earth and the Moon is taken from the planetary ephemerides DE430. While the DE430 ephemeris provides a more accurate lunar orbit for current epochs, the lunar orbit from the D431 ephemeris is more accurate for times a few centuries

in the past (Folkner et al., 2014). Since data covering the timeframe from 2009 to 2014 was analyzed, the DE430 ephemeris was used.

In the following the sensitivity of the relativistic correction to uncertainties of the nominal LRO trajectory is derived. A regular laser ranging pass from a ground station to LRO was used to derive the position and the velocity of the spacecraft from the nominal LRO trajectory throughout the pass. The position and the velocity were shifted for a certain amount and used to calculate the LRO clock rate and from that the offset (see section 3.5.3). The offset integrated from the shifted trajectory was then compared to the offset integrated from the trajectory without a shift. The difference provided the sensitivity of the corrections to variations in the position and the velocity.

In actuality, the trajectory would need to be propagated from shifted initial conditions in order to retrieve the positions throughout the pass. However, just shifting the position and the velocity directly was assumed to be an acceptable approximation within this analysis.

Between mid July 2009 and the beginning of January 2010 the arc overlaps of the nominal LRO trajectory had a mean total difference of 5.5 m. The largest differences of the position were thereby in along- and cross-track direction (Mazarico personal communication, 2016). A shift of 100 m was applied on the LRO position in these directions. This conservative guess of the uncertainty is ≈20 times larger than the mean total difference. The mean total difference of the velocity was 4.9 mm/s during the same timeframe, with the largest differences in radial direction (Mazarico personal communication, 2016). Analog to the position a ≈20 times larger shift of 0.1 m/s was applied on the velocity, but in radial direction.

Table 25 lists the differences of the correction due to a 100 m shift of the position and a 0.1 m/s shift of the velocity for a ≈32 min long pass, when Wettzell station (WETL) was ranging to LRO on the 15th of November 2011 at 00:11:46 UTC. As can be seen from Table 25, the relativistic corrections are more sensitive to variations in the velocity than the position – as also expressed by equation 10 in research paper 1. The offset of 44 ps accumulated over the 32 min of the pass is equivalent to an average rate of $\approx 2 \times 10^{-14}$. This rate is below the stability of the LRO clock ($\approx 2 \times 10^{-13}$ up to 10000 s) or any other error source (e.g. missing temperature correction; see later in this section). Even with this conservative scaling of the spacecraft position and velocity (factor of ≈20) the resulting offset and average trend are small throughout a pass. Thus the relativistic corrections are insensitive to the errors of the nominal LRO trajectory.

Table 25: Difference of the relativistic correction due to a shift of the LRO position and the velocity during a 32 min long pass from WETL station from the 15th of November 2011 00:11:46 UTC. Both the position and the velocity were shifted in the listed directions for an amount of ≈20 times their observed uncertainty.

Shift	Direction of shift	Amount	Difference of correction
Position	Along-track	100 m	-3.3 fs
	Cross-track	100 m	-5.6 fs
	Along- and cross-track*	100 m	-5.6 fs
Velocity	Radial	0.1 m/s	44 ps
Position and velocity	Along-, cross-track* & Radial	100 m & 0.1 m/s	44 ps

*) Norm of the shift in along- and cross-track is equal to the listed amount.

Influence on the results from both research papers

Contrary to the pairing and the relativistic correction all further results in research paper 1 (see Figure 39) are sensitive to the errors of the nominal LRO trajectory. The predicted receive times derived from the nominal LRO trajectory are used for the characterization of the LRO and the ground station clocks as well as in the referencing of MET to TDB. Only the measurement of the ground station clock differences from simultaneous passes is insensitive to orbit errors up to 100 m as discussed by Sun et al. (2013a; see also section 3.6.3 in research paper 1).

Both the spacecraft state vector and the timing of all involved clocks were estimated within the orbit determination in research paper 2. Consequently the results (trajectories, the LRO and the ground station clock parameters as well as the post-fit measurement residuals) were affected by the completeness and the accuracy of the applied corrections as well as the dynamical and clock modeling but not by the nominal trajectory. However, since many correlated timing parameters had to be estimated simultaneously with the spacecraft state vector, a priori constraints were applied on the state vector and the involved clocks. These a priori constraints were taken directly from the nominal LRO trajectory for the state vector and from the clock characterization from research paper 1 that is based upon it. Furthermore the estimated trajectories were compared to the nominal LRO trajectory and the estimated clock parameters to their a priori initial constraints (see Figure 39). This causes the results from research paper 2 to be indirectly affected by the accuracy of the nominal LRO trajectory as well. However, since the accuracy of the nominal trajectory is 9 m (30 ns) at the arc overlaps (Mazarico et al., 2013) it provides an accurate basis and reference for the results in the research papers 1 and 2. Within the estimation of research paper 2, the a priori covariance were set to the precision the timing parameters were derived in research paper 1 with. This could have been done with the a priori covariance of the initial state as well. But instead of setting it to 9 m (accuracy of the nominal LRO trajectory), it was set to $1x10^6$ m. With that the solution was not tied to the nominal LRO trajectory and the differences to the estimated trajectories could be used to evaluate their accuracy independently. However, systematics might have been introduced to various aspects because a radio-based product from an inversion was applied for the analysis of laser ranging data. Furthermore, the radio data was recorded with different techniques and different hardware than the laser data. Since the spacecraft state and all involved clocks have to be estimated with the one-way observables, constraints and a priori information are required. Consequently this approach as well as comparing the estimated orbits to the nominal LRO trajectory has also been used by other authors (Mao et al., 2014, Löcher et al., 2015, Buccino et al., 2016).

5.2 Implications of the clock estimation

The LRO and ground station clock behavior was modeled and characterized by polynomial fits of different length and order within this work. Following Tapley et al. (2004) the application of polynomial fits is appropriate for the modeling of the behavior of the clocks. Due to the empirical approach, also unmodeled systematics of the clocks can be approximated while the model is simple and the number of parameters that have to be estimated is small. Within the orbit determination for example, 2nd order fits provided a good compromise on the number of parameters and the approximation accuracy (seen from the post-fit measurement residuals). An approximation of the LRO and ground station clocks with 1st order fits yielded larger post-fit measurement residuals and larger differences of the estimated with respect to the nominal LRO trajectory. Also all other authors, who used one-way laser ranging data to LRO for orbit determination, applied polynomial fits of similar order for the

approximation of the involved clocks (Mao et al., 2014; Löcher et al., 2015; Buccino et al., 2016; see discussion at the end of this section).

Clock approximation with polynomial fits

Figure 1 of Dirkx et al. (2015) illustrates how well fits of a certain arc length represent the behavior of a clock. Thereby the fits have to cover the actual behavior of the clock and all kinds of errors, such as from the incomplete corrections for example and from the fitting itself. Short clock arc lengths (per pass at minimum) allow for an exact representation, since the fits can approximate the clock behavior including the errors well. However, with decreasing arc length, more fits are required for the approximation of a clock over a certain timeframe and with that more parameters have to be estimated simultaneously. If they are estimated concurrently with other parameters, such as the state vector, the correlations can become so large that signal from the other parameters is absorbed by the timing parameters (Dirkx et al., 2015). In that case, the timing and the other parameters cannot be estimated accurately anymore.

With an extended clock arc length, less correlated parameters have to be estimated. Since the concurrent estimation of the spacecraft state vector and all involved clocks is required with the one-way data, such extended clock arc lengths are generally of interest. However, with an increased clock arc length, the approximation of short term variations by the polynomial fits becomes less accurate which can be seen from increasing post-fit measurement residuals (Figure 1 of Dirkx et al., 2015).

This effect was present with the post-fit measurement residuals in both research papers. The MET to TDB referencing from 3rd order fits (research paper 1) had a 1–σ residuals variation of ≈60 ns (≈18 m) over 7 days, 171 ns (51.3 m) over 28 days and 256 ns (76.8 m) over 5 years (see Figure 41 and section 3.6.2). Within the orbit determination (research paper 2) the 1–σ variation of the residuals was 0.6 ns (0.19 m) over 2 days and ≈23 ns (≈7 m) over 7 days (see section 4.5.1).

Comparison of the clock estimation of the research papers

Even though polynomial fits of the same order were applied for the estimation of the involved clocks in both research papers, the residuals were different, even while using the same observation passes. Figure 41 shows the post-fit measurement residuals from the multiple-pass analysis from research paper 1 and the orbit determination in research paper 2. The same single and simultaneous LRO laser ranging passes from a 7 day timeframe during Science Mission phase SM02 were used in both approaches.

While the orbit was kept fixed in the multiple-pass analysis in research paper 1, only the LRO clock was approximated with polynomial fits, but not the ground station clocks. Consequently the timing differences between the ground station clocks were not removed and can be seen in the residuals. Within the orbit determination in research paper 2, the LRO and all involved ground station clocks were approximated with polynomial fits. Consequently the post-fit measurement residuals did not show the ground station clock differences and were smaller than the residuals from the multiple-pass analysis (see Figure 41). The residuals of the individual passes from the orbit determination were, however, larger than the residuals of the individual passes from the multiple-pass analysis. While the applied polynomial fit removed the long-term trend of the ground station clocks, the drifts of the individual passes with respect to that long-term trend became more prominent. The incorporation of simultaneous passes to the observation data did not change the measurement residuals significantly within both approaches.

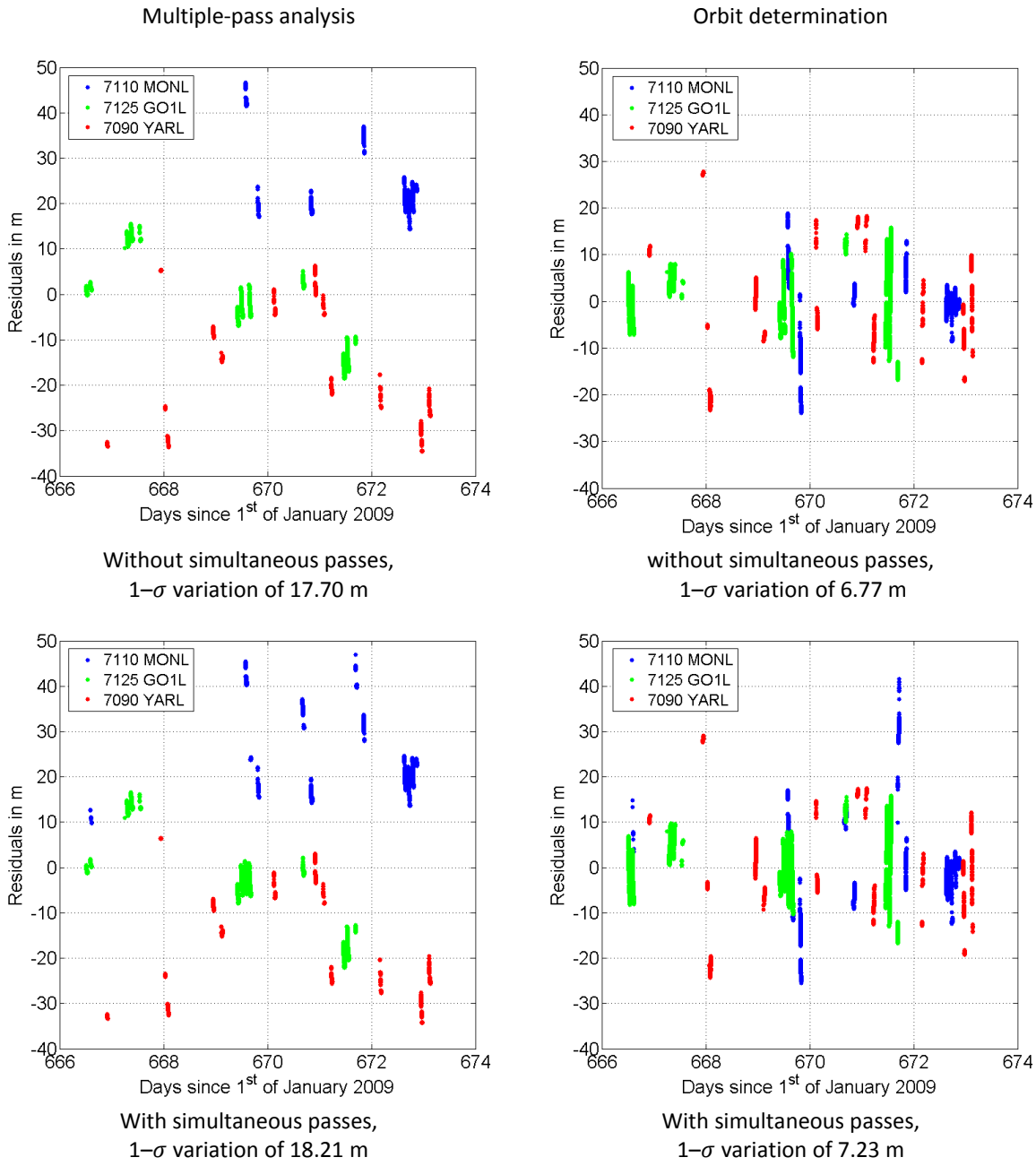

Figure 41: Post-fit measurement residuals derived from the multiple-pass analysis (left) and the orbit determination (right) while utilizing the same observation data (single as well as simultaneous passes) covering a timeframe of 7 days during Science Mission phase SM02.

Estimated clock parameters and their detectability

The parameters of the involved clocks were obtained from the polynomial fits as shown in section 4.4.1 in research paper 2. The 0th order parameter of the fit provided the offset, the 1st order parameter the rate, the 2nd order parameter the aging and the 3rd order parameter the change of the aging. Even though the offset was estimated as well, the analysis of the estimated parameters focused on the higher order parameters rate, aging and its change. With the one-way data, the estimated offsets only referenced MET to TDB and did not represent a system bias – they only represented the difference between the two timescales at a certain epoch. Furthermore the offsets were represented by large numbers at the order of 10^8 s while having a precision of $1x10^{-10}$ s at the same time (also see section

3.7.2 in research paper 1). Consequently the presentation of the clock parameters in research paper 1, 2 and the discussion focuses on the LRO clock rate, its aging and the change of the aging.

Depending on the length of the clock arc, the order of the polynomial fits that were applied for the LRO clock modeling, were varied. It takes clock arcs of a certain length before the LRO clock parameters cause an offset that is larger than the LOLA timestamp precision (0.5 ns) and thus become detectable. The LRO clock rate is detectable immediately since it has a value on the order of 10^{-8}. With aging values at the order of 10^{-17} /s, it takes a clock arc length of at least 2 h. In the case of the change of the aging that is at orders of 10^{-24} /s^2, it takes a length of at least 22 hours, until the effect becomes detectable. For an accurate estimation of the parameters even longer arc lengths are desirable. As discussed in research paper 1, only 1st order fits were used for single passes that have an average length of 33 min (see section 3.6.1 research paper 1). In research paper 2, 2nd order polynomial fits were used over timeframes between 1 and 7 days (see section 4.4.1). 3rd order fits over timeframes of ≈28 days (one mission phase) were applied within the multiple-pass analysis (see section 3.7.2 in research paper 1).

The ground station clock differences were derived from 1st order polynomial fits applied to the common-view observations (see research paper 1, section 3.6.2 and 3.6.3). Within this work the exact average simultaneous pass length could not be estimated since a manual editing of all 1215 simultaneous passes would have been required. However, since the participating stations had to range successfully to LRO simultaneously, the average simultaneous pass length was shorter than the average single pass length (33 min). Due to the average length of less than 33 min, only relative offsets and rates but no higher order differences were estimated.

Corrections applied to the observation data

Before the LRO and the ground station clocks were modeled with polynomial fits (e.g. in order to estimate their parameters), corrections were applied to the receive times (see Figure 39). While the atmospheric correction was applied to the predicted receive times, the relativistic and the range-walk correction were applied to the measured receive times (see equation 13 and 14).

Within this work, the terms clock modeling and corrections are kept separated, since they are different aspects. The corrections addressed influences, which were not related to the onboard clock itself, as the atmospheric correction for example. Also the range-walk correction addresses a detector and not a clock issue. Even though the relativistic correction affected the receive times measured by the onbobard clock, it only represented a transformation caused by the selected reference frame and timescale – TDB in this work.

Atmospheric correction

As outlined in research paper 1, the atmospheric correction was applied in form of a constant offset throughout a pass. If the environmental conditions were changing throughout a pass, drifts might have been introduced. Such drifts might have affected the post-fit measurement residuals of the MET to TDB referencing for example. However, the ranging to LRO was usually done at high elevations while change of the elevation was small throughout a pass (e.g. 53° to 45° for the example pass in section 3.5.1 in research paper 1).

Compared to Earth satellites, which can cross the whole sky above a ground station within few minutes, the angular change of LRO in the sky was small, because of the large distance between the

Earth and the Moon. Due to Earth's rotation the angular position of the Moon changed by ≈8° during the average length of 33 min and by ≈11° during the 42 min long example pass. However, only the elevation and its change were relevant for the calculation of the atmospheric correction. Due to the inclination of the lunar orbit with respect to Earth's equator between 18.2° and 28.5° (Herman and Conway, 1998), the change of elevation always stayed below the change of the angular position of the Moon and was thus small.

Approximating the atmospheric correction with a constant offset caused a drift of $5x10^{-13}$ over the 45 min of the example pass from section 3.5.1 in research paper 1. Such remaining drifts influenced the LRO clock rate estimated from single passes. However, in order to compare the single-pass rates with multiple-pass rates, they were grouped and averaged over the same timeframes (see section 3.7.2 in research paper 1). Thereby the variations of the single-pass rates due to the simplified atmospheric correction were not present anymore, after the rate was averaged over multiple passes. Furthermore the drifts were not affecting the estimation of the LRO clock rate, since it was derived at a precision of 10^{-11} (see section 3.7.2 in research paper 1) and thus 2 orders of magnitude larger than the drifts from the simplified atmospheric correction. Contrary the relative ground station clock rates were measured to values between $2x10^{-13}$ and $6x10^{-12}$ (see section 3.7.3 in research paper 1) and were thus sensitive to the introduced drifts. However, solely the smaller relative rates (between $2x10^{-13}$ and $\approx 5x10^{-13}$) were affected and only if the conditions were changing during the passes.

The ground station clock differences derived within the orbit determination (research paper 2) were not affected by the simplified atmospheric modeling at a significant level. Potentially the introduced drifts might have affected the smaller relative rates rates (between $2x10^{-13}$ and $\approx 5x10^{-13}$) as well. However, due to the limited approximation accuracy of the ground station clocks within the orbit determination, the relative rates from research paper 1 and 2 could only be compared at their order of magnitude (see section 4.5.3 in research paper 2). Furthermore, the accumulated offset of ±0.2 m (± 0.7 ns) in case of the example pass was smaller than the measured relative offsets (33 ns to 560 ns; see section 3.7.3 in research paper 1). Consequently the drifts and the offset introduced from the simplified atmospheric corrections did not affect the relative rates and offsets of the orbit determination.

The simplified model (constant offset) was implemented for the atmospheric corrections since it enabled a simplified processing of the data. While the update of the model itself would be simple, the whole dataset including single and simultaneous passes would need to be reprocessed in order to update the results. The reprocessing of the single passes is an automated process that consumes an intermediate amount of time. However, the reprocessing of the simultaneous passes requires manual data editing at the first iteration. The reprocessing of all simultaneous passes that were analyzed so far would require too much time for this work. Since only the smaller relative ground station clock rates would be improved by the update, this task could be carried out within future work.

Range-walk correction

Due to the impulse response of the LOLA detector electronics, the shape of a recorded laser pulse changes as a function of the intensity which causes an offset on the derived range (Riris and Cavanaugh, 2009). During a pass for example, this also increases the measurement precision as the intensity of the received pulses and with that the offset is varying. While without range-walk correction the measurement precision estimated from the passes of the various stations was 30 – 50 cm, only

with applied correction the LOLA time stamp precision of 15 cm could be achieved. The range-walk correction was implemented via an empirical correction formula (see section 3.5.2 in research paper 1).

Within this formula station factors were required, that were optimized from a series of passes for every ground station. Thereby the station factor was varied, until a minimum 1–σ variation of the residuals with respect to a 4th order fit was found (see section 3.5.4 in research paper 1). Since only a residual minimization was used as criteria, this approach could lead to over optimized station correction factors. However, since no other correction formula was available or has been published by the LOLA team, this approach was considered to be sufficient. Moreover, the correction does not influence the observation data accuracy but only the precsision, which gets further averaged with the formation of the NPT data from the FR data.

Relativistic correction

The relativistic correction allowed for the conversion of the measured receive times from MET to TDB. After applying the corrections, the clock behavior can be analyzed directly without systematics (see Figure 23 in research paper 1). For the calculation of the corrections, the distance of the selected solar system bodies to the spacecraft was derived from the planetary JPL ephemerides DE430 (Folkner et al., 2014) and the nominal LRO trajectory within the NAIF software SPICE. As discussed in section 5.1, the correction is insensitive to the uncertainties of the nominal LRO trajectory. Since the orbit of the bodies taken into account (the Earth, the Moon as well as the Sun) is known at submeter accuracy (Folkner et al., 2014), they do not affect the relativistic correction.

Temperature correction

So far no model was available to correct for the variation of the LRO clock rate due to temperature change. As discussed in research paper 1 and 2, the typically observed temperature variation of 0.3°C caused an offset of 13–39 ns over one day. This was equivalent to an average linear trend of 1.5–4.5x10^{-13} with variations with an amplitude of ≈2–6 ns around it. Assuming a sinusoidal curve an average rate of ≈±1–3x10^{-13} between the turnover points every 21600 s was found which resulted in a maximum LRO clock rate change of ≈7.5x10^{-13}. Variations due to changes in the power consumption of close-by instruments or the orbit height could have caused further changes of the rate. Since ground station clocks were shielded properly, they did not experience changes of their rate like the LRO clock did. How this missing correction affected the results is included in the following discussion.

LRO clock stability

Besides the corrections, also the stability of the LRO clock affected the accuracy of its approximation. The LRO clock (2x10^{-13} over up to 10000 s) was less stable than the involved ground station clocks (1x10^{-12} to 1x10^{-15} over periods of 10^3 to 10^7 s). However since the stability was constant over one LRO orbit (≈120 min which is 7200 s) no additional periodic error was introduced over one LRO orbit. As with the missing temperature correction, the effect of the LRO clock stability on the results is included the following discussion.

Influence of the corrections, the LRO clock stability and the orbit on the LRO clock approximation

How well a fit of certain length and order could approximate the stochastic trend of a clock depended on the stability of the clock as well as the completeness and the accuracy of the corrections for

systematic effects. In case of incomplete corrections, remaining systematic effects mixed with random errors and had to be approximated as well. Because more noise was present in that case, the approximation becames less accurate in general and with increasing clock arc length.

Since the clock modeling only meant the approximation of the clock behavior via a polynomial fit, the orbit is not directly a part of it. However, since it was used for the estimation of the LRO and the ground station clock parameters it is discussed in the following.

At first it is described how the order of the polynomial fit influenced the estimation of the LRO clock parameters within the different methods. Furthermore it will be discussed how the parameters from the different methods were compared and to which precision they could be derived. Following that, it will be highlighted how the arc length affected the estimated parameters and the approximation of the LRO clock. Moreover, the effect of the accuracy of the ground station clock approximation on the measurement of their differences (ground to ground time transfer) will be discussed. Finally the section closes with a comparison of the results from the clock modeling to the literature.

Estimation of the LRO clock parameters, fit order and accuracy/precision from the comparison

In the single-pass analysis, 1st order fits were applied for the estimation of the offset and the rate. By applying a 2nd order fit to the rate over time, the higher order LRO clock parameters (aging and its change) were estimated. In the multiple-pass analysis, 3rd order fits were utilized to estimate all parameters directly (rate, aging and its change). The single-pass parameters were grouped and averaged accordingly to the multiple-pass analysis. Since then the parameters were averaged or estimated over the same timeframes, they were subject to the same errors that affected the LRO clock. Consequently their precision could be derived from the 1–σ variation of their differences.

With increasing order, the parameters described effects at a smaller magnitude and were thus more sensitive to errors (see section 3.7.2 in research paper 1). Consequently the precision of the estimated parameters became larger with increasing order (Table 12 of research paper 1). While the LRO clock rate was estimated at a precision 8500 times smaller than the value itself (≈6.9104±0.0008x10^{-8}), the aging had a precision at the order of magnitude of its actual value (≈1.6±1.2x10^{-12} /day). The change of the aging was estimated at a ≈4 times larger precision (≈-2.3±9.2x10^{-14} /day²).

Response of the LRO clock parameters to the clock arc length

Figure 42 shows the response of the LRO clock rate to an increasing clock arc length. If estimated over short timeframes (from single passes), the estimated rates covered the short term variations reasonably. However, due to remaining uncertainties from the clock modeling, incomplete corrections and the nominal LRO trajectory, the single pass rates scattered with respect to the interpolated trend of the multiple pass rates (see Extended Science mission phase ES09 and ES10 in Figure 42). The trend estimated over longer timeframes (up to one mission phase) covered the LRO clock long-term trend much better. However, with too large changes of the LRO clock rate, the trend was not covered well if the timeframe was too long (see Extended Science mission phase ES08 in Figure 42). In that case, the timeframe over which the rate was estimated had to be further split as during Extended Science mission phase ES07 (see Figure 42 and also the discussion in section 3.6.2 in research paper 1).

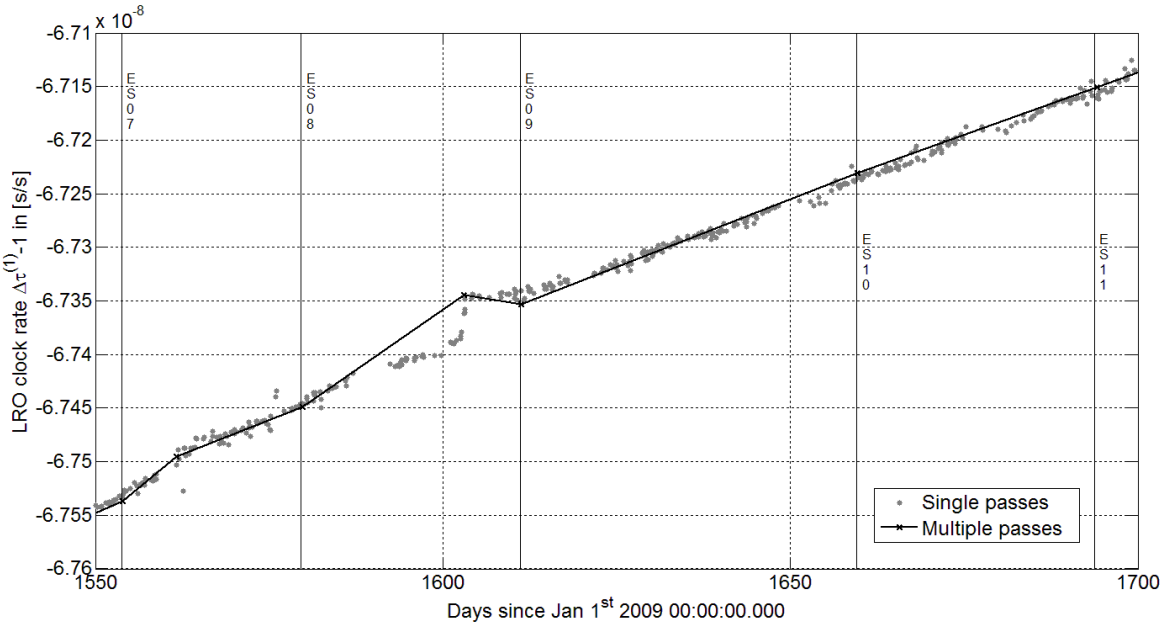

Figure 42: LRO clock rate estimated from single and multiple passes. Within the multiple pass analysis, the rate is usually estimated over 28 days as within the Extended Science mission phase ES09 and ES10. In case of larger changes of the rate, the timeframes were further split as within Extended Science mission phase ES07 and ES08.

Analogously the rates from the orbit determination had a larger scatter with respect to the mean trend of the single-pass rates when they were estimated over 1 and 2 days (arcs 1, 2 and 5 to 10 in Figure 35). When the rates were estimated over 7 days (arcs 3 and 4 in Figure 35), the scatter was smaller.

Compared to the LRO clock rate, the aging described changes on a smaller scale and was thus more sensitive to errors from described influences (clock arc length, completeness of the corrections, the LRO clock stability as well as the nominal LRO trajectory). As discussed in section 3.6.1 (research paper 1), single passes were too short (≈33 min on average) to estimate the aging. A clock arc length of at least 2 h was required before the offset became detectable (see discussion above). Within the multiple-pass analysis from research paper 1, the aging was typically estimated over one mission phase (≈28 days) and to values at the order of 10^{-17} /s (10^{-13} /day). These values were in agreement with the aging values of Mao et al. (2011).

Table 26 shows the order of magnitude of the aging parameters that were estimated in research paper 1 and 2 while utilizing different clock arc lengths. While the aging was usually not derived from single passes, within this analysis 2nd order fits were also applied to single passes for its estimation. Consequently the derived values (at the order of 10^{-15} /s which is 10^{-11} /day) were two orders above the actual order of magnitude. Within the orbit determination (estimation of both the orbit and the clocks – research paper 2), the values agreed on the order of magnitude (10^{-17} /s, 10^{-13} /day) for clock arc lengths of 1 day. For clock arc lengths of 2 days, values 1 to 2 orders of magnitude larger were retrieved and for clock arc lengths of 7 days, the values were 3 to 4 orders larger (see Table 26). The values were increasing with increasing clock arc length due to accumulating errors that affected the LRO clock approximation (see section 4.5.2 in research paper 2).

Table 26: LRO clock aging values estimated with different methods and over different clock arc lengths. Note that for this comparison 2nd order fits were also applied to single passes, while regularly the aging is not estimated from single passes.

Method	Orbit is	Clock arc length	Aging order of magnitude
Single-pass analysis	Fixed (Research paper 1)	≈33 min*	10^{-15} /s (10^{-15} /day)
Multi-pass analysis		≈28 days	10^{-17} /s (10^{-13} /day)
7-day arcs, per day, without simultaneous passes	Estimated (Research paper 2)	1 day	10^{-16}–10^{-17} /s (10^{-12}–10^{-13} /day)
7-day arcs, per day, with simultaneous passes		1 day	10^{-16}–10^{-17} /s (10^{-12}–10^{-13} /day)
2-day arcs, per full period, without simultaneous passes		2 days	10^{-15}–10^{-16} /s (10^{-11}–10^{-12} /day)
7-day arcs, per full period, without simultaneous passes		7 days	10^{-13} /s (10^{-09} /day)
7-day arcs, per full period, with simultaneous passes		7 days	10^{-14} /s (10^{-10} /day)

*) Average pass length is used (see section 7.1 in research paper 1).

Response of the LRO clock approximation to the clock arc length

Table 27 lists the 1–σ variation of the post-fit measurement residuals as a function of the LRO clock arc length for the methods that were used in research paper 1 and 2 – 3rd order fit for the MET to TDB referencing and 2nd order fit for the LRO clock approximation. While the short clock arcs of each method have small 1–σ residual variations, the 1–σ residual variations of the longer clock arcs are larger due to accumulating errors that affect the clock approximation (see section 4.5.2 in research paper 2). If the LRO clock was approximated over the same timeframe (7 days) with both approaches, the residuals were larger for the referencing than for the orbit determination. Since only the LRO and not the ground station clocks were approximated within the referencing (see discussion at the beginning of this section) their systematics and trends are present in the residuals and increase them.

Table 27: 1–σ variation of the post-fit measurement residuals while the LRO clock is estimated via different methods and over different arc lengths.

Method	Orbit is	LRO clock arc length	State arc length	1–σ variation of the measurement residuals
Orbit determination	Estimated	2 days	2 days	0.19 m≈0.6 ns
		1 day	7 days	3.69 m≈12.3 ns
		7 days	7 days	7.23 m≈24.1 ns
MET to TDB referencing	fixed	7 days*	-	17.7 m≈59 ns
		56 days**	-	49.8 m≈166 ns
		≈5 years***	-	76.8 m≈256 ns

*) See Figure 41.

**) Referencing done with 3rd order fits over the 2 Science Mission phases SM02 and SM03 (see section 3.7.2 in research paper 1).

***) Referencing done with 3rd order fits over all mission phases CO until ES24 which covers the timeframe from July 2009 until September 2014 (see section 3.7.2 in research paper 1).

Optimum clock arc length

Introducing an optimum clock arc length would balance the maximum possible arc length and the accumulation of errors. With increasing arc length, the number of correlated timing parameters that had to be estimated concurrently, were reduced (see section 4.4.4 research paper 2). Consequently longer clock arcs were favorable within the orbit determination with one-way data, even though the post-fit measurement residuals increased and the clock parameters became less accurate. However, the clock arc length could be optimized so that the number of parameters and the accumulation of errors and thus the degradation of the residuals and the LRO clock parameters are balanced. Since the residuals and clock parameters were steadily degrading with increasing clock arc length, a certain minimum does not exist. However, the degradation of the residuals and the clock parameters could kept at a tolerable level.

Compared to the LRO clock, the ground station clocks are more stable (see Table 9 in research paper 1) and less affected by environmental influences. Thus fewer errors are accumulating with increasing clock arc length and the residuals as well as the clock parameters degrade less. Consequently their optimized clock arc length might be different to an optimized LRO clock arc length.

Estimation of the ground station clock differences, influence of the clock approximation accuracy

In research paper 1, the ground station clock differences were estimated from a 1st order fit applied over the length of a simultaneous pass. In research paper 2 the differences were derived from 2nd order fits that approximated the ground station clocks over the whole arc length (e.g. 2 or 7 days). Furthermore, in research paper 1 the differences were measured for one certain ground station clock combination, while in research paper 2 all ground station clocks were estimated concurrently before individual differences were derived. Due to the longer ground station clock arcs, the approximations within the orbit determination had limited accuracy. Consequently, the differences could not be approximated as accurate as they could be measured from the simultaneous passes and were only compared at their order of magnitude. However, except for one outlier the differences agreed quite well with each other and with the values reported for the ground station clock stabilities (see Table 23 and Table 17 in research paper 2). Furthermore, this is in agreement with the recommendation of the ILRS, that the stations should keep their offset to UTC smaller than 100 ns (see section 2.1).

The limited accuracy of the ground station clock approximations also was the reason, why the incorporation of simultaneous passes to the regular single pass observation data provided no improvement within the orbit determination of this work. Due to correlated ground station clocks and errors from the LRO clock approximation (random clock errors and incomplete corrections), the simultaneous passes could not be resolved at timestamp precision (see Figure 40 and see section 4.5.1 in research paper 2). Improvement of the dynamical, the clock modeling as well as the corrections might enable a more accurate approximation of the ground station clocks and with that of the simultaneous passes, which could finally enable the expected positioning improvement (Neumann et al., 2014). However, even with an improved modeling, it might not be possible to resolve the post-fit measurement residual differences at the timestamp precision during a simultaneous pass. With a ground station clock approximation over 2 or 7 days and strong correlations, errors will always accumulate, which cause the residuals to be off. But the difference of the residuals during a simultaneous pass might be used for monitoring an improvement of the ground station clock approximation, when they become smaller upon improvement of the modeling.

Within the estimation of research paper 2, it would have been possible, to estimate the ground station clocks with respect to a fixed one. Accordingly Mao et al., (2014) kept GO1L station fixed and estimated all other ground station clocks with repsect to it. However, due to larger offsets of the GO1L timing with respect to the other stations (up to 10 µs – see section 3.7.2), this station was not selected as reference within this work. Since other stations did not provide a comparable amount of data and all stations were subject to outages, the ground station clocks were estimated individually within this work.

During common-view observations the LRO clock is subject to the same errors, so that only the differences between the ground station clocks remain and can be measured accurately (see section 3.6.3 in research paper 1). However with longer clock arcs (e.g. 7 days – see Figure 41) the approximation of the LRO clock is less accurate and trends and systematics are introduced to the measurement residuals. Due to these variations in the residuals, the measurement of ground station clock differences from consecutive passes (ground to ground time transfer from non-common view observations) becomes subject to too much interpretation and is thus unfeasible.

Comparison to literature

Mao et al. (2014), Löcher et al. (2015) and Buccino et al. (2016) also used polynomial fits for the approximation of the involved clocks as done within this work. Further they applied fits of similar order over timeframes of similar lengths – 3rd order fits for the LRO clock analysis over multiple months (Mao et al., 2014) and 2nd order fits for the LRO clock within the orbit determination (Mao et al., 2014; Löcher et al., 2015; Buccino et al., 2016). However, Mao et al. (2014) and Löcher et al. (2015) provided no information, which length they used for the LRO clock fit, if they did variations of this length and whether they also used polynomial fits for the approximation of the ground station clocks. Since they provided no results about their clock modeling, no comparison could be done.

Buccino et al. (2016) reported further information about their clock analysis. At first the LRO clock behavior was characterized similarily to the approach of this work – with 2nd order polynomial fits while using the nominal LRO trajectory. Thereby post-fit measurement residuals with a 1-σ variation of 900 ns were observed over the timeframe of on year. If the fits were applied over shorter timeframes, the residuals were smaller (160 ns over 2 to 4 weeks), which is in agreement with this work – see discussion at the beginning of this section and Table 9 (residuals between 160 and 170 ns over 26 to 28 days). Within the orbit determination 2nd order fits were applied for the LRO clock approximation over a timeframe of 7 days but only a 0th order fit (bias) was used for the ground station clocks. The authors assumed the ground station clock drift to be negligible compared to the LRO clock drift. The post-fit measurement residuals over 7 days were 0.26 m. Since this result included Doppler data, it is not directly comparable to our post-fit measurement residuals. However, since a bias is estimated for every pass such small residuals over this timeframe were possible – in contrast to residuals of 1 m over 2 days and 4 to 7 m over 7 days with a 2nd order polynomial fit within this work.

Furthermore a variation of the clock modeling was introduced while the authors used laser ranging data only. Over a timeframe of 1.5 days, both the LRO and the ground station clocks were either estimated with one 2nd order fit for every pass or with a bias only (0th order) every 30 s (white noise approach). The authors already stated that even though the ground station clock errors will be small compared to the ones from the LRO clock, if just one fit is used it will absorb errors of both clocks. Since this approach allowed for a more frequent adjustment of the clocks (per pass insteado f over 7

days), the post-fit measurement residuals become smaller (1-σ variation of 0.09 m over 1.5 days). If the clock fit is estimated every 30 s, the residuals become even smaller (1-σ variation of 0.03 m over 1.5 days). However, with such a frequent estimation, the biases absorb all unmodeled errors and even absorb physical signal (Buccino et al., 2016), which is in agreement with this work (see discussion at the beginning of this section).Overall only little details were published by the authors Mao et al. (2014), Löcher et al. (2015) and Buccino et al. (2016) regarding the clock modeling and the analysis of their approximation. The results that could be compared were in agreement with this work.

5.3 Implications of the dynamical modeling

While the orbit was kept fixed in research paper 1, the dynamical modeling described in section 4.4.2 (research paper 2) was used to integrate the LRO orbit in research paper 2 (see Figure 39). Compared to the modeling that was used for the estimation of the nominal LRO trajectory (Mazarico et al., 2012), the dynamical modeling of this work was less accurate. The individual differences between the modeling of Mazarico et al. (2012) and the dynamical modeling of this work are discussed in the following.

Simplified solar radiation pressure

Contrary to a 3-dimensional spacecraft model, including orientation and self-shadowing, a simplified cannon-ball model following Montenbruck and Gill (2000) was applied within this work. The equation

$$a_{SRP} = P_{SRP} C_R \frac{A}{m} \frac{AU^2}{r_{Sun-LRO}{}^2} \quad (37)$$

was used in a vectorized form for the calculation of the solar radiation pressure. Thereby P_{SRP} was the solar radiation pressure in the vicinity of the Earth with a value of $P_{SRP} \approx 4.56 \times 10^{-6}$ N/m², $C_R$the solar radiation pressure coefficient for which C_R = 1.2 was used and A the surface of the satellite which was assumed to A = 10 m². The mass m was changing over time, as fuel was consumed during the regular station keeping and orbital maneuvers. The spacecraft mass was derived from the Small Forces Files (SFF) which were taken from the LOLA/LRORS PDS data node (Imbrium website, 2016). However, the files that were available on the website, only covered the timeframe from June 2009 until December 2011.

Table 28 shows the corresponding solar radiation pressure that was calculated from equation 37, while using the spacecraft mass from the SFF as well as a maximum and minimum distance $r_{Sun-LRO}$. This distance is at maximum at Earths aphel plus the lunar orbit and at minimum at Earths perihel minus the lunar orbit during Earth's orbit around the Sun. The corresponding distances are listed in Table 28.

Table 28: Solar radiation pressure a_{SRP} calculated for LRO at different dates and with the corresponding mass and distance to the Sun.

Approximate date	Spacecraft mass in kg	Distance LRO–Sun in km	Resulting a_{SRP} in m/s²
September 2009	1280	$152100 \times 10^3 + 384400$	4.1×10^{-8}
December 2011	1071	$147095 \times 10^3 - 384400$	5.3×10^{-8}

Smith et al. (2008) provided a plot, where the solar radiation pressure value is derived from different models for LRO. In order to derive the error introduced by the simplified model described above, its values were compared to the values from the more detailed models from Smith et al. (2008). However, the plot was provided without any date or period but with a time step only. When a time step of 5 s was assumed, which was used by Mazarico et al. (2012) during the integration of the nominal LRO trajectory, a period of the LRO orbit of ≈117 min was derived, which is a reasonable value.

The value (≈$5x10^{-8}$ m/s²) from the simplified model used in this work, agreed quite well with the value (≈$5x10^{-8}$ m/s²) Smith et al. (2008) derived with their macro-model. Furthermore, both values were similarly constant throughout the sunlit phase of an LRO orbit. With the incorporation of self-shadowing to the macro-model, the behavior of the solar radiation pressure from Smith et al. (2008) was not that constant anymore. Simplified the solar radiation pressure was changing as following. From the begin of the sunlit phase of an LRO orbit to ≈2500 s (≈42 min) later, the acceleration was steadily increasing from $1x10^{-8}$ m/s² to $3x10^{-8}$ m/s². From there the acceleration steadily decreased until it reached a value of $2x10^{-8}$ m/s² after ≈4500 s (≈75 min), when LRO was entering the shade of the Moon.

In order to derive the difference in velocity and position, the differences between the acceleration from the simplified model and the macro-model that includes self-shadowing were integrated over time. After one LRO orbit with a length of 117 min, the integrated difference of the acceleration resulted in a velocity of $1.25x10^{-4}$ m/s and a distance of ≈0.3 m. The differences added up to an error of ≈3.7 m over one day and of ≈25.8 m after 7 days. The equivalent average trend of ≈$1.4x10^{-13}$ m/s² was absorbed by the constant empirical accelerations, which were estimated to values between $1x10^{-9}$ and $1x10^{-8}$ m/s².

However, the variations around the mean trend introduced systematics that affected the residuals. First, the change of the solar radiation pressure was not as simple as it was assumed above. Second variations around the average trend were caused by the change between the sunlit and the shade phases during the LRO orbit. Since the solar radiation pressure only was active in the sunlit phase, variations were introduced to the residuals around the transitions from the shade to the sunlit phase and vice versa.

Thermal radiation and reflected sunlight from the lunar surface

The influence of thermal radiation and reflected sunlight from the lunar surface was not incorporated within the dynamical modeling. As discussed in research paper 2, these two effects caused a maximum error in the position of 15 m over 7 days, which was equivalent to an acceleration of $5x10^{-11}$ m/s². Due to the small order of magnitude, this value was absorbed by the empirical accelerations as well (see section 4.4.2 research paper 2).

Lunar gravity field truncation

Within updates of the nominal LRO trajectory, the GRAIL gravity field was used up to degree and order 420 (Mazarico et al., 2013). The application of the gravity field thereby allowed for an improvement of the LRO nominal trajectory accuracy from ≈14 m to ≈9 m over all mission phases (estimated from the arc overlaps). Due to limitations of the estimation software used in this work, the GRAIL gravity field was truncated at degree and order 180. Due to the less detailed gravity field errors were accumulating and the resulting trajectories were less accurate than the ones from Mazarico et al. (2013). This can be

seen from the larger arc overlap differences of this work (41 m), compared to the arc overlap differences of Mazarico et al. (2013; 9 m). However, the truncation of the gravity field at degree and order 180 kept the calculation times of the trajectories and the individual runs at a reasonable level.

Empirical accelerations and optimum state arc length

The estimation of constant empirical accelerations allowed for an estimation of 7-day long orbit arcs with an accuracy comparable to 2-day long orbit arcs. This is shown by the agreement of their differences with respect to the nominal LRO trajectory of ≈25 m on average for the 2-day and for the best 7-day arc (see section 4.5.1 in research paper 2). However, errors were accumulating with increasing state arc length which increased the difference to the nominal LRO trajectory and the post-fit measurement residuals (see Table 20 in research paper 2). Analog to the clock arc length, the state arc length could be optimized so that the maximum possible length and the accumulation of errors are balanced. While this would limit the number of parameters, the effect of the errors on the results – increasing difference to the nominal LRO trajectory and post-fit measurement residuals – could be kept at a certain tolerable limit. Since completely different aspects are modeled, the state and the clock arc lengths do not need to be identical.

5.4 Implications of the observation data coverage and type

Table 29 lists the coverage of LRO radio and laser observation data during various timeframes for comparison. Since all correlated ground station clocks had to be estimated simultaneously, observation data from only three ground stations was included – from the two US stations GO1L and MONL and the Australian station YARL. The timeframe of 7 days during SM02 was selected for LRO orbit determination because of good coverage of the observation data (see Table 29).

With ≈6 passes per day, the number of passes per timeframe (40 over 7 days) was much larger during the timeframe selected for orbit determination, than during SM02 (≈2 passes per day) and during SM03 (≈3 passes per day). Furthermore, the average and maximum gap in time between consecutive observation passes was smaller than during SM02 and SM03 phase. Because an important focus of this work was the analysis of the issues of the one-way laser ranging data application, more variations were made in the clock approximation instead of in the data selection. Instead of processing multiple 7 day long timeframes, the selected timeframe was used for extensive variations in the clock analysis. Due to the better data coverage of the selected compared to other timeframes (e.g. SM02 and SM03), the results are not transferable to the overall mission. However, also Mao et al. (2014) observed large variations within their difference to the nominal LRO trajectory (5 – 30 m). These variations show, that the results from individual timeframes were also not transferable to the overall mission.

The table also lists the coverage of the radio passes, which were used within the estimation of the nominal LRO trajectory, during the timeframe selected for orbit determination. As can be seen from the number of passes and the average and maximum gap in time, the coverage of the radio data is better than the coverage of the laser data.

The gaps in the observation data coverage were also present in the LRO clock rate estimated from the single passes. The LRO clock parameters esimtated from multiple passes did not have these gaps, since the used polynomial fits provided continuous coverage. However the accuracy of the approximation of the LRO clock behavior via the long-term fits might have been limited during those gaps – in particular the approximation of the short-term behavior.

Table 29:Observation data coverage during Science Mission phase SM02 and SM03 for LRO laser ranging and radio data.

Timeframe	OD* during SM02		SM02	SM03
Type	Radio**	Laser	Laser	Laser
Length in days	7	7	28	26
Number of selected passes	88	40	66	88
Average pass length in minutes	≈42	≈38	≈33	≈33
Average gap between consecutive passes in hours	≈1.3	≈4	≈9.2	≈6
Largest gap between consecutive passes	≈3.3 hours	≈20 hours	≈5 days	≈3 days

*) Orbit determination.

**) Includes both radio range and Doppler data.

Within the observation data used for the orbit determination, two gaps with a length of 12 hours (on day 666 and 670) and one gap with a length of 20 hours (on day 668) were present. The gaps on day 668 and 670 significantly affected the quality of the 2-day arcs (Nr. 6, 8 and 9). The arcs had larger differences to the nominal LRO trajectory and larger overlap differences (Nr. 6&7, 7&8, 8&9) than the other arcs (see Table 4 in research paper 2).

Longer arcs (7 days) and the estimation of empirical accelerations allowed for the estimation of results with differences to the nominal LRO trajectory similar to the 2-day arcs even in the presence of the data gaps. Since the coverage of the radio data is better, the nominal LRO trajectory has a better accuracy – ≈9 m at the arc overlaps over all mission phases. However, with ≈25 m difference to the nominal LRO trajectory for 2 and 7 day long arcs, the results of this work were in agreement with the differences of 5–30 m that Mao et al. (2014) reported with their 14-day long laser rangin data only arcs.

Besides the regular passes, the dataset featured 1215 simultaneous passes. The common-view observations had much larger gaps, since multiple stations had to range successfully at the same time. 52% of the simultaneous passes were carried out on consecutive LRO orbits and up to 0.5 days (≈5 LRO orbits), 26% between 0.5 and 1.5 days and 21% between 1.5 and 25 days. Furthermore, the limited field of view of the optical receiver only allowed for simultaneous passes between US stations. Due to this limitation, no common-view observations were available between stations from different continents (e.g. between the US and the Australian station).

The limitations on the coverage of the simultaneous passes highlight the difficulty to monitor the whole station network with one-way observations only. Furthermore, non-common view observations were not possible within the LRO mission (see section 5.2). Even though non-common view time transfer was not possible, the multiple-pass analysis allowed the monitoring of the station clock differences over long timeframes at a rough scale.

The coverage of the common-view observations was limited in time and to certain ground station clock combinations. Consequently the basis for developing a priori constraints and comparing estimated ground station clock differences was limited as well. This constrained the selection of data from ground stations for the orbit determination, when no or only very few simultaneous passes were available for the stations.

Overall the simultaneous passes did not affect the quality of the results of research paper 2 significantly. As shown in section 5.1 and 5.2, the estimated trajectories and LRO clock parameters only

changed slightly due to the incorporation of the simultaneous passes. The fact that they did not provide the positioning improvement as expected by Neumann et al. (2014) was due to the limited accuracy of the ground station clock approximation (see section 5.2).

5.5 Implications of the Normal Point data formation

From the results on the experiment and ground station performance large variations in the amount of observation data from the different ground stations was observed (see Table 11 in research paper 1). Since GO1L is firing in phase and frequency with the LOLA Earth Range Gate the station provided 85 % of the FR data. The averaging of the FR to the NPT data provided a reduced and uniform data rate for all stations. For the LRO mission the specific settings for the bin length of 5 s and a minimum shot criteria of 1 shot per bin was applied during the formation (ILRS website, 2016). The formation of the FR to NPT data reduces the overall amount by a factor of 41 to ≈1.6 million shots and thus simplified its storage and handling. Furthermore, the uniform data rate balanced the shares of data coming from the different stations (see Table 11 in research paper 1). The continuous data rate furthermore removed the need to apply weights on the observation data from the different ground stations within the orbit determination. Moreover the NPT formation improved the precision of the data (see Figure 17 in research paper 1).

5.6 Incorporation of the one-way laser ranging data within orbit determination

While the goal of this work was the successful application of laser ranging data within orbit determination of LRO, an overall goal of the mission was to derive improved spacecraft positioning from the combined application of different datasets within orbit determination (see section 1). Table 30 compares the LRO orbit determination results from this work and various authors whereby laser, radio and altimetric crossover data were used on their own or in combination. With that the laser ranging only solutions from this work as well as the latest state of research on the orbit determination from multiple datasets can be compared. However, none of the listed authors reported results specifically for the 7-day long timeframe during mission phase SM02 selected within this work. Consequently the accuracy could only be compared from the reported overall averaged numbers. Since one main focus of this work was the analysis of the issues of the one-way data application, more variations were introduced on the clock approximation instead of in the data selection – by processing multiple and different periods of data.

The results of Mazarico et al. (2012 and 2013) provided the nominal LRO trajectory, whereby only the first result incorporated altimetric crossover data. Following the incorporation of the GRAIL gravity field within their orbit determination, Mazarico et al. (2013) did not use the crossovers anymore. However, Mazarico et al. (2012 and 2013) did not incorporate laser ranging data in any solution. All other authors used the nominal trajectory from Mazarico et al. (2013) as reference and evaluated the quality of their results via the differences.

The results show that the radio only solutions provided more accurate positioning than the one-way laser ranging only solutions (except for Buccino et al., 2016). This is most likely due to the issues of one-way compared to two-way data (see section 2.1). Furthermore the incorporation of the laser to the radio data did not always improve the positioning.

Table 30: Results of the LRO orbit determination from different authors. Various combinations of laser, radio and crossover observation data were used.

Authors	Data used	Reported accuracy	Accuracy estimated from	Comment
Mazarico et al. (2012)	Radio range and Doppler, crossovers	14 m	Arc overlaps	nominal LRO trajectory, LLGM-1 gravity field used
Mazarico et al. (2013)	Radio range and Doppler	9 m	Arc overlaps	nominal LRO trajectory GRAIL gravity field used
Mao et al. (2014)	Radio*	5–20 m	Difference to nominal LRO trajectory	14 day long arcs
	Laser ranging	5–30 m		
	Radio, Laser ranging	5–17 m		
Löcher et al. (2015)	Radio Doppler	10.53 m	Difference to nominal LRO trajectory	2.5 day long arcs covering the timeframe from September 2011 to 2012
	Radio range and Doppler	10.05 m		
	Radio Doppler, Laser ranging	11.24 m		
	Radio range and Doppler, Laser Ranging	10.21 m		
Buccino et al. (2016)	Radio Doppler	23.0 m	Difference to nominal LRO trajectory	7 day long arcs
	Radio range	90.5 m		
	Laser ranging	7.2 m		
	Radio Doppler, Laser ranging	20.9 m		
	Radio range and Doppler, Laser Ranging	33.0 m		
Bauer et al. (2016)**	Laser Ranging	25 m	Difference to nominal LRO trajectory	7 day long and 2 day long arcs

*) It was not specified in the work if radio range, radio Doppler data or both types were used.
**) Research paper 2.

Only Mao et al. (2014), Buccino et al. (2016) and this work (research paper 2) featured laser ranging only solutions. While Mao et al. (2014) derived 5–30 m differences to the nominal trajectory, the differences of this work (≈25 m) are in this range, but above the results from Buccino et al. (2016). Only Mao et al. (2014) achieved an improvement of LRO positioning from the joint application of radio and laser data. With Löcher et al. (2015) and Buccino et al. (2016), the accuracy of the positioning slightly or significantly decreased, respectively. Both papers did not provide possible reasons for this. In this work, radio observation data could not be incorporated due to limitations of the estimation software (see section 4.4.2 in research paper 2).

No discussion is provided by Mao et al. (2014), Löcher et al. (2015) or Buccino et al. (2016) about the background or the issues of the combined application of radio and laser data within orbit determination. Thus it can only be assumed that the differences in the setup (one- vs. two-way), the measurement technique (pulse detection vs. phase and frequency offset) as well as the hardware (clocks, detection equipment, etc.) complicates the combined application and did not allow for an improved positioning per se. The different datatypes are subject to different issues and errors which all have to be modeled, calibrated before or estimated concurrently within the estimation.

While the results of this work directly supported the research of the one-way data appliccation, the research of a combined solution is supported indirectly. Once all aspects of the individual datasets are understood, the combined application can be analyzed in particular.

The following list contains important aspects and issues of the one-way laser ranging data processing and application which were identified within this work. For issues that were overcome, the solutions are provided, for issues that were not solved yet, next steps or requirements are formulated. These next steps and the requirements could be picked up in future research or missions. The important aspects and issues are:

- The application of the nominal LRO trajectory and the MET to TDB time conversion (SCLK – see section 5.1) enabled a simplified pairing and processing of the separated fire and receive times. With the LRO laser ranging experiment the pairing is quite robust against uncertainties in the spacecraft positioning, due to the 28 Hz cycle and the 8 ms long Earth Range Gate (see section 5.1). Contrary to the pairing, the further analysis of the LRO and the ground station clocks was sensitive to spacecraft positioning uncertainties. More accurate spacecraft positioning (e.g. nominal LRO trajectory compared to the FDF trajectories – see section 5.1) allowed for a more accurate analysis of the clocks.
- Due to the high rate of the Full Rate data (e.g. measurements at a ≈14 Hz rate in case of GO1L station – see Table 11 in research paper 1), the processing and the application became time and memory consuming. Furthermore weights were required for the observation data from the different stations within the orbit determination. The averaging of the Full Rate to Normal Point data reduced the total amount of data and thus the time and memory required during the processing and the application of the data. Moreover, the shares of data from the different stations were balanced by the uniform data rate, station dependent characteristics were removed and the data precision was improved (see section 5.5).
- Using the nominal LRO trajectory allowed to characterize the LRO clock and reference onboard to ground time with a fixed orbit. The polynomial fits that were used, had limited capability to approximate the short-term behavior of a clock accurately when they were applied over longer arc lengths. The accuracy of the LRO clock characterization and the referencing depended on the length of the timeframe over which the fit was applied, the order of the polynomial fit, the completeness of the corrections applied to the fire and the receive times and the accuracy of the nominal LRO trajectory (see section 5.2).
- Furthermore, the ground station clock differences were characterized from the post-fit measurement residuals of the onboard to ground time (MET to TDB) referencing and simultaneous passes. The laser ranging stations had differences in their total time with respect to UTC and thus with each other. Their differences could be measured almost independently from onboard clock and orbit errors from simultaneous passes (common-view observations – see section 3.6.3 in research paper 1). However, time transfer from non common-view observations was not possible due to the limited accuracy of the clock modeling (polynomial fits), the limited LRO clock stability, the incomplete corrections and uncertainties from the nominal LRO trajectory.
- In order to continuously monitor the ground station clock differences, continuous simultaneous pass coverage over time and between all participating stations would be required. Carrying out as many passes as possible between, at best, all participating stations is challenging regarding the scheduling, the local weather conditions and the requirement that

all stations have to successfully hit LRO during a pass. Furthermore, the coverage is limited by the field of view of the optical receiver and the required pointing of the High Gain Antenne towards White Sands in New Mexico (USA) to which the receiver is attached. This limited the coverage of the simultaneous passes to US stations only.

- With the one-way setup, the spacecraft state vector of LRO, the timing of its clock and all involved ground station clocks had to be estimated simultaneously within the orbit determination. This concurrent estimation of all timing system introduced strong correlations between the parameters (see section 4.4.2 in research paper 2). Furthermore the transmit delay of the stations, as well as the offset of the total time referencing to UTC were not provided by the ground stations. This was most likely caused by the fact, that one-way observations were not common practice for the ILRS stations. In order to separate the LRO and all involved ground station clocks, a priori constraints (initial and covariance values) were applied within the orbit determination. The results from the LRO and ground station clock characterization from research paper 1 were used for the a priori constraints on the timing systems. The LRO state vector also required a priori information (see section 4.4.2 in research paper 2), which was taken from the nominal LRO trajectory directly.
- In order to reduce the number of correlated parameters within the orbit determination, longer arc lengths for the state and the clocks were used. Within this work, the maximum possible length was 7 days, since accumulating errors reduced the quality of the results (the trajectories, the LRO and ground station clock parameters as well as the post-fit measurement residuals). Mao et al. (2014) used 14 day long arcs, which was the maximum possible timeframe between consecutive LRO spacecraft maneuvers.
- Within the orbit determination accurate dynamical modeling was required in order to reduce accumulating errors that affected the accuracy of the trajectories. With increasing state arc length, simplified or neglected effects increased the difference to the nominal LRO trajectory and introduced trends as well as systematics in the post fit measurement residuals. The incorporation of empirical accelerations allowed for the estimation of 7 day long arcs at a quality comparable to 2 day long arcs.
- The dynamical modeling applied in this work, was less accurate than the modeling of Mazarico et al. (2012; 2013). Due to a simplified radiation pressure model, neglected thermal radiation and reflected sunlight from the lunar surface and the truncation of the GRAIL gravity field at degree and order 180, errors were accumulating which degraded the accuracy of the results (trajectories and post-fit measurement residuals, see section 5.3).
- The optimization of the state arc length may balance the maximum possible length and the accumulation of errors that affect the quality of the results (difference of estimated to the nominal LRO trajectory as well as post-fit measurement residuals).
- The corrections that were applied on the fire and the receive times have to be complete and accurate. Errors due to missing or simplified corrections affected the clock approximation with the polynomial fits. The errors mixed with the random errors of the LRO and the ground station clocks and introduced systematics and trends to the post-fit measurement residuals. These systematics and trends were accumulating with increasing clock arc length.
- Besides the corrections, the stability of the LRO and the ground station clocks affected the accuracy of the clock approximations. The LRO clock was less stable than the ground station clocks and introduced more random errors (see section 4.4.2 in research paper 2). However, multiple ground station clocks had to be estimated simultaneously which resulted in more correlated approximations and parameters. As it was seen from the incorporation of the

simultaneous passes within the orbit determination (see section 4.5.1 in research paper 2), the correlated ground station clocks could not be separated exactly, since their differences only agreed at the order of magnitude with the differences from research paper 1 (see section 4.5.3 in research paper 2). Improved corrections would allow for a better separation and approximation of the ground station clocks and might enable the expected improvement of spacecraft positioning from simultaneous passes (Neumann et al., 2014).

- As with the state arc length, an optimized clock arc length each for the LRO and the ground station clocks may balance the maximum possile length and the accumulation of errors that affect the quality of the results (clock parameters and post-fit measurement residuals). Due to different errors, the optimum state, LRO and ground station clock arc lengths do not need to be identical.
- The coverage of the laser ranging observation data needs to be continuous. In research paper 1, gaps in the data coverage were compensated with the averaging from the polynomial fits. Within the orbit determination of research paper 2, it was found that data gaps over 12 hours significantly reduced the quality of the results (the trajectories, the LRO and ground station clock parameters as well as the post-fit measurement residuals). These gaps were present, since only three correlated ground station clocks could be estimated at a time with the accuracy of the modeling and the corrections of this work. Improved corrections could allow for the incorporation of observation data from more than three ground stations and thus further close data gaps.
- Accordingly continuous observation data coverage is required for the simultaneous passes since ground station clock differences can only be derived from common-view observations. The goal should be a continuous coverage with common-view observations between as many stations ranging to LRO as possible. This would provide more measurements for the development of a priori constraints and for the comparison of the results from the orbit determination.

5.7 Future work and outlook

In the following, various aspects are outlined, that should be improved within future work and research. Besides discussing the effect of the improvements on the results, methods are provided that could be used as a basis for future work.

Estimation of the ground station clocks within research paper 1

As described in section 5.2 both the LRO and the ground station clocks were estimated within the orbit determination, but only the LRO clock within its characterization in research paper 1. Consequently the differences of the ground station clocks are present in the post-fit measurement residuals (see Figure 41). As within the orbit determination, the different ground station clocks could be approximated with polynomial fits within the multiple-pass analysis as well. From the approximation of the ground station clocks further information for the a priori constraints within the orbit determination could be derived. Utilizing values that were derived via the same approach (2nd order polynomial fits) might improve the constraints, the approximation and the comparison of the results. The ground station clocks thereby would need to be adjusted concurrently with the LRO clock. Consequently the analysis would become more complicated than the current approach where only one 3rd order fit is applied to the observation data. Since all clocks would need to be estimated simultaneously, the clock approximations and thus the timing parameters might become correlated as

within the orbit determination. Due to the limited approximation accuracy of the 2nd order fits, error signal of the clocks could be distributed between their approximations. However, the actual value of the approach would need to be addressed within future work.

Solar radiation pressure model

As highlighted above, an important aspect of the orbit determination is the accuracy of the dynamical modeling. Differences of ≈3.6 m are accumulating between the simplified cannonball model and a 3-dimensional model featuring self-shadowing over a single LRO orbit (≈120 min; see section 5.3). The average trend introduced by the differences was compensated by constant empirical accelerations. However, variations of the solar radiation pressure introduce variations in the post-fit measurement residuals (e.g. during the change from the sunlit to the shade phase). In order to avoid these errors, a full 3 dimensional model including self-shadowing should be implemented. Such a model could be based on the spacecraft macro-model provided in Smith et al. (2008) and the orientation from the NAIF SPICE "C-Kernels".

Thermal radiation and reflected sunlight from the lunar surface

Furthermore the influence of thermal radiation and reflected sunlight from the lunar surface should be incorporated preventing, the accumulation of errors of ≈15 m over 7 days (see section 5.3). Spherical harmonic expansion models, as described in Floberghagen et al. (1999), could be used as a basis for the incorporation of the reflected sunlight and thermal radiation from the lunar surface. However, the accumulated error is smaller than the error due to the simplified solar radiation pressure (25 m compared to 15 m over 7 days respectively). Consequently the solar radiation pressure model should be updated first.

Improving the dynamical modeling reduces the accumulation of errors over the state arc length. This would for longer trajectories at a better accuracy and fewer parameters that have to be estimated within the orbit determination.

Furthermore, the accuracy of the results (clock parameters and measurement post-fit residuals) is affected by the clock modeling. In order to improve the LRO and the ground station clock approximation, the corrections have to be improved. Potential improvements affect the correction for atmospheric effects and the variation of the LRO clock rate due to temperature change.

Atmospheric correction

As discussed in section 5.2 the atmospheric correction was employed as a constant offset. When the environmental conditions were changing throughout a pass, an error in the form of a drift was introduced. Updating the model is simple, however reprocessing of the dataset and the simultaneous passes in particular is required. While the first step is a mostly automated process, the reprocessing of the simultaneous passes requires a manual data editing on the first iteration which is time consuming. This update could be carried out within future work. This would improve the measurement of the smaller values of the relative ground station clock rates (between 2×10^{-13} and 5×10^{-13}, see section 5.2).

Temperature correction

Moreover, the corrections did not feature a correction of the variation of the LRO clock rate due to temperature change. The missing correction introduced an average trend of $1.5–4.5 \times 10^{-13}$ with

variations of 2–6 ns at a daily period around it (see section 5.2). When a turnover point was assumed every 21600 s these variations translated into average trends of $\approx \pm 1\text{–}3 \times 10^{-13}$. The introduced error mixed with the random errors of the LRO clock and had to be approximated with the polynomial fits as well. These errors increased the measurement post-fit residuals and degraded the estimated clock parameters in general and with increasing arc length. Mao et al. (2013) provides some information about a model that could potentially be used as a basis for a correction model.

Implementing the correction would improve both the LRO and the ground station clock modeling, since their timing parameters were correlated. Due to the correlations, errors of the LRO clock may have been absorbed by the ground station clock approximations and vice versa. Fewer errors would have to be approximated with the polynomial fits beside the stochastic noise of the LRO clock.

Within the LRO clock analysis, the improved approximation would allow for the estimation of more accurate LRO clock parameters and a more accurate referencing of onboard time to ground time time (MET to TDB). Within the orbit determination an improved clock approximation would allow for reduced post-fit measurement residuals, a better separation of the clocks and consequently the incorporation of observation data from more than three ground stations within this work. This could further close gaps in the observation data and improve the quality of the results. Furthermore, the improved ground station clock approximation might enable the improvement of positioning upon the incorporation of simultaneous passes to the observation data, as expected by Neumann et al. (2014). Whether the measurement of ground station clock differences from non-common view observations would become feasible should be investigated as well.

Optimum state and clock arc length

As discussed in the sections 5.2, 5.3 and 5.6 the length of the state, the LRO and the ground station clock arcs could be optimized. This would balance the maximum possible length and thus the number of parameters with the accumulating errors. The optimized arc lengths for the state as well as the LRO and the ground station clocks do not have to be identical. Since less correlated parameters had to be estimated, longer arc lengths (7 to 14 days) were generally of interest. Limitations in time prevented an extensive search for optimized state and clock arc lengths within this work. However, optimized arc lengths would provide the optimum settings for the laser ranging data when it is used in combination with other datasets within orbit determination.

Estimation software

Since the utilized estimation software is currently not capable of applying radio or altimetric crossover observation data, the observation models for these datatypes should be implemented within future work. This would allow investigation of joint application of the different datatypes within the LRO orbit determination in order to derive spacecraft positioning improvement (see section 1).

Next steps

Alltogether, the listed improvements should be applied in order to evaluate the complete potential of the positioning accuracy and improvement enabled by the one-way laser ranging data to LRO. After that, the orbit determination with all types of LRO mission data should be researched with the individual optimum settings. Even though the joint application seems to be affected by yet not fully resolved discrepancies (Löcher et al., 2015), the various datasets provide a good basis for the research

of it. The observation data has an extensive coverage (e.g. 5 years with the laser ranging data) and the different types are available from one mission. The results from this research could further provide a basis for the analysis and simulation of future missions, which intend to derive spacecraft positioning from the joint application of different types of observation data.

5.8 Differenced range-rate measurements from consecutive one-way ranges

Within this work an aspect was found, that could not be investigated in detail due to time limitations. Following Tapley et al. (2004), consecutive one-way range measurements of a pass could be used to derive a differenced range-rate measurement. While Tapley et al. (2004) discuss this for a downlink from a satellite to a ground station, in the following such range-rate measurements are derived for the uplink to LRO. Two consecutive range measurements ρ from a ground station to LRO are provided by

$$t_{R1} = t_{T1} + \rho_1/c \quad (38)$$

and

$$t_{R2} = t_{T2} + \rho_2/c, \quad (39)$$

where t_T are the transmit times at the stations, t_R the receive times at LRO and c the speed of light. The approach of Tapley et al. (2004) is adapted and the onboard clock is modeled with a linear fit via

$$t = T + a + b(T - T_0) + \epsilon', \quad (40)$$

where t is the time measured by the onboard clock, T true time, a a constant offset between the onboard and the ground station clock, b a linear clock drift (rate), T_0 is a reference time and ϵ' are other errors coming from incomplete corrections and random LRO clock errors for example. Incorporating equation 40 into equation 38 and 39 provides

$$T_{R1} + a + b(T_{R1} - T_0) + \epsilon' = t_{T1} + \rho_1/c \quad (41)$$

and

$$T_{R2} + a + b(T_{R2} - T_0) + \epsilon' = t_{T2} + \rho_2/c. \quad (42)$$

A range-rate measurement is retrieved by differencing the two consecutive range measurements (equation 38 and 39) via

$$t_{R2} - t_{R1} = t_{T2} - t_{T1} + (\rho_2 - \rho_1)/c, \quad (43)$$

which is simplified to

$$\delta t_R = \delta t_T + (\rho_2 - \rho_1)/c, \quad (44)$$

where δt_R is the difference between the receive times at LRO and δt_T the difference between the transmit times. Incorporating the first order clock approximation (see equation 41 and 42) in the differenced range-rate measurement (equation 44) and simplifying yields

$$\delta T_R(1 + b) = \delta t_T + (\rho_2 - \rho_1)/c. \quad (45)$$

As seen from equation 45, the constant offset a and the error term ϵ' are cancelled out. Consequently the onboard receive times are only affected by the onboard clock drift over the differencing time, when a 1st order fit is applied for the modeling of the onboard clock.

Table 31 lists various error sources that were identified within this work that could affect the accuracy of such differenced range-rate measurements in order to obtain a guess on their achievable accuracy.

The error sources are distinguished between effects that can be calibrated or calculated (LRO clock errors from rate, aging and change and relativistic corrections), their uncertainty (rate, aging, change of aging, relativistic corrections) and effects that cannot be corrected (NPT measurement precision, LRO random clock errors, variation of LRO rate due to temperature variations). Even though some effects can be removed by calibration or calculation, their uncertainties are present and affect the differenced range-rate measurements. Effects that are random or for which no correction model was available, affect the measurements as well. The error of the ranges, which were used in the differencing, affect the accuracy of the retrieved measurements as well. In the following, the influence of the measurement precision on the differenced range measurement is derived. Simplified a differenced range measurement $\dot{\rho}$ is derived via

$$\delta\dot{\rho} = \frac{\rho_2 - \rho_1}{t_{R2} - t_{R1}} = \frac{\rho_2 - \rho_1}{\Delta t_R}, \tag{46}$$

where $\rho_{1/2}$ are the consecutive ranges with their receive times $t_{R1/2}$ and the time difference Δt_R in between them. If the time difference is assumed to be a constant that is defined, the error of the ranges is propagating via

$$\Delta\dot{\rho} = \frac{\sqrt{\Delta\rho_1{}^2 + \Delta\rho_2{}^2}}{\Delta t_R} = \sqrt{2}\,\frac{\Delta\rho}{\Delta t_R}. \tag{47}$$

Since the differenced ranges $\dot{\rho}$ are derived from the NPT data, their measurement precision of 5.6 cm (see research paper 1) is used for $\Delta\rho$. A length of 30 s was assumed for the differencing time.

The results from research papers 1 and 2, as well as the discussion (section 1) are used to quantify the numbers for the uncertainties of the various effects. For the timeframe, over which the range-rate measurements are differenced, 30 s were selected. Even though NPT ranges were available every 5 s, it will be shown, that only after ≈24 s the propagated error of the NPT precision becomes smaller than all other errors together. The offsets caused by the rate, the aging, its change as well as for their uncertainties over the timeframe of 30 s are listed in Table 31 as well.

As summarized in Table 31, a total uncertainty of ≈$2\text{x}10^{-11}$ (≈6 mm/s) was retrieved for range-rate measurements differenced over 30 s. The NPT measurement uncertainty and the uncertainty of the estimated LRO clock rate were the largest influence factors. Compared to this, Mazarico et al. (2012) reported errors of the Doppler LRO tracking data of 0.3 mm/s for White Sands station and of 0.4–0.8 mm/s for the USN. Consequently the accuracy of the differenced range-rate data based in this first guess would be only ≈8–20 times larger than the LRO Doppler data accuracy. This accuracy and the fact that some of the issues of the one-way data are removed (onboard clock offset) is promising regarding the application of this data within orbit determination. However, the actual spacecraft positioning accuracy that could be achieved with this data would need to be analyzed in detail. Furthermore, the actual accuracy of the data would need to be analyzed from the data itself, since here it is predicted from the results of this work.

As it can be seen from Table 31, the offsets, accumulated by the aging and the change of aging (≈$1.7\text{x}10^{-14}$ s and ≈$8.3\text{x}10^{-20}$ s respectively) were smaller than the offset of accumulated by the rate (≈$2.1\text{x}10^{-6}$ s). Since the uncertainties of the onboard clock are only accumulating over the differencing time, a linear fit is sufficient for the modeling of the onboard clock (equation 43). Even with a maximum

possible differencing time of 33 min (average pass length), the aging and its change would not be detectable by LOLA (smaller than the timestamp precision of $5x10^{-10}$ s, see section 5.2).

With a timeframe of 30 s, not every consecutive NPT pair is used for the differencing, but only every 6th NPT. However, the differencing could be done for NPT's every 5 s by using its corresponding range 30 s later (see Figure 43). With that approach only few measurements are lost, which would also be the case with even with larger differencing times. Other configurations, such as varying differencing times throughout one pass or the multiple use of the same NPT range for multiple differenced range measurements, are theoretically possible. However, such variations would also introduce variations in the measurement accuracy throughout the pass.

Table 31: Error influences that may affect differenced range measurements along with their magnitude. A potential overall error is summed from relevant error influences.

Effect	Order of magnitude	Comment	Relevant?
Uncertainty from range precision and averaging time	$\approx 8.8x10^{-12}$	Error propagation of NPT measurement precision of 5.6 cm over a measurement differencing time of 30 s	**Yes**
LRO clock rate	$\approx 6.9x10^{-8}$, causes an offset of $\approx 2.1x10^{-6}$ s over 30 s	Derived from a posteriori clock calibration*, removed from the data	No
Uncertainty of estimated LRO clock rate	$\approx \pm 1x10^{-11}$, causes an offset of $\approx 3.0x10^{-10}$ s over 30 s	Derived from comparison of the results derived with different methods*	**Yes**
Aging of LRO clock	$\approx 1.6x10^{-12}$ /day, causes an offset of $\approx 1.7x10^{-14}$ s over 30 s	Derived from a posteriori clock calibration*, removed from the data	No
Uncertainty of estimated aging	$\approx 1.2x10^{-12}$ /day, causes an offset of $\approx 1.3x10^{-14}$ s over 30 s	Derived from comparison of the results derived with different methods*	Yes but neglected due to small order of magnitude
Change of aging of LRO clock	$\approx -2.3x10^{-14}$ /day², causes an offset of $\approx 8.3x10^{-20}$ s over 30 s	Derived from a posteriori clock calibration*, removed from the data	No
Uncertainty of the change of aging	$9.2x10^{-14}$ /day², causes an offset of $\approx 3.3x10^{-19}$ s over 30 s	Derived from comparison of the results derived with different methods*	Yes but neglected due to small order of magnitude
Relativistic effects	$\pm 1x10^{-9}$	Data is corrected for this effect	No
Uncertainty of relativistic corrections	$\approx 2x10^{-14}$	Derived from the sensitivity analysis of the relativistic corrections due to uncertainties of the nominal LRO trajectory (see section 5.1)	Yes but neglected due to small order of magnitude
LRO clock stability	$1x10^{-13}$ over up to 100 s	Random error of the LRO clock*	**Yes**
LRO clock rate variation due to temperature variation	Average trend of $\approx 1.5–4.5x10^{-13}$ with variations of $\approx \pm 1–3x10^{-13}$ around it, so $7.5x10^{-13}$ at maximum	Systematic effect for which no correcting model was available within this work*	**Yes**
Total	**$\approx 2x10^{-11}$**	**≈6 mm/s**	**-**

*) See research paper 1.

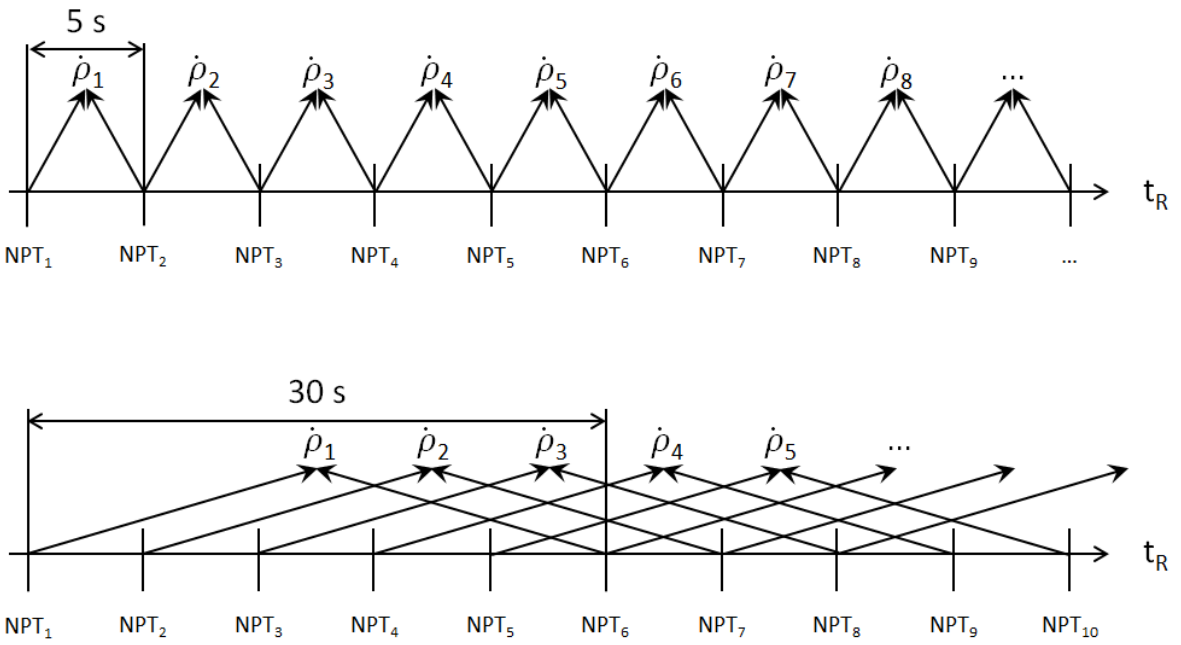

Figure 43: Possible scheme for the differencing of rate-range measurements from the combination of different NPT's by varying the timeframe in between them. While here lengths of 5 and 30 s are shown, also other lengths as well as varying lengths throughout a pass are theoretically possible.

Future work addressing this topic should incorporate an appropriate observation model within the estimation software. With that the application of the data within the LRO orbit determination as well as the errors actually affecting it, could be investigated.

5.9 Benefit of one-way laser tracking of spacecraft and further applications

Compared to two-way tracking systems, one-way tracking is subject to issues regarding the processing, the application of the data and the accuracy of the results (see section 5.6). However, various characteristics of the LRO laser ranging experiment highlight the potential of one-way laser tracking systems in particular for future missions that carry a laser altimeter.

Since the on-board laser altimeter of LRO was used for both the altimetry measurements and the Earth-based tracking, no additional laser ranging terminal was required. Furthermore, the one-way uplink does not require an active laser terminal onboard the spacecraft. This reduces the number of required instruments (1 instrument for 2 tasks), the mass, the hardware size, the power consumption and the complexity of the operation (passive instrument requires no active pointing). The laser ranging experiment itself was enabled by adding an optical receiver to the High Gain Antenna, a fiber optics cable that forwarded incoming laser pulses and modification of the LOLA instrument. Since the amount of additionally required hardware and the modifications were small, incorporating a laser ranging capability within missions with a laser altimeter seems to be feasible at little effort. The ESA Asteroid Impact Mission (AIM) for example intends to utilize its onboard optical terminal for collecting altimetric measurements to the asteroid surface and for communicating to Earth. Furthermore, the additional observation data is supposed to provide accurate orbit determination of the spacecraft (Michel et al., 2016).

The LRO mission goal of deriving improved spacecraft positioning from the joint application of multiple types of observation data also highlights multiple advantages. Once a successful joint orbit determination is possible, ground-based tracking could be optimized between radio tracking and laser

ranging regarding costs, accuracy, availability of and observability at the stations. Furthermore, an increased application of local altimetric observations within the orbit determination might enable a reduction of ground-based tracking.

In order to retrieve improved performance from a one-way tracking system, onboard clock stability is crucial. Recent developments such as the miniaturized onboard Deep Space Atomic Clock (DSAC) from NASA's JPL provide stabilities of better than $2x10^{-14}$ /day. This improved performance (even stabilities of $1x10^{-15}$ /day were demonstrated with first test models) would allow for improved spacecraft positioning while using one-way data only (Ely et al., 2012). Such an improved onboard clock stability could allow for time transfer in non-common view.

Furthermore, an extensive pre-launch characterization of the onboard clock would improve the performance of a one-way tracking system as well. By calibrating the influence of external effects (e.g. temperature change) on the onboard clock comprehensively, they could be modeled and applied in forms of corrections. With that, the the errors are removed, leaving only the stochastic behavior of the clock in an optimum case. This would improve the clock approximation with polynomial fits and with that the accuracy of the results (trajectories and post-fit measurement residuals). Additionally the stations should introduce a calibration for the transmit path (Tx) delay and report the station clock offset to UTC in order to provide these values for the orbit determination. Since ILRS ground stations typically perform two-way laser ranging to retro-reflectors, these values were not reported because one-way observables were not a common practice for them (see section 2.5). Providing these values would reduce the variations affecting the LRO clock approximation and with that improve it as well as the accuracy of the results. While these values might be required for future campaigns, such as space debris tracking, they could provide improvement in the performance of future one-way tracking systems. Consequently ground stations should be encouraged to measure the values if it is not part of their routine operation already, even at extra effort.

Further capabilities were demonstrated with the laser ranging to LRO experiment. Sun et al. (2013b) also utilized the uplink to LRO for demonstration of optical communication. Furthermore the LOLA laser boresight pointing offset, the far field pattern and the receiver pointing as well as their change were estimated from successful two-way experiments. The measurements were taken from the Goddard Geophysical and Astronomical Observatory located at NASA's Goddard Space Flight Center at the beginning of the mission and 5 years later (Sun et al., 2014).

The general future potential of laser technology is further demonstrated by recent scientific and commercial interests and developments. Some interplanetary missions proposed two-way Interplanetary Laser Ranging (ILR) for a more precise estimation of planetary, relativistic and solar system parameters from cm accurate two-way ranges. A Mars and Phobos mission for example, involving an ILR link, would allow for the accurate estimation of the gravitational, tidal and rotational parameters and with that of their interior (Dirkx et al. 2014) as well as improved basic dynamical solar system parameters (Hemmati et al.,2009). Furthermore, tests of gravitational theory could be improved with such a mission – in particular the test of the equivalence principle. Furthermore, the geodetic precession, the PPN parameters α and γas well as possible variations of the gravitational constant G could be measured accurately (Turyhsev et al, 2004).

While the communications experiment to LOLA only achieved a transmission rate of 300 kbps, the lunar mission LADEE demonstrated laser based communication at a 622 Mbps rate (Sun et al., 2013;

D'Ortenzio et al., 2015). The recently launched European Data Relay Satellite is supposed to provide laser based communication at rates of 5.6 Gbps from a geostationary orbit via its Laser Communication Terminal (LCT; Heine et al., 2011 and Zech et al. 2014). Thereby the LCT represents the next step towards the commercialization of optical communication. The laser technology thereby allows for faster, more focused and thus more secure as well as more efficient communication.

Laser ranging also seems to be a potential technique to compete with the problem of man-made space debris which was first described by Kessler et al. (1978). By having all of the required hardware for detection, tracking and removal on ground, using laser systems might be a feasible option to solve to the problem. After the precise tracking of debris, high powered lasers might be able to gradually alter the orbit of debris in order to avoid collision with spacecraft or other debris (Stupl et al., 2012). Depending on the size also a de-orbiting of debris might be possible (Esmiller et al., 2015).

The previous examples highlight the versaitility of the one-way laser ranging experiment to LRO and of two laser ranging in general. However, as shown in this work, compared to two-way, one-way observables are subject to more issues and higher requirements. Clocks on ground and in space are involved that effect the measurement with their timing errors and have to be estimated concurrently. They require existing orbit information for the pairing of the separated data and complete corrections for external influences in order to characterize the involved clocks. From that a priori constraints can be derived, which, in combination with complete and accurate dynamical modeling, is required within the orbit determination. Furthermore the one-way observables are affected directly by the stability of the clocks on ground and in space, as well as their sensitivity to external effects. While ground station clocks are properly shielded, a comprehensive pre-launch campaign would be required to calibrate the behavior of the onboard clock with respect to external influences. Furthermore the ground stations would be required to monitor their transmit delay and their total time offset – which was not routine operation for the ILRS ground stations ranging to LRO. Consequently the requirements on the involved elements of a one-way tracking system are higher compared to a two-way system, if good positioning performance shall be provided. Consequently the effort would be high with current technology, in order to provide a one-way tracking system with good performance, while it still would be affected by the listed issues. With that, it seems to not very likely, that a dedicated one-way tracking system will be incorporated in a near future mission. However, adding a one-way tracking capability to a spacecraft might be beneficial, if the requirements are met by future technology developments or other mission drivers anyway. Also an existing onboard laser altimeter certainly might provide an incorporation of a one-way tracking capability with small effort. If a dedicated laser ranging capability is required within a mission beyond Earth orbit, it will have to incorporate two-way laser ranging with active segements both on ground and in space. With that the signal loss caused by retro-reflectors, as well as the issues that are related to one-way systems can be overcome. In simplest form such experiments could be carried out with an onboard laser altimeter, while the spacecraft is pointing it towards Earth. However, this will most likely only allow for a few session during cruise, which could be used for calibration but not for continuous two-way tracking of a spacecraft.

References

Buccino, D.R., Seubert, J.A., Asmar, S.W. and Park, R.S., Optical Ranging measurement with a lunar orbiter: limitations and potential, *J. Spacecr. Rockets* **53**, 2016.

Dirkx, D., Noomen, R., Prochazka, I., Bauer, S. and Vermeersen, L., Influence of atmospheric turbulence on planetary transceiver laser ranging, *Adv. Space Res.* **54**, 2014.

Dirkx, D., Noomen, R., Visser, P.N.A.M., Bauer, S. and Vermeersen, L.L.A., Comparative analysis of one- and two-way planetary laser ranging concepts, *Planet. Space Sci.* **117**, 2015b.

Ely, T.A., Koch, T., Kuang, D., Lee, K., Murphy, D., Prestage, J., Tjoelker, R. and Seubert, J., 2012. The deep space atomic clock mission. In: Proceedings of the 23rd International Symposium on Space Flight Dynamics (ISSFD). Pasadena, California, USA, October 29th–November 2nd.

Esmiller, B., Space debris removal by ground-based lasers: main conclusions of the European project CLEANSPACE, *Appl. Opt.* **53**, 2015.

Floberghagen, R., Visser, P. and Weischede, F., Lunar albedo force modeling and its effect on low lunar orbit and gravity field determination, *Adv. Space Res.* **23**, 1999.

Folkner, W.M., Williams, J.G., Boggs, D.H., Park, R.S. and Kuchynka, P., The planetary and lunar ephemerides DE430 and DE431, *IPN Prog. Rep.* **42-196**, 2014.

Heine, F., Kämpfner, H., Lange, R., Czichy, R., Lutzer, M. and Meyer, R., Laser communication applied for EDRS, the European data relay system, *CEAS Space J* **2**, 2011.

Hemmati, H., Birnbaum, K.M., Farr, W.H., Turyshev, S. and Biswas, A., Combined laser-communications and laser-ranging transponder for Moon and Mars, in Free-Space Laser Communication Technologies XXI, *Proceedings of SPIE* **7199**, 2009.

Herman, A.L., Bruce, A.C., Optimal, Low-Thrust, Earth-Moon Orbit Transfer, *J GUID CONTROL DYNAM* **21**, 1998.

International Laser Ranging Service (ILRS) Website. <http://ilrs.gsfc.nasa.gov> retrieved in July 2016.

Imbrium website. <http://imbrium.mit.edu> retrieved in August 2016.

Kessler, D.J., Burton G.C., Collision frequency of artificial satellites: The creation of a debris belt, *J. Geophys. Res.: Space Physics* **83**, 1978.

Löcher, A., Hofmann, F., Gläser, P., Haase, I., Müller, J., Kusche, J. and Oberst, J., Towards improved lunar reference frames: LRO orbit determination, in: International Association of Geodesy Symposia, Springer, 2015.

Mao, D., Sun, X., McGarry, J., Skillman, D., Torrence, M., Mazarico, E., Hoffman, E., Rowlands, D., Neumann, G., Golder, J., Barker, M., Zuber, M. and Smith, D., 2013. Laser Ranging to Lunar Reconnaissance Orbiter: Timing and Orbits. In: Proceedings of the American Geophysical Union, Fall Meeting. San Francisco, California, USA, December 9th–13th.

Mao, D., Sun, X., McGarry, J., Mazarico, E., Torrence, M., Rowlands, D., Neumann, G., Barker, M., Golder, J., Smith, D. and Zuber, M., 2014. LRO orbit determination with laser ranging data. In: Proceedings of the 19th International Laser Ranging Service workshop Annapolis. Maryland, USA, 27th–31st October.

Mazarico, E., Rowlands, D.D., Neumann, G.A., Smith, D.E., Torrence, M.H., Lemoine, F.G. and Zuber, M.T., Orbit determination of the Lunar Reconnaissance Orbiter, *J. Geod.* **86**, 2012.

Mazarico, E., Goossens, S., Lemoine, F., Neumann, G., Torrence, M., Rowlands, D., Smith, D. and Zuber, M., 2013. Improved orbit determination of lunar orbiters with lunar gravity fields obtained by the GRAIL mission. In: Proceedings of the 44th Lunar and Planetary Science Conference (LPSC). Woodlands, Texas, USA, 18th–23rd March.

Michel, P., Cheng, A:, Küppers, M., Pravec, P., Blum, J., Delbo, M., Green, S.F., Rosenblatt, P., Tsiganis, K., Vincent, J.-B., Biele, J., Ciarletti, V., Hérique, A., Ulamec, S., Carnelli, I., Galvez, A., Benner, L., Naidu, S.P. Barnouin, O.S., Richardson, D.C, Rivkin, A., Scheirich, P., Moskovitz, N., Thirouin, A., Schwart, S.R., Campo Bagatin, A. and Yua, Y., Science case for the Asteroid Impact Mission (AIM): A component of the Asteroid Impact & Deflection Assessment (AIDA) mission, *Adv. Space Res.* **57**, 2016.

Montenbruck, O. and Gill, E., Satellite Orbits, 2000, Springer.

Neumann, G.A., Barker, M.H., Mao, D., Mazarico, E., McGarry, J.F., Smith, D.E., Sun, X., Torrence, M.H. and Zuber, M.T., 2014. Interplanetary laser ranging: the quest for 1 AU. In: Proceedings of the 19th International Laser Ranging Service workshop. Annapolis, Maryland, USA, 27th–31st October.

Riris, H. and Cavanaugh, J., Calibration document for the Lunar Orbiter Laser Altimeter (LOLA), 2009, NASA, Goddard Space Flight Center.

Slojkowski, S., 2014. Lunar Reconnaissance Orbiter Orbit Determination Accuracy Analysis. In: Proceedings of the 24th International Symposium on Space Flight Dynamics. Laurel, Maryland, USA, 5-9 May.

Smith, D., Zuber, M., Lemoine, F., Torrence, M. and Mazarico, E., 2008. Orbit determination of LRO at the Moon. 16th International Workshop on Laser Ranging. Poznan, Poland, October 13th–17th.

Stupl, J., Mason, J., De Vries, W., Smith, C., Levit, C., Marshall, W., Salas, A.G., Pertica, A., Olivier, S. and Ting, W., 2012. LightForce: An Update on Orbital Collision Avoidance Using Photon Pressure. In: Proceedings of the 63rd International Astronautical Congress. Naples, Italy, October 1st–5th.

Sun, X., Skillman, D.R., McGarry, J.F., Neumann, G.A., Mao, D., Torrence, M.H. and Hoffman, E., 2013a. Time transfer between satellite laser ranging stations via simultaneous laser ranging to the Lunar Reconnaissance Orbiter. In: Proceedings of the 18th International Laser Ranging workshop. Fujiyoshida Japan, 11th–15th November.

Sun, X., Skillman, D.R., Hoffman, E.D., Mao, D., McGarry, J.F., McIntire, L., Zellar, R.S., Davidson, F.M., Fong, W.H., Krainak, M.A., Neumann, G.A., Zuber, M.T. and Smith, D.E., Free space laser communication experiments from Earth to the Lunar Reconnaissance Orbiter in lunar orbit, *Opt. Express* **21**, 2013b.

Sun, X., Barker, M.K., Mao, D., Marzarico, E., Neumann, G.A., Skillman, D.R., Zagwodzki, T.W., Torrence, M.H., Mcgarry, J. and Smith, D.E. and Zuber, M.T., 2014. In-orbit calibration of the Lunar Orbiter Laser Altimeter via two-way laser ranging with an Earth station. In: Proceedings of the American Geophysical Union, Fall Meeting. San Francisco, California, USA, December 15th–19th.

Tapley, B., Schutz, B. and Born, G.H., Statistical Orbit Determination, 2004, Academic Press.

Turyshev, S.G., Williams, J.G., Shao, M., Anderson, J.D., Nordtvedt Jr., K.L. and Murphy Jr., T.W., 2004. Laser Ranging to the Moon, Mars and Beyond. In: Proceedings of the 2004 NASA/JPL Workshop on Physics for Planetary Exploration. Solvang, California, USA, April 20th–22nd.

Zech, H., Heine, F. and Motzigemba, M., 2014. Laser Communication Terminal: Product Status and Industrialization Process. In: Proceedings of the International Conference on Space Optical Systems and Applications (ICSOS). Kobe, Japan, May 7th–9th.

6 Synthesis

This cumulative thesis consists of two papers which investigated the processing and the application of one-way laser ranging data from Earth-based ground stations to the Lunar Orbiter Laser Altimeter (LOLA) onboard the Lunar Reconnaissance Orbiter (LRO) for onboard clock characterization, time transfer and orbit determination. Thereby the issues of one- compared to two-way observables, regarding the processing and the application, were analyzed in particular.

In the first research paper, a method for the pairing of the separated fire and receive times was developed. Thereby time conversion and spacecraft positioning information were utilized, which allowed to establish the pairing outside an orbit determination. It was found that the pairing required an accuracy of only ±9 ms for the time conversion and of ±2700 km for the spacecraft positioning information. Corrections for range walk within the laser altimeter, as well as for atmospheric and relativistic effects were applied to the fire and the receive times.

Overall ≈3000 hours of tracking data covering a timeframe of 5 years (from June 2009 until September 2014) were processed, featuring 64 million Full Rate and 1.5 million Normal Point observations. Thereby the formation of Normal Points reduced the overall data amount by a factor of ≈41 which reduced the time and the memory required for processing. Furthermore, the uniform data rate of the Normal Point observations removed station specific characteristics, balanced the data shares from the different stations and removed the need for station specific weights in the orbit determination. Moreover, the Full Rate data measurement precision of 12.3 cm was improved to 5.6 cm with the averaging to Normal Point observations. Through a statistical analysis of the dataset the experiment and the ground station performance was evaluated, which is valuable input for mission analysis and simulation.

The LRO clock was characterized via polynomial fits and estimated to an average value of 6.9×10^{-8} for the rate, of 1.6×10^{-12} /day for the aging and of 2.3×10^{-14} /day² for the change of aging over all mission phases. The values were in agreement with the literature. Furthermore, the fits were utilized for referencing spacecraft onboard time to the TDB time scale. The accuracy of the ground to space time transfer was 166 ns over two mission phases (≈56 days) and 256 ns over all mission phases (≈5 years). Common view observations from these fits as well as simultaneous passes were used to measure ground station clock differences, allowing for ground to ground time transfer. Thereby relative offsets ranging from 33 to 560 ns and relative rates varying between 2×10^{-13} and 6×10^{-12} were observed during selected mission phases.

In research paper 1, the LRO clock as well as the ground station clock differences were estimated with the nominal LRO trajectory and thus with a fixed orbit. In research paper 2 the LRO state vector as well as the timing of the LRO and all ground station clocks was estimated simultaneously, which introduced strong correlations between the parameters. A priori constraints for the state vector and the clock parameters were derived from the nominal LRO trajectory and the clock analysis in research paper 1, respectively. While arc lengths of up to 14 days can be found in the literature, within this work orbit arcs with lengths of 2 and 7 days were estimated during Science Mission phase 02 (SM02, November 2010). The results of the orbit arcs were their trajectories, the post-fit measurement residuals and the estimated clock parameters.

The orbit arcs estimated with one-way laser ranging data only had differences of ≈25 m with respect to the nominal LRO trajectory. This was within the 5–30 m range of differences which was found in the

literature. While the estimated LRO clock rate agreed with the a priori constraints, the aging absorbed clock modeling errors with increasing clock arc length. Due to high correlations between the involved ground station clock parameters and limited clock modeling accuracy, the derived differences agreed only at the order of magnitude with the values from the clock analysis from research paper 1. Gaps in the observation data coverage longer than 12 hours (≈6 successive LRO orbits) affected the results significantly. The incorporation of simultaneous passes did not change the results significantly and provided no improvement in spacecraft positioning. With enhanced dynamical modeling and corrections, the accuracy of the trajectories, the clock approximations and thus the spacecraft positioning could be improved. Then the one-way laser ranging could provide valuable input within a joint orbit determination of LRO from radio, laser and altimetry data.

It was found that an optimum arc length could be derived for the LRO state, the LRO clock and all ground station clocks. With such arc lengths, the maximum possible length as well as the accumulation of errors would be balanced. This would keep the number of parameters small and the errors at a defined level. Thereby the optimum lengths for the LRO state, the LRO clock and the ground station clocks could be different.

The results of this work were also used to analyze errors that could influence range-rate measurements which were differenced from the one-way laser ranges. After summing up relevant error influences a potential uncertainty of 6 mm/s was found for such measurements.

Within the literature the issues of one- compared to two-way laser ranging observables has not yet been discussed. The issues that affected the processing, the application were highlighted and summarized within this cumulative thesis. While this supports the research of the application of one-way laser ranging data within orbit determination directly, also the overall mission goal of improved positioning from a joint orbit determination is promoted. Once the aspects of the laser ranging data application are understood, the joint application with radio and altimetry data can be analyzed in detail.